n°ordre : 42200

Université des Sciences et Technologies de Lille 1

UFR des Sciences de la Terre

UMR 8198 « Evolution, Ecologie, Paléontologie » Université Lille 1 – CNRS

Ecole doctorale 104 – Science de la Matière, du Rayonnement et de l'Environnement

Filière Géosciences, Ecologie, Paléontologie et Océanographie

Doctorat de l'Université de Lille 1

Géologie

par Maxime PADEL

Influence cadomienne dans les séries pré-sardes des Pyrénées Orientales : approche géochimique, stratigraphique et géochronologique

Thèse co-dirigée par José Javier Álvaro et Sébastien Clausen

Soutenance Publique prévue le 9 Décembre 2016

JURY

Josep Maria CASAS	Université de Barcelone, Espagne ; Rapporteur
Abderrahmane SOULAIMANI	Université Cadi Ayyad, Maroc ; Rapporteur
Olivier BLEIN	BRGM, France ; Examinateur
Thomas SERVAIS	Université Lille 1, France ; Examinateur
José Javier ÁLVARO	Université Lille 1, France ; Directeur
Sébastien CLAUSEN	Université Lille 1, France ; Co-directeur
Olivier AVERBUCH	Université Lille 1, France ; Invité
Bernard LAUMONIER	Université de Lorraine, France ; Invité
César WITT OLIVO	Université Lille 1, France ; Invité

Université des Sciences et Technologies de Lille 1

UFR des Sciences de la Terre

UMR 8198 « Evolution, Ecologie, Paléontologie » Université Lille 1 – CNRS

Ecole doctorale 104 – Science de la Matière, du Rayonnement et de l'Environnement

Filière Géosciences, Ecologie, Paléontologie et Océanographie

Ph.D of Université de Lille 1

Geology

by Maxime PADEL

Cadomian Influence on the pre-Sardic Series of the Eastern Pyrenees: Geochemical, Stratigraphic and Geochronological Approach

Ph.D thesis supervised by José Javier Álvaro et Sébastien Clausen

Public defence on the 9th December 2016

JURY

Josep Maria CASAS	Barcelona University, Spain ; Reviewer
Abderrahmane SOULAIMANI	Cadi Ayyad University, Morocco ; Reviewer
Olivier BLEIN	BRGM, France ; Examiner
Thomas SERVAIS	Lille 1 University, France ; Examiner
José Javier ÁLVARO	Lille 1 University, France ; Supervisor
Sébastien CLAUSEN	Lille 1 University, France ; Supervisor
Olivier AVERBUCH	Lille 1 University, France ; Invited
Bernard LAUMONIER	Lorraine University, France ; Invited
César WITT OLIVO	Lille 1 University, France ; Invited

UMR 8198 « Evolution, Ecologie, Paléontologie » Université Lille 1 – CNRS
UFR des Sciences de la Terre – Bâtiment SN5
Avenue Paul Langevin
59655 Villeneuve d'Ascq Cedex France

Résumé

La stratigraphie de l'Ediacarien-Ordovicien Inférieur des Pyrénées Orientales est révisée. Le découpage stratigraphique est similaire aux successions de la Montagne Noire (France) et de la Sardaigne (Italie) tenant compte de (1) l'absence de déformation cadomienne au cours de la transition Ediacarien-Cambrien, (2) la présence, comme dans la Montagne Noire septentrionale, d'un volcanisme acide proche de la limite Ediacarien-Cambrien, et (3) l'absence des corps régressifs du Guzhangien (Cambrien moyen terminal) comme au Sud-Ouest de la Sardaigne. Les analyses géochimiques du volcanisme de l'Ediacarien supérieur des Pyrénées Orientales suggèrent deux affinités distinctes, une tholéitique liée à un contexte d'extension (métabasites des Formations de Nyer et d'Olette) et une autre calco-alcaline et à dominance acide liée à l'orogénèse Cadomienne (sommet de la Formation d'Olette et Formation du Pic de la Clape). Une révision des zircons détritiques des dépôts terreneuviens de la partie nord-occidentale péri-gondwanienne (Maroc, massif Ibérique, Montagne Noire, Pyrénées et Sardaigne) reflète l'influence relative des principales sources de sédiments suivant une polarité SO-NE : les sources panafricaines et atlasiennes prédominent dans les successions les plus sud-occidentales, tandis que l'influence du craton Arabo-Nubien et du méta-craton Saharien augmente vers le NE. Cette tendance disparait ensuite, reflétant une possible homogénéisation géodynamique et des sources continentales le long de cette marge.

Mots clés. Stratigraphie, complexe volcano-sédimentaire, géochimie, datation U-Pb sur zircon, Pyrénées Orientales, Montagne Noire, Gondwana Occidentale.

Abstract

The Ediacaran-Lower Ordovician stratigraphy of the Eastern Pyrenees is updated and revised. The similar stratigraphic framework is compared with neighbouring outcrops from the Montagne Noire (France) and Sardinia (Italy), which take into account: (i) the absence of Cadomian deformation close to the Ediacaran-Cambrian boundary interval, (ii) the presence, like in the northern Montagne Noire, of acidic-dominated volcanosedimentary complexes punctuating the Ediacaran-Cambrian transition, and (iii) the lack of the Guzhangian (mid Cambrian) regression, also absent in SW Sardinia. The geochemical analyses of the uppermost Ediacaran volcanism in the Eastern Pyrenees suggest two distinct affinities linked to extensional conditions (metabasites of the Nyer and Olette formations) followed by the influence the Cadomian orogeny (acidic and calk-alkaline magmatism recorded at the top of the Olette Formation and in the overlying Pic de la Clape Formation). Detrital zircons from Terreneuvian siliciclastic sediments of West Gondwana (Morocco, Iberian Massif, Montagne Noire, Pyrenees and Sardinia) reflect a distinct SW-NE trend in the relative influence of major sediment sources: the Panafrican-Atlasian sources predominate throughout the southwesternmost successions, whereas the influence of the Arabian-Nubian Shield and the Sahara Metacraton sources increases northeastward. This trend tends to disappear afterwards, possibly reflecting a common geodynamic evolution throughout this margin.

Key-words. Stratigraphy, volcanosedimentary complex, geochemistry, U-Pb zircon dating, Eastern Pyrenees, Montagne Noire, West Gondwana.

Sommaire

1 Version Française Abrégée

1. Contexte

A la suite du plan national de cartographie géologique au 1/50 000, le Bureau de Recherches Géologiques et Minières (BRGM) a mis en place un nouveau programme national d'acquisition de données géologiques à travers le *Référentiel Géologique de France* (RGF ; Derenne, 2013). La réalisation du RGF, suite du programme de la carte géologique terminée en 2011, constitue le premier objectif du contrat Etat-BRGM 2013-2017. L'objectif du RGF est de constituer une base de données tridimensionnelle rassemblant toutes les données du sol et du sous-sol confrontées aux dernières interprétations scientifiques. Elle se présentera sous la forme d'un modèle 3D disponible sur une plate-forme numérique unifiée d'échange d'information pour l'ensemble de la communauté géologique. La gouvernance de ce chantier pluri-décennal est pour cela confiée au comité directeur assisté d'un comité scientifique où siègent 42 membres académiques (universitaires, personnels CNRS, grandes écoles). Ces derniers ont décidé de construire le RGF selon une succession de projets régionaux voués à de grands ensembles géologiques. Le premier chantier régional s'est ouvert sur les Pyrénées en 2013.

Parmi les objectifs affichés de ce chantier Pyrénées se trouve l'établissement d'un lexique hiérarchisé et d'une charte stratigraphique unifiée permettant de construire une légende générale des formations et structures. Cette légende harmonisée permettra d'unifier et de vectoriser les contours géologiques dans un SIG, pour l'ensemble du massif des Pyrénées, et la construction d'une base de données numériques structurée sur ce lexique hiérarchisé. De plus le RGF Pyrénées, sous la responsabilité de T. Baudin (BRGM), entend intégrer une quatrième dimension à sa base de données : la dimension temps, depuis la genèse des objets géologiques jusqu'aux Pyrénées actuelles. Il se propose pour cela de réaliser des cartes événementielles. Un rôle important a été donné aux campagnes de terrains afin de répondre à des questions ciblées, de tester les données existantes et de faire l'acquisition de données nouvelles. La sélection des projets financés se fait après appel à déclaration d'intérêt auprès de la communauté des géosciences (Derenne, 2013). C'est dans ce cadre que ce projet doctorale a été mis en œuvre.

2. Cadre géologique et stratigraphique préliminaire

Le massif des Pyrénées forme un axe orographique orienté Est-Ouest qui a résulté de la collision entre la microplaque ibérique et la plaque européenne durant une période allant du Crétacé Supérieur au Néogène. Cette collision s'est produite au cours de l'orogenèse alpine et traduit plus généralement la remontée de la plaque africaine vers la plaque européenne avec la fermeture de l'océan Téthys et l'ouverture de l'océan Atlantique (Roest & Srivastava, 1991 ; Barnolas et al., 1996 ; Fitzgerald et al., 1999 ; Lagabrielle et al., 2010). Le cœur de la chaîne des Pyrénées est constitué de la Zone Axiale autour de laquelle se repartissent quatre autres grandes unités morpho-structurales, qui sont la Zone Sud Pyrénéenne, l'avant-pays plissé méridional, la Zone Nord Pyrénéenne et l'avant-pays plissé septentrional (Barnolas et al., 1996 ; Fig. 1).

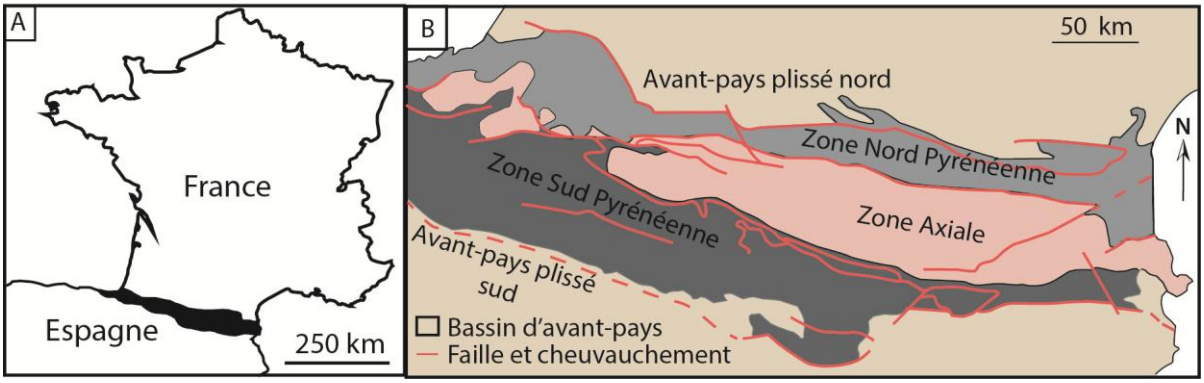

Fig. 1 : A. Localisation de la chaîne des Pyrénées. B. Grandes unités morpho-structurales du Massif des Pyrenées.

La Zone Axiale des Pyrénées est principalement composée de terrains paléozoïques affectés ou issus de l'orogenèse hercynienne et considérés comme faisant partie de l'Arc Ibéro-Armoricain (Fig. 2 ; Pouclet et al., 2016). Cet arc se compose de deux branches, l'une Sud-Ouest, l'autre Nord-Est, et sépare deux marges édiacariennes à ordoviciennes du Gondwana occidental. La branche Sud-Ouest est formée du massif ibérique. La branche Nord-Est comprend les Domaines Nord-Armoricain, Central Armoricain et Sud-Armoricain (Bretagne méridionale et Vendée), le Massif Central septentrional, le Domaine Occitan (Albigeois, Montagne Noire, Mouthoumet, Cévennes et Massif Central méridional), la Corse, la Sardaigne et les Pyrénées (Martínez-Catalán, 2012 ; Pouclet et al., 2016). Dans cette branche Nord-Est, une partie du Domaine Occitan (Montagne Noire, Mouthoumet), du Domaine Sud-Armorcain (Vendée), de la Sardaigne et des Pyrénées, est marquée par la

présence d'un événement tectono-thermique d'âge Ordovicien Moyen à l'origine d'un hiatus stratigraphique appelé discordance sarde. Cette discordance, parfois angulaire mais aussi paraconforme, met en contact les séries dites pré-sardes et les dépôts souvent conglomératiques marquant la reprise de la sédimentation à l'Ordovicien Supérieur (Casas & Fernández, 2007 ; Casas et al., 2010 ; Pouclet et al., 2016).

Quelques datations radiométriques réalisées sur des niveaux volcanoclastiques, et de rares données biostratigraphiques obtenues pour les séries pré-sardes, ont permis d'estimer une mise en place de ces dépôts depuis l'Ediacarien supérieur à l'Ordovicien Inférieur (Abad, 1988 ; Perejón et al., 1994 ; Cocherie et al., 2005 ; Castiñeiras et al., 2008 ; Casas & Palacios, 2012 ; Casas et al., 2015 ; Laumonier et al., 2015). Longtemps considérés comme représentant un socle cadomien métamorphisé des séries pré-sardes, les orthogneiss de la Zone Axiale des Pyrénées et de la Montagne Noire ont récemment été datés de l'Ordovicien (Deloule et al., 2002; Roger et al., 2004 ; Cocherie et al., 2005 ; Castiñeiras et al., 2008 ; Liesa et al., 2011 ; Martínez et al., 2011).

D'Ouest en Est, les âges radiométriques des gneiss pyrénéens sont les suivants : 472±2 Ma et 470±6 Ma au massif d'Aston-Hospitalet (Denele et al., 2004), 472±6 à 467±7 Ma dans le massif du Canigou (Cocherie et al., 2005), 477±4 à 476±5Ma dans le massif du Roc de Frausa (Cocherie et al., 2005 ; Castiñeiras et al., 2008) et 470±3 Ma dans le massif d'Albera (Liesa et al., 2011). Ce volcanisme (Floien-Dapingien) est différencié du volcanisme interstratifié dans l'Ordovicien Supérieur (étalé depuis 452±4 à 458±3 Ma) des massifs des Gavarres, des Guilleries et du Canigou (Navidad et al., 2010 ; Martínez et al., 2011). Ainsi ces orthogneiss ne sont plus interprétés comme des soubassements mais comme des plutons intrusifs dans des successions de l'Ediacarien-Ordovicien Inférieur.

La cartographie à l'échelle 1/50 000 d'une partie des Pyrénées Orientales (feuilles d'Argèles-Cerbère, Arles-su-Tech, Céret, Prades, Prats-de-Molló, Mont-Louis, Saillagouse) représente une nouvelle phase dans la reconstitution stratigraphique et géodynamique de l'Ediacarien-Ordovicien de cette marge gondwanienne (cartes géologiques au 1/50 000 éditées par le BRGM pour le territoire français ; Llac et al., 1988 ; Guitard et al., 1998 ; Autran et al., 2004 ; Baudin et al., 2008 ; Donzeau et al., 2010 ; Calvet et al., 2012 ; Laumonier et al., 2015, sous presse ; cartes géologiques au 1/50 000 éditées par l' IGME et l'ICGC pour le territoire espagnol ; Carreras et al., 1994 ; Cirés et al., 1994a,b, 1995 ; Muñoz et al., 1994). Les « séries » classiques de Canaveilles et de Jujols (Cavet, 1957) ont été révisées et sous-divisées en deux groupes par Laumonier (1988). Ce découpage

lithostratigraphique a par la suite souffert de nombreuses modifications (Laumonier et al., 1996, 2004, 2015) (Fig. 3). La réalisation des dernières cartes géologiques est basée sur le dernier découpage proposé par Laumonier et al. (2015).

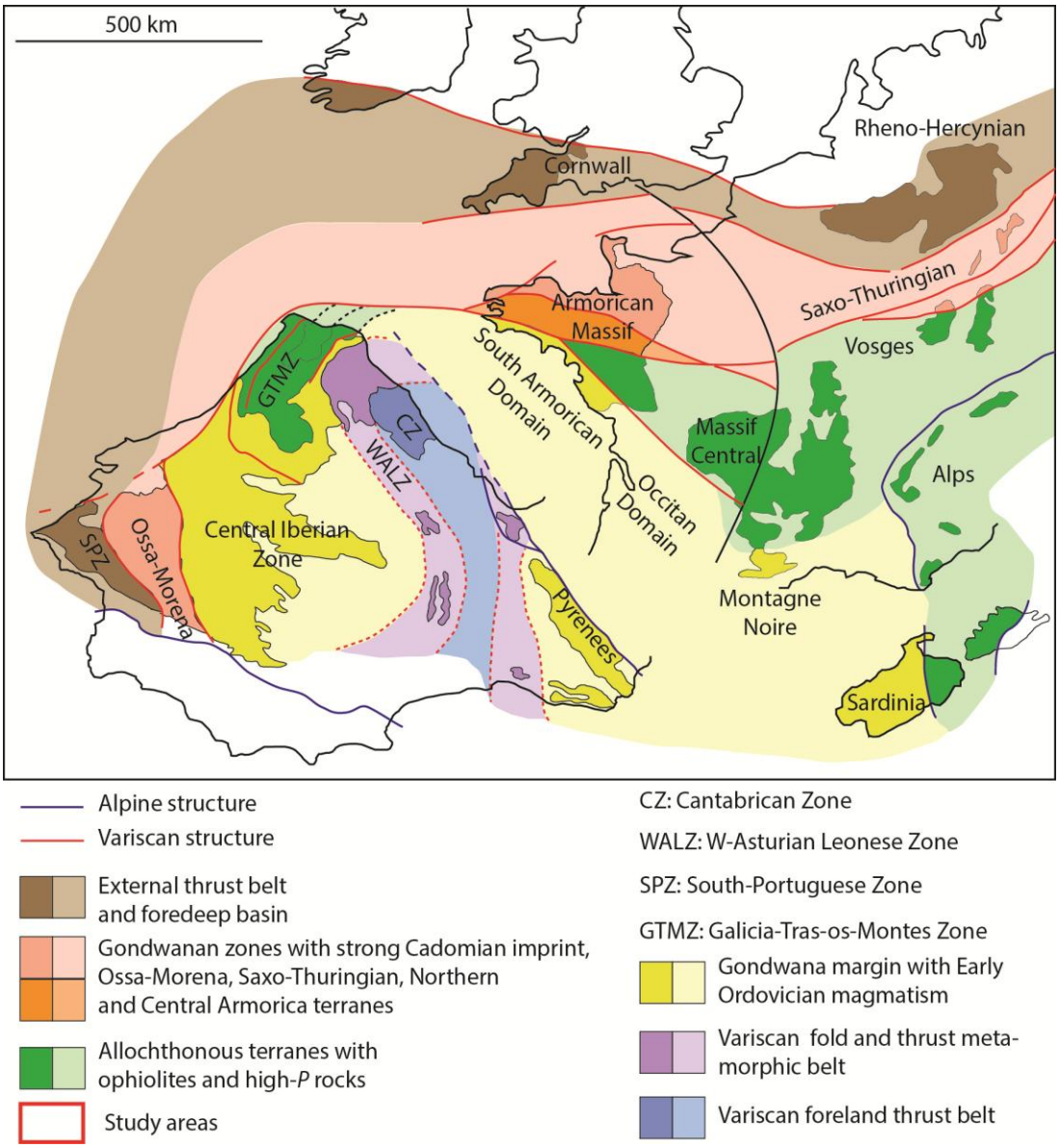

Fig. 2 : Carte de la chaîne Varisque dans l'Europe de l'ouest et représentation des différents domaines de la marge péri-gondwanienne au sein des grandes unités varisques (modifié d'après Ballèvre et al., 2009 ; Martínez-Catalán, 2012 ; Pouclet et al., 2016) ; issu de Padel et al. (submitted ; Article 4).

Dans ce découpage lithostratigraphique, Laumonier et al. (2015) a sous-divisé les deux groupes de la façon suivante (Fig. 3):

(1) Le Groupe de Canaveilles, ~ 2 km d'épaisseur, affleure dans les massif du Canigou, du Roc de France, des Albères et du Cap de Creus. Il comprend les Formations de Canaveilles et de Cabrils, composées de schistes homogènes à intercalations de marbres et de

gneiss à silicates calciques et « granulés ». Les niveaux volcano-sédimentaires ou « granulés » affleurant dans les feuilles d'Arles-sur-Tech et de Prats-de-Molló s'étalent depuis ~580 à 550 Ma (Cocherie et al., 2005 ; Castiñeiras et al., 2008). L'orthogneiss métagranitique du Mas Blanc (feuille Arles-sur-Tech), daté de ~560 Ma (Castiñeiras et al., 2008), renforce l'attribution du Groupe de Canaveilles à l'Ediacarien.

(2) Le Groupe de Jujols, ~ 3-5 km d'épaisseur, affleure du Vallespir à la Cerdagne, ponctuellement dans le massif des Albères et dans le massif des Aspres. Le groupe est sous-divisé en : (2a) Formation basale de Tregurà, « olistostromique » et carbonatée ; (2b) Formation d'Evol, composée de schistes rubanés et niveaux gréso-microconglomératiques, représentée par les formations d'Alos d'Isil et d'Alins, séparées par un niveau carbonaté associé à la Formation Lleret-Bayau ; (2c) Formation de Valcebollère, composée de marbres, calcschistes, alternances schisto-calcaires et schistes à nodules carbonatés ; et (2d) Formation de Jujols, ou schistes rubanés, parfois supprimée par la discordance sarde. L'âge du Groupe de Jujols est considéré comme Cambrien *s.l.*

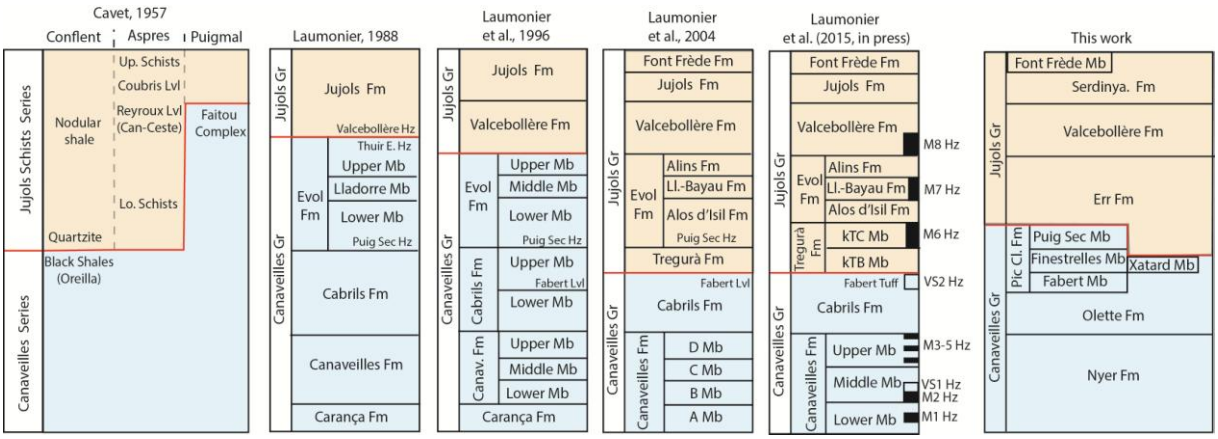

Fig. 3 : Historique de l'évolution des groupes de Canaveilles et Jujols depuis les travaux de Cavet (1957) jusqu'au découpage lithostratigraphique de Laumonier et al., (2015) ; issu de Padel et al., (in prep a ; [article 1]).

3. Objectifs

Les cibles de recherche proposées pour cette thèse de doctorat rentrent dans le cadre du chantier RGF-Pyrénées et sont:

- La révision stratigraphique des successions pré-sardes des Pyrénées Orientales.
- Son calage biostratigraphique et géochronologique.
- La corrélation lithostratigraphique avec les régions avoisinantes présentant des successions d'âge équivalent (principalement, la Montagne Noire et la Sardaigne) et la

relation paléogéographique des domaines de la marge nord-occidentale du Gondwana, depuis la Sardaigne aux Domaines Sud-Armoricain et Occitan (Montagne Noire et Mouthoumet, France), le massif ibérique et l'Anti-Atlas (Maroc).

4. Méthodologie

La mise en place d'une méthodologie pluridisciplinaire, fondée sur le travail de géologie de terrain, a été nécessaire afin de répondre aux objectifs de ce projet. Les résultats issus de ce projet, qu'ils soient acceptés (Padel et al., in press, [article 3] ; Chapitre 4), soumis (Padel et al., submitted [article 4], chapitre 5), ou en préparation (Padel et al., in prép. a, b [articles 1 et 2], chapitre 2 et 3), fondés sur les différents axes méthodologiques, sont indiqués entre parenthèses après ces derniers.

4.1 Etude de terrain

La région d'étude est principalement située dans les Pyrénées Orientales, dans les unités tectonostratigraphiques du Conflent (partie méridionale du synclinal de Villefranche), des Aspres, du Puigmal, du Vallespir et du Roc de France/Frausa. Pour une étude et une compréhension plus globale, les terrains étudiés s'étendent depuis la Cerdagne au cap de Creus, en passant par les massifs des Albères/Albera, des Aspres, de l'Agly/Aglí et du Canigou/Canigó.

Au total, 5 missions de terrain et d'échantillonnage (pour un total de 68 jours) ont été effectuées entre juin 2014 et mai 2016 afin de compléter la cartographie 1/50 000 existante par des levés de coupes stratigraphiques clés et relevés d'informations sédimentologiques pertinentes (Fig. 4). L'échantillonnage a porté sur 1) les séries carbonatées et silicoclastiques pour l'analyse des microfaciès et l'extraction des microfossiles à intérêt biostratigraphique ; et 2) les séries volcanosédimentaires et silicoclastiques pour la réalisation de datations géochronologiques et l'étude des sources sédimentaires des terrains étudiés (approche géodynamique et paléogéographique).

Les études géochronologiques ont également intégré des échantillons des séries volcanosédimentaires et silicoclastiques de la transition Ediacarien-Cambrien de la Montagne Noire prélevés et fournis par J.J. Álvaro, S. Clausen, E. Monceret et D. Vizcaïno.

Etablissement d'un nouveau cadre stratigraphique des successions étudiées (chapitre 2 [article 1]).

Sur la base des observations de terrain, de nouvelles données acquises en laboratoire et de l'analyse de l'évolution historique du découpage lithostratigraphique, la mise en œuvre du nouveau cadre stratigraphique présenté ici (Fig. 3) s'appuie sur les règles établies par la Commission Stratigraphique Internationale (ICS) et présentées dans son Guide Stratigraphique International (Salvador, 1994).

Dans les Pyrénées, les modifications successives des différentes unités lithostratigraphiques qui composent les successions pré-sardes n'ont pas toujours respectées les règles de nomenclature. De fait, la modification des limites et du contenu de ces groupes et formations n'a que rarement été suivie d'un changement de nom et du stratotype de ces dernières. L'un des apports principaux de cette thèse est donc la révision du cadre lithostratigraphique utilisé jusqu'ici pour la réalisation des cartes géologiques au 1/50 000 du BRGM. Cette révision s'inscrit dans l'un des objectifs principaux du chantier RGF-Pyrénées : la définition d'un « lexique lithostratigraphique des séries anté-ordoviciennes (pré-sardes) ». Une corrélation de ce nouveau cadre lithostratigraphique avec les successions voisines des Pyrénées et de la marge occidentale péri-gondwanienne (Montagne Noire et Sardaigne) est ensuite proposée. Celle-ci s'appuie sur les résultats des études stratigraphiques, mais aussi géochronologiques. Même si ce travail découle de l'ensemble des travaux menés au cours de ce projet, il est ici présenté en chapitre 3 [article 1], afin d'introduire la nomenclature stratigraphique appliquée dans les autres travaux [articles 2, 3 et 4].

4.2 Etude biostratigraphique

L'un des objectifs de ces travaux était de tester la potentialité biostratigraphique des niveaux carbonatés et silicoclastiques des groupes de Canaveilles et de Jujols. L'étude biostratigraphique s'est focalisée sur la recherche de taxons à fort potentiel chronostratigraphique du Cambrien-Ordovicien : les microfossiles à squelette minéralisé (« small shelly fossils », SSF) dans les intercalations carbonatées interprétées comme de l'Ediacarien-Cambrien qui apparaissent dans les formations de Canaveilles, Jujols, Tregurà et Valcebollère *sensu* Laumonier et al. (2015) ; et les palynomorphes, particulièrement les acritarches, qui ont déjà été cités dans les formations carbonatées (Valcebollère ; Laumonier et al., 2015) et silicoclastiques étudiées (Serdinya ; Casas & Palacios, 2012).

La recherche des SSF a consisté en l'attaque de la matrice calcaire par bains répétés de 24h à 48h des échantillons dans une solution d'acide acétique à 10 % suivis de tamisage des résidus à 50 µm, 125 µm, 250 µm, 500 µm, 1 mm et 2 mm et tri des différentes fractions obtenues sous loupe binoculaire avant éventuelles observations au microscope électronique à balayage. Pour chaque échantillon de carbonates passés à l'acide acétique dans le but d'extraire des microfossiles à squelette minéralisé, 3 à 6 kg de roches ont été utilisés pour un total de poids de roches traitées estimé à ~ 120 kg (sur la période de juillet 2014 à avril 2016). Sur les 26 échantillons traités, seuls 5 ont fourni des microfossiles à squelette minéralisé (Fig. 4). 4 proviennent du site dit de Terrades (Unité de Salud, Espagne), situé dans la Zone Pyrénéenne méridionale, d'où ont été décrits des bioconstructions à archéocyathes (Abad, 1988 ; Perejón et al., 1994). Les microfossiles obtenus ont fait l'objet d'une étude réalisée par E. Wallet dans le cadre d'un stage de Licence de Sciences de la Terre, des Planètes et de l'Univers à l'université de Lille (en prép.). Le cinquième échantillon, prélevé dans la Formation de Valcebollère, dans la coupe du Faitou (chapitre 2), n'a fourni que des restes de microfossiles sans intérêt biostratigraphique.

La recherche de palynomorphes s'est effectuée selon les procédés palynologiques standards, par la dissolution de la matrice calcaire et/ou silicoclastique d' échantillons de 50 g à 100 g par des attaques successives à l'acide chlorhydrique et fluorhydrique. Les résidus obtenus ont été neutralisés dans de l'eau distillée après chaque traitement. Pour chacun des 20 échantillons traités, deux fractions ont été obtenues par tamisage sur tamis de nylon de 15 µm (élimination des débris fins) et 50 µm. 4 frottis (lames palynomorphiques) des deux fractions ont été réalisés après concentration des résidus par centrifugation et examinés au microscope optique à lumière transmise. Aucune de ces 80 lames n'a révélé la présence de palynomorphes.

La présence de microrestes minéralisés dans la Formation de Valcebollère, bien que non exploitable, suggère que le manque de données paléontologiques est attribuable à la surimpression de phases de déformation et de métamorphisme (régional et de contact) liés aux cycles orogéniques hercynien et alpin. La Zone Sud Pyrénéenne (Fig. 1), d'où proviennent les seuls microfossiles à squelette minéralisé cambriens exploitables, témoigne de la différence entre les zones les plus déformées de la Zone Axiale, et les zones périphériques moins affectées. Néanmoins, la possibilité de trouver des microfossiles dans des secteurs en partie préservées de la déformation reste envisageable.

4.3 Etude géochronologique (datation U/Pb sur zircon) [articles 2, 3 et 4]

Trois méthodes de datation U/Pb sur zircon existent et peuvent être utilisées suivant que l'objectif soit : 1) de dater la roche ; 2) de comprendre les différents événements géologiques enregistrés par celle-ci ; ou 3) de déterminer, dans le cas de roches détritiques, l'âge des sources qui ont alimenté les sédiments. La méthode TIMS (« Thermal Ionization Mass Spectrometry »), dite conventionnelle, est basée sur la dissolution chimique du zircon avant analyse (Gehrels 2014). Si cette méthode est la plus précise à ce jour, elle peut cependant induire un âge erroné si le zircon étudié, s'il présente une histoire complexe (e.g. cœur hérité plus vieux que la bordure du minéral).

Les deux autres méthodes, SIMS (« Sensitive High-Resolution Ion Microprobe ») et LA-ICPMS (« Laser Ablation–Inductively Coupled Plasma–Mass Spectrometry ») permettent quant à elles de palier à ces inconvénients en effectuant une analyse dite *in situ* sur une zone choisie du minéral (Gehrels 2014). L'avantage de cette technique d'analyse localisée est qu'elle offre la possibilité de dater le ou les événements géologiques enregistrés par le zircon. La méthode LA-ICPMS est moins précise que la méthode SIMS, mais permet d'effectuer un plus grand nombre de mesures dans un temps donné. L'objectif est ici à la fois de dater les roches volcanoclastiques et d'étudier la source sédimentaire des roches détritiques. Pour des résultats robustes, il est nécessaire d'étudier environ 30 à 50 zircons par échantillon de roche volcanoclastique (Bowring et al. 2006), et plus 100 zircons par échantillon de roche silicoclastique afin de s'assurer de la représentation de l'ensemble des sources du dépôt (Andersen, 2005). C'est donc la méthode LA-ICPMS qui a été choisie. Les datations ont été réalisées à l'Université de Rennes 1 dans le laboratoire Géosciences Rennes (UMR 6118), sur un appareil ICP-MS Agilent 7700x couplé à un laser ESI Excimer (NWR193UC). La méthode de datation propre à cette technique est détaillée dans le chapitre 5 [article 3]. Au total, 1345 analyses de zircons ont été effectuées, dont 981 ont pu être exploitées dans le temps imparti à ce projet.

Unités tectono-stratigraphiques	Coupes	Groupes	Formations	Biostratigraphie		U-Pb Zircon	Missions
				"SSF"	Palyno.		
Puigmal	Vacebollère	J	Valcebollère	1/4	0/3	/	M1; M2; M3
	Tregurà	C	Pic de la Calpe	0/5	0/1	/	M1; M2; M3; M5
	Roques Blanquès	J	Valcebollère	0/2	/	/	M2; M5
	Finestrelles	C/J	Pic de la Clape / Err	0/2	0/1	1/1	M2; M3
	Espinavelle	C	Nyer	/	0/1	/	M1
	Queralbs	J	Valcebollère / Err	0/3	0/1	/	M2; M4; M5
	Pic de la Clape	C	Pic de la Clape / Err	/	0/2	2/2	M1; M2; M4; M5
	Fabert-Molló	C	Pic de la Clape / Err	/	0/2	1/1	M1; M2; M4; M5
	Gironella	J	Valcebollère	0/1	/	/	M3
	Molina	J	Serdinya	/	0/1	/	M2
	Saillagouse	J	Err	/	0/1	/	M2
Conflent	Jujols	J	Serdinya	/	0/2	/	M1; M5
	Thuir d'Evol	J	Valcebollère / Err	0/2	0/1	/	M1
Aspres	Montauriol	J	Serdinya	/	0/1	1/1	M1; M3; M5
	Xatard	C	Olette	/	0/1	/	M1; M5
	St Colombe	J	Valcebollère	0/1	0/1	/	M1; M5
Pallaresa	Alos d'Isil	J?	Alos d'Isil	/	/	(1)	M3; M4
	Alins	J?	Alins	/	(1)	(1)	M3; M4
	Lleret/Boldis	J?	Lleret-Bayau	0/2	/	/	M3; M4
Albères	Cap Cerbère	C	Pic de la Clape / Err	/	/	1/1	M3
	Cap de Creus	C	Montjoi	/	/	(1)	M3
Salud	Terrades	J	Terrades	4/4	/	/	M1

X/X: nombre d'échantillons ayant fournis des résultats / nombre d'échantillons traités (en vert, résultats exploitables, en rouge, résultats non exploitables). (X) : échantillons disponibles, non analysés à ce jour.

Fig. 4 : Aperçu des travaux menés au cours de la thèse après la première mission de terrain M1 en juin 2014. Missions : M1, juin 2014 (9 jours) ; M2, août 2014 (9 jours) ; M3, mai-juillet 2015 (33 jours) ; M4, août 2015 (7 jours) ; M5, mai 2016 (10 jours). C : Canaveilles ; J : Jujols.

Etude U-Pb des zircons volcanosédimentaires : datation des complexes volcanosédimentaires de la transition Ediacarien-Cambrien en Montagne Noire et aux Pyrénées [articles 2-3]

La partie supérieure du Groupe de Canaveilles est caractérisée par la présence d'un complexe volcanosédimentaire. Les différentes datations U-Pb disponibles dans la littérature (Cocherie et al., 2005 ; Castiñeiras et al., 2008 ; Casas et al., 2015) ont été révisées et comparées à celles acquises durant cette thèse. L'analyse de la géochimie des niveaux volcaniques (basiques et acides) et l'étude des faciès qui composent ce complexe apportent une réponse quant à son mode de mise en place.

Un complexe volcanosédimentaire similaire a été décrit dans le flanc nord de la Montagne Noire (France ; Álvaro et al., 2014), pour lequel aucune datation n'avait été effectuée. Les datations radiométriques des niveaux volcanoclastiques effectuées ici ont donc eu pour but d'obtenir un contrôle de l'âge de ces successions pré-sardes des Pyrénées

Orientales [article 2] et de la Montagne Noire septentrionale [article 3], notamment de mieux contraindre la limite Ediacarien-Cambrien dans les niveaux analysés et de discuter l'origine de cette activité magmatique décrite le long de la marge occidentale péri-gondwanienne.

Etude U-Pb des zircons détritiques : analyse des sources sédimentaires des successions cambro-ordoviciennes, et paléoposition relative des plates-formes et/ou bassins de la marge occidentale péri-gondwanienne **[articles 3-4]**

La paléoposition des Pyrenées le long de la marge occidentale péri-gondwanienne reste énigmatique. Ainsi, ces dernières sont la plupart du temps ignorées dans les tentatives de reconstitution paléogéographique (Murphy et al., 2004 ; Nance et al., 2008 ; voir cependant hypothèses dans Von Raumer et al., 2003 ; Pouclet et al., 2016).

Or, l'analyse de zircons détritiques permet non seulement d'identifier les potentielles sources qui alimentent un influx sédimentaire, mais également de comparer les sources de différentes plates-formes le long d'une marge et donc d'en proposer une paléoposition relative.

Ainsi, plusieurs échantillons cambriens à ordoviciens du Groupe de Jujols (Pyrénées), et de certaines formations d'âges supposés équivalents de la Montagne Noire, ont été analysés et comparés à des données déjà publiées sur la Sardaigne, l'Anti-Atlas (Maroc) et les Zones d'Ossa-Morena et Centrale en Espagne.

Un test K-S (Kolmogorov-Smirnov) puis une analyse de diagramme CA-DA (Age de Cristallisation – Age de Dépôt ; Cawood et al., 2012) ont ainsi été utilisés pour comparer les sources et essayer d'illustrer l'évolution géodynamique de cette marge gondwanienne.

5. Synthèse des principaux résultats

5.1 Nouveau découpage lithostratigraphique

Sur la base des travaux antérieurs (cartographiques, litho- et biostratigraphiques et géochronologiques), et grâce aux nouvelles données acquises, le nouveau cadre stratigraphique a permis de redéfinir les groupes de Canaveilles et de Jujols. Le Groupe de Canaveilles, de la base au sommet, se compose des formations de Nyer, d'Olette et du Pic de la Clape. A la base du groupe, l'ancienne Formation de Canaveilles est remplacée par la nouvelle Formation de Nyer. Si le nom et le stratotype de cette formation sont nouvellement

introduits pour respecter les règles établies par la Commission Stratigraphique Internationale (ICS), son contenu et ses limites restent tels que définis au préalable. La nouvelle Formation d'Olette est essentiellement silicoclastique, tandis que la nouvelle Formation du Pic de la Clape est composée d'un complexe volcanosédimentaire représenté par les Membres de Fabert (métaryolites), de Finestrelles (appareils volcano-sédimentaires à dominance acide) et du Puig Sec (carbonates péritidaux). Au dessus, le Groupe de Jujols présente, de la base au sommet, les formations d'Err, de Vacebollère et de Serdinya. Les formations d'Err et de Serdinya sont composées de dépôts silicoclastiques, séparés par les carbonates et les alternances schisto-carbonatées de la Formation de Vacebollère.

5.2 Corrélation stratigraphique régionale

Faisant partie de la même branche de l'Arc Varisque Ibero-Armoricain, l'Ediacarien-Ordovicien Inférieur de la Montagne Noire, les Pyrénées Orientales et la Sardaigne partagent de nombreuses affinités stratigraphiques. Ces trois domaines partagent les caractéristiques suivantes : (1) l'absence de déformation cadomienne proche de la limite Ediacarien-Cambrien ; (2) la présence dans la Montagne Noire septentrionale et dans les Pyrénées Orientales d'un volcanisme acide et explosive ponctuant la transition Ediacarien-Cambrien ; (3) la mise en place dans ces deux mêmes domaines d'une productivité carbonatée qui marque la base du Cambrien, absente dans des domaines affectés par la déformation cadomienne et par des apports terrigènes significatives ; et (4) de l'absence de la régression qui marque le Cambrien moyen terminal (Guzhangien) dans la Montagne Noire (Formation de Ferrals), suggérant l'érosion des paléo-reliefs significatifs dans la source continentale qui nourrissait les bassins des Pyrénées Orientales et de la Sardaigne sud-occidentale.

La conservation exceptionnelle des monticules récifales à calcimicrobes et archéocyathes dans l'écaille alpine de Terrades, qui n'ont pas subi ni la déformation ni le métamorphisme caractéristique de la Zone Axiale des Pyrénées Orientales, permet de discuter le caractère allochtone de certains chevauchements alpins. L'assemblage des archéocyathes de cette Formation de Terrades comprend de nombreux genres communs avec la Sardaigne (formations de Matoppa et de Punta Manna) et, en moindre proportion, avec la Montagne Noire (formations de Pardailhan et de Lastours). Cet affleurement représente *a priori* une partie allochtone au bassin cambrien des Pyrénées, dont la provenance pourrait être mise en relation avec des déplacements alpins depuis des positions plus septentrionales appartenant au Domaine Occitan et à sa prolongation orientale sarde.

5.3 Datation des complexes volcanosédimentaires

Les datations U-Pb sur zircon effectuées conjointement sur les métarhyolites et les dépôts volcano-sédimentaires de la transition Ediacarien-Cambrien des Pyrénées Orientales (Formation du Pic de la Clape) et de la Montagne Noire (Formation de Rivernous) ont permis de contraindre géochronologiquement l'enregistrement des épisodes volcaniques cadomiens dans ce secteur péri-gondwanien.

La datation de zircon à partir de la méthode d'ablation laser (LA−ICP−MS) a permis de préciser les âges de dépôt de la métarhyolithe appartenant au Membre de Fabert (Formation Pic de la Clape) et de brèches volcanoclastiques et de grès tuffacés appartenant au Membre Fabert (Formation du Pic de la Clape), ainsi que la révision de 5 des datations radiométriques publiés depuis 2005. Cette révision géochronologique a permis de reconnaitre trois complexes volcano-sédimentaires au sein des Membres de Fabert et de Finestrelles respectivement datés à ca. 577-558 Ma, ca. 559−554 Ma et ca. 542−532 Ma.

5.4 Analyse géochimique des épisodes volcaniques

L'analyse géochimique des différents niveaux volcanogéniques (basiques et acides) interstratifiés dans le Groupe de Canaveilles suggère la succession de deux types de magmatisme : l'un tholéitique à dominance basaltique (Formation de Nyer et partie inférieure de la Formation d'Olette) lié à des conditions extensives, suivi d'un magmatisme à dominance acide et calco-alcalin, identifié au sommet de la Formation d'Olette et au sein des Membres de Fabert et de Finestrelles (Formation du Pic de la Clape), mis en relation avec l'orogénèse cadomienne.

5.5 Etude des zircons détritiques du Cambro-Ordovicien de la marge occidentale péri-gondwanienne

La méthode employée pour étudier les sources sédimentaires et la paléoposition relative des différents bassins de la marge occidentale péri-gondwanienne est basée sur l'analyse des zircons détritiques des dépôts silicoclastiques. Cette approche permet à la fois de déterminer leur âge géochronologique, de déduire leur sources continentales, de situer leur paléo-position relative (en fonction des modifications des populations des sources continentales) et, par comparaison avec l'affinité géochimique des épisodes volcaniques, de leur situer dans un contexte géodynamique.

Les résultats obtenus montrent, au Terreneuvien, une polarisation Est-Ouest de la marge occidentale péri-gondwanienne. Cette marge (actuellement « pliée » par l'Arc Varisque

Ibéro-Armoricain) est subdivisée en (1) marge sud-occidentale, représentée par les Rifts de l'Atlas (Maroc) et d'Ossa-Morena (Espagne) qui occupent une position marginale (distale) du continent, séparées de ce dernier par le bassin ibérique composé, actuellement, par les Zones (Varisques) Centro-Ibérique, Astur-Occidental Léonaise et Cantabrique ; et (2) marge nord-orientale composée des Domaines marginales Armoricain Septentrionale et Centrale et des Domaines internes Sud-Armoricain, Occitan (prolongé vers la Corse et la Sardaigne) et Pyrénéen. La polarisation qui caractérise la population des zircons hérités est particulièrement marquée par l'augmentation progressive vers l'Est des zircons appartenant à l'intervalle ca. 1.2-0.9 Ga, liée à l'influence de sources du craton Arabo-Nubien et du méta-craton Saharien.

Au cours du Cambrien, et jusqu'à l'Ordovicien Inférieur, cette tendance s'atténue et l'apport sédimentaire semble s'homogénéiser. Ceci se traduise par une distribution plus équilibrée des populations chronologiques des zircons. Cette évolution reflèterait : (1) l'érosion des reliefs cadomiens et panafricains, (2) un changement du contexte géodynamique depuis un système orogénique (cadomien et panafricain) vers un régime extensif, de type rift au Cambrien et drift (marge passive) à l'Ordovicien Inférieur.

La modification SO-NE le long de la marge occidentale péri-gondwanienne des populations des zircons permet de suggérer une hypothèse quant à la paléoposition relative des Pyrénées. La superposition des orogénèses Varisque et Alpine ne permet pas de situer ces trois bassins, mais la proportion des âges de zircon compris dans l'intervalle 1.2-0.9 Ga suggère une position du Bassin Pyrénéen intermédiaire entre les Bassins de la Montagne Noire et de la Sardaigne (Fig. 5).

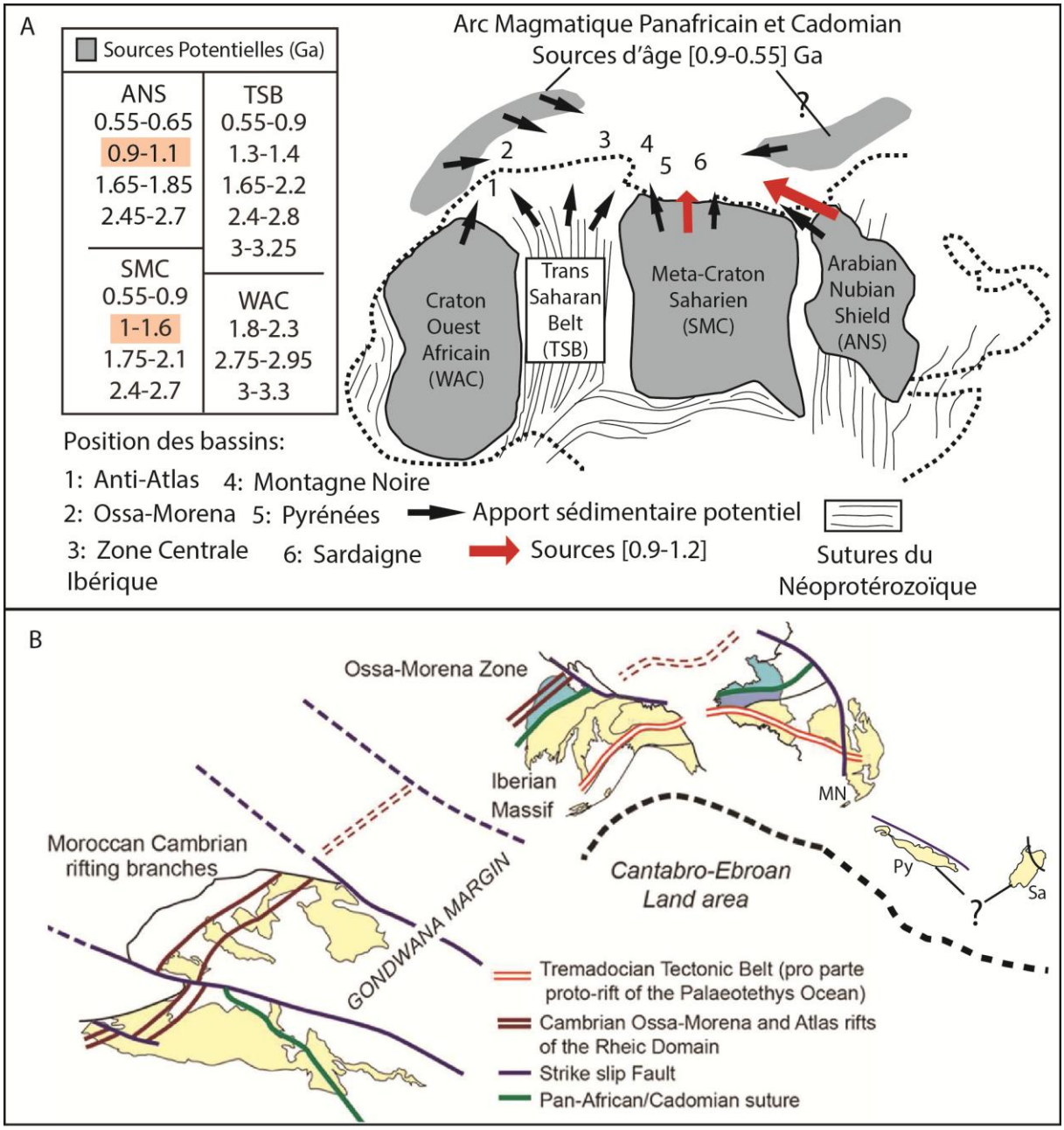

Fig. 5. Proposition de paléoposition relative des différents domaines analysés de la marge périgondwanienne. A. Au cours du Cambrien inférieur (Terreneuvien), d'après l'analyse des zircons détritiques de l'intervalle 1.2-0.9 Ga. B. Proposition de reconstitution paléogéographique de la marge occidentale péri-gondwanienne, replaçant les principales sutures et structures cambriennes ; modifiée d'après le modèle de Pouclet et al. (2016) pour localiser les Pyrénées et la Sardaigne par rapport à la Montagne Noire.

6. Références

Abad, A., 1988. El Cámbrico inferior de Terrades (Gerona). Estratigrafía, facies y paleontología. Batallería 2, 47–56.

Álvaro, J.J., Bauluz, B., Clausen, S., Devaere, L., Imaz, A.G., Monceret, E., Vizcaïno, D., 2014. Stratigraphy of the Cambrian-Lower Ordovician volcanosedimentary complexes in the northern Montagne Noire, France. Stratigraphy 11, 83–96.

Andersen, T., 2005. Detrital zircons as tracers of sedimentary provenance: limiting conditions from statistics and numerical simulation. Chem. Geol. 216, 249-270.

Autran, A., Calvet, M., Delmas, M., 2004. Carte géologique de la France (1/50 000), feuille Mont-Louis (1094). BRGM, Orléans.

Ballèvre, M., Bosse, V., Ducassou, C., Pitra, P., 2009. Palaeozoic history of the Armorican Massif: Models for the tectonic evolution of the suture zones. C. R. Geosci. 341, 174–201.

Casas, J.M., Fernández, O., 2007. On the Upper Ordovician unconformity in the Pyrenees: New evidence from the La Cerdanya area. Geol. Acta 5, 193–198.

Barnolas, A., Chiron, J.C., 1996. Synthèse géologique et géophysique des Pyrénées. Tome 1: Cycle hercynien. BRGM-ITGE, Orléans-Madrid, 729 p.

Baudin, T., Autran, A., Guitard, G., Laumonier, B., 2008. Carte géologique de la France (1/50 000), feuille Arles-Sur-Tech (1100). BRGM, Orléans.

Bowring, S.A., Schoene, B., Crowley, J.L., Ramezani, J., Conon, D.J., 2006. High-precision U-Pb zircon geochronology and the stratigraphic record: progress and promise. Geochronology: Emerging Opportunities, Paleontological Society Short Course. Paleontol. Soc. Pap. 11, 23-43.

Calvet, M., Autran, A., Wiazemsky, M., Laumonier, B., Guitard, G., 2012. Carte géol. France (1/50 000), feuille Argelès-sur-Mer – Cerbère (1097-1101). Orléans: BRGM.

Carreras, J., Losantos, M., Palau, J., Escuer, J., 1994. Memoria explicativa del mapa geológico de España a escala 1:50.000, hoja de Roses (nº259). ITGE, Madrid.

Casas, J.M., Fernández, O., 2007. On the Upper Ordovician unconformity in the Pyrenees: New evidence from the La Cerdanya area. Geol. Acta 5, 193–198.

Casas, J.M., Castiñeiras, P., Navidad, M., Liesa, M., Carreras, J., 2010. New insights into the Late Ordovician magmatism in the Eastern Pyrenees: U–Pb SHRIMP zircon data from the Canigó massif. Gondwana Res. 17, 317–324.

Casas, J.M., Palacios, T., 2012. First biostratigraphical constraints on the pre-Upper Ordovician sequences of the Pyrenees based on organic-walled microfossils. C. R. Geosci. 344, 50–56.

Casas, J. M., Navidad, M., Castiñeiras, P., Liesa, M., Aguilar, C., Carreras, J., Hofman, M., Gärtner, A., & Linnemann, U., 2015. The Late Neoproterozoic magmatism in the Ediacaran series of the Eastern Pyrenees: new ages and isotope geochemistry. Int. J. Earth Sci. 104, 909–925.

Castiñeiras, P., Navidad, M., Liesa, M., Carreras, J., Casas, J.M., 2008. U-Pb zircon ages (SHRIMP) for Cadomian and Lower Ordovician magmatism in the Eastern Pyrenees: new insights in the pre-Variscan evolution of the northern Gondwana margin. Tectonophysics 461, 228-239.

Cavet, P., 1957. Le Paléozoïque de la zone axiale des Pyrénées orientales françaises entre le Roussillon et l'Andorre. Bull. Ser. Carte géol. Fr. 55, 303–518.

Cawood, P.A., Hawkesworth, C.J., Dhuime, B., 2012. Detrital zircon record and tectonic setting. Geology 40, 875–878.

Cirés, J., Domingo, F., Roca, E., Ecuer, J., Sanz, J., 1994a. Memoria explicativa del mapa geológico de España a escala 1:50.000, hoja de Puigcerda (n°217). ITGE, Madrid.

Cirés, J., Morales, V., Liesa, M., Carreras, J., Escuer, J., Pujadas, J., 1994b. Memoria explicativa del mapa geológico de España a escala 1:50.000, hoja de La Jonquera (n°217). ITGE, Madrid.

Cirés, J., Casas, J.M., Muñoz, J.A., Fleta, J., Barbera, M., 1995. Memoria explicativa del mapa geológico de España a escala 1:50.000, hoja de Molló (n°218). ITGE, Madrid.

Cocherie, A., Baudin, T., Autran, A., Guerrot, C., Fanning, M., Laumonier, B., 2005. U-Pb zircon (ID-TIMS and SHRIMP) evidence for the early Ordovician intrusion of metagranites in the late Proterozoic Canaveilles Group of the Pyrenees and the Montagne Noire (France). Bull. Soc. géol. Fr. 176, 269-282.

Deloule, E., Alexandrov, P., Cheilletz, A., Laumonier, B., Barbey, P., 2002. In situ U–Pb zircon ages for Early Ordovician magmatism in the eastern Pyrenees, France: The Canigou orthogneisses. Int. J. Earth Sci. 91, 398–405.

Denele, Y., Barbey, P., Deloule, E., Pelleter, E., Olivier, Ph., Gleizes, G. 2004. Middle Ordovician U-Pb age of the Aston and Hospitalet orthogneissic laccoliths: their role in the evolution of the Pyrenees. Bull. Soc. géol. France 180, 209-216.

Derenne, J.L., 2013. Le référentiel Géologique de la France. La carte géologique entre dans la troisième dimension. Georama 28, 2-8.

Donzeau, M., Laumonier, B., Guitard, G., Autran, A., Llac, F., Baudin, T., Calvet, M., 2010. Carte géologique de la France (1/50 000), feuille Céret (1096). BRGM, Orléans.

Fitzgerald, P.G., Muñoz, J.A., Coney, P.J., Baldwin, S.L., 1999. Asymmetric exhumation across the Pyrenean orogen: implications for the tectonic evolution of a collisional orogen. Earth Planet. Sc. Lett. 173, 157–170.

Gehrels, G., 2014. Detrital zircon U-Pb geochronology applied to tectonics. Annu. Rev. Earth Planet. Sci. 42, 127-149.

Guitard, G., Laumonier, B., Autran, A., Bandet, Y., Berger, G.M., 1998. Notice explicative, Carte géologique de la France (1:50.000), feuille Prades (1095). BRGM, Orléans.

Lagabrielle, Y., Labaume, P., Saint-Blanquat, M., 2010. Mantle exhumation, crustal denudation and gravity tectonics during Cretaceous rifting in the Pyrenean realm (SW Europe): insights from the geological setting of the lherzolite bodies. Tectonics 29, 1–26.

Laumonier, B., 1988. Les groupes de Canaveilles et de Jujols (‘‘Paléozoïque inférieur’’) des Pyrénées orientales – arguments en faveur de l’âge essentiellement Cambrien de ces séries. Hercynica 4, 25–38.

Laumonier, B., Abad, A., Alonso, J.L., Baudelot, S., Bessière, G., Besson, M., Bouquet, C., Bourrouilh, R., Brula, P., Carreras, J., Centène, A., Courjault-Radé, R., Courtessole, R., Fauconnier, D., García-Sansegundo, Guitard, G., Moreno-Eiris, E., Perejón, A., Vizcaïno, D., 1996. Cambro–Ordovicien. In: Synthèse géologique et géophysique des Pyrénées. Edition BRGM-ITGE, 1, 157-209.

Laumonier B., Autran, A., Barbey, P., Cheilletz, A., Baudin, T., Cocherie, A., Guerrot, C., 2004. Conséquences de l’absence de socle cadomien sur l’âge et la signification des séries pré-varisques (anté–Ordovicien supérieur) du sud de la France (Pyrénées, Montagne Noire). Bull. Soc. géol. France 175, 105–117.

Laumonier, B., Calvet, M., Wiazemsky, M., Barbey, P., Marignac, C., Lambert, J., Lenoble, J.L., 2015. Notice explicative Carte géologique de la France (1/50.000), feuille Céret (1096). Orléans, BRGM.

Laumonier, B., Le Bayon, B., Calvet, M., in press. Carte géologique de la France (1/50 000), feuille Prats-de-Mollo (1099). BRGM, Orléans.

Liesa, M., Carreras, J., Castiñeiras, P., Casas, J.M., Navidad, M., Vila, M., 2011. U-Pb zircon of Ordovician magmatism in the Albera Massif (Eastern Pyrenees). Geol. Acta 9, 93–101.

Llac, F., Autran, A., Guitard, g., Robert, J.F., Gourinard, Y., Santanach, P., 1988. Carte géologique de la France (1/50 000), feuille Saillagouse (1098). BRGM, Orléans.

Martínez-Catalán, 2012. The Central Iberian arc, an orocline centered in the Iberian Massif and some implications for the Variscan belt. Int J Earth Sci. 101, 1299–1314.

Martínez, F.J., Iriondo, A., Dietsch, C., Aleinikoff, J.N., Peucat, J.J., Cirès, J., Reche, J., Capdevila, R., 2011. U-Pb SHRIMP-RG zircon ages and Nd signature of Lower Paleozoic rifting-related magmatism in the Variscan basement of the Eastern Pyrenees. Lithos 127, 10–23.

Murphy, J.B., Pisarvesky, S.A., Nance, R.D., Keppie, J.D., 2004. Neoproterozoic–Early Paleozoic evolution of peri-Gondwana terranes: implications for Laurentia-Gondwana connections. Int. J. Earth Sci. 93, 659-682.

Muñoz, J.A., Vergés, J., Martínez-Ríus, A., Fleta, J., Pujadas, J., Tosquella, J., Samsó, J.M., Sanz, J., Saula, E., Mató, E., Barberà, M., 1994. Memoria explicativa del mapa geológico de España a escala 1:50.000, hoja de Ripoll (n°256). ITGE, Madrid.

Nance, R.D., Murphy, J.B., Strachan, R.B., Keppie, J.D., Gutiérrez-Alonso, G., Fernández-Suárez, J., Quesada, C., Linnemann, U., D'lemos, R., Pisarevsky, S.A., 2008. Neoproterozoic–early Palaeozoic Tectonostratigraphy and palaeogeography of the peri-Gondwanan terranes: Amazonian v. West African connections. From Ennih, N., Liégeois, J.-P., (eds), The Boundaries of the West African Craton. Geol. Soc. London Spec. Publ. 297, 345–383.

Navidad, M., Casas, J.M., Castiñeiras, P., Barnolas, A, Fernández-Suárez, J., Liesa, M., Carreras, J. & Gil-Peña, I. 2010. Geochemical characterization and isotopic age of the Caradocian magmatism from North-Eastern Iberian Peninsula: Insights from the Late Ordovician evolution of the northern Gondwana margin. Gondwana Res. 17, 325-337.

Padel, M., Álvaro, J.J., Clausen, S., Guillot, F., Poujol, M., Chichorro, M., Monceret, E., Pereira, M.F., Vizcaïno, D., in press [article 3]. U-Pb laser ablation ICP-MS zircon dating across the Ediacaran–Cambrian transition of the Montagne Noire, southern France. C. R. Geosci.

Padel, M., Clausen, S., Poujol, M., Álvaro, J.J., submitted [article 4]. Cambrian-Lower Ordovician sedimentary provenance shifts in Northwest Gondwana. Gondwana Res.

Padel, M., Clausen, S., Álvaro, J.J., Laumonier, B., in prep a [article 1]. Stratigraphic review of the Ediacaran-Lower Ordovician (pre-Sardic) volcanosedimentary framework in the Eastern Pyrenees, France and Spain.

Padel, M., Álvaro, J.J., Sánchez-García, T., Clausen, S., Poujol, M., Laumonier, B., Guillot, F., in prep b [article 2]. Cadomian volcanosedimentary complexes across the Ediacaran-Cambrian transition of the Eastern Pyrenees, France and Spain.

Perejón, A., Moreno-Eiris, E., Abad, A., 1994. Montículos de arqueociatos y calcimicrobios del Cámbrico inferior de Terrades, Gerona (Pirineo oriental, España). – Bol. R. Soc. Esp. Nat. (Sec. Geol.) 89, 55-95.

Pouclet, A., Álvaro, J.J., Bardintzeff, J.-M., Gil Imaz, A, Monceret, E., Vizcaïno, D. (2016). Cambrian–Early Ordovician volcanism across the South Armorican and Occitan Domains of the Variscan Belt in France: Continental break-up and rifting of the northern Gondwana margin. Geosci. Frontiers, doi: 10.1016/j.gsf.2016.03.002.

Roest, W.R., Srivastava, S.P., 1991. Kinematics of the plate boundaries between Eurasia, Iberia and Africa in the North Atlantic from the late Cretaceous to the present. Geology 19, 613–616.

Roger, F., Respault, J.P., Brunel, M., Matte, P., Paquette, J.L., 2004. Première datation U- Pb des orthogneiss œillés de la zone axiale de la Montagne Noire (Sud du Massif-Central) : nouveaux témoins du magmatisme ordovicien dans la chaine varisque. C. R. Geosci. 336, 19-28.

Salvador, A., 1994. International stratigraphic guide, 2nd. edition. Boulder, CO: Geological Society of America, 214 pp.

Von Raumer, J.F., Stampfi, G.M., Bussy, F., 2003. Gondwana-derived microcontinents — the constituents of the Variscan and Alpine collisional orogens. Tectonophysics 365, 7 –22.

2 Révision stratigraphique des séries volcanosédimentaires de l'Ediacarien-Ordovicien Inférieur (pré-sarde) des Pyrénées Orientales, France et Espagne [Article 1]

Stratigraphic review of the Ediacaran-Lower Ordovician (pre-Sardic) volcanosedimentary framework in the Eastern Pyrenees, France and Spain

Maxime Padel[1]*, Sébastien Clausen[1], J. Javier Álvaro[2] and Bernard Laumonier [3]

[1]UMR 8198 EEP CNRS, Université de Lille 1, Bâtiment SN5, Avenue Paul Langevin, 59655 Villeneuve d'Ascq Cedex, France, maxime.padel@etudiant.univ-lille1.fr and sebastien.clausen@univ-lille1.fr
[2]Instituto de Geociencias (CSIC-UCM), Novais 12, 28040 Madrid, Spain, jj.alvaro@csic.es
[3]Université de Lorraine, GeoRessources, École des Mines, CS 14234, F-54042 Nancy Cedex, France ; bernard.laumonier@univ-lorraine.fr
100 avenue du Général Leclerc, 54000 Nancy, France ; blaumonier@wanadoo.fr

* Corresponding author

Abstract

The Ediacaran-Lower Ordovician stratigraphy of the volcanosedimentary successions exposed in the Eastern Pyrenees is updated and revised here. The review is based on recent U-Pb zircon radiometric ages, intertonguing relationships of carbonate-dominated strata and onlapping patterns marking the top of volcanosedimentary complexes. A comparison with neighbouring pre-Variscan outcrops from the Montagne Noire (Occitan Domain, France) and Sardinia (Italy) is made. A similar stratigraphic evolution with these areas is related to: (i) the absence of Cadomian deformation close to the Ediacaran-Cambrian boundary interval, (ii) the presence of an episodic, Cadomian-related, acidic-dominated volcanism and carbonate production punctuating the Ediacaran-Cambrian transition, like in the northern Montagne Noire; and (iii) the lack of Guzhangian (late Cambrian Epoch 3) regressive shoal complexes, like in SW Sardinia.

1. Introduction

The Pyrenean massif is an intracontinental fold and thrust belt that mostly resulted from the convergence between the Iberian and European plates during the Alpine orogenesis (Roest an Srivastava, 1991; Barnolas and Chiron, 1996; Fitzgerald et al., 1999; Lagabrielle et

al., 2010). The Axial Zone of the Pyrenees belongs to the NE branch of the Variscan Ibero-Armorican Arc (Barnolas and Chiron, 1996; Pouclet et al., 2016) and, as other neighbouring Palaeozoic massifs (such as Sardinia and the Montagne Noire), has recorded the Sardic Phase (Santanach, 1972; Casas and Fernández, 2007; Álvaro et al., 2015).

Pre-Sardic (Ediacaran-Lower Ordovician) successions are affected by the intrusion of numerous Sardic and Variscan plutons and the imprint of regional and contact metamorphic conditions. The onset of the these orogeneses resulted in a complex tectonic structure, which can be subdivided into numerous tectonostratigraphic units including major orthogneissic, metagranite intrusions located at the core of the so-called metamorphic dome (Zwart, 1986; Soliva et al., 1989; Vissers, 1992; Carreras and Capella, 1994; Laumonier and Autran, 2001; Denèle et al., 2009; Mezger, 2009; Laumonier et al., 2010; García-Sansegundo et al., 2011; Olivier et al., 2016; Cochelin et al., in press). The interplay of high deformation and metamorphic patterns partly explains the almost complete lack of valuable biostratigraphically significant fossils in the Ediacaran-Lower Ordovician succession of the Pyrenean Axial Zone (Cochio, 1981).

The Variscan granite of Mont-Louis, can be used to mark the boundary between the Central and Eastern Pyrenees (Figs. 1-2). The first pioneer studies on the pre-Variscan considered the orthogneissic dome of the Canigou massif as a Precambrian basement covered by a Cambro-Ordovician succession that started with a characteristic marble marker bed. Roussel (1893, 1904) was the first to attribute a Precambrian-Cambrian age to these marbles bordering the Canigou orthogneiss (“marbre de base” *sensu* Guitard, 1970; Laumonier and Guitard, 1986; Laumonier et al., 1996; Barbey et al., 2001). The geochronological reappraisal of the pre-Variscan intrusions, including the Canigou massif, as Ordovician drastically changed former stratigraphic interpretations (see e.g. Deloule et al., 2002; Cocherie et al., 2005; Martínez et al., 2011). Current models describe a complete Ediacarian-Lower Ordovician succession, later intruded by Sardic and Variscan plutons (Barbey et al., 2001; Laumonier et al., 2004; Martínez et al., 2011). Cavet (1957) defined the two principal pre-Sardic stratigraphic units of the Axial Zone in the Eastern Pyrenees, the Canaveilles and the Jujols Schists Series (Fig. 3), later assigned to groups (Laumonier and Guittard, 1986; Laumonier, 1988; Laumonier et al., 1996, 2004, 2015, in press). Their definition, geographical extension and subdivision have been varying continuously.

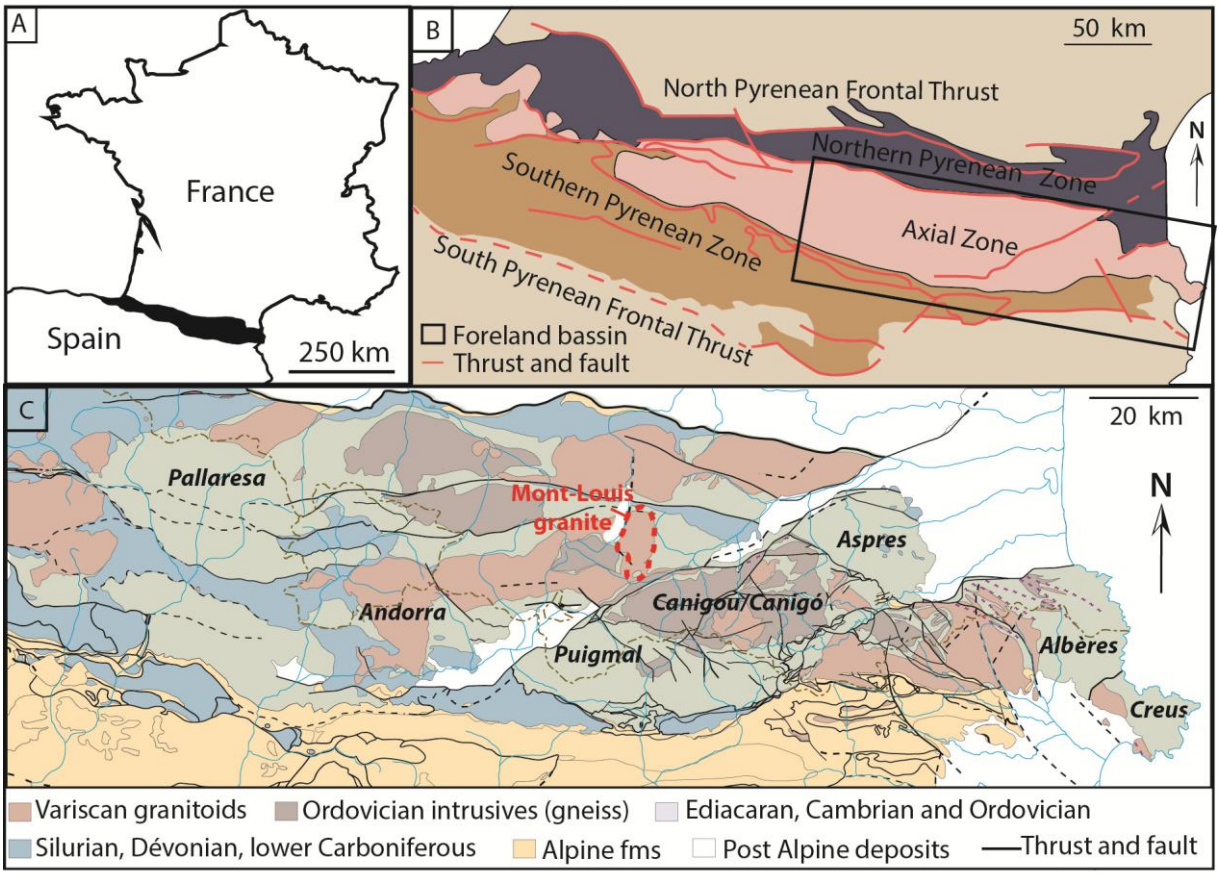

Fig. 1 : A. location of the Pyrenees marking the Spanish/French border. B. Main structural units of the Pyrenees. C. Simplified geological map of the Central and Eastern Pyrenees; modified from Laumonier (2015).

Recent 1/50 000 geological maps (Arles-sur-Tech, Argelès-sur-Mer-Cerbère, Prats-de-Mollo in crossing the Spanish/French border; Céret, Mont-Louis, Prades, in the French flank; Guitard et al., 1998; Autran et al., 2004; Baudin et al., 2008; Donzeau et al., 2010; Calvet et al., 2012; Laumonier et al., in press) have been trying to correlate and homogenise the pre-Sardic lithostratigraphic units from both sides of the Eastern Pyrenees. However, a formal definition of formations and members (including stratotype designation, selection of contacts and intertonguing relationships) are commonly absent, leading to nomenclatural confusion. In addition, the correlation throughout numerous tectonostratigraphic units remains contentious. The scarcity of biostratigraphic data in the Ediacaran-Lower Ordovician succession (Perejón et al., 1994; Casas and Palacios, 2012; Wallet et al., in prep) has been partly compensated by reporting of geochronologic U/Pb datings of zircon (Cocherie et al., 2005; Castiñeiras et al., 2008, Casas, 2015; Padel et al., in prep [article 2].). Palaeogeographic reconstructions and stratigraphic correlations with other basins of Northwest Gondwana are, as a consequence,

very hypothetical: the Pyrenees are often absent from the palaeogeographic reconstructions of this margin of Gondwana.

The aim of this paper is to propose an updated revision of the Ediacaran-Lower Ordovician (pre-Sardic) stratigraphic framework in the Eastern Pyrenees, based on recent geochronologic data coupled with field work. Previous, emended and new stratigraphic units are formally introduced, which are subsequently correlated, at the stage level, with neighbouring platforms of the eastern branch of the Variscan Ibero-Armorican Arc.

2. Geological setting

The geologic mapping at a scale of 1:50 000 made by the Spanish and Catalan Geological Surveys (IGME and ICGC; Carreras et al., 1994; Cirés et al., 1994a,b, 1995; Muñoz et al., 1994) and the French Geological Survey (BRGM) in the eastern Pyrenees (Llac et al., 1988; Guitard et al., 1998; Autran et al., 2004; Baudin et al., 2008; Donzeau et al., 2010; Calvet et al., 2012; Laumonier et al., 2015, in press) were based on lithosomes (Spanish side) and a late Ediacaran-Lower Ordovician stratigraphic framework proposed by Laumonier et al. (1996, 2004, 2015, in press) for the French side in everlasting nomenclatural evolution. The tectonostratigraphic units and sections reported below comprise the Albère-Cap de Creus, Aspres, Canigou, Puigmal, Vallespir, Roc de France, and Salud units (Baudin et al., 2008; Laumonier et al., 2015, in press).

2.1 Tectonic setting

Geologically speaking, the Pyrenees consist of an elongated E-W Axial Zone bounded by northern and southern flanks (Barnolas and Chiron, 1996; Laumonier, 2015). The imprint in its basement of the Variscan orogenic events has led to several tectonic models which are still debated (Zwart, 1986; Eeckhout and Zwart, 1988; Soliva et al., 1989; Vissers, 1992; Carreras and Capella, 1994; Druguet, 2001; Laumonier and Autran 2001; Denèle et al., 2009; Mezger, 2009; Laumonier et al., 2010, 2015; García-Sansegundo et al., 2011; Sengör, 2013; Olivier et al., 2016; Cochelin et al., in press).

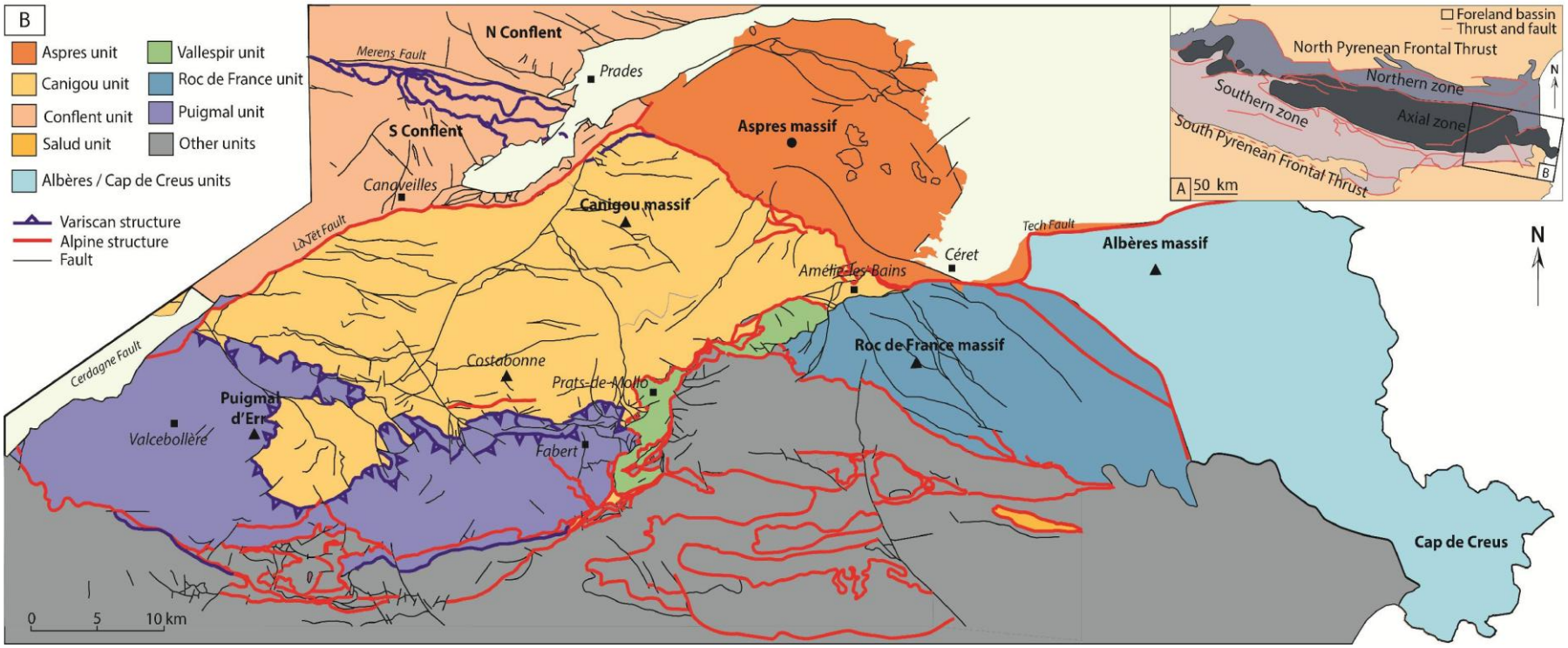

Fig. 2 : A. Main structural units of the Pyrenees with location of eastern Pyrenees. B. Main tectonostratigraphic units of the Eastern Pyrenees used herein.Many authors agree with the existence of two Varican-related structural domains (Zwart, 1986; Vissers, 1992; Carreras and Capella, 1994; Denèle et al., 2009; Cochelin et al., in press): a deeper domain, named infrastructure, composed of high-grade metamorphic rocks and including the metamorphic domes and metasedimentary rocks (sillimanite to andalusite zones); and an upper domain, named suprastructure, made of low grade metamorphic rocks (biotite and chlorite zones). The core of these gneissic domes is generally composed of Ordovician metagranites, previously interpreted as the Precambrian basement of a Cambro-Ordovician succession.

2.2 Sardic intrusions

The intrusions that form the core of metamorphic domes have recently been dated based on U-Pb zircon methods: the orthogneisses intruding the Canaveilles Group of the high-grade metamorphic infrastructure domain have been dated as Lower (Floian) to Upper Ordovician, ranging from ca. 456-446 Ma (Casas et al., 2010) to ca. 475-467 Ma (Deloule et al., 2002; Cocherie et al., 2005) in the Canigou massif, ca. 458 Ma (Martínez et al., 2001) in the Freser dome, and ca. 477-460 Ma (Castiñeiras et al., 2008; Liesa et al., 2011; Cocherie et al., 2005) in the Roc de France and Albères/Albera massifs (orthogneiss and metaporphiric dykes). The Ribes granophyres intruding Upper Ordovician conglomerates located in the low-grade metamorphic suprastructure have yielded an age of ca. 458 Ma (Martínez et al., 2011).

3. Stratigraphic framework

The lithostratigraphic framework of the Pyrenees has been in a permanent nomenclatural flux throughout the Spanish and French geological maps (Fig. 3). Even Laumonier et al. (in press) has suggested in the latest lithostratigraphic framework that their proposal should be regarded as provisional. As a consequence, an updated revision of the Ediacaran-Lower Ordovician volcanosedimentary framework in the Eastern Pyrenees is proposed below based on recent U-Pb radiometric ages, intertonguing relationships of carbonate-dominated strata and onlapping relationships capping volcanosedimentary complexes. Previous nomenclatures have been maintained if their lithologies and original base and top have suffered no changes; otherwise, a new nomenclature is proposed to avoid ambiguities among lithostratigraphic units that have been used to represent different lithologies and contacts in successive geological maps. Exception is made with the Canaveilles and Jujols groups: although their contact has been continually modified, their nomenclature is maintained due to traditional use.

3.1 Canaveilles Group (emended)

The Canaveilles Series of Cavet (1957) was broadly defined to encompass the lowermost carbonate-bearing levels interbedded in a monotonous schist-dominated succession, then interpreted as directly onlapping a Precambrian metamorphic dome, the so-called Canigou/Canigó massif. According to Cavet (1957), the base of the Canaveilles Series was located at the contact between the Cadomian orthogneisses and the micaschist cap, whereas its top was placed between some black shales cropping out across Oreilla and Olette

villages (Conflent Unit; Fig. 2) and quartzitic levels then assigned to the Jujols Schists Series (Fig. 3). The resulting Canaveilles Series extended throughout all the tectonostratigraphic units forming the Albères, Aspres, Canigou, Puigmal, Roc de France and Vallespir units (Fig. 2). Subsequently, Laumonier and Guitard (1986), Laumonier (1988) and Laumonier et al. (1996) successively redefined the Canaveilles Series as a group subdivisable into the Canaveilles, Cabrils and Evol formations (Fig. 3). Recently, Laumonier et al. (2004, 2015) excluded the Evol Formation from the Canaveilles Group, which was included in the overlying Jujols Group (see below). The Canaveilles Group, as reviewed herein, contains scattered volcanogenic levels (the so-called “gneiss granulés” of Guitard and Lafitte, 1956), and is covered, in the Puigmal unit, by a thick volcanosedimentary complex. This has been mapped and reported in previous works as the Tregurà Formation and marks the top of a succession characterized by the presence of episodic volcanic products that have not yet been reported in the overlying Jujols Group. Despite the everlasting nomenclatural modifications proposed for the Canaveilles Group, this lithostratigraphic unit has been traditionally used and is maintained herein. The thickness of the group, as revised below in the Eastern Pyrenees, was estimated between 2 and 3 km by Laumonier et al. (2004).

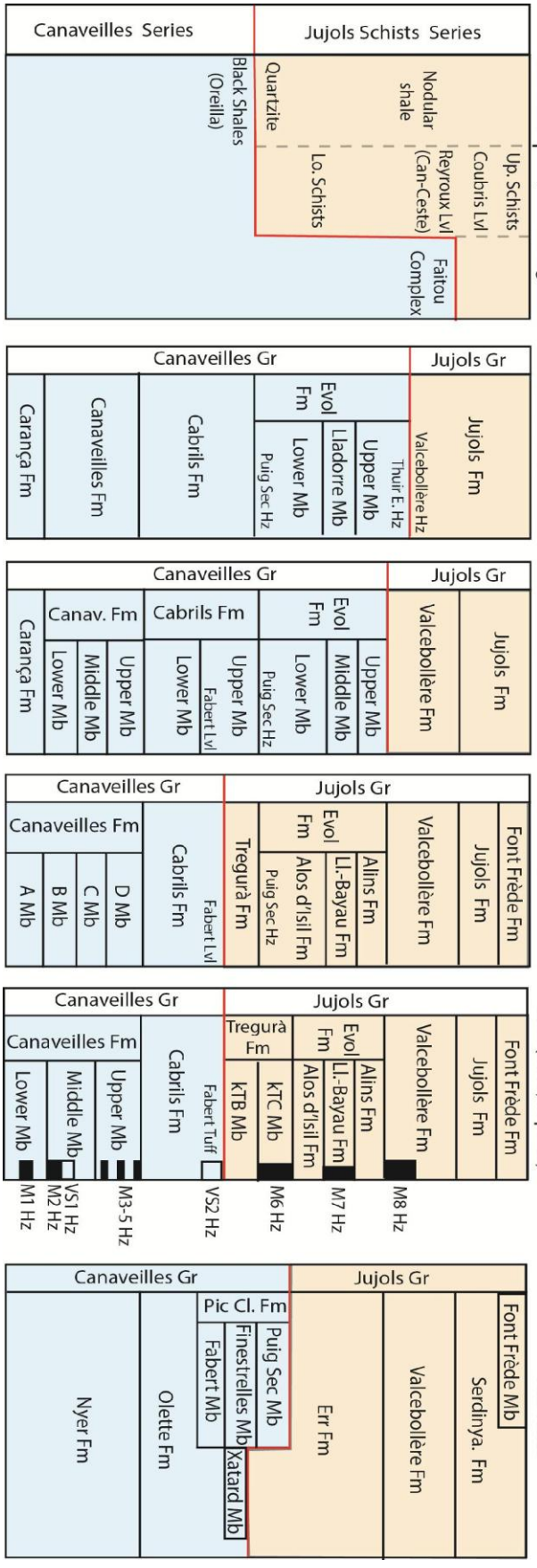

Fig. 3 : Evolution of the lithostratigraphic nomenclature in the Ediacaran-Lower Ordovician succession of the Eastern Pyrenees (Fm, formation; Gr, groupe; Hz, horizon; Lvl, level; Lo, lower; M, marble; Mb, member; VS, volcanosedimentary; Up, upper). Correlation between the different levels of the Jujols Schists Series was not introduced by Cavet (1957) and is therefore tentative.

The basal formation of the Canaveilles Group (Canaveilles Formation *sensu* Laumonier et al., 2015) is renamed here Nyer Formation to remove potential ambiguity caused by the previous homonymy between a group and its own formation (see Owen, 2009). The Olette Formation is restricted herein to the upper carbonate-free, shale-dominated package, of the Cabrils Formation sensu Laumonier et al. (2015). The uppermost rhyolitic tuffs and volcanosedimentary complexes recognized in the Puigmal Unit (Tregurà Formation *sensu* Laumonier et al., 2004; Fabert level or VS2 *sensu* Laumonier et al., 2015; kTB Member *sensu* Laumonier et al., in press) are grouped below in the Pic de la Clape Formation (Fig. 3).

3.1.1 Nyer Formation (new)

The Canaveilles Formation *sensu* Laumonier et al. (2004, 2015), is renamed here Nyer Formation after the homonymous village, in the vicinity of Canaveilles village. It is the basal unit of the Canaveilles Group and is restricted to the Eastern Pyrenees, where it surrounds the Variscan and Sardic intrusions and metamorphic domes. The stratotype is located along the road D28 around the Canaveilles village (42°31'58.80"N; 2°15'6.54"E); a parallel section crops out along the neighbouring road N116. A hypostratotype is recognized in the Canigou unit, around the Freser dome (southern Canigou massif), between Queralbs and the Núria station, which starts at 42°22'2.59"N- 2° 9'28.36"E.

The Nyer Formation (Figs. 3-4), about 2000 m thick, consists of heterolithic metasedimentary rocks (Laumonier et al., 1996, 2015) dominated by micaschists but including subsidiary marbles, metasandstones, metabasites and, at least, a metaryodacite layer (VS1 of Laumonier et al., 2015). The latter, 10 to 200 m thick, is exclusively recognized to the south of the Canigou massif.

Laumonier et al. (2015) have differentiated at least 5 marble marker-beds (M1 to M3-5; Fig. 3), up to 300 m thick, and considered the top of the uppermost as the base of the overlying Cabrils Formation. The maximum thickness of the Canaveilles (=Nyer) Formation was estimated by Laumonier et al. (2015) in the Queralbs area; however, this estimate includes a tectonic contact thrusting over the Cambrian Valcebollère Formation. As a result, the maximum thickness of the Nyer Formation should be re-evaluated. The number of marble interbeds varies throughout the tectonostratigraphic units, due to both intertonguing and tectonic truncations.

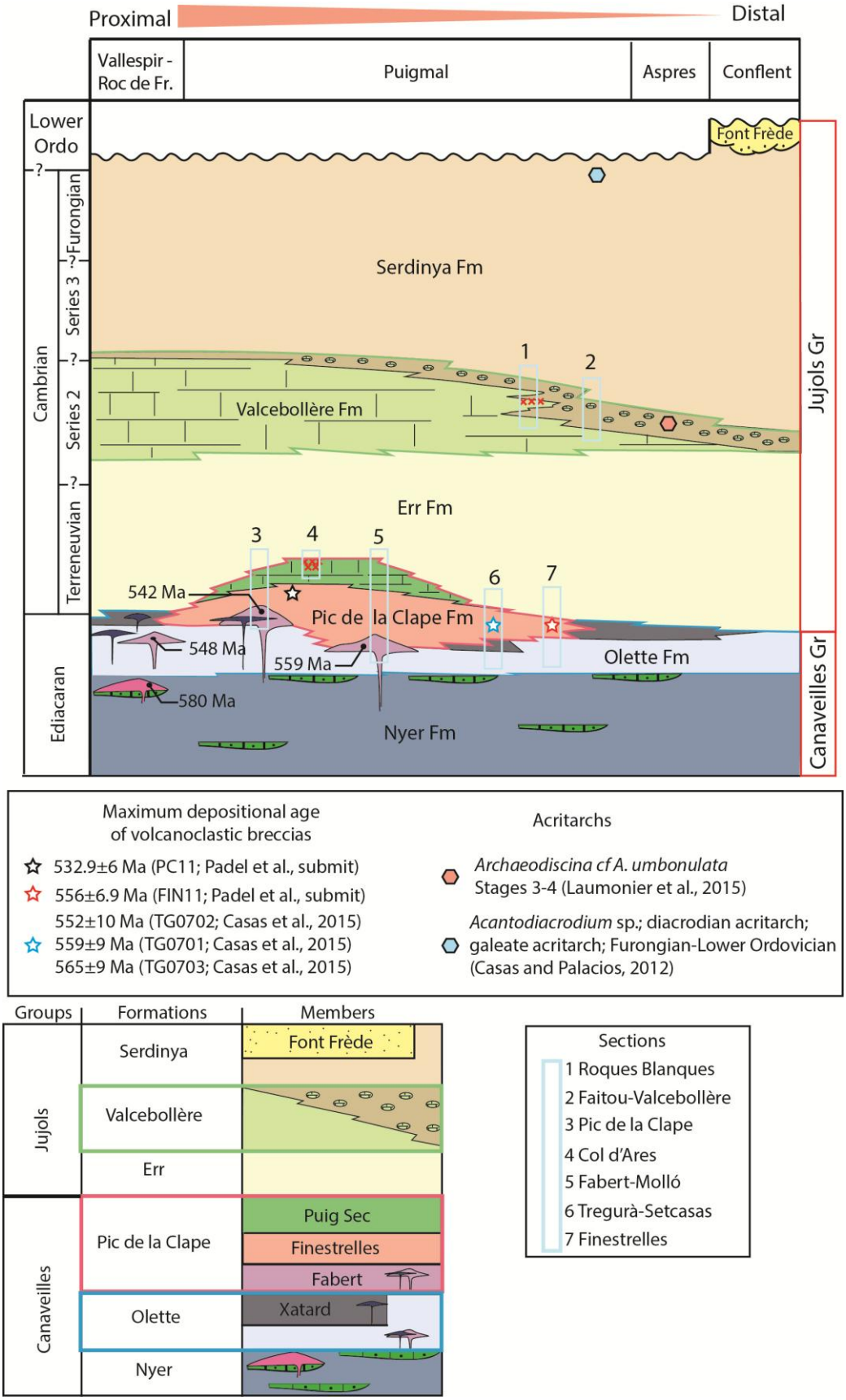

Fig. 4 : New stratigraphic framework proposed for the Ediacaran-Lower Ordovician of the Eastern Pyrenees. Not to scale.

The only radiometric constraint is yielded by the volcanic level VS1 that, according to Laumonier et al. (2015), overlies M2 south of the Canigou massif. Nevertheless, the age of VS1 (580±10 Ma; Cocherie et al., 2005), obtained by U-Pb dating on zircon, should be re-evaluated (see discussion in Padel et al., in prep [article 2].). At present, the lateral correlation of the M1-M5 marble beds included in the Nyer Formation may be considered as tentative. M3-M5 marbles are unknown in some areas, such as the northeast of Nuria Station in the Canigou unit, near Taulis village northeast of the Canigou massif, and southeast of Prats-de-Mollo-la-Preste village in the Vallespir Unit, as a result of which, the Nyer/Olette contact is not distinguishable (Donzeau et al., 2010; Laumonier et al., in press). This formation is still in need of a more detailed stratigraphic study to better understanding its extension and relationships with overlying formations.

3.1.2 Olette Formation and Xatard Member (new)

The Olette Formation (uppermost Canaveilles Series in the Conflent unit by Cavet, 1957) represents the marble-free and shale-dominated part of the Cabrils Formation *sensu* Laumonier et al. (1996, 2004, 2015) (see Fig. 3). The upper volcanic level (Fabert level *sensu* Laumonier et al., 1996), overlain by a volcanosedimentary complex locally rich in carbonate clasts, was described as the upper member of the Cabrils Formation, south of the Canigou massif (Laumonier et al., 1996). Laumonier et al. (2004) defined the Tregurà Formation to include these conglomerates, representing the lowermost part of the Jujols Group; by contrast, the Fabert level, disconnected lithostratigraphically from the overlying volcanosedimentary complex, marked the top of the Canaveilles Group. As both volcanogenic episodes are genetically related (Padel et al., in prep [article 2].), the Fabert volcanic level and the overlying volcanosedimentary “conglomerates” (or breccias) are included below as members of the Pic de la Clape Formation.

The Olette Formation (Figs. 3-4), conformably overlying the Nyer Formation, is therefore reduced herein to 400-500 m of greenish and black shales, schists, greywackes, feldspathic sandstone. The uppermost black shale interbeds, commonly named “ampelites” or “schistes carburés” by previous authors, are included here in the new Xatard Member of the Olette Formation.

The stratotype of the Olette Formation is selected along the Cabrils river (GPS42°33'49.18"N; 2°15'24.42"E), in the Conflent Unit, and the stratotype of the Xatard Member along the road D13, near the Col du Xatard (42°33'12.36"N; 2°37'0.66"E) in the

Aspres Unit. A parastratotype of the Xatard Member, located in the Conflent Unit, was reported as the Oreilla Schists by Guitard et al. (1998) between Oreilla and Olette villages, along the D4 road and south of the Pic Lluomet. These black shales are well exposed in the Puigmal Unit, between el Catllar and Setcasas villages, along the road GIV 5264. The base of the Xatard Member is visible in its stratotype, but its top is absent there due to faulting (Laumonier et al., 2015). The top of the Xatard Member is seen on the right cliffy bank of the Ter river at the Tregurà section (42°21'30.68"N; 2°17'34.44"E), where it is marked by the occurrence of the tuffaceous sandstones and volcanoclastic breccias of the overlying Pic de la Clape Formation. The latter is absent in the Aspres and Conflent units, where the Err Formation conformably overlies the Xatard Member. The Xatard Member pinches out laterally and grading into the greenish shales of the Err Formation.

3.1.3 Pic de la Clape Formation (new)

The Pic de la Clape Formation (Figs. 3-4) includes a succession of genetically related volcanic pulsations linked to the episodic development of carbonate production. The formation is subdivided, from bottom to top, into (i) the Fabert level *sensu* Laumonier et al. (1996) and VS2 *sensu* Laumonier et al. (2004, 2015), named Fabert Member herein; (ii) the Finestrelles Member, corresponding to the Tregurà Formation *sensu* Laumonier et al. (2004) and the basal volcanosedimentary member of the Tregurà Formation (kTB) *sensu* Laumonier et al. (in press), and (iii) the Puig Sec Member (Puig Sec horizon *sensu* Laumonier, 1988; kTC or M6 *sensu* Laumonier et al., 2015). These three members are genetically linked and are representative of a major tectono-magmatic pulsation recording episodes of carbonate production (Padel et al., in prep [article 2].).

The Pic de la Clape Formation crops out south of the Canigou massif in the Vallespir, Roc de France and Puigmal units, around the Tregurà and Fabert villages, and at the Pic de Finestrelles and Pic de la Clape. Its type section is defined at the Pic de la Clape (42°23'47.64"N; 2°26'40.99"E). The age of the Pic de la Clape Formation is considered as upper Ediacaran to Terreneuvian based on new and revised U-Pb dating (Padel et al., in prep [article 2]).

The Fabert Member (Figs. 3-4), up to 50 m thick, crops out discontinuously from the Puigmal to the Vallespir-Roc de France units. Its stratotype is located along the Fabert Torrent, 200 m east of Fabert village. Guitard and Lafitte (1956) referred this unit to as “gneiss granulés” and interpreted them as metamorphized volcanic or volcanosedimentary

protoliths. The Fabert level *sensu* Laumonier et al. (1996), or VS2 of Laumonier et al. (2015) is considered herein as a metarhyolithe (Padel et al., in prep [article 2]), that exhibits lenticular shapes and conformably overlies fine to medium quartzo-feldspatic greywackes (Olette Formation). At the Pic de la Clape, a basic lava flow is interbedded in the member. In the Puigmal unit, two divergent radiometric ages were estimated for the Fabert metarhyolites: 559.1+1.75/-1.35 Ma near Fabert village, and 542.9+ 5/-1.30 Ma at the Pic de la Clape (Padel et al., in prep [article 2]), suggesting this unit does not record a single volcanic event but successive pulsations. In the Vallespir-Roc de France unit, an acidic tuff lying in the Olette Formation was dated at 548±8 Ma (Concordia Age, n=7, MSWD= 0.004) by Castiñeiras et al. (2008), and subsequently recalculated at 544.8±3.2 Ma (Concordia Age, n= 8, MSWD=0.020) by Padel et al. (in prep [article 2]) These ages and the stratigraphic position of sampled rocks confirm that the upper part of the Olette Formation was deposited laterally and coeval to the onset of the Fabert Member (Fig. 4).

The Finestrelles Member (Figs. 3-4), is a heterolithic unit, up to 500 m thick, composed of tuffaceous sandstone and volcanoclastic breccias and subsidiary shale, pristine-to-volcaniclastic limestone, showing sharp intertonguing relationships. The matrix of the volcanoclastic breccias and tuffaceous sandstone is variously carbonate cemented. Locally (e.g. in the uppermost Tregurà-Setcasas section, 42°20'36.04"N; 2°17'52.95"E), massive volcanoclastic breccias include carbonate boulders more than 2 m large. The typical facies is locally overlies by shale and greywacke (e.g. in the Mollo section). The stratotype of the Finestrelles Member is selected at the Pic du Finestrelles (42°24'30.54"N; 2° 7'29.76"E; section 7 in Fig. 4), NW to the Núria station, where it consists of about 150 m of volcanoclastic breccias, tuffaceous limestone sandstone and shale preserved in inverse position. There, U-Pb dating of zircon of tuffaceous sandstone has yielded a maximum depositional age of 556± 6.9 Ma (MSW=0.061, Padel et al., in prep [article 2]). The volcanoclastic deposits of the Finestrelles Member are conformably overlying the Olette Formation in the Finestrelles and Setcasas-Tregurà sections, the Fabert Member in the Molló-Fabert and Pic de la Clape sections, and are overlain by the Puig Sec Member in the Molló-Fabert and Pic de la Clape sections and the Err Formation in the Finestrelles and Setcasas-Tregurà transects (Fig. 4).

Another parastratotype is defined at the Puig Sec, near the Pic de la Clape, in which the breccias include variegated volcanic clasts. However, here, the fine to medium greywacke matrix is depleted of carbonate cement; limestone clast and boulder are also absent. U-Pb

dating of zircon of breccias from this parastratotype has yielded a maximum depositional age of 532.9 ±6 Ma (MSW=1.2, Padel et al., in prep [article 2]). Rejuvenation of the maximum depositional age versus age of the underlying metarhyolithe, attest that the breccias deposited during cogenetic volcanic activity (Padel et al., in prep [article 2]).

The Puig Sec Member (Puig Sec Horizon *sensu* Laumonier, 1988; M6 and kTC *sensu* Laumonier et al., in press; Figs. 3-4), up to 180 m thick, consists of bedded and massive limestone, dolostone and marble strata. The base of the member is well exposed in the Fabert-Molló transect (42°21'3.10"N; 2°24'26.06"E), and its contact with the siliciclastic strata of the Err Formation at the homonymous stratotype (Col d'Ares section; 42°22'2.80"N; 2°27'17.00"E; Pic de la Clape section, 42°23'20.49"N; 2°25'55.29"E). The stratotype is located at the Puig Sec (42°23'40.00"N; 2°25'56.36"E) and can also be observed along the D115 road at the Col d'Ares (42°22'2.80"N; 2°27'17.00"E).

3.2 Jujols Group (emended)

The Jujols Group (Figs. 3-4) was firstly described as the Jujols Schists Series by Cavet (1957), as a monotonous succession of alternating shale and sandstone. However, Cavet (1957) included in the Series what is now considered as Upper Ordovician conglomerate and volcanic deposits. The latter are distinctly post-Sardic and underlain by a significant unconformity, and therefore excluded from the Jujols Group (Laumonier, 1988). According to Cavet (1957), the base of the Jujols Schists was characterized by the presence of grey shales with carbonate nodules and quartzite interbeds. Laumonier (1988) elevated the Jujols Schists Series *sensu* Cavet (1957) and Jujols Series of Laumonier and Guitard (1986) as an invalid group including a single, eponymous formation. Laumonier et al. (1996) included in the Jujols Group the so-called Valcebollère Formation (previously described as a horizon), which included bedded and massive limestones and shales with carbonate nodules described by Cavet (1957). Laumonier et al. (2004, 2015), extended the Jujols Group to include the Tregurà, Evol, Valcebollère, Jujols and Font Frède formations. As a consequence, three carbonate levels, interstratified within the mostly siliciclastic Jujols Group, were recognized in the Eastern Pyrenees by Laumonier et al. (2015) (Fig. 3): the Puig Sec Horizon or M6 (uppermost part of the Tregurà Formation), the Lleret Bayau Formation or M7 (including the Can Ceste and Reyroux levels of Cavet, 1957 and invalidly incorporated in the Evol Formation), and the Valcebollère Formation (M8, including the Courbis level of Cavet, 1957). The lowermost marble level, called Puig Sec Horizon by Laumonier (1988) and Laumonier et

al. (1996), corresponds to the new Puig Sec Member of the Pic de la Clape Formation that should not be separated from the Pic de la Clape Formation because similar facies occur interbedded in its Finestrelles Member. The two uppermost levels (Lleret-Bayau and Valcebollère formations) never co-occur in a same continuous section, whatever the tectonostratigraphic unit. In addition, only the Coubris level of Cavet (1957; Valcebollère Formation), from the Aspres Unit, has been biostratigraphically constrained (acritarch record mentioned in Laumonier et al., 2015). Therefore, in absence of indisputable lithologic markers and until better age constraints are available, we consider herein these two carbonate levels cannot be stratigraphically differentiated in the Eastern Pyrenees. As a consequence, the Valcebollère Formation is the only considered carbonate level herein.

As a result, the base of the Jujols Group coincides with the base of the Err Formation (Figs. 3-4), which onlaps the palaeorelief formed by the Pic de la Clape Formation south to the Canigou Massif. Where the Pic de la Clape Formation is absent, the Err Formation conformably overlies the Olette Formation. The top of the Jujols Group is highlighted by the Middle-Upper (part) Ordovician hiatus associated with the Sardic Phase (Zwart, 1979; Degardin et al., 1996; Laumonier et al., 1996, 2004, 2015; García Sansegundo et al., 2004). The thickness of the group can be estimated at about 3 to 4 km.

3.2.1 Err Formation (new)

As mentioned above, the limits and content of the Evol Formation *sensu* Laumonier et al. (1996, 2004, 2015) has often changed through time (Fig. 3). In addition, the invalidly included Lleret-Bayau Formation is not recognized herein in the Eastern Pyrenees. As a consequence, the new Err Formation is defined as fully siliciclastic and depleted of carbonate level, therefore differing form the previously defined Evol Formation

As a results, the Err Formation (Figs. 3-4) is considering as a relatively monotonous shale-dominated, up to about 2000 m thick unit. It consists of grey to brownish and greenish shale and centimetre-to-decimetre thick, fine-grained sandstone, locally punctuated by gravelly sandstone (“microconglomérat” *sensu* Laumonier et al., 1996, 2004, 2015). These sandstones never exceed 10 m thick and can be observed, (1) in the Puigmal unit, near the summit of the Puigmal d’Err massif (42°22'28.54"N; 2° 7'5.85"E), and eastward, and (2) at the Pic de la Clape (42°23'31.60"N; 2°26'26.91"E) where they overlie the Puig Sec Member. These sandstones are also well developed in the Aspres and Conflent units. The base of the Err Formation is well exposed at the Pic de Finestrelles, where it conformably overlies the

Finestrelles Member, and its top south of the Pic de Duraneu, where it is conformably overlain by the Valcebollère Formation (42°22'43.01"N; 2° 4'32.54"E). Its stratotype is located in the Puigmal d'Err Massif, near the summit (42°22'29.04"N; 2° 7'18.90"E).

3.2.2 Valcebollère Formation (emended)

The Valcebollère Formation (Figs. 3-4) consists of a lower massive-to-bedded limestone package (up to 300 m thick), overlain and passing westward to a 15 to 200 m thick, shale/carbonate alternation that changes up section into green shales bearing carbonate nodules.

The stratotype of the Vacebollère Formation was defined south to the Canigou massif in the Puigmal Unit (42°22'37.14"N; 2° 4'35.34"E), eastward to the Valcebollère village, between the Duraneau and the Puigmal d'Err summits, along the Faitou valley (Laumonier et al., 1996). There, Cavet (1957) first described a greenish and shaly-carbonate alternation (named the Faitou Complex), which was included into the Canaveilles Series. Laumonier (1988) named it the Valcebollère horizon and used it as the base of the Jujols Group, directly overlying the Thuir d'Evol carbonate horizon (defined in the Conflent Unit). Laumonier et al. (1996), subsequently grouped the Thuir d'Evol and Valcebollère horizons into a single Valcebollère Formation, thus lowering the base of the Jujols Group. They correlated this Valcebollère Formation with the massive carbonate levels of the Carliba (Vallespir unit) and Llanars (Puigmal Unit). Laumonier et al. (2004) revised the Jujols Group, moving its lower boundary to the base of the Tregurà Formation.

Nodular shales are absent in the Roques Blanques section, along the road N260 (parastratotype), which consists of two massive carbonate layers ranging between 10 to 30 m thick, separated by a thin 5-8 m thick green marly interval.

Thick, massive limestones were not deposited in the Faitou section, (where the former Faitou Complex was defined by Cavet, 1957), along the Faitou Valley (42°22'37.14"N; 2° 4'35.34"E).

In addition to its stratotype (located eastward to the Valcebollère village), remarkable outcrops of the Valcebollère Formation in the Puigmal Unit are located near Llanars and Roca Bella villages (42°19'28.63"N; 2°20'23.30"E); in the Vallespir Unit along the Gorges de la Fou (42°27'33.35"N; 2°36'24.90"E); in the Aspres Unit, along the road D2 near Saint Colombe de las Illas (42°37'24.31"N; 2°38'28.15"E). Finally, in the Conflent Unit, the

formation is exposed 200 m north to the Thuir d'Evol Village. The thickness of the formation diminishes northward.

The Courbis Limestone of the Valcebollère Formation in the Aspres Unit (Fig. 4) has yielded the acritarch *Archaeodiscina* cf *umbonulata* Volkova 1968. *A. umbonulata* is a cosmopolitan species ranging approximately from Cambrian Age 3 to early Cambrian Age 4 (Laumonier et al., 2015; T. Palacios, pers. com. 2016).

3.2.3 Serdinya Formation (new) *and Font Frède Member*

In the Jujols Schists Series of the Aspres unit, Cavet (1957) differentiated two siliciclastic units (named lower and upper Jujols Schists) differentiated by carbonate interbeds (the above-reported Valcebollère Formation). In the Aspres unit, the Serdinya Formation defined herein corresponds to the Upper Jujols Schists *sensu* Cavet (1957) once excluded the (post-Sardic) Upper Ordovician deposits. In the remaining tectonostratigraphic units, the new Serdinya Formation corresponds to the Jujols and Font Frède formations *sensu* Laumonier et al. (2004). Cavet (1957) characterized this part of the succession by the presence of lenticular and coarse sandstones ("micro-conglomérates") alternating with quartzite and shale strata. In the northern part of the Aspres Unit, Laumonier (1988) and Laumonier et al. (1996, 2015) reinterpreted the coarse sandstone of the Jujols Upper Schists (i.e. Mas d'Escossy) as cropping out in reverse position and deposited below the Valcebollère Formation, so as part of the Evol Formation (former Alins Formation). New field work questions this interpretation, as depositional structures (scouring bases and grading of coarse-grained sandstones) suggest an opposite way-up. In addition, as we consider here the Coubris, Can-Ceste and Reyroux levels as part of the Vacebollère Formation, we interpret the overlying coarse-grained sandstone strata as part of the Serdynia Formation. In addition, the rank of the Font Frède Formation *sensu* Laumonier et al. (2004) is changed into member within the Serdinya Formation due to reduced lateral extension and gradual character of its lowermost part.

The stratotype of the Serdinya Formation is located near the Col Diagre, in the Conflent Unit (42°35'2.40"N, 2°16'35.90"E). This formation consists of grey to greenish shales alternating with thin centimetre to decimetre-thick sandstone beds. The Serdinya Formation (Figs. 3-4) conformably overlies the Valcebollère Formation and is topped by the Sardic unconformity. Acritarchs recovered from the uppermost part of the Serdinya Formation in the Puigmal Units has yielded a broad Furongian-Early Ordovician age for the microphytoplancton assemblage (Casas and Palacios, 2012).

4. SE-NW palaeogeographic trends

In the Eastern Pyrenees, the metamorphic domes and granitic intrusions (e.g., Canigou, Roc de France and Albères massifs) are flanked to the northern Conflent and Aspres units, and to the southern Puigmal, Vallespir, Roc de France and Albère-Cap de Creus units (Fig. 2). In the Puigmal, Vallespir and Roc de France units, the top of the Canaveilles Group illustrates the onset of volcanosedimentary complexes (Fabert and Finestrelles members of the Pic de la Clape Formation) covering deep, clayey, offshore environments (Olette Formation). The influence of volcanic outflows away from this area is limited as stated by the absence of the Finestrelles-type facies in the northern Conflent and Aspres units. The presence of the Puig Sec Member of the Pic de la Clape Formation, which developed on topographic highs of these complexes, is also recognized in the same southern tectonostratigraphic units.

The Valcebollère Formation displays a distinct southeast-to-northwest proximal-distal trend of lithologies (Fig. 4), grading from massive-to-bedded marbles/limestones in the Puigmal (Llanars, Roca Bella, Roques Blanques) and Vallespir (Gorge de la Fou) units to shale/carbonate alternations and shales bearing carbonate nodules parallel to stratification in the northern units (Faitou section). Obviously, the latter lithology (named “schistes troués” in the Montagne Noire and “facies rizadas” in the Iberian Chains; Courtessole, 1973; Álvaro and Vennin, 1997) shows an opposite, southeastward thinning with a maximum thickness observed at Faitou. The thickness of the formation also decreases west-and northward, as observed in the Conflent and Aspres units.

5. Correlation with surrounding Pyrenean units

Laumonier et al. (1996, 2004) proposed different correlation schemes throughout the Central and Eastern Pyrenees. Three areas are selected here for comparison: the Cap de Creus Unit, the Pallaressa valley (Central Pyrenees) and the Salud Unit (Southern Pyrenean Zone).

Recent research on the pre-Sardic, volcanosedimentary deposits of the Cap de Creus Unit (Figs. 1-2) has avoid reporting the stratigraphic setting in any lithostratigraphic framework (Carreras et al., 1994; Losantos et al., 1997; Carreras and Druguet, 2013), precluding any detailed correlation with the lithostratigraphy of the Eastern Pyrenees (see remarks in Laumonier et al., 1996). Recently, a volcanosedimentary succession has been described including U/Pb dating of zircon (Castiñeiras et al., 2008; Casas et al., 2015). The authors dated these volcanoclastic breccias to 577.9±3Ma (MSWD= 2.8) and 558 ±3 Ma

(MSWD= 0.43). As a consequence, the volcanosedimentary series developed in the Cap de Creus area can be considered herein as reflecting the easternmost development of the volcanic episodes recorded by the Fabert and Finestrelles members of the Pic de la Clape Formation. Further correlation of the pre-Sardic deposits of the Cap de Creus with surrounding Pyrenean areas would require detailed reappraisal and dating of the complete succession.

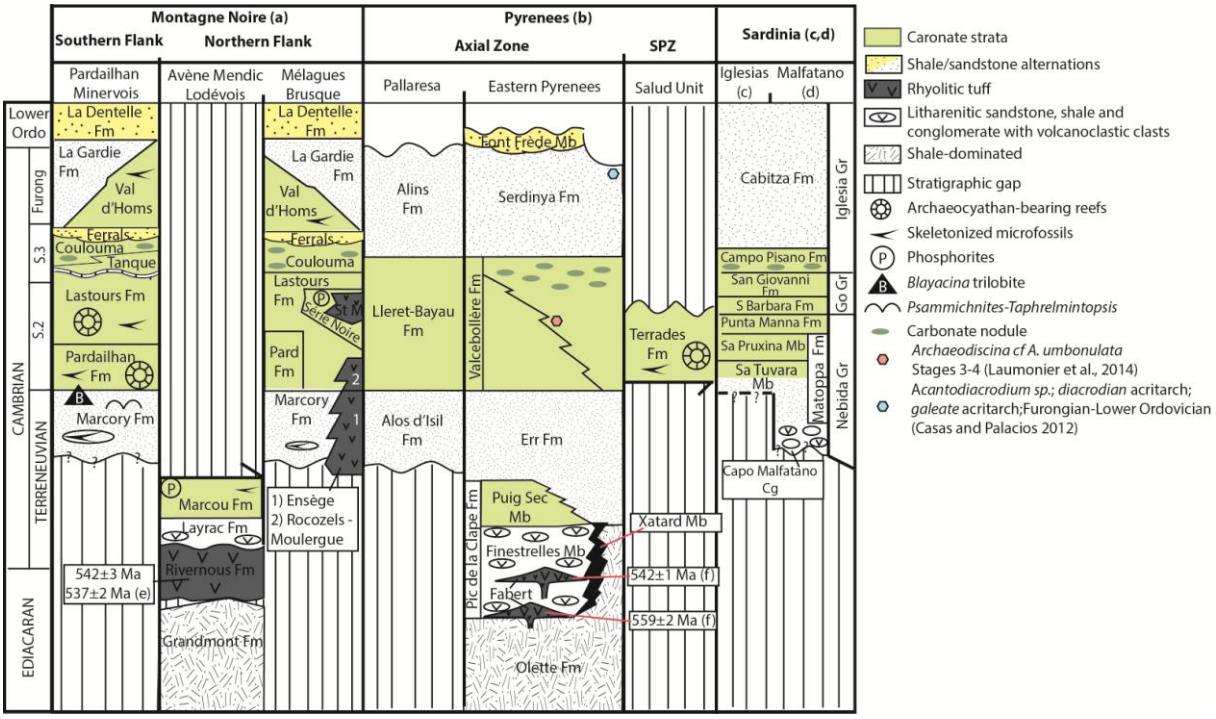

Fig. 5 : Stratigraphic comparison of the Ediacaran-Lower Ordovician successions from the Montagne Noire, the Eastern Pyrenees and Sardinia. SPZ: Southern Pyrenean Zone; S: Series; Furong: Furongian; Ordo: Ordovician; Pard: Pardailhan; St M: St Meen; Go Gr: Gonnessa Group; Fm: Formation; Mb: Member; Gr: Group; Cg: conglomerate. References: (a) stratigraphy of the Montagne Noire after Álvaro et al. (2014); (b) this study; (c) stratigraphy of Sardinia after Pillola et al. (1994); (d) stratigraphy of Sardinia after Costamagna et al. (2014); (e) et al. (in press [article 3]) (f) Padel et al. (in prep [article 2]).

Zandvliet (1960), Wennekers (1966), Hartevelt (1970), Zwart (1979) and García Sansegundo (1992) contributed, among others, to the elaboration of the pre-Sardic stratigraphic framework ofthe Central Pyrenees. In the Pallaresa valley (Central Pyrenees), a thick (more than 4000 m), siliciclastic-dominated succession crops out from the Certascan lake to the Llavorsi anticline (Laumonier et al., 1996). It is divided into three formations (according to Laumonier et al., 1996): the Alos d'Isil, Lleret-Bayau and Alins formations. The base of the Alos d'Isil Formation is thrusting by Devonian strata (Laumonier et al., 1996) and is crosscut by Variscan intrusions and Ordovician metagranites. The top of the Alins

Formation is unconformably overlain by the Upper Ordovician Rabassa conglomerate Formation (Zandelviet, 1960; Zwart, 1979). The Alos d'Isil and Alins formations are dominated by shales locally alternating with thin- to medium-grained sandstones. They are separated by the metasandstones and marbles of the Lleret-Bayau Formation. The latter was studied by Zandvliet (1960) and redefined by Zwart (1979), who suggested its lateral equivalence with the Jujols Schists Series *sensu* Cavet (1957), broadly equivalent to the Jujols Group as reviewed above. Laumonier et al. (1996, 2004) correlated the Pallaresa series with the Evol Formation from the Eastern Pyrenees (Fig. 4). However, as mentioned above, the Lleret-Bayau Formation of Laumonier et al. (2015, in press) cannot be lithologicaly differentiated from the Valcebollère Formation in the Eastern Pyrenees, where it is therefore not recognized (see discussion above). In addition, the Lleret-Bayau and Valcebollère formations never co-occur in a single section. It is also noticeable that all the carbonate units in the Central Pyrenees (i.e. Lleret Bayau Formation from the Pallaressa valley and Ransol Formation from the Hospitalet Massif) were considered as synonymous, and grouped in the Lleret Bayau Formation in the Aspres Unit (Can Ceste, Riuros and Coubrils limestones; Eastern Pyrenees) by Laumonier et al. (1996, 2004). Lower Cambrian Acritarchs were subsequently reported from the Coubris limestone (Eastern Pyrenees), which was moved from the Lleret-Bayau to the Valcebollère formations, whereas all other previously reported limestone levels remained in the Lleret-Bayau Formation without further lithological arguments (Laumonier et al., 2015, in press), despite the lack of any other geochronologic or biostratigraphic control. Finally, Laumonier (2015, in press) consider both the Lleret-Bayau and Valcebollère formations as a lateral equivalence of the Terrades Formation (Salud Unit; Laumonier et al., 1996, 2004, 2015, in press).

Considering the fluctuating concept and correlations of the Lleret-Bayau Formation, and the lack of any other stratigraphic constraint, we suggest the Pallaressa succession should be correlated with the Jujols Group (as revised above), being the Alos d'Isil, Lleret-Bayau and Alins formations equivalent to the Err, Valcebollère and Serdinya formations, respectively (Fig. 5). Dating of a volcanic tuff, discovered during this study at the base of the Alins Formation in the Pallaressa unit, will probably help assessing this tentative correlation scheme between the Central and the Eastern part of the Pyrenees.

The Terrades Formation of the Salud Unit, Southern Pyrenean Zone, up to 50 m thick, is the only Cambrian formation of the Pyrenees bearing shelly fossils. Abad (1989) described the presence of archaeocyathan patch reefs alternating with green to brownish shales, and

assigned the sponges to the Cambrian Age 3. Restudies by Perejón et al. (1994) and Menéndez et al. (2015) confirmed a late Cambrian Age 3. Current investigation on skeletonized microfossils from peri-reefal limestones of the Terrades Formation suggests a Cambrian Age 3-4 (Wallet et al., in prep). The detailed preservation of pristine microfacies and microbial textures in these limestone strata, contrasting with the traditional marble aspect of any carbonate bed of Cambrian age, points to an allochthonous provenance of this Alpine thrust slice (Laumonier, 1998), where the Cambrian limestones are thrusting Eocene strata and unconformably overlain by Eocene strata. Biogeographic affinities of archaeocyaths point to close similarities with similar assemblages from SW Sardinia and the Montagne Noire (Perejón et al., 1994). A pre-Alpine setting to the north of the North Pyrenean Thrust, so from the Occitan Domain and its lateral prolongation in Sardinia, may be envisaged.

6. Correlation with surrounding domains from North Gondwana

Since the pioneer work of Cavet (1957), the Ediacaran-Lower Ordovician succession of the Pyrenees has been traditionally compared to well-constrained successions from the southern Montagne Noire. These lithostratigraphic correlations between both Variscan massifs have remained, up to recently, the main way to interpolate the age of the Canaveilles and Jujols groups (Cavet, 1957; Laumonier et al., 1996, 2004). The stratigraphic framework of the southern and northern Montagne Noire has recently been updated (Álvaro et al., 1998, 2014) and better constrain based on recent biostratigraphic (Devaere et al., 2013, 2014) and geochronologic studies (et al., in press [artilcle 3]).

The metarhyolite of the Rivernous Formation (542.5±2.4 Ma and 539.2±2.7 Ma in the Avène-Mendic parautochthon; Padel et al., in press [article 3]) and the volcaniclastic breccias and litharenites of the Layrac Formation have been suggested as lateral equivalents of the Fabert and Finestrelles members of the Pic de la Clape Formation in the Eastern Pyrenees, respectively (Padel et al., in prep [article 2]). Underlying both volcanogenic units, the sulfidic black shales and arkoses of the Grandmont (Avène-Mendic parautochthon) and Olette formations (Eastern Pyrenees) are consequently age-correlated, dating their uppermost part as upper Ediacaran. In the same way, a common episode of carbonate productivity can be correlated throughout the overlying Marcou Formation (Cambrian Age 2-3) of the Mélagues unit in the northern Montagne Noire (Devaere et al., 2013) and the Puig Sec Member of the Pic de la Clape Formation (Puigmal unit, Pyrenees). The Valcebollère Formation and, as tentatively suggested above, the Lleret Bayau Formation from the Central Pyrenees, can be

confidently considered as representative of the important Cambrian Age 3-4 episode of carbonate production highlighted by the Lastours and Pardhailhan formations (Devaere et al., 2014). The upper part of the Valcebollère Formation (limestone/shale alternations and monotonous shales bearing carbonate centimetre-thick nodules) is laterally equivalent with the La Tanque-Coulouma transition. A distinct lithological difference between the Eastern Pyrenees and the Montagne Noire is marked by the absence, in the former, of the Guzhangian (regional Languedocian) regression represented by the onset of the Ferrals Formation. This sandstone-dominated formation is absent both in the Eastern Pyrenees and SW Sardinia (Fig. 5). The regression recorded by the input of sandstones marking the uppermost part of the Serdinya Formation (Font Frède Member) may represent the onset of the early Tremadocian regression represented in the Montagne Noire by the La Dentelle Formation.

The 3500-4000 m thick Cambrian-to-Lower Ordovician succession of Sardinia is divided into the Nebida, Gonnessa and Iglesia groups (Cocozza and Gandin, 1991; Pillola et al., 1998). In the Malfatano Cap, the base of the Nebida Group is represented by the polygenic and volcanoclastic Malfatano Conglomerate Member of the Matoppa Formation (Costamagna et al., 2008; Costamagna, 2014). The Bithia Formation, a complex package including metarhyolithes, schists and marbles, underlies these conglomerates at the Malfatano Cap and is commonly presented as the basal unit of the succession (Costamagna et al., 2014). However, age, thickness and contacts of the Bithia Formation are debated (Pillola et al., 1998; Costamagna et al., 2008; Costamagna, 2014). Some biostratigraphic data suggest a Precambrian to earliest Cambrian age (Pittau Demelia and Del Rio, 1982; Gandin et al., 1987; Bechstädt and Boni, 1994), but conventional U-Pb dating (CA-TIMS) of an interlayered magmatic level reported an Ordovician age (Pavaneto et al., 2012). Costamagna et al. (2014) recovered some metamorphised archaeocyaths from the marbles of the Bithia Formation but their poor preservation precludes any precise taxonomic determination. Bechstädt and Schledding (1988) considered the Bithia Formation as a metamorphized tectonic repetition of the overlying formations. The Malfatano Conglomerate Member of the Matopa Formation is considered herein as the base of the Cambrian succession until the enigma of the Bithia Formation is solved. This member is interpreted as reflecting the last stage of the Cadomian Orogeny (Costamagna, 2014). The Malfatano Metaconglomerate is therefore interpreted herein as a possible equivalent of the Finestrelles Member (Eastern Pyrenees) and the Layrac Formation (Montagne Noire). The lower siliciclastic deposits of the Sa Tuvara Member (Matoppa Formation) overly the metaconglomerate, and should represent a lateral equivalent

of the Err (Eastern Pyrenees) and Marcory (Montagne Noire) formations. The upper carbonate and siltstone alternations of the Matoppa Formation have yielded a Cambrian Age 3-4 fauna (Pilllla et al., 1994), which was correlated with the Pardhaillan Formation of Montagne Noire (Álvaro et al., 2010).

The Matoppa Formation is conformably overlain by the Punta Manna Formation, the uppermost heterolithic unit of the Nebida Group. The following Gonnessa Group, mainly composed of massive carbonates bearing reefal complexes, is correlated with the Lastours Formation (Álvaro et al., 2010). The upper part of the Matoppa Formation, the Punta Manna Formation and the Gonnessa Group were deposited during the Cambrian Epoch 2 and are interpreted as lateral equivalents of the Valcebollère and Terrades formations (Fig. 5). The carbonate sequence of the Gonnessa Group is overlain by carbonate-shale alternations and/or nodular limestones grading upward into shales bearing carbonate nodules of the Campo Pisano Formation, a lateral equivalent of the Coulouma Formation (Álvaro et al., 2010) and the upper part of the Valcebollère Formation. The Campo Pisano Formation (Cambrian Series 3 to Lower Ordovician; Pillola et al., 1994) is conformably overlain by the clastic rocks of the Cabitza Formation, correlated herein with the Serdinya but not with any formation of the Montagne Noire, which has recorded the regressive Guzhangian Ferrals Formation (Álvaro et al., 2003, 2007) (Fig. 5). The lack of this regression in the Eastern Pyrenees and SW Sardinia might be related to peneplanation of source areas, unable to yield coarse-grained sediments.

7. Conclusions

The Eastern Pyrenees display a (pre-Sardic) Ediacaran-Lower Ordovician succession similar to neighbouring basins of the eastern branch of the Ibero-Armorican Arc, such as those recorded in the Montagne Noire and SW Sardinia. A distinct volcanic activity is episodically recorded in the Ediacaran Canaveilles Group, characterized by interbedded metabasites and the onset of acidic-dominated volcanosedimentary complexes (Pic de la Clape Formation) which led to development of carbonate production on the top of volcanogenic palaeoreliefs (Puig Sec Member) in the southern (palaeogeographically proximal) part of the Eastern Pyrenees. The influence of the Cadominan Orogeny and development of carbonate platforms across the Ediacaran-Cambrian boundary interval mimics the evolution recorded in the northern Montagne Noire. The Cambrian Series 2 comprises another episode of carbonate production (Valcebollère Formation) similar to those recorded in the Montagne Noire (Pardailhan and Lastours formations) and SW Sardinia (upper part of the Nebida Group and

Gonnessa Group). A distinctive lithology characterizes the Cambrian Series 3, due to the absence of the Guzhangian Ferrals Regression (Montagne Noire) and the dominance of clayey-dominated substrates across Furongian and earliest Tremadocian times (Serdinya and Cabitza formations in the Eastern Pyrenees and SW Sardinia, respectively). Based on acritarchs, we suggest the Font Frède Member as representative of the regressive conditions documented by the onset of the Tremadocian La Dentelle Formation. An unconformable and erosive contact marks the top of the Ediacaran-Lower Ordovician succession, represented in the three Variscan massifs by the onset of the Sardic Phase.

8. References

Abad, A., 1988. El Cámbrico inferior de Terrades (Gerona). Estratigrafía, facies y paleontología. Batallería 2, 47–56

Álvaro, J.J., Vennin, E., 1997. Episodic development of Cambrian eocrinoid-sponge meadows in the Iberian Chains (NE Spain). Facies 37, 49–64.

Álvaro, J.J., Courjault-Radé, P., Chauvel, J.J., Dabard, M.P., Debrenne, F., Feist, R., Pillola, G.L., Vennin, E., Vizcaïno, D., 1998. Nouveau découpage stratigraphique des séries cambriennes des nappes de Pardailhan et du Minervois (versant sud de la Montagne Noire, France). Géologie de la France 1998 (2), 3–12.

Álvaro, J.J., González-Gómez, C., Vizcaïno, D., 2003. Paleogeographic patterns of the Cambrian-Ordovician transition in the southern Montagne Noire (France): preliminary results. Bulletin de la Société géologique de France 174 (3), 23–31.

Álvaro, J.J., Ferretti, F., González-Gómez, C., Serpagli, E., Tortello, M.F., Vecoli, M., Vizcaïno, D., 2007. A review of the Late Cambrian (Furongian) palaeogeography in the western Mediterranean region, NW Gondwana. Earth-Science Reviews 85, 47–81.

Álvaro, J.J., Monceret, E., Monceret, S., Verraes, G., Vizcaïno, D., 2010. Stratigraphic record and palaeogeographic context of the Cambrian Epoch 2 subtropical carbonate platforms and their basinal counterparts in SW Europe, West Gondwana. Bulletin of Geosciences 85, 573–584.

Álvaro, J.J., Bauluz, B., Clausen, S., Devaere, L., Imaz, A.G., Monceret, E., Vizcaïno, D., 2014. Stratigraphy of the Cambrian-Lower Ordovician volcanosedimentary complexes in the northern Montagne Noire, France. Stratigraphy 11, 83–96.

Álvaro, J., Colmenar, J., Monceret, E., Pouclet, A., Vizcaïno, D., 2015. Late Ordovician (post-Sardic) rifting branches in the North Gondwanan Montagne Noire and Mouthoumet massifs of southern France. Tectonophysics 681, 111–123.

Autran, A., Calvet, M., Delmas, M., 2004. Carte géologique de la France (1/50 000), feuille Mont-Louis (1094). BRGM, Orléans.

Barbey, P., Cheilletz, A., Laumonier, B., 2001. The Canigou orthogneiss (Eastern Pyrenees, France, Spain): an Early Ordovician rapakivi granite laccolith and its contact aureole. Comptes Rendus de l'Académie des Sciences, Paris 333, 129–136.

Barnolas, A., Chiron, J.C., 1996. Synthèse géologique et géophysique des Pyrénées. Tome 1: Cycle hercynien. BRGM-ITGE, Orléans-Madrid, 729 p.

Baudin, T., Autran, A., Guitard, G., Laumonier, B., 2008. Carte géologique de la France (1/50 000), feuille Arles-Sur-Tech (1100). BRGM, Orléans.

Bechstädt, T., Schledding, T., Selg, M., 1988. Rise and fall of an isolated, unstable carbonate platform: The Cambrian of Southwestern Sardinia. Geologische Rundschau 77, 389–416.

Bechstädt, T., Boni, M. (eds.), 1994. Sedimentological, stratigraphical and ore deposits field guide of the autochthonous Cambro-Ordovician of Southwestern Sardinia. Servizio Geologico d'Italia. Memorie Descrittive della Carta Geologica d'Italia 48, 434 p.

Calvet, M., Autran, A., Wiazemsky, M., Laumonier, B., Guitard, G., 2012. Carte géol. France (1/50 000), feuille Argelès-sur-Mer – Cerbère (1097-1101). Orléans: BRGM.

Carreras, J., Capella, I., 1994. Structures and tectonics at different lithospheric tectonic levels in the Palaeozoic basement of the Pyrenees: a review and a new interpretation. Journal of Structural Geology 16 (11), 1509–1524.

Carreras, J., Losantos, M., Palau, J., Escuer, J., 1994. Memoria explicativa del mapa geológico de España a escala 1:50.000, hoja de Roses (nº259). ITGE, Madrid.

Carreras, J., Druguet, E., 2013. Illustrated field guide to the geology of Cap de Creus. Universidad Autónoma de Barcelona ed., Barcelona, 123 p.

Casas, J. M., Navidad, M., Castiñeiras, P., Liesa, M., Aguilar, C., Carreras, J., Hofman, M., Gärtner, A., & Linnemann, U., 2015. The Late Neoproterozoic magmatism in the Ediacaran series of the Eastern Pyrenees: new ages and isotope geochemistry. Int. J. Earth Sci. 104, 909–925.

Casas, J.M., Fernández, O., 2007. On the Upper Ordovician unconformity in the Pyrenees: New evidence from the La Cerdanya area. Geologica Acta 5, 193–198.

Casas, J.M., Castiñeiras, P., Navidad, M., Liesa, M., Carreras, J., 2010. New insights into the Late Ordovician magmatism in the Eastern Pyrenees: U–Pb SHRIMP zircon data from the Canigó massif. Gondwana Research 17, 317–324.

Casas, J.M., Palacios, T., 2012. First biostratigraphical constraints on the pre-Upper Ordovician sequences of the Pyrenees based on organic-walled microfossils. Comptes Rendus Geoscience 344, 50–56.

Castiñeiras, P., Navidad, M., Liesa, M., Carreras, J., Casas, J.M., 2008. U-Pb zircon ages (SHRIMP) for Cadomian and Lower Ordovician magmatism in the Eastern Pyrenees: new insights in the pre-Variscan evolution of the northern Gondwana margin. Tectonophysics 461, 228–239.

Cavet, P., 1957. Le Paléozoïque de la zone axiale des Pyrénées orientales françaises entre le Roussillon et l'Andorre. Bulletin du Service de la Carte géologique de France 55, 303–518.

Cirés, J., Domingo, F., Roca, E., Ecuer, J., Sanz, J., 1994a. Memoria explicativa del mapa geológico de España a escala 1:50.000, hoja de Puigcerda (n°217). ITGE, Madrid.

Cirés, J., Morales, V., Liesa, M., Carreras, J., Escuer, J., Pujadas, J., 1994b. Memoria explicativa del mapa geológico de España a escala 1:50.000, hoja de La Jonquera (n°217). ITGE, Madrid.

Cirés, J., Casas, J.M., Muñoz, J.A., Fleta, J., Barbera, M., 1995. Memoria explicativa del mapa geológico de España a escala 1:50.000, hoja de Molló (n°218). ITGE, Madrid.

Cocchio, A.M., 1981. Microflores des séries du Paléozoïques inférieur du massif de Mouthoumet. Etude systématique et comparaison avec les séries des Pyrénées orientales et de la Montagne-Noire. PhD, University of Toulouse (unpublished).

Cochelin, B., Chardon, D., Denèle, Y., Gumiaux, C., Le Bayon, B., in press. Space-time structural relationships between mid- and upper-levels of hot orogenic crust: strain field and kinematics of the Variscan Pyrenees. Tectonics.

Cocherie, A., Baudin, T., Autran, A., Guerrot, C., Fanning, M., Laumonier, B., 2005. U-Pb zircon (ID-TIMS and SHRIMP) evidence for the early Ordovician intrusion of metagranites in the late Proterozoic Canaveilles Group of the Pyrenees and the Montagne Noire (France). Bulletin de la Société géologique de France 176, 269–282.

Cocozza, T., Gandin, A., 1991. Carbonate deposition during early rifting: the Cambrian of Sardinia and the Triassic-Jurassic of Tuscany, Italy. Special Publication of the International Association of Sedimentologists 9, 9–37.

Courtessole, R., 1973**.** Le Cambrien moyen de la Montagne Noire. Biostratigraphie. Imprimerie de la Charite, Montpellier.

Costamagna, L., Cruciani, G. & Franceschelli, M., 2008. The Bithia Formation, upper part of an Infracambrian?–Early Cambrian tecto-sedimentary cycle in Southwestern Sardinia (Italy). Rendiconti della Società Geologica Italiana 3, 272–273.

Costamagna, L.G., 2014. The Capo Malfatano Metaconglomerates in the Early Cambrian of SW Sardinia, Italy: key level for a new stratigraphic setting and evidence of Cadomian tectonics. Zeitschrift der Deutschen Gesellschaft für Geowissenschaften 166, 21–33.

Dégardin, J.M., Alonso, J.L., Bessière, G., Bodin, J., Bouquet, C., Brula, P., Centène, A., Duran, H., Garces-Cocchio A.M., García-López, J., García-Sansegundo, J., Guérangé, B., Julivert, B., Laumonier, B., Losantos, M., Palau, J., Pari, F., Pouit, G., Raymond, D., Richard, P., Sanz, M., Truyols-Massoni, M., Villas, E., 1996. Ordovician supérieur-Silurien. In: Synthèse Géologique et Géophysique des Pyrénées. In: Synthèse géologique et géophysique des Pyrénées. Edition BRGM-ITGE, 1, 211-233.

Deloule, E., Alexandrov, P., Cheilletz, A., Laumonier, B., Barbey, P., 2002. In situ U–Pb zircon ages for Early Ordovician magmatism in the eastern Pyrenees, France: The Canigou orthogneisses. International Journal of Earth Sciences 91, 398–405.

Denèle, Y., Olivier, P., Gleizes, G., Barbey, P., 2009. Decoupling between the middle and upper crust during transpression-related lateral flow: Variscan evolution of the Aston gneiss dome (Pyrenees, France), Tectonophysics 477 (3–4), 244–261.

Devaere, L., Clausen, S., Steiner, M., Álvaro, J.J., Vachard, D., 2013. Chronostratigraphic and palaeogeographic significance of an early Cambrian microfauna from the Heraultia Limestone, northern Montagne Noire, France. Palaeontologia Electronica, 16, 17A, 1–91.

Devaere, L., Clausen, S., Monceret, E., Vizcaïno, D., Vachard, D., Genge, M.C., 2014. The tommotiid *Kelanella* and associated fauna from the early Cambrian of southern Montagne Noire (France): implications for Camenellan phylogeny. Palaeontology 57, 979–1002.

Donzeau, M., Laumonier, B., Guitard, g., Autran, A., Llac, F., Baudin, T., Calvet, M., 2010. Carte géologique de la France (1/50 000), feuille Céret (1096). BRGM, Orléans.

Druguet, E., 2001. Development of high thermal gradients by coeval transpression and magmatism during the Variscan orogeny: insights from the Cap de Creus (Eastern Pyrenees). Tectonophysics, 332, 275-293.

Eeckhout, B., van den, Zwart, H.J., 1988. Hercynian crustal-scale extensional shear zone in the Pyrenees, Geology 16 (2), 135–138.

Fitzgerald, P.G., Muñoz, J.A., Coney, P.J., Baldwin, S.L., 1999. Asymmetric exhumation across the Pyrenean orogen: implications for the tectonic evolution of a collisional orogen. Earth and Planetary Science Letters 173, 157–170.

Gandin, A., Minzoni, N., Courjault-Radé, E., 1987. Shelf to basin transition in the Cambrian-Lower Ordovician of Sardinia (Italy). Geologische Rundschau 76, 827–836.

García-Sansegundo, J., 1992. Estratigrafía y estructura de la Zona Axial pirenaica en la transversal del Valle de Arán y de la Alta Ribagorça. Publicaciones Especiales del Boletín Geológico y Minero de España 102-103, 1–167.

García-Sansegundo, J., Gavaldá, J., Alonso, J.L., 2004. Preuves de la discordance de l'Ordovicien supérieur dans la Zone Axiale des Pyrénées: exemple du Dôme de la Garonne (Espagne, France). Comptes Rendus Geoscience 336, 1035–1040.

García-Sansegundo, J., Poblet, J., Alonso, J.L., Clariana, P., 2011. Hinterland-foreland zonation of the Variscan orogen in the Central Pyrenees: comparison with the northern part of the Iberian Variscan Massif. In: Kinematic Evolution and Structural Styles of Fold-and-Thrust Belts (Poblet, J., Lisle, R.J., eds.). Geological Society, London, Special Publications 349, 169–184.

Guitard, G., Laffite, P., 1956. Sur l'importance et la nature des manifestations volcaniques dans le Paléozoïque inférieur des Pyrénées orientales. Comptes Rendus de l'Académie des Sciences, Paris 242, 2749–2752.

Guitard, G., 1970. Le métamorphisme hercynien mésozonal et les gneiss oeillés du massif du Canigou (Pyréné es orientales). Orlé ans: Mém. B.R.G.M. 63, 353 p.

Guitard, G., Laumonier, B., Autran, A., Bandet, Y., Berger, G.M., 1998. Notice explicative, Carte géologique de la France (1:50.000), feuille Prades (1095). BRGM, Orléans.

Hartevelt, J.J.A., 1970. Geology of the upper Segre and Valira valleys, central Pyrenees, Andorra/Spain. Leidse Geologische Mededelingen 45, 167–236.

Lagabrielle, Y., Labaume, P., Saint-Blanquat, M., 2010. Mantle exhumation, crustal denudation and gravity tectonics during Cretaceous rifting in the Pyrenean realm (SW Europe): insights from the geological setting of the lherzolite bodies. Tectonics 29, TC4012, 1–26.

Laumonier, B., 1988. Les groupes de Canaveilles et de Jujols (''Paléozoïque inférieur'') des Pyrénées orientales – arguments en faveur de l'âge essentiellement Cambrien de ces séries. Hercynica 4, 25–38.

Laumonier, B., 1998. Les Pyrénées centrales et orientales au début du Paléozoïque (Cambrien *s.l.*) : évolution paléogéographique et géodynamique. Geodinamica Acta, 11, 1-11.

Laumonier, B., 2015. Les Pyrénées alpines sud-orientales (France, Espagne) – essai de synthèse. Revue de Géologie pyrénéene 2, 1–44.

Laumonier, B., Autran, A., 2001. Un chevauchement hercynien majeur dans les Pyrénées orientales : le chevauchement du Puigmal. Comptes Rendus de l'Académie des Sciences, Paris (série 2) 332, 585–594.

Laumonier, B., Guitard, G., 1986. Le Paléozoïque inférieur de la moitié orientale de la Zone Axiale des Pyrénées. Essai de synthèse. Comptes Rendus de l'Académie des Sciences, Paris (série 2) 302, 473–478.

Laumonier, B., Abad, A., Alonso, J.L., Baudelot, S., Bessière, G., Besson, M., Bouquet, C., Bourrouilh, R., Brula, P., Carreras, J., Centène, A., Courjault-Radé, R., Courtessole, R., Fauconnier, D., García-Sansegundo, Guitard, G., Moreno-Eiris, E., Perejón, A., Vizcaïno, D., 1996. Cambro–Ordovicien. In: Synthèse géologique et géophysique des Pyrénées. Edition BRGM-ITGE, 1, 157-209

Laumonier B., Autran, A., Barbey, P., Cheilletz, A., Baudin, T., Cocherie, A., Guerrot, C., 2004. Conséquences de l'absence de socle cadomien sur l'âge et la signification des séries pré-varisques (anté-Ordovicien supérieur) du sud de la France (Pyrénées, Montagne Noire). Bulletin de la Société géologique de France 175, 105–117.

Laumonier, B., Marignac, C., Kister, P., 2010. Polymétamorphisme et évolution crustale dans les Pyrénées orientales pendant l'orogenèse varisque au Carbonifère supérieur. Bulletin de la Société géologique de France 181, 411–428.

Laumonier, B., Calvet, M., Wiazemsky, M., Barbey, P., Marignac, C., Lambert, J., Lenoble, J.L., 2015. Notice explicative de la Carte géologique de la France (1/50.000), feuille Céret (1096). BRGM, Orléans.

Laumonier, B., Le Bayon, B., Calvet, M., in press. Carte géologique de la France (1/50 000), feuille Prats-de-Mollo (1099). BRGM, Orléans.

Liesa, M., Carreras, J., Castiñeiras, P., Casas, J.M., Navidad, M., Vila, M., 2011. U-Pb zircon of Ordovician magmatism in the Albera Massif (Eastern Pyrenees). Geologica Acta 9, 93–101.

Llac, F., Autran, A., Guitard, g., Robert, J.F., Gourinard, Y., Santanach, P., 1988. Carte géologique de la France (1/50 000), feuille Saillagouse (1098). BRGM, Orléans.

Losantos, M., Palau, J., Carreras, J., Druguet, E., Santanach, P., Cirés, J., 1997. Mapa geològic de Catalunya, Escala 1:25.000 Fulls: Roses 259-1-1, Cap de Creus, 259-2-1, Far de Roses 259-1-2.

Martínez, F.J., Iriondo, A., Dietsch, C., Aleinikoff, J.N., Peucat, J.J., Cirès, J., Reche, J., Capdevila, R., 2011. U-Pb SHRIMP-RG zircon ages and Nd signature of Lower Paleozoic rifting-related magmatism in the Variscan basement of the Eastern Pyrenees. Lithos 127, 10–23.

Menéndez, S., Perejón, A., Moreno-Eiris, E., 2015. Late Ovetian (Cambrian Series 2, Stage 3) archaeocyathan. biostratigraphy of Spain. Ann. Paléontol.101 (2015) 161–166

Mezger, J. E., 2009. Transpressional tectonic setting during the main Variscan deformation: evidence from four structural levels in the Bossòst and Aston-Hospitalet mantled gneiss domes, central Axial Zone, Pyrenees. Bulletin de la Société géologique de France 180 (3), 199–207.

Muñoz, J.A., Vergés, J., Martínez-Ríus, A., Fleta, J., Pujadas, J., Tosquella, J., Samsó, J.M., Sanz, J., Saula, E., Mató, E., Barberà, M., 1994. Memoria explicativa del mapa geológico de España a escala 1:50.000, hoja de Ripoll (n°256). ITGE, Madrid.

Olivier, P., Druguet, E., Castaño, L.M., Gleizes, G., 2016. Granitoid emplacement by multiple sheeting during Variscan dextral transpression: The Saint-Laurent – La Jonquera pluton (Eastern Pyrenees). Journal of Structural Geology 82, 80–92.

Owen, D.E., 2009. How to use stratigraphic terminology in papers, illustrations, and talks. Stratigraphy 6, 106–116.

Padel, M., Álvaro, J.J., Clausen, S., Guillot, F., Poujol, M., Chichorro, M., Monceret, E., Pereira, M.F., Vizcaïno, D., in press [article 3]. U-Pb laser ablation ICP-MS zircon dating across the Ediacaran–Cambrian transition of the Montagne Noire, southern France. Comptes Rendus Geoscience.

Padel, M., Álvaro, J.J., Sánchez-García, T., Clausen, S., Poujol, M., Laumonier, B., Guillot, F., in prep [article 2]. Cadomian volcanosedimentary complexes across the Ediacaran-Cambrian transition of the Eastern Pyrenees, France and Spain.

Pavanetto, P., Funedda, A., Northrup, C.J., Schmitz, M., Crowley, J., Loi, A., 2012. Structure and U-Pb zircon geochronology in the Variscan foreland of SW Sardinia, Italy. Geological Journal 47, 426–445.

Perejón, A., Moreno-Eiris, E., Abad, A., 1994. Montículos de arqueociatos y calcimicrobios del Cámbrico inferior de Terrades, Gerona (Pirineo oriental, España). Boletín de la Real Sociedad Española de Historia Natural (Sección Geológica) 89, 55–95.

Pillola, G.L., Leone, F., Loi, A., 1998. The Cambrian and Early Ordovician of SW Sardinia. Giornale di Geologia, ser. 3, vol. 60, Special lssue, ECOS VII-Sardinia Guide-book, 25–38.

Pittau Demelia, P., Del Rio, M., 1982. Acritarchi e loro significato stratigrafico nelle successioni paleozoiche della Sardegna. In: Guida alla geologia del Paleozoico sardo (Carmignani, L., Cocozza, T., Ghezzo, C., Pertusati, P.C., Ricci, C.A., eds.). Società Geologica Italiana, 33–35.

Pouclet, A., Álvaro, J.J., Bardintzeff, J.M., Gil Imaz, A, Monceret, E., Vizcaïno, D., 2016. Cambrian-Early Ordovician volcanism across the South Armorican and Occitan Domains of the Variscan Belt in France: Continental break-up and rifting of the northern Gondwana margin. Geosciences Frontiers, doi: 10.1016/j.gsf.2016.03.002.

Roest, W.R., Srivastava, S.P., 1991. Kinematics of the plate boundaries between Eurasia, Iberia and Africa in the North Atlantic from the late Cretaceous to the present. Geology 19, 613–616.

Roussel, J., 1893. Etude stratigraphique des Pyrénées. PhD, University of Lille (unpublished).

Roussel, J., 1904. Tableau stratigraphique des Pyrénées. Bulletin du Service de la Carte géologique de France 15, 97, 199, p. 166.

Santanach, P., 1972. Sobre una discordancia en el Paleozoico inferior de los Pirineos orientales. Acta Geologica Hispánica 5, 129–132.

Sengör, A.M.C., 2013. The Pyrenean Hercynian Keirogen and the Cantabrian Orocline as genetically coupled structures. Journal of Geodynamics 65, 3–21.

Soliva, J., Salel, J.F., Brunel, M., 1989. Shear deformation and emplacement of the gneissic Canigou thrust nappe (Eastern Pyrenees). Geologie en Mijnbouw 68, 357–366.

Vissers, R.L.M., 1992. Variscan extension in the Pyrenees. Tectonics 11 (6), 1369–1384.

Volkova, N.A., 1968. Acritarchs from Precambrian and Cambrian deposits in Estonia. In: Probelmatics of Riphean and Cambrian on the Russian Platform, Urals and Kazakhstan.

Volkova, N.A., Zhuravleva, Z.A., Zabordin, V.Y., Klinger, B.S., (eds.). Akademiya Nauk SSSR, Geologicheskii Istitut, trudy, 188, 8-48.

Wallet, E., Padel, M., Clausen, S., Álvaro, J.J., in prep. Cambrian Stage 3 ‘small shelly fossils’ from the Terrades inlier, Southern Pyrenees: palaeobiogeographic implications.

Zandvliet, J., 1960. The geology of the upper Salat and Pallaresa valleys, Central Pyrenees, France/Spain. Leidse Geologische Mededelingen 25, 1–127.

Zwart, H.J., 1979. The geology of the central Pyrenees. Leidse Geologische Mededelingen 50, 1–74.

Zwart, H.J., 1986. The Variscan geology of the Pyrenees. Tectonophysics 129, 9–27.

3 Complexes volcanosédimentaires cadomiens de la transition Ediacarien-Cambrien des Pyrénées Orientales, France et Espagne. [Article 2]

Cadomian volcanosedimentary complexes across the Ediacaran−Cambrian transition of the Eastern Pyrenees, France and Spain

Maxime Padel[1]*, J. Javier Álvaro[2] , Teresa Sánchez-García[3], Sébastien Clausen[1], Bernard Laumonier [4], François Guillot[5] and Marc Poujol[6]

[1]UMR 8198 EEP CNRS, Université de Lille 1, Bâtiment SN5, Avenue Paul Langevin, 59655 Villeneuve d'Ascq Cedex, France, maxime.padel@etudiant.univ-lille1.fr and sebastien.clausen@univ-lille1.fr

[2]Instituto de Geociencias (CSIC-UCM), Novais 12, 28040 Madrid, Spain, jj.alvaro@csic.es

[3] IGME, Ríos Rosas 23, 28003 Madrid, Spain.

[4]Université de Lorraine, GeoRessources, École des Mines, CS 14234, F-54042 Nancy Cedex, France ; bernard.laumonier@univ-lorraine.fr

100 avenue du Général Leclerc, 54000 Nancy, France ; blaumonier@wanadoo.fr

[5]UMR 8187 LOG CNRS, Univ. Lille-Univ. Littotal Côte d'Opale, SN5 Sciences de la Terre, 59655 Villeneuve d'Ascq Cedex, France, e-mail: Francois.Guillot@univ-lille1.fr

[6]Géosciences Rennes, UMR 6118, Université de Rennes1, Campus de Beaulieu, 35042 Rennes, France, e-mail: marc.poujol@univ-rennes1.fr

* Corresponding author

Abstract

The volcanism embedded in the Ediacaran Canaveilles Group of the Eastern Pyrenees displays two distinct geochemical affinities: (i) the metabasites of the Nyer and Olette formations reflects the emplacement of a tholeiitic magmatism linked to extensional conditions; whereas (ii) the acidic and calk-alkaline magmatism recorded at the top of the Olette Formation and in the overlying Fabert and Finestrelles members (Pic de la Clape Formation) is representative of the Cadomian orogeny. A distinct diachronism can be outlined following a SW-NE trending throughout West Gondwana. Pan-African and Cadomian deformation is recorded in outer peri-Gondwanan margins (e.g. Anti-Atlas, Ossa-Morena, Cantabrian and West Asturian-Leonese Zones, and North- and Central-Armorican Domains), whereas it is absent in back-arc settings (Central Iberian Zone) and in some inner peri-

Gonwanan margins (Montagne Noire and Pyrenees). Despite the absence of deformation, the latter inner margins have recorded a delayed SW-NE trending of Cadomian-related, calk-alkaline, acidic volcanism. This is represented by the Fabert and Finestrelles members cropping out in the Puigmal and Cap de Creus units of the Eastern Pyrenees. There, three volcanosedimentary edifices can be identified based on palaeotopography and distance from the sources, the so-called Creus (ca. 577-558 Ma), Fabert-Tregurà-Finestrelles (ca. 559−552 Ma) and Pic de la Clape (ca. 542−532 Ma) edifices. The top of the palaeorelief formed by the two latter edifices recorded the nucleation of centres of microbial carbonate productivity (Puig Sec Member) linked to synsedimentary fissuring (unstable substrates) and karstification. The presence of carbonate production across the Ediacaran–Cambrian transition is exclusively located in areas far from the Cadomian subduction and devoid of significant terrigenous input, such as those reported in the Eastern Pyrenees and the northern Montagne Noire.
Keywords: stratigraphy, carbonate production, volcanism, geochemistry, Gondwana.

1. Introduction

In West Gondwana, the Ediacaran−Cambrian transition is characterized by the onset and aftermath of the Pan-African, Cadomian and Avalonian orogenies (Ballèvre et al., 2001; Kroner and Stern, 2004; Murphy et al., 2004), recording an arc-to-rift transition (Linnemann et al., 2007, 2008, 2014; Álvaro et al., 2014a; Pouclet et al., 2016) by the way of strike-slip and transform faults (Murphy et al., 1999; Nance et al., 2002; Keppie et al., 2003). The Cadomian Orogeny is differently recorded in the southwestern (Iberian Massif) and northeastern (North-, Central and South-Armorican Domains, Occitan Domain and Pyrenees) branches of the Variscan Ibero-Armorican Arc. A distinct angular discordance is recorded in the former branch (except in the Central-Iberian Zone, interpreted as a back-arc setting; Bandrés et al., 2002; Pereira et al., 2011) and the outer margin of the latter (North- and Central Armorican Domains), whereas the Ediacaran−Cambrian transition is conformable in the inner margin of the eastern branch (Ballèvre et al., 2001; Álvaro et al., 2014b; Pouclet et al., 2016).

Despite the recent publication of numerous U−Pb zircon dates from the Pyrenees (e.g., Cocherie et al., 2005; Castiñeiras et al., 2008; Casas et al., 2015), the age of some Cadomian-related volcanosedimentary complexes remains contentious, many of their correlations are still exclusively based on lithostratigraphic comparisons, and the record of the Cadomian

Orogeny far from the subduction sutures (such as those preserved in the Anti-Atlas, Ossa-Morena and Armorican Massif) is still incompletely understood. In the Eastern Pyrenees, these volcanogenic levels have served as reliable markers for correlation along short distances, but they are subject to drastic facies changes and intertonguing relationships.

A stratigraphic framework of acidic volcanosedimentary complexes associated with subsidiary basic lava flows and centres of carbonate production has been recently proposed by Laumonier et al. (2004, 2015) for the Eastern Pyrenees. Unfortunately, U−Pb dating of their related zircon grains has yielded some confusion in what was considered a handful of stratigraphic marker beds encompassing a geochronological interval of ca. 32 m.y. (580−548 Ma; Cocherie et al., 2005; Castiñeiras et al., 2008; Casas et al., 2015). A revision of previous radiometric ages, completed with new U−Pb dating of zircon by LA−ICP−MS, seemed necessary to understand the volcanogenic record preserved in the Eastern Pyrenees across the Ediacaran−Cambrian transition. The aim of this paper is to examine the stratigraphy, sedimentology and geochemistry of the volcanosedimentary complexes that separate the Canaveilles and Jujols groups in the Eastern Pyrenees, completed with new U−Pb zircon dating of key volcaniclastic levels arranged in an updated stratigraphic framework, as a geodynamic refining of the Cadomian influence in the Eastern Pyrenees.

2. Geological setting and stratigraphy

The Eastern Pyrenees is the repository of a thick Ediacaran−Cambrian record. These rocks are part of the Variscan basement and mainly crop out in the eastern part of its axial zone, from the Mediterranean Sea to the Noguera-Pallaresa valley (Laumonier et al., 1996). The dominance of unfossiliferous fine-grained siliciclastic sediments interrupted by marbles and scattered igneous rocks has rendered correlation and dating difficult (Laumonier et al., 1996, 2004; Deloule et al., 2002; Cocherie et al., 2005; Liesa et al., 2011; Martínez et al., 2011). Despite the localized strong penetrative strain and regional greenschist-to-amphibolite facies metamorphism, delicate primary fabrics and textures are locally still preserved. The implications of lithostratigraphic variation to the geodynamic history of the Ediacaran−Cambrian transition have recently been the focus of reconnaissance geological mapping (Baudin et al., 2008; Donzeau et al., 2010; Laumonier et al., 2015, in press) and the "Référentiel Géologique de France" Program led by the French Geological Survey (BRGM). These differentiated several feldspar-rich tuffs and tuffites (or "micro-granulés") and

volcanosedimentary bodies (referred in the geological maps to VS1-VS2 marker levels and Tregurà Formation, respectively) recognized in the Puigmal, Vallespir, Roc de France and Albères tectonostratigraphic units (Fig. 1).

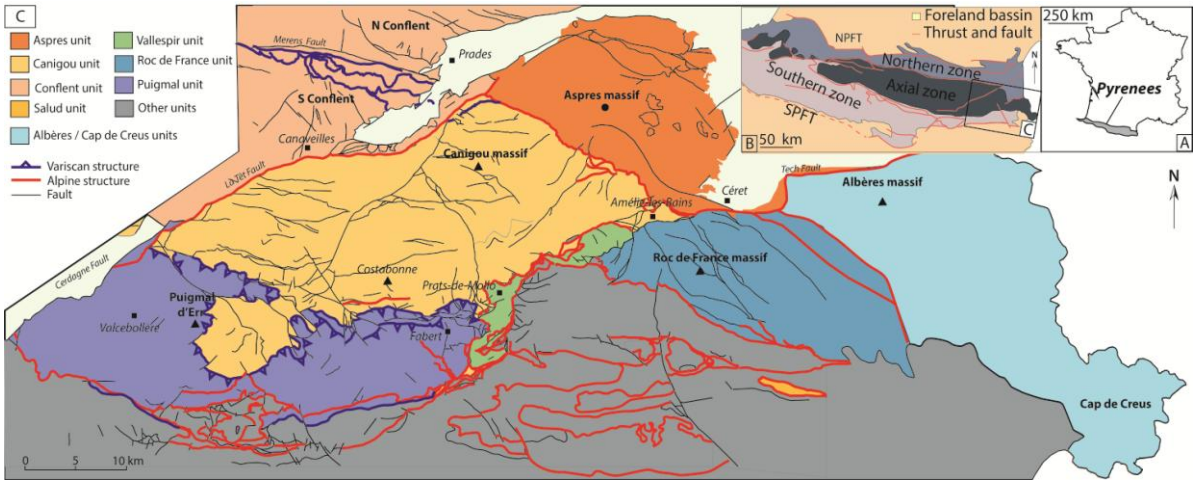

Fig. 1 : Geological sketch of the Eastern Pyrenees. A. Pre−Variscan exposures of the Pyrenees marking the French/Spanish border. B. Main tectonostratigraphic units of the Eastern Pyrenees. SPFT: South Pyrenean Frontal Thrust, NPFT: North Pyrenean Frontal Thrust. C. Variscan and Alpine tectonostratigraphic units of the Eastern Pyrenees, named Albères-Cap de Creus, Aspres, Canigou, Conflent, Puigmal, Roc de France and Vallespir; modified from Baudin et al. (2008) and Laumonier et al. (2015).

The traditional subdivision of the Ediacaran−Cambrian succession into the Canaveilles and Jujols groups (Cavet, 1957; Laumonier et al., 1996, 2004, 2015) reflects an inherited stratigraphic framework based on the supposed intrusion of Cadomian granitic plutons surrounded by gneissic aureoles that, in the Canigou/Canigó massif and the Freser dome (Puigmal unit), were definitively dated as Mid−Late Ordovician and related to the Sardic Phase (Casas et al., 2010; Martínez et al., 2011). The resulting Canaveilles Group, the base of which is irregularly intruded by Ordovician and Variscan granitoids (Deloule et al., 2002; Cocherie et al., 2005; Liesa et al., 2011; Martínez et al., 2011), is a micaschist-dominated succession locally punctuated by marbles, acidic tuffs and metabasites of the Nyer Formation (Laumonier et al., 1996, 2004). A metarhyodacite (VS1 *sensu* Laumonier et al., 2015) dated at 581±10 Ma by Cocherie et al. (2005) was subsequently reinterpreted (with the same data) at ca. 545 Ma by Castiñeiras et al. (2008). The uppermost part of the Canaveilles Group, the so-called Olette Formation, is a monotonous shaly succession bearing subsidiary local feldspar-rich tuffs, which have yielded variable U−Pb zircon ages, ranging from ca. 575 Ma in the Puigmal unit (Casas et al., 2015) to 548±8 Ma in the Roc de France unit, and 560±11 Ma in the Cap de Creus (Castiñeiras et al., 2008). Despite the different U−Pb methods

followed by the authors, this handful of ages pointed to a succession of volcanic pulsations throughout the late Ediacaran.

In the Puigmal unit, the top of the Olette Formation is marked by the occurrence of metre- to hectometre-thick volcanic and volcanosedimentary units, surrounded and capped by the shale-dominated Err Formation (Jujols Group). Due to the proliferation of local toponymies to differentiate local lithostratigraphic terms (Laumonier et al., 1996, 2004, 2015, in press), we propose to name this volcanosedimentary complex the Pic de la Clape Formation (stratotype at its homonymous hill: 42°23'47.64"N; 2°26'40.99"E), and subdivide it, from bottom to top, into the Fabert, Finestrelles, and Puig Sec members. Their respective names refer to their homonymous stratotypes (Fig. 2). The Fabert metarhyolites (VS2 *sensu* Laumonier et al., 2015) crop out in the Puigmal, Vallespir, Roc de France and Albères-Cap de Creus units. The Finestrelles volcanosedimentary bodies occur south and southeast of the Canigou massif: from Cerdagne to Cap de Creus in the Vallespir unit and at Cap Cerbère in the Albère unit (Laumonier et al., 1996, in press; Baudin et al., 2008). The Puig Sec Limestone appears in the Puigmal unit, from Mollo village to Pic de la Clape. The Pic de la Clape Formation intertongues northward and is not recognisable in the Aspres and Conflents tectonostratigraphic units (Figs. 1-2). As a result, the Canaveilles/Jujols contact cannot be precisely recognized outside the Puigmal, Vallespir, Roc de France and Albère units.

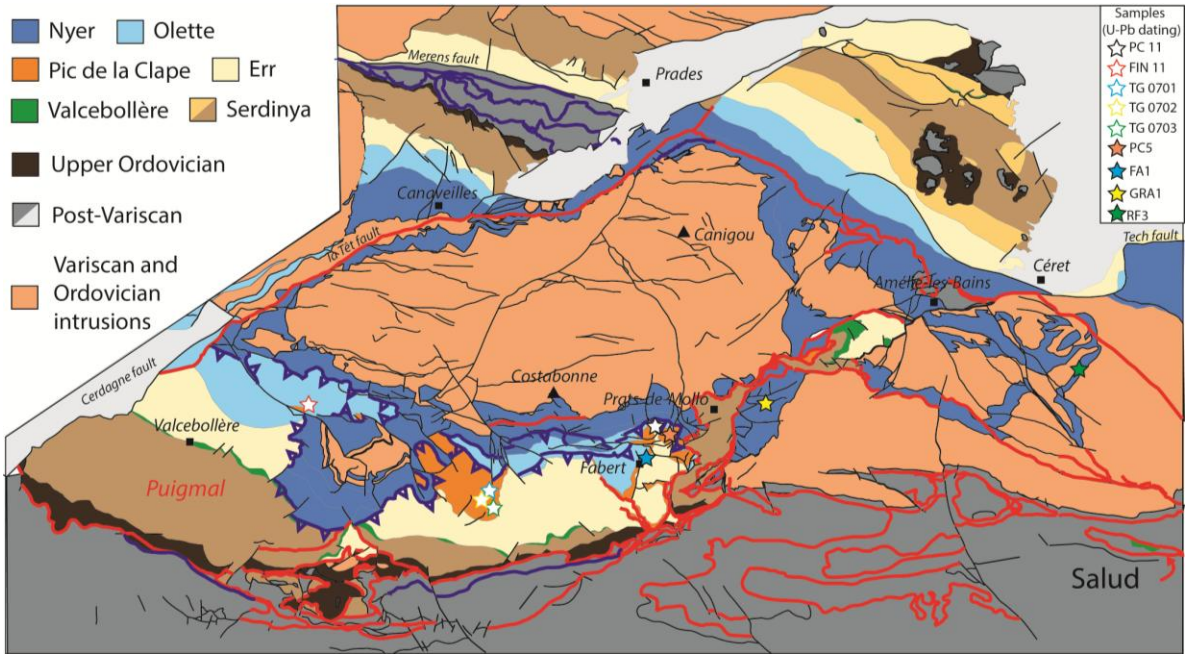

Fig. 2 : Setting of the study samples in the tectonostratigraphic units surrounding the Canigou/Canigó Massif; modified from Laumonier et al. (2015).

3. Material and methods

The heterolithic Pic de la Clape Formation has been studied and sampled at four localities of the Puigmal unit, which are, from west to east: Pic du Finestrelles, along the road GIV-5265 in the vicinity of Tregurà village (locality sampled by Casas et al., 2015), the Fabert village, and the Pic de la Clape summit (Fig. 2).

Geochemical data are based on 17 chemical analyses of representative volcanic samples (Table 1). Major, trace, and rare-earth elements were determined using X-ray fluorescence and inductively coupled plasma mass spectrometry (ICP-MS) at AcmeLabs, Canada. Precision for major, trace and rare elements is usually better than 2%, 5−10% and 3−7%, respectively.

Zircon separation from fresh volcanogenic samples started with rock grinding using a steel crusher. The resulting powders were sieved in the range 50–250 µm. Grains were separated first using heavy liquid (sodium heteropolytungstates 2.85 g.cm-3 density), then using Frantz magnetic separator. Following Sláma and Košler (2012), the selected grains were obtained from random hand-picking under binocular microscope whatever their size, shape, or colour in order to avoid any operator bias. They were finally set in an epoxy resin puck and polished to expose their core.

U−Pb dating of zircon was determined by Laser ablation inductively coupled with plasma source mass spectrometry (LA−ICP−MS) at the Geosciences Laboratory, Rennes. The methodology for data treatment and analytical process are detailed in Padel et al. (in press). All data and analytical results are presented in the supplementary data. Concordia age is obtained using the Isoplot 3.75 software (Ludwig, 2012) and plotted in an inverse Terra-Wasserburg diagram. Associated to the Concordia Age, the mean square weighted deviation (MSWD) is statistic index calculated which should be around 1 to insure a valuable age (Wendt and Carl, 1991). If MSWD > $1+2(2/f)^{1/2}$ at 2σ, where f is the degree of freedom (Wendt and Carl, 1991), the calculated age have to be rejected. For U–Pb dating, f=n–1, where n is the number of dating use to calculate the age, condition to respect this rules is detailed by Spencer et al. (2016).

Probability density plot are built using density plotter (Vermeesch, 2004). $^{207}Pb/^{206}Pb$ ages are used for U−Pb analysis giving an age older than 1000 Ma when $^{206}Pb/^{238}U$ ages are preferred for U−Pb analysis yielding an age younger than 1000 Ma. Only analysis include in the [90−110] concordance interval are considering for the interpretations. The depositional

age is given for a cluster age including at least 3 concordant ages. In sedimentary rock samples, about 110 grains were analysed in order to get the best representation of the detrital zircon populations. For volcanic level more than 50 grains were analyzed, following Bowring et al. (2006). Ages of tuffs were calculated using the TuffZirc Age algorithm (Ludwig and Mundil, 2002) and compared with the Concordia Age.

4. Facies associations

As stated above, the Pic de la Clape Formation is a heterolithic succession composed, from bottom to top, of the Fabert Metarhyolite, the Finestrelles Volcanosedimentary Complex and the Puig Sec Limestone members (Figs. 3–4). Their facies and sedimentological interpretations are reported below.

4.1 Fabert metarhyolites

Firstly described by Guitard and Laffite (1956), the Fabert Member crops out south of the Canigou Massif, from the vicinity of the homonymous village to the Pic de la Clape summit. In a detailed petrographic description, Guitard (1970) described this unit (named "gneiss granulé" by Guitard and Laffite, 1956), as a metamorphic rock derived from a volcanic or volcanosedimentary protolith, displaying a lapilli structure and a high-to-medium content of SiO_2 (~ 64%; Guitard, 1970). Subsequently, the term "gneiss granulé" has been broadly used in the description of these and other acidic levels with similar macroscopic aspect interbedded in the Canaveilles Group (Casas et al., 1986; Cirés et al., 1995; Laumonier et al., 1996, 2004).

The member is massive, lenticular-shaped (intertonguing toward the NE and SW) and up to 50 m thick. At the Pic de la Clape summit, the member contains rare intraformational breccias and fine- to medium-grained arkose, black shale and basic lava flow interbeds (Fig. 5A). The latter interbeds are the source of some mafic clast lags, which occur lining scouring contacts

Similar metarhyolites and metabasite interbeds have been described in the underlying Nyer and Olette formations of the Canaveilles Group, but their age and relationship with host rock remain uncertain (Casas et al., 1986; Navidad et al., 1996; Navidad and Carreras, 2002; Castiñeiras et al., 2008).

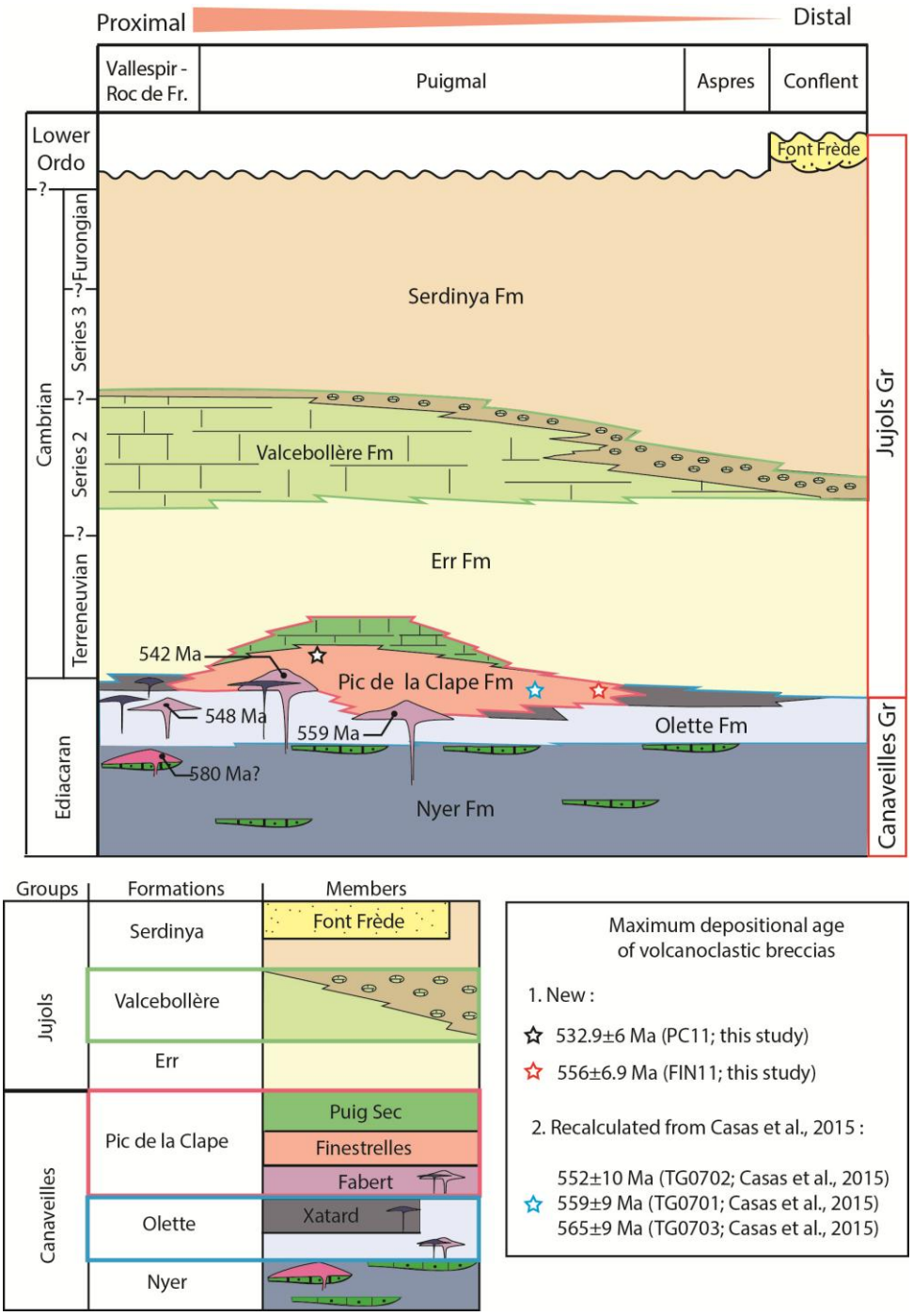

Fig. 3 : Stratigraphic chart of the Canaveilles and Jujols groups in the Eastern Pyrenees.

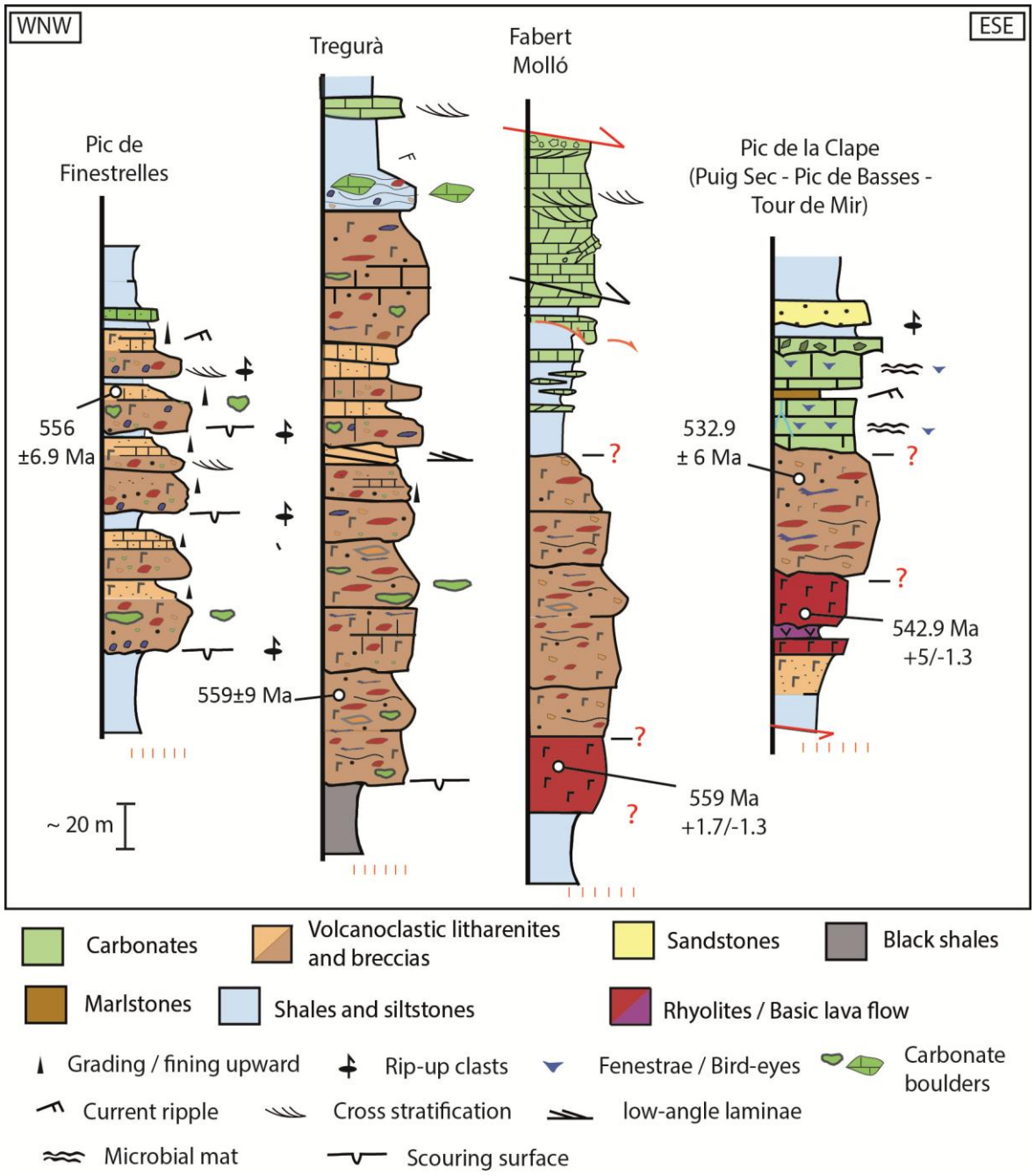

Fig. 4 : Stratigraphic logs of the Pic de la Clape Formation reported in the text; for a tectonostratigraphic setting, see Figure 2.

4.2 Finestrelles volcanosedimentary complex

The heterolithic Finestrelles Member, up to 500 m thick in the Puigmal unit, is not stratiform but displays an irregular geometry: it (para)conformably overlies either the Olette Formation or the Fabert Member, and is onlapped by both the Puig Sec Member and the Err Formation (Jujols Group) (Fig. 3). The member consists of volcanoclastic breccias, tuffaceous

sandstones and siltstones, and is locally punctuated by shale, litharenite and pristine-to-volcaniclastic limestone interbeds (Fig. 5B–F). Thicker beds are dominated by volcanoclastic breccias, whereas the remaining facies are more abundant in thinner lenses.

Lithofacies and their distribution are mainly heterogeneous, with exposures of varying composition and facies interlayered on a 10−100 m scale and displaying complex interfingering relationships. Heterolithic volcaniclastic breccias are the most characteristic facies, which typically occur as thick (>10 m), matrix-supported and structureless units separated by thin (<1 m) clast-supported volcaniclastic breccias, and tuffaceous sandstones and siltstones (Fig. 5G–H). Breccias (>25% blocks) contain angular-to-subrounded volcaniclasts, centimetric to pluridecimetric in size. Clasts are polygenic and dominated by unsorted, composite (polyphasic) volcaniclasts, although carbonate, sandy and shaly clasts are locally abundant (Fig. 6–B). The tuffaceous matrix is rich in subrounded quartz and feldspar-rich siltstone, irregularly cemented with sparry calcite and dolomite (Fig. 6C–D). Rusty rhyolitic clasts are common in the lower part of the member suggesting local reworking and erosion of a rhyolitic basement (Fabert Member).

Despite the massive aspect of the breccias, distinct intra-breccia scouring contacts are locally common. They are capped with heterolithic lags with normal grading. The sharp scouring base of some breccias and litharenitic sandstones is highlighted by the presence of rip-up clasts sourced from interbedded shales. At the Pic du Finestrelles, some metre-scale volcaniclastic breccia and tuffaceous sandstone strata fine upward and are interrupted by laminated shale interbeds, up to 0.5 m thick. Fine- to medium-grained litharenitic interbeds are poorly sorted, lenticular in shape and display cross- to low-angle stratification and parallel lamination (Fig. 5G–H). In the vicinity of Tregurà village and at the Pic du Finestrelles, several decimetre-thick interbeds are volcaniclastic-rich to pristine sparry limestones, grading both laterally and vertically into litharenites rich in sparry (poikilotopic) calcite and dolomite cement (Fig. 6C–E). In the same areas, the uppermost part of the member contains subrounded carbonate granules and boulders (up to 2 m in size) “floating” in a shaly-to-tuffaceous matrix. Some carbonate boulders show injection dykes infilled with host sediment. In contrast, between Fabert and Pic de la Clape, the volcanoclastic breccias and tuffaceous sandstones are free of both carbonate matrix and clasts. Glassy textures (fiammes or shards) have been locally described near Tregurà (Casas et al., 2015).

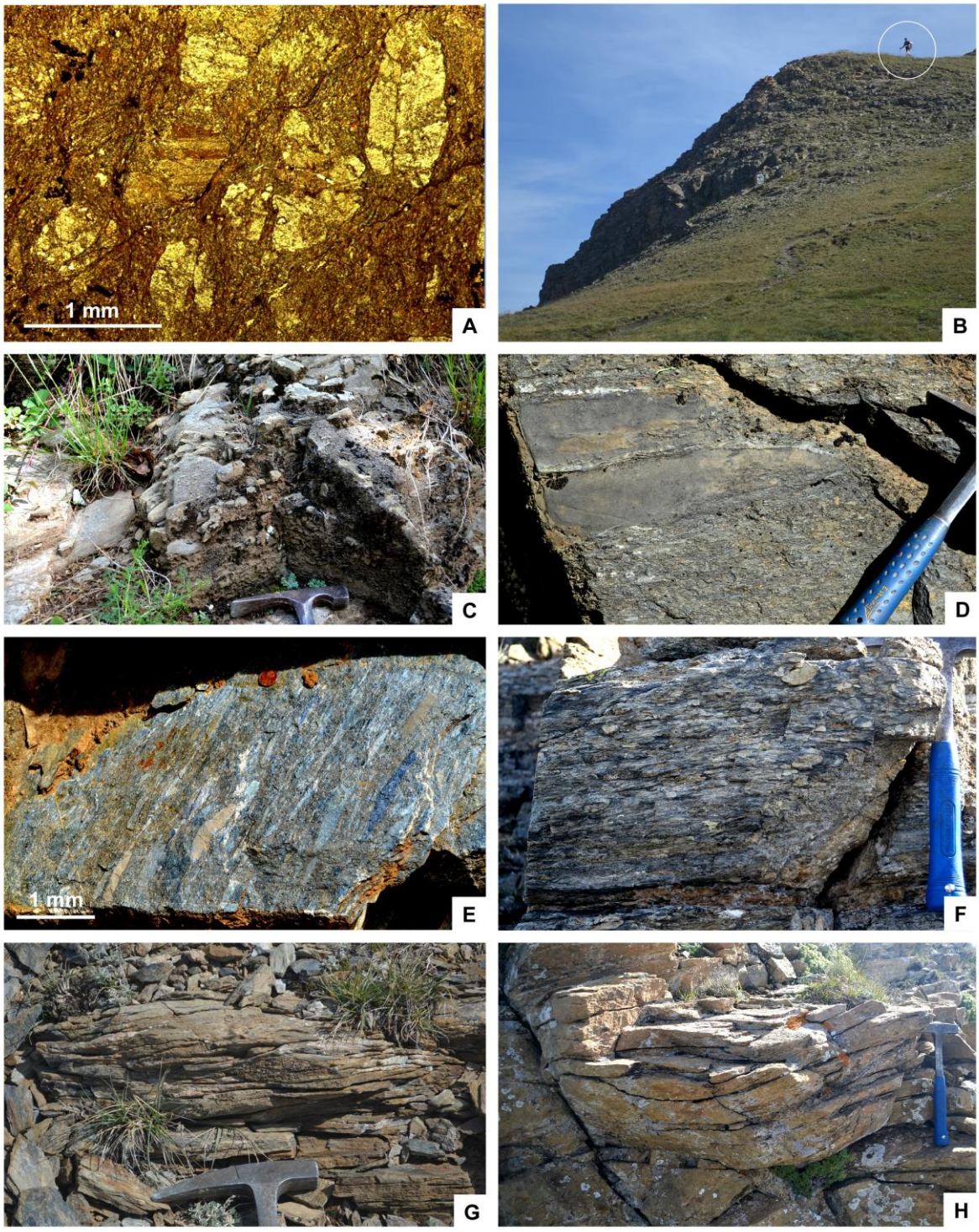

Fig. 5 : A. Thin-section photomicrograph of the basic lava interflow embedded in the metarhyolites of the Fabert Member at Pic de la Clape. B. Exposure of the Finestrelles Member at its homonymous stratotype upside down. C. Weathered breccias of the Finestrelles Member at Tregurà. D-F. Field aspect of the Finestrelles unsorted breccias at Tregurà (D-E) and Finestrelles (F). G-H. Trough cross-stratified sets of tuffaceous sandstones at the Finestrelles stratotype.

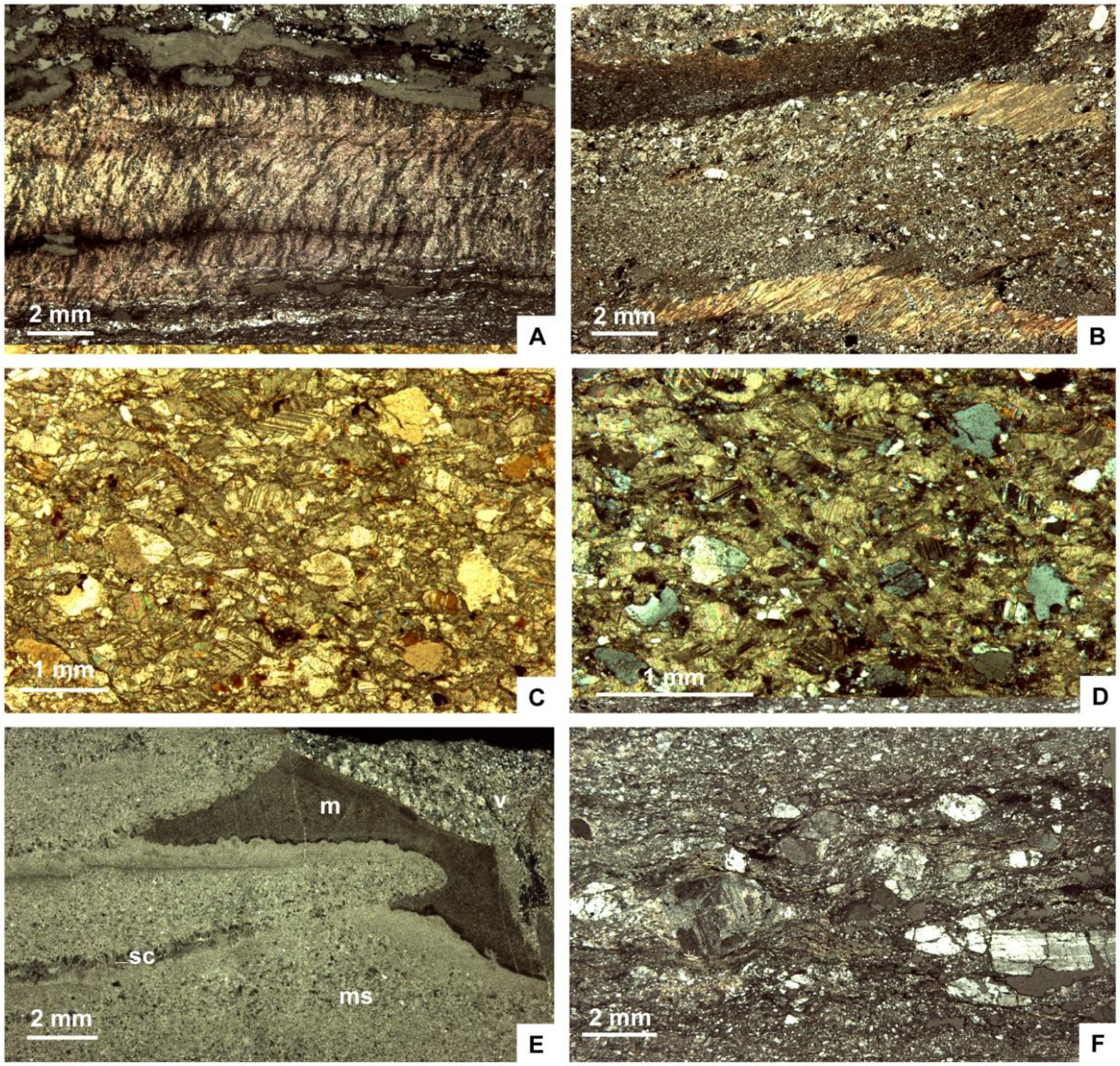

Fig. 6 : Thin-section photomicrographs of the Finestrelles Member. A-B. Schist clasts derived from the underlying Olette Formation exhibiting crenulated cleavage and embedded in a tuffaceous silty matrix at Tregurà. C-D. Sparry limestone comprising scattered quartz and feldspar phenocrysts at Finestrelles; parallel light and cross polarized light, respectively. E. Limestone granule showing alternations of microsparite (ms) and sparry crusts, partially surrounded by micrite (m), encased in a volcanosedimentary matrix (v); Finestrelles, F. Feldspar-rich tuff ("granulé") embedded in shales at Finestrelles.

The dominated massive and structureless, matrix-supported fabric of the Finestrelles Member, containing poorly sorted, angular to subrounded, polygenic and polyphasic clasts, and local presence of mafic and rusty rhyolitic clasts are consistent with deposition from volcaniclastic debris flows. The fluidal-pumiceous or amoeboid clasts and fiammes described by Casas et al. (2015) inside the volcanoclastic breccias are considered as evidence of hot emplacement of pyroclastic deposits (Bull and McPhie, 2007). Carbonate boulders displaying injection dykes infilled with host sediment attest that the clasts were not yet lithified during

deposition. Although the presence of euhedral or broken single crystals suggests these deposits were originally deposited as pyroclastic debris (Fig. 6F), the final facies point to reworking before definitive subaqueous deposition.

Such kind of syneruptive, resedimentary ("cannibalistic") deposition reflects slope-related, downslope instability from the site of eruption and episodes of mass-wasting volcanic explosive eruptions. Dominance of volcaniclastic debris in resedimentary syneruptive units with abrupt vertical and lateral facies changes and overall poorly bedded nature prone to mass-wasting and reworking of pyroclastic debris. Slope aprons may be associated with active syndepositional faulting in the vicinity of volcanic centres recording alternation of explosive (acidic) and calm (mafic) emplacements in a marine setting.

The presence of both interbedded pristine-to-volcaniclastic limestones and tuffaceous sandstones rich in calcite/dolomite cements points to development of carbonate productivity, episodically interrupted by successive syneruptive pulsations. Locally, the Finestrelles Member displays the record of reworked subrounded carbonate granules and boulders linked to contemporaneous development of carbonate factories leading to the onset of irregular palaeoreliefs capped by centres of carbonate production (both older and laterally equivalent to the carbonate-dominated Puig Sec Member), then destabilized by tectono-volcanic events and included in the debris avalanche deposits.

4.3 The Puig Sec limestone

This member, up to 180 m thick, consists of massive-to-bedded limestones and marbles, locally dolomitized. The main features are the abundance of fenestral (birdseyes cemented by drusy and equant calcite cements) fabrics interrupted by polygonal mudcracks and tepee structures infilled with brownish silty sediment (Fig. 7A–D). Karstic pockets infilled with brownish marlstones rich in illite (after XRD analysis) and intraformational breccia, crosscut with synsedimentary fissuring, are significant in the Col d'Ares stratotype (Fig. 8A–F). Subsidiary sparry layers and peloidal wackestones/packstones show parallel to low-angle lamination. Microstromatolitic laminae are locally interrupted by clotted textures mimicking complex cauliflower-like fabrics (Fig. 9A–G). In contrast, in the lower part of the stratotype and in the vicinity of Mollo village, the bedded limestones display interbedded lenses with scouring contacts and grading of intraclastic rip-up clasts, up to 1.2 m thick. These are characterized by the abundance of trough and planar cross-bedding, and low-angle and parallel laminae.

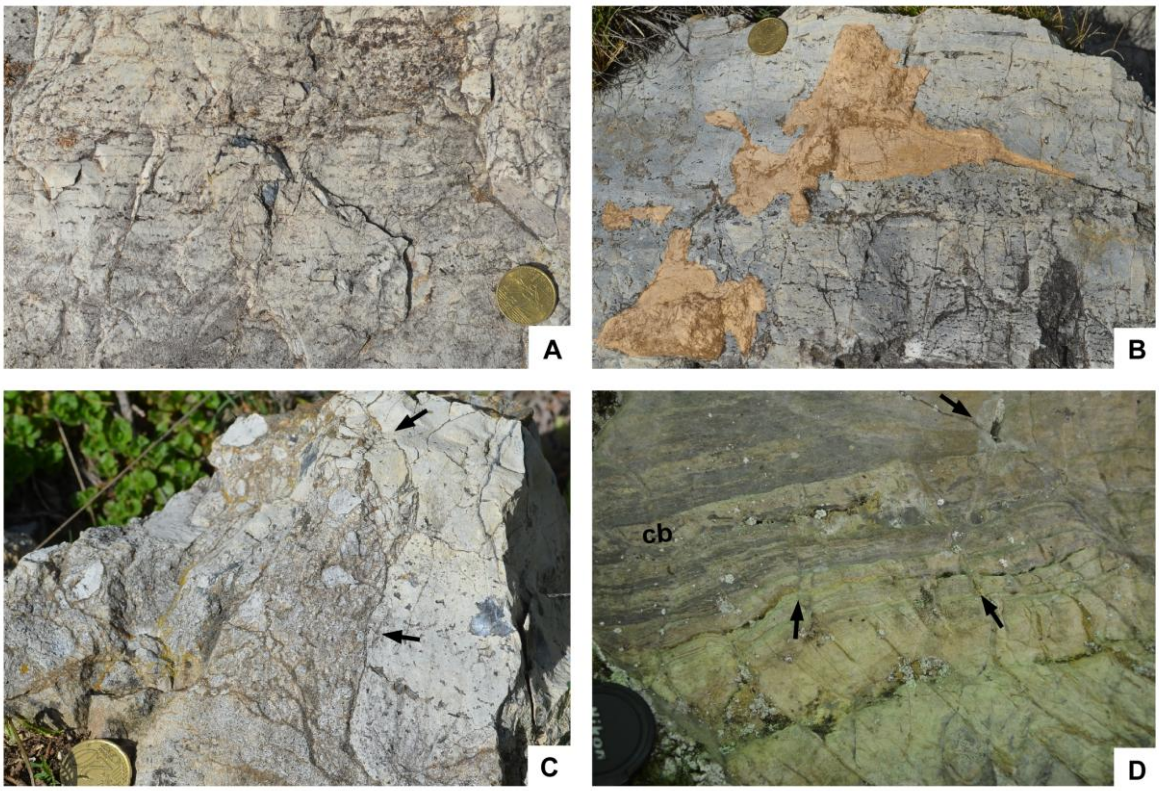

Fig. 7 : Sedimentary structures preserved in the Puig Sec Member at its stratotype of Col d'Ares. A. Fenestral limestone exhibiting parallel laminae. B. Fenestral limestone with disturbed pockets (false orange) infilled with contorted and intraformational breccia. C. Arrowed contact of breccia infill crosscutting the pristine fenestral limestone. D. Contorted lamination (cb) showing disturbed tepee structures, affected by synsedimentary fissures and microfaults (arrowed)

The facies association described at the stratotype and at Tour du Mir represents the establishment of peritidal environments, rich in microbial mats and biofilms, episodically submitted to subaerial exposure, karstic emplacement and synsedimentary fissuring; fenestrae and birdseyes are interpreted as release of fluids by organic decay. The interbedded limestones found in Mollo and the lower part of the stratotype point to episodic development of shoal barriers protecting the above-reported peritidal environments. As a result, a retrogradational trend of shoal barrier complexes protecting (back-barrier) peritidal environments can be suggested migrating centripetally throughout elevated areas of the Finestrelles composite palaeorelief.

5. Magmatic affinity of volcanic products: preliminary results

17 new geochemical analyses are compared with those reported by Navidad et al. (1996) from Roc de Frausa and Navidad and Carreras (2002) from the Canigou massif.

Unfortunately, the stratigraphic control of their samples is not well constrained and complete descriptions about their relationship with the host rock (lava flow, sill or dyke) and their pre-, syn- or post−Sardic setting are not available. As a result, the previous dataset (included in Table 1) should be considered with caution. In addition, data from the Canigou massif are necessarily incorrect because they do not fit with the geochemical diagrams published in the same paper. In order to check the validity of these data, we sampled again the lower part of the Canaveilles Group in the Puigmal area (Canigou unit; samples JM, Pir and Pyr).

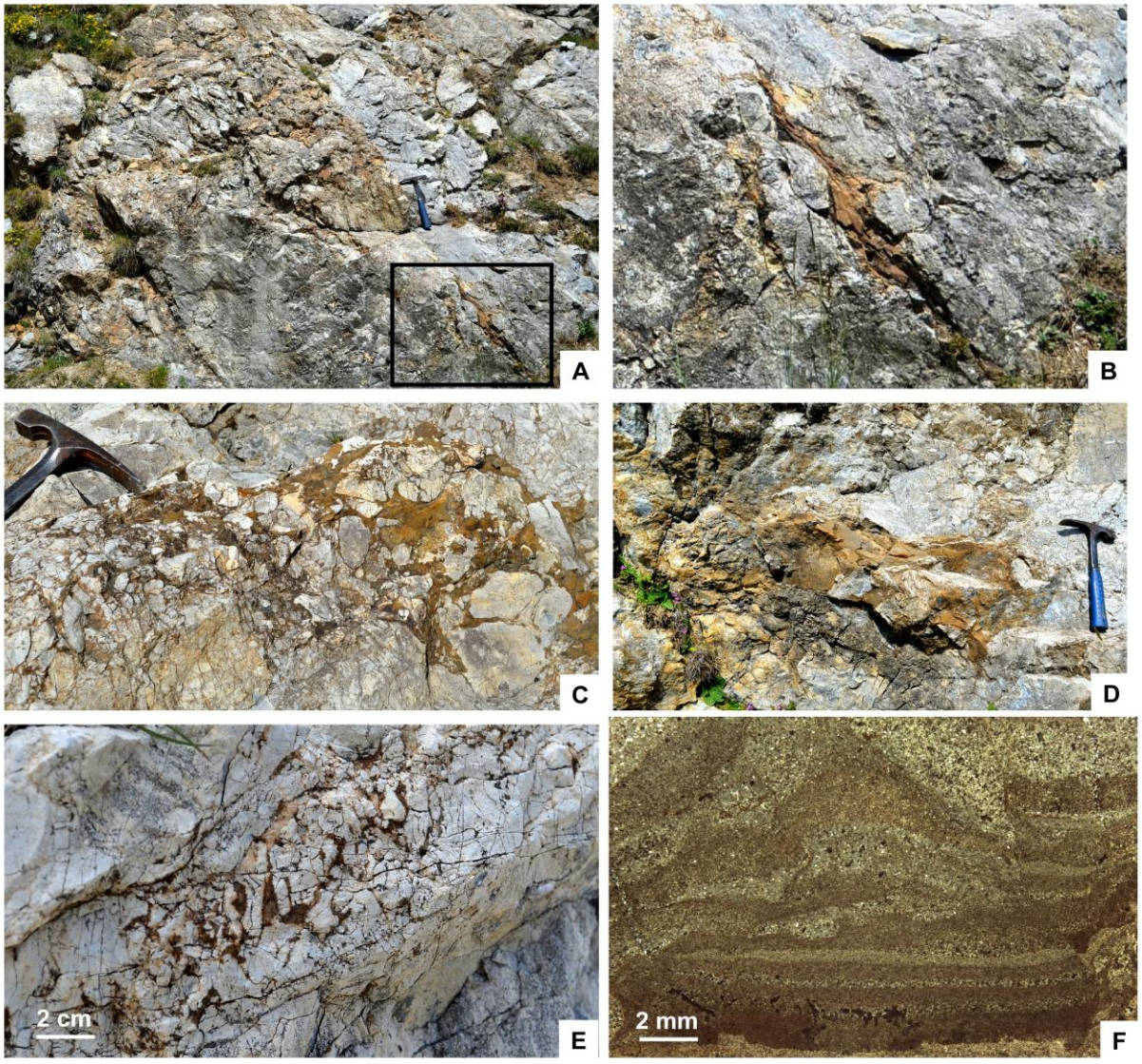

Fig. 8 : Karstic features of the Puig Sec Member at its stratotype of Col d'Ares. A. Karstic cavity complex with sealed top (close to hammer) and lower digitations. B. Detail of boxed area in previous picture. C-E. Breccia-to-conglomerate intraformational infill. F. Karstic infill composed of banded illite-rich marlstone affected by synsedimentary fissuring.

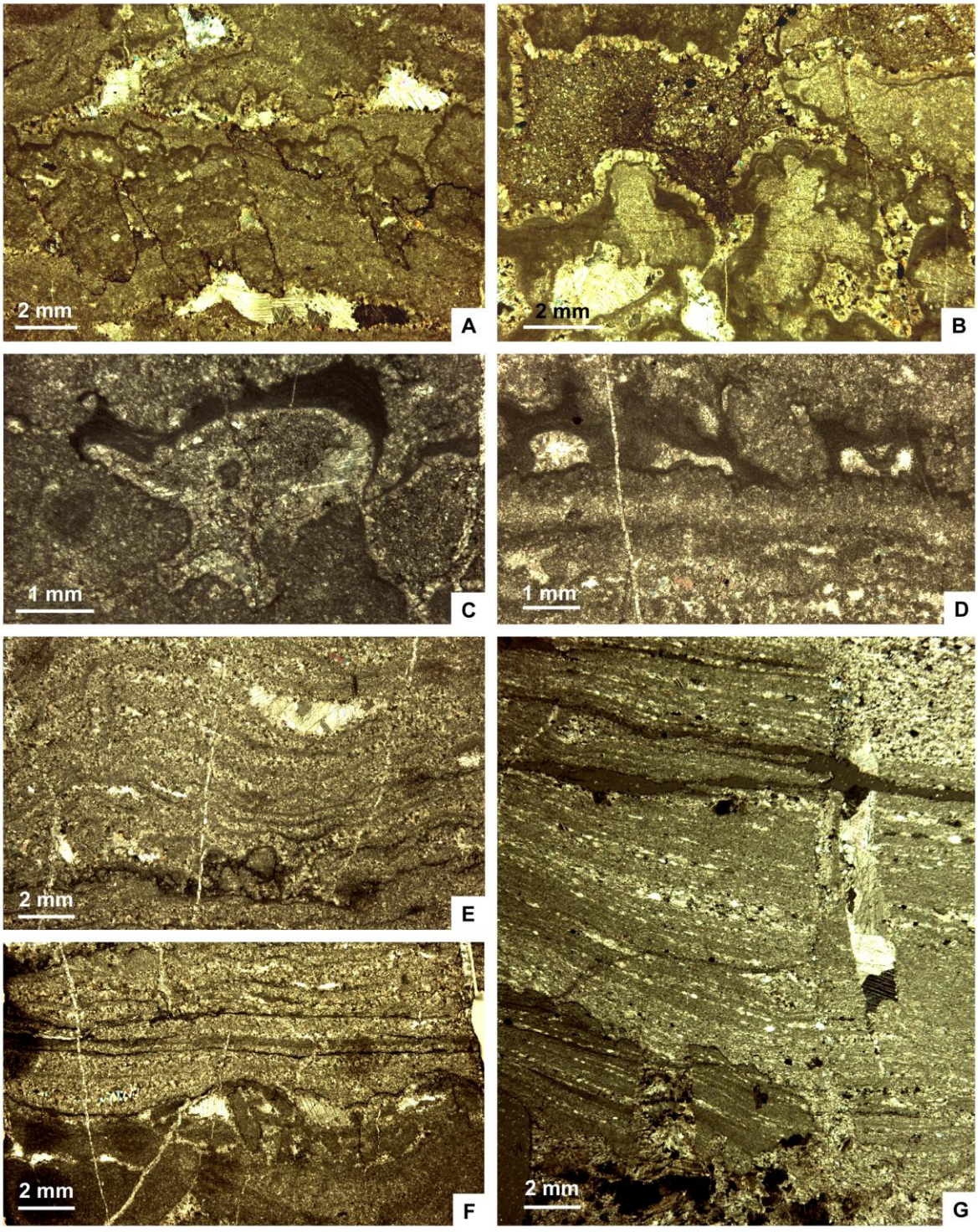

Fig. 9 : Thin-section photomicrographs of microbial limestones from the Puig Sec Member at Pic de la Clape and Tour du Mir sections. A-D. Clotted textures outlined with microbial crusts (darker) forming cauliflower-like fabrics. E-G. Microstromatolitic laminations alternating with peloidal packstones, overlying intraformational breccias and locally affected (G) by synsedimentary fissuring.

5.1 Basic rocks

Basic volcanic products are represented by some basalt and basaltic andesite lava flows and sills interbedded in the Nyer Formation and the lower part of the Olette Formation (including those from Roc de Frausa; Navidad et al., 1996), and a basanite embedded within the Fabert Member at Pic de la Clape (PC-6). These comprise mafic rocks with SiO_2 contents ranging from 52 to 41 wt. %. According the CIPW norm content, the basic rocks are undersaturated in silica, the 35% of which are subaluminous (A/CNK = 0.85) and subalkaline, and the 5% subaluminous and peralkaline (ol-ne normative). In the Pearce's (1996) diagram (Fig. 10A), the samples plot in the subalkaline field, except sample 2MB from Roc de Frausa (Navidad et al., 1996) that plots in the alkaline field.

Most samples from the Nyer and lower Olette formations plot in the tholeiitic field (Irvine and Baragar, 1971) of the AFM diagram (Fig. 10B), whereas sample PC-6 (Fabert Member) plot in the calc-alkaline field. A chondrite-normalised plot of basalts (Sun and McDonough, 1989) reveals a subdivision into two groups (Fig. 10C): one with less LREE fractionation (Nyer group) and another one displaying higher fractionation. The latter includes the Fabert basanite and the basalts from Roc de Frausa (Navidad et al., 1996). The first group shows moderate fractionation of LREE/HREE with $(La/Sm)_n$ = 1.89, $(Gd/Yb)_n$ =1.44 and without Eu anomalies (Eu/Eu* =1.07) suggesting little plagioclase fractionation. The second group shows $(La/Sm)_n$ = 3.98, a similar value of $(Gd/Yb)_n$ =1.43, and higher fractionation patterns of plagioclase with Eu/Eu* = 0.98.

In the Wood's (1980) tectonic discrimination diagram (Fig. 10D), the basic members plots in the arc-basalt domain, with two exceptions belonging to Roc de Frausa (Navidad et al., 1996). Sample 10LV plots in the E-MORB field and sample 2MB in the OIB field. In the Th/Yb vs. Nb/Yb tectonic diagram of Pearce (2008; Fig. 10E), a crustal input via subduction into the source of melts may be suggested, represented by an array displacement to higher Th/Nb ratios. Sample PC6 is displaced to more continental field. Finally, in the TiO2/Yb vs. Nb/Yb diagram (Pearce, 2008; Fig. 10F), sample PC6 shows E-MORB characteristics, whereas the remaining samples display higher Nb/Yb ratios that could indicate deeper melting.

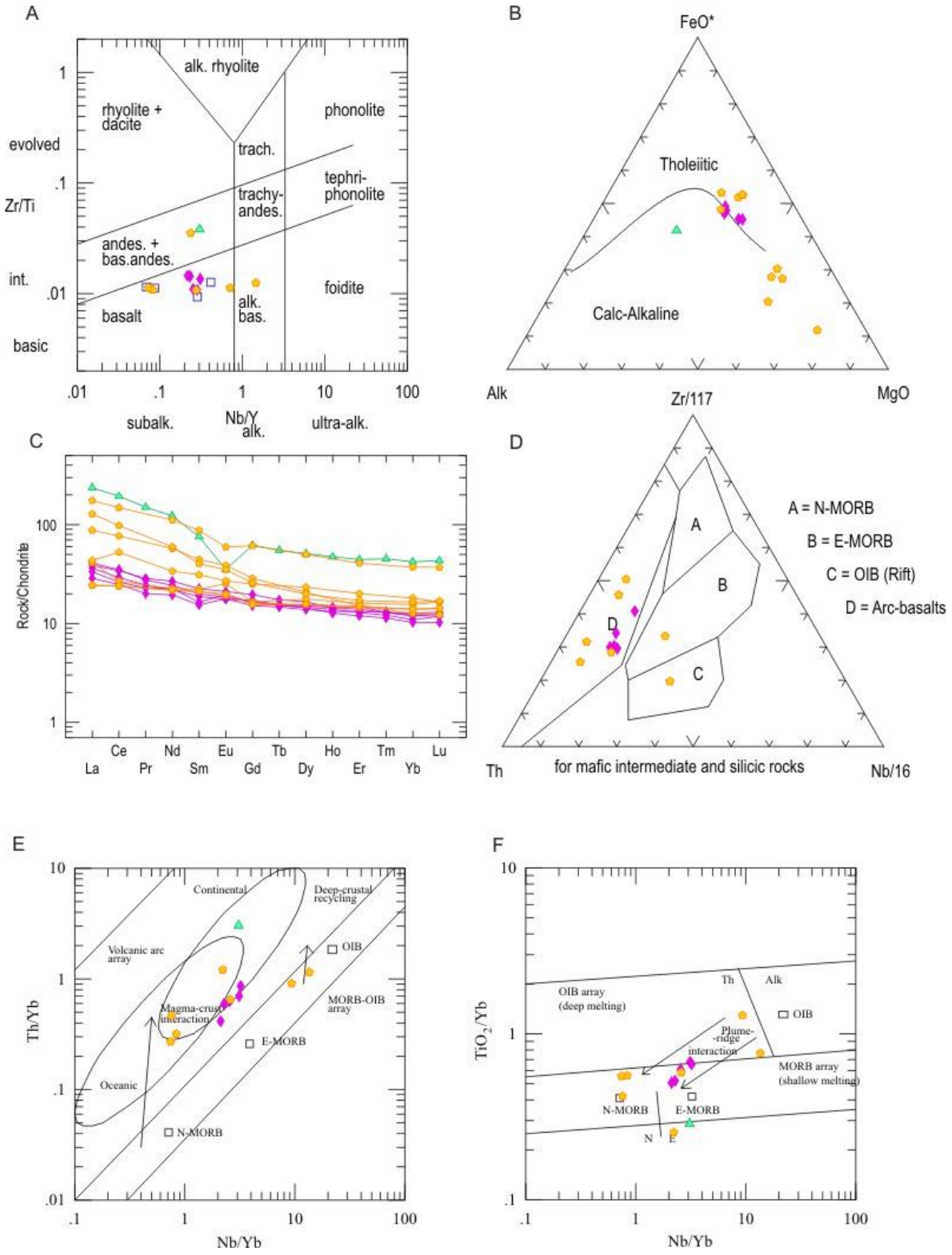

Fig. 10 : Geochemical features of the Ediacaran basic rocks from the Canaveilles Group, Eastern Pyrenees. A. Zr/Ti vs. Nv/Y diagram (Pearce, 1996). B. AFM diagram of Irvine and Baragar (1971). C. Chondrite-normalized REE patterns (normalizing values from Sun and McDonough, 1989). D. Tectonic discriminating diagram of Wood (1980). E. Th/Yb vs. Nb/Yb tectonic discriminating diagram of Pearce (2008). F. TiO_2/ Yb vs. Nb/Yb tectonic discriminating diagram of Pearce (2008).

5.2 Acid and intermediate rocks

Felsic and intermediate rocks are represented by a complex sequence of volcanic and volcanosedimentary rocks, belonging to the Nyer, Olette and Pic de la Clape formations. These rocks are oversaturated with SiO_2, whose content ranges from 52 to 75 wt. %. They are peraluminous to metaluminous (A/CNK = 1.20). These rocks are mainly plotted in the subalkaline field of the Pearce's (1996) diagram (Fig. 11A), and in the calk-alkaline field of Irvine and Baragar (1971) (Fig. 11B), except sample 1MB from Roc de Frausa (Navidad et al., 1996). The dataset is represented as a moderately fractionated chondrite normalized diagram, with $(La/Sm)_n$ = 2.58, $(Gd/Yb)_n$ =1.45, and strong Eu negative anomalies (Eu/Eu* = 0.58) (Fig. 11C), indicating plagioclase fractionation.

The geochemical characterization of the tectonic setting (Fig. 11D–E) is not straightforward, as they overlap both the anorogenic and orogenic fields in the Pearce et al.'s (1984) diagram. In the Zr vs.TiO_2 diagram of Syme (1998), their geochemical signature is not very clear: most of samples plot in the arc association, whereas sample LPT2 plots in the field related to extension.

All the geochemical characteristics outlined above suggest that these rocks were mainly derived from a continental crust source, though they have some features that evidence a more important subcrustal influence.

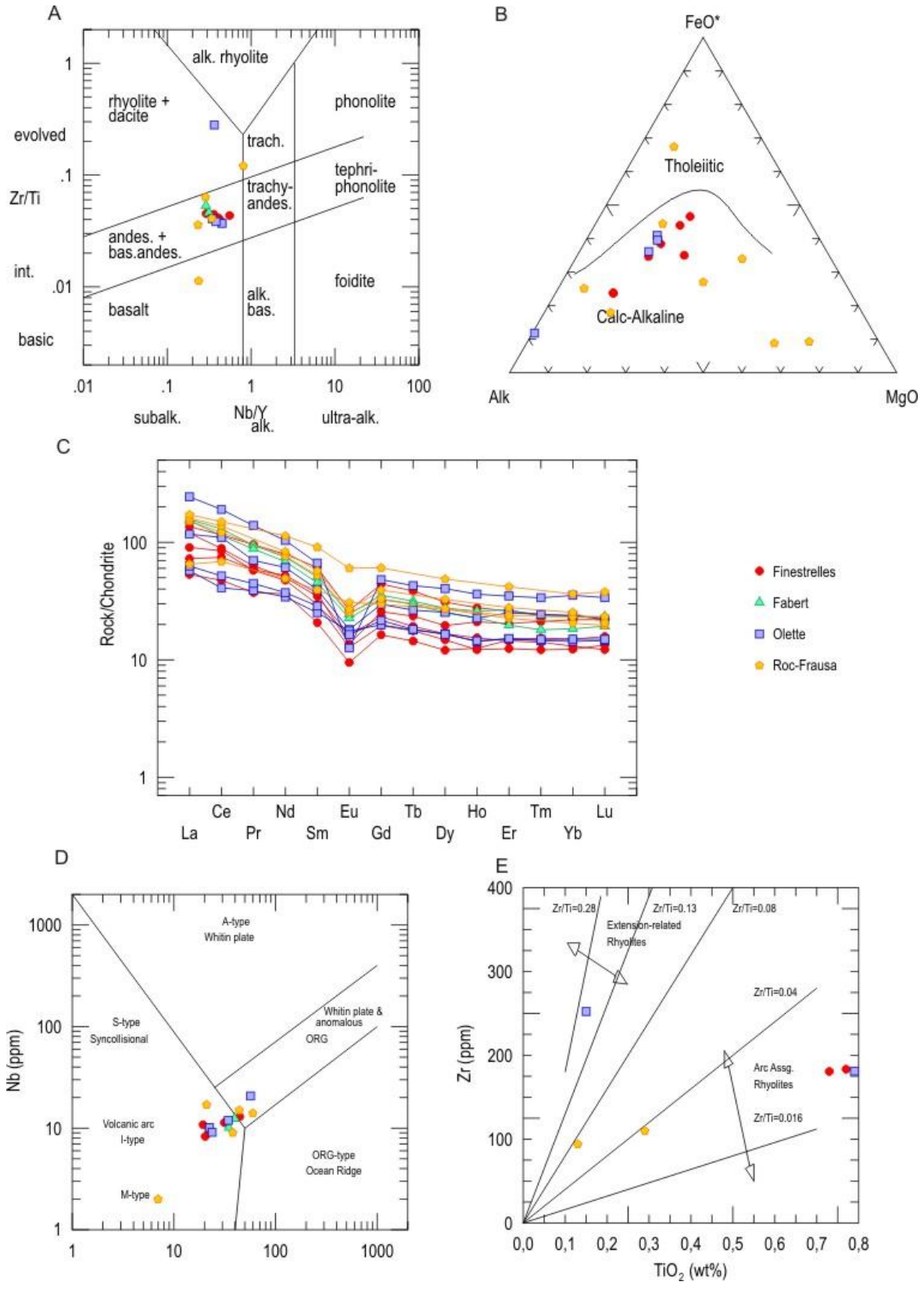

Fig. 11 : Geochemical features of the Ediacaran acidic and intermediate rocks from the Canaveilles Group sampled in the Eastern Pyrenees. A. Zr/Ti vs. Nv/Y diagram (Pearce, 1996). B. AFM diagram of Irvine and Baragar (1971). C. Chondrite-normalized REE patterns (normalizing values from Sun and McDonough, 1989). D. Y vs. Nb diagram (Pearce et al., 1984). E. Zr vs. TiO2 diagram (Syme, 1998).

6. U−Pb zircon dating

The homogeneity in geochemical composition of the above-reported volcanic and volcanosedimentary products does not allow a differentiation of geochemically distinctive volcanic pulsations. A revision of previous U−Pb zircon dates and a selection of key volcanic levels are documented below in order to reconstruct the geometrical relationships of their volcanosedimentary bodies.

6.1 Revision of previous radiometric ages

During the two last decades, several U−Pb datings on zircon have followed two different radiometric approaches (LA−ICPMS and SIMS), which allowed an estimate of the age of the Canaveilles volcanic and volcanosedimentary deposits preserved in the Puigmal and Vallespir units.

6.1.1. The first U−Pb dating, obtained with the SHRIMP (SIMS) method, yielded an age of 580±10 Ma (sample GRA1, n=8/22) for some metarhyolitic layers (VS1 *sensu* Laumonier et al., 2004) interbedded in the Nyer Formation of the Vallespir unit (Cocherie et al., 2005). This age was calculated with a MSWD=2.2, whereas Wendt and Carl (1991) and Spencer et al. (2016) stated that this value should not exceed 2. In addition, this age was calculated after excluding the two youngest zircon ages. The obtained TuffZirc Age was calculated at 590+4/−7 Ma (n=4/22). The high MSWD value and the exclusion of the youngest ages to calculate the Concordia Age point to a distinction between depositional and reworking ages. We propose here to reconsider the previous result until obtaining new dating of level VS1 by using LA–ICPMS with at least 50 analyses.

6.1.2. In the Roc de France unit, one metatuff interlayered in schists was dated using SHRIMP (SIMS) at 548±8 Ma (sample RF3, n=7/11; Castiñeiras et al., 2008) with a (recalculated) MSWD=0.0043. The radiometric data available in this contribution have been used herein to recalculate a Concordia age at 544.8±3.2 Ma (n=8/22) with a better MSWD=0.020 (Fig. 12). The Tuffzirc algorithm has yielded an age of 541+10/−5 Ma (n=5/11).

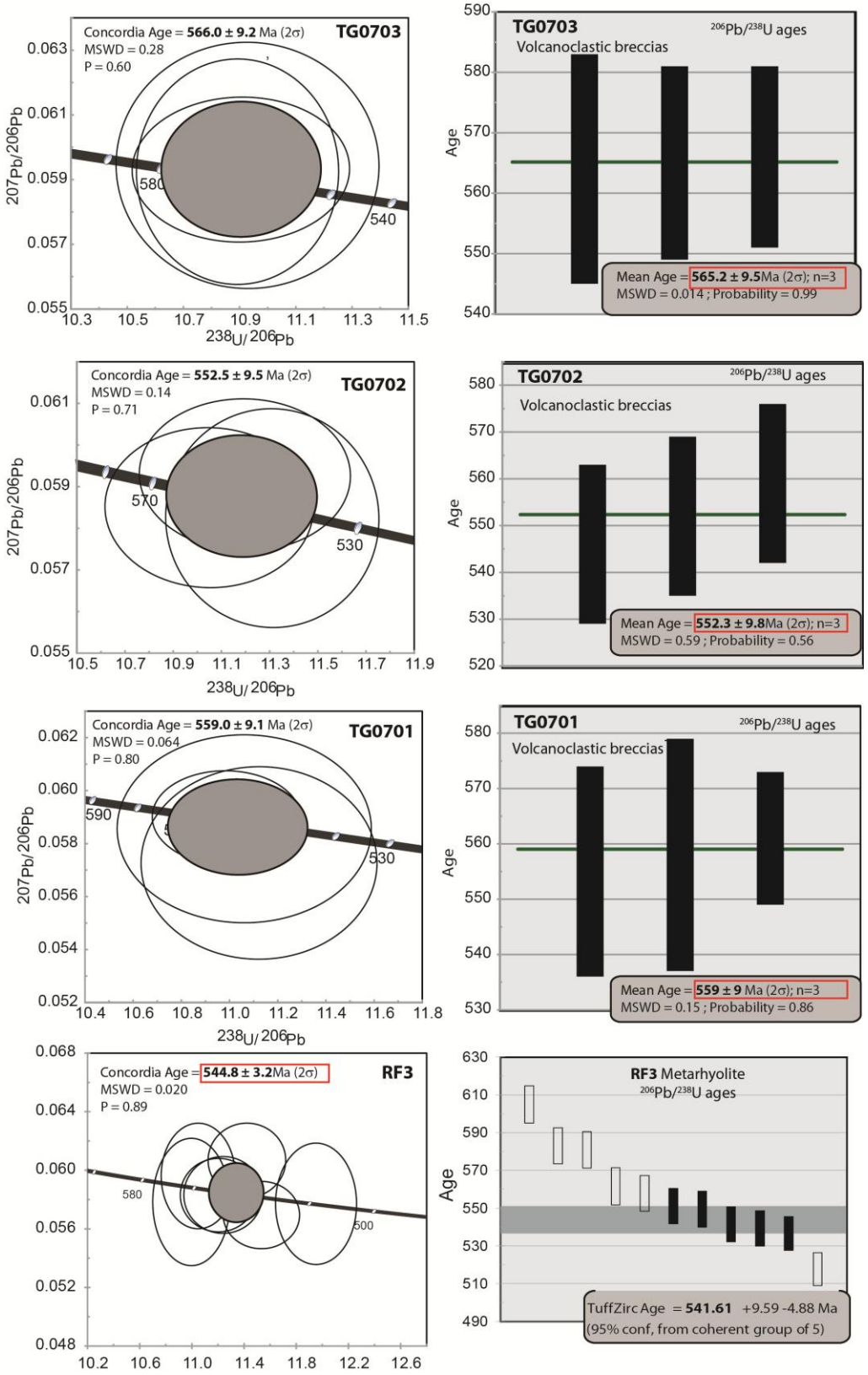

Fig. 12 : Revision of previous radiometric ages. The Terra-Wasserburg Concordia diagrams are in the left side. The TuffZirc and Weighted Average diagrams are in the right side. The maximum depositional age of the voclanoclastic breccias (TG0701; TG0702, TG0703) and depositional age of the metarhyolite (RF3) chosen are indicated in the red boxes.

6.1.3. The Finestrelles Member was previously dated by Casas et al. (2015) in the vicinity of Tregurà, who interpreted the analysed rocks as primary ignimbrites. Most of the outcrops have been reinterpreted above as volcaniclastic breccia-dominated aprons made up after reworking of ignimbritic deposits. In addition, the method previously used to separate zircon grains presents operator biases *sensu* Slama and Košler (2012). We propose here to reconsider the zircon distribution of the three samples from the Puigmal unit (TG0701–02–03) based on the sedimentary slope-related mixing recorded by the involved ignimbrites. As a result, we suggest recalculating the age as a maximum (re)depositional age better than as volcanic depositional age. The new age proposed herein is based on the three youngest, concordant and equivalent dates within error, using the mean weighted average age: TG0701= 559±9 Ma, TG0702= 552±10 Ma and TG0703= 565±9 Ma (Fig. 12).

6.2 New U-Pb dating

Four new U-Pb datings are analysed below (Fig. 13)

(i) The two exposures of the metarhyolithic Fabert Member cropping out in the Puigmal unit have been sampled to obtain their depositional age.

FA1 was sampled at the stratotype (near the Fabert torrent). 104 of the 113 analyses were considered as concordant [90−110%]. The density distribution curve shows one distinct single peak at 560 Ma with scattered Proterozoic and Archean inherited dates (Fig. 14). Using the 25 youngest concordant dates, we obtain a Concordia Age of 558.9±2.4 Ma (MSW=0.91 at 2σ).The TuffZirc algorithm has calculated an age of 559.1+1.75/−1.35 Ma, using 50 of the 104 dates, which is considered here as the depositional age.

PC5 was sampled at the Pic de la Clape summit. 47 of the 60 analyses were considered as concordant [90−110%]. Again, the density distribution curve shows one distinct single peak at 542 Ma with scattered Proterozoic inherited dates (Fig. 14). Using the 5 youngest concordant dates, we obtain a Concordia Age of 542.8±5.4 Ma (MSW=0.78 at 2σ). The TuffZirc algorithm has calculated an age of 542.9 + 5/−1.30 Ma, using 33 of the 47 dates, which is considered here as the depositional age.

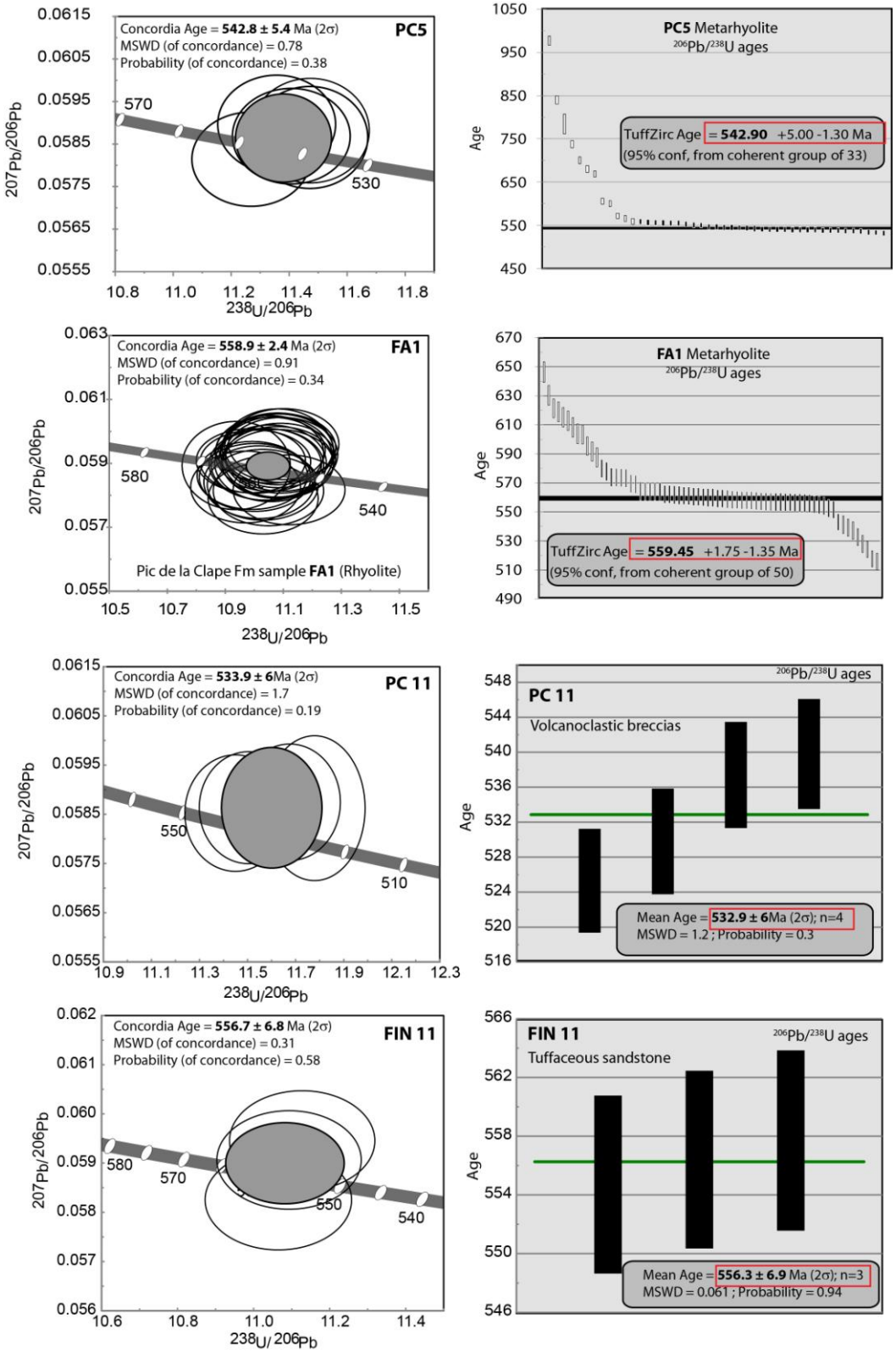

Fig. 13 : New dating. The Terra-Wasserburg Concordia diagrams are in the left side. The TuffZirc and Weighted Average diagrams are in the right side. The maximum depositional age of the voclanoclastic breccias and the tuffaceous sandstone (PC11; FIN11), and depositional age of the metarhyolites (PC5; FA1) chosen are indicated in the red boxes.

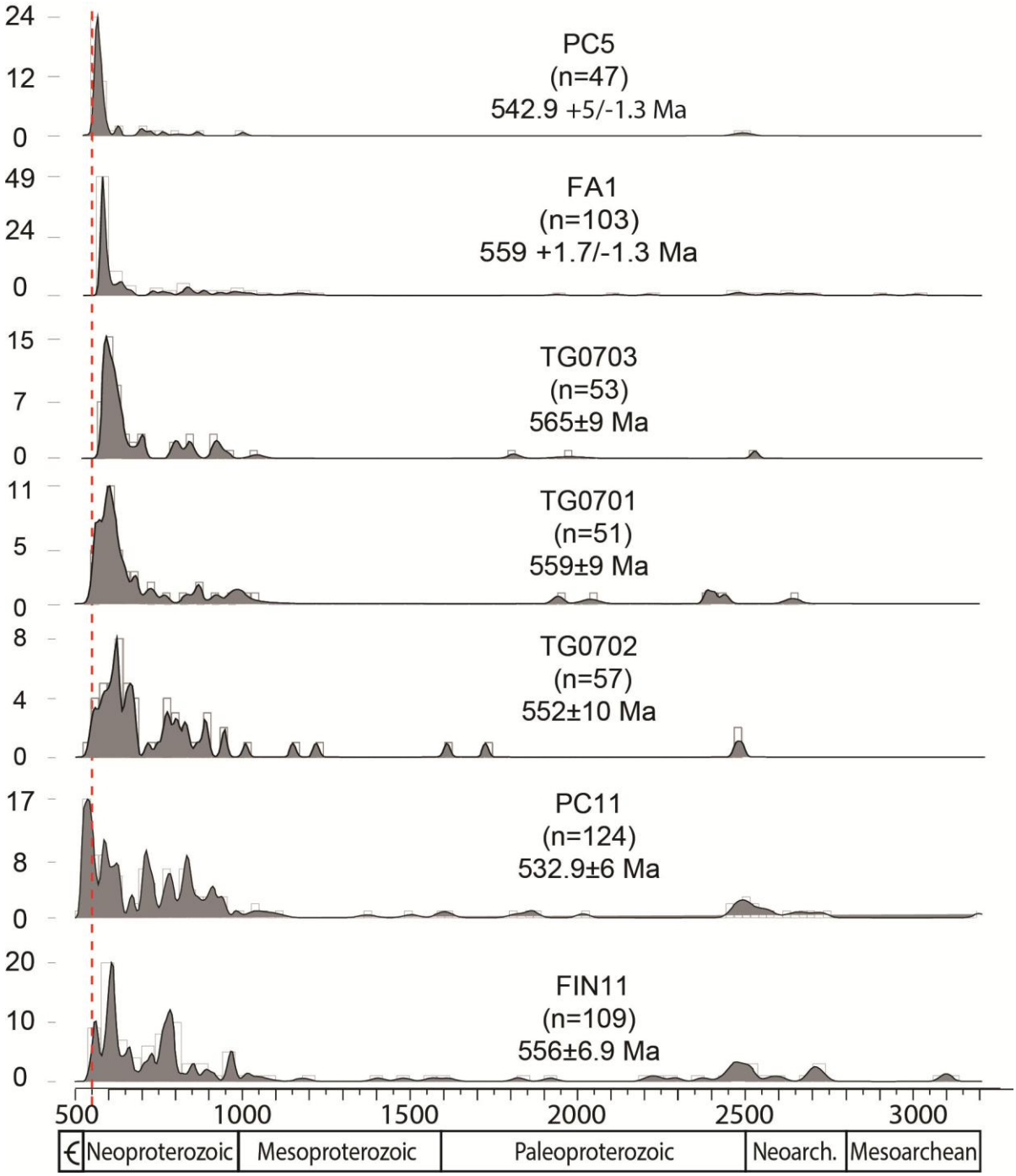

Fig. 14 : Age distribution curve and age repartition of zircons from the metarhyolithes (PC5 and FA1), the volcanoclastic breccias (TG0701, TG0702, TG0703, PC11) and a tuffaceous sandstone (FIN11).

(ii) The volcanosedimentary breccias and tuffaceous sandstones of the Finestrelles Member have been sampled at the Pic du Finestrelles (FIN11) (stratotype) and Pic de la Clape (PC11) summits, as a comparative checking with the maximum depositional ages yielded for these deposits by Casas et al. (2015). In the tuffaceous sandstone FIN11, 109 of the 111

analyses were considered as concordant [90−110%]. The density distribution curve shows one principal peak at ca. 610 Ma, with 5 other secondary peaks at ca. 560 Ma, 785 Ma, 970 Ma, 2.5 Ga, 2.7 Ga and scattered Proterozoic and Archean dates (Fig. 14). The three youngest concordant dates, ranging between 554 and 557 Ma, yielded an average age of 556±6.9 Ma (MSW=0.061), which is considered as the maximum depositional age.

In the breccia sample PC11, 124 of the 140 analyses were considered as concordant [90−110%]. The density distribution curve shows one principal peak at ca. 537 Ma, with six other secondary peaks at ca. 600 Ma, 710 Ma, 780 Ma, 830 Ma, 910 Ma, 2.5 Ga and scattered Proterozoic and Archean dates (Fig. 14). The four youngest and most concordant dates, ranging between 525 and 539 Ma, have yielded an average age of 532.9 ±6 Ma (MSW=1.2), which is considered as the maximum depositional age.

7. Geometry of Cadomian volcanosedimentary complexes

By means of the above-reported sedimentary and geochronological data, the Cadomian volcanosedimentary evolution recorded in the Eastern Pyrenees can be outlined. Abrupt lithofacies changes and pinch-and-swelling (or lenticular) geometries suggest significant modifications in eruption, transport and depositional processes over short distances.

Although the Fabert Member has previously been interpreted as a single stratigraphic marker bed, two metharhyolites of the member have yielded ages separated by ca. 17 m.y. (559+1.75/−1.35 Ma at Fabert village, 542.9+5/−1.30 Ma at Pic de la Clape). This reflects the onset of successive acidic pulsations, with similar petrographic and geochemical compositions.

The overlying Finestrelles Member displays complex lateral facies associations, which change from thick, massive or normal graded volcaniclastic breccias close to vent areas, to thin- and medium-bedded tuffaceous sandstones, displaying plane-parallel and through cross-stratification, toward distal areas. Three volcanosedimentary edifices can be recognized based on palaeotopography and distance from the sources, from near-vent to distal areas: the so-called Cap de Creus (ca. 577−558 Ma; Casas et al., 2015), Tregurà (following the transect Fabert-Tregurà-Finestrelles, ca. 559−552 Ma) and Col d'Ares (linking to Pic de la Clape summit; ca. 542−532 Ma) edifices. The two latter edifices represent explosive acidic eruptions that dispersed over large (km-scale) areas, and comprise two unconformity-bounded

units with similar petrochemical features but differentiable geochronological data. The edifices represent pyroclastic-dominated, planoconvex-like bodies, up to 500 m thick, with gradual topographically-controlled north- and northwesternward decreasing thicknesses. Onlapping discontinuities marked by short-term episodes of carbonate production point to unconformity-bounded inter-eruptive episodes. These carbonate interbeds mark successive calm episodes, interrupted by volcanic eruption and remobilization of volcanosedimentary edifices. The definitive end of volcanic activity was marked in the two above-reported volcanosedimentary edifices by nucleation and development of fringing centres of carbonate factories. These favoured microbial carbonate production close to subaerial exposure on the top of palaeorelief highs. These episodically recorded substrate instability linked to development of fissuring and tilting.

The volcanic activity recorded in the Pic de la Clape Formation began on a deep ocean with a substrate covered with black sulfidic shales. After cessation of volcanism and local development of carbonate production, the volcanic edifices rapidly subsided and were subsequently sealed by the Err shale-dominated strata. Contemporaneous tectonic activity (or substrate instability) was exclusively located at the above-reported volcanosedimentary edifices and may be explained as episodes of seafloor instability developed in response to overall differential subsidence determined by surrounded volcanosedimentary topography. No synsedimentary faulting has yet been reported in laterally equivalent strata crossing the Canaveilles/Jujols contact. The shallowing associated with the onset of the Pic de la Clape Formation is exclusively restricted to the Puigmal unit and related to the onset of volcanic activity.

8. From late Ediacaran extensional pulses to the Cadomian arc-related orogeny

The basic lava flows and sills embedded in the Nyer and Olette formations (Table 1; Figs. 10–11) reflects the emplacement of a tholeiitic magmatism probably linked to Ediacaran extensional conditions and preceding the record of Cadomian magmatism. Similar pre−Pan-African and pre−Cadomian, rift-related magmatic products are recorded in the Tonian(?)−Cryogenian Lkest-Taghdout Group of the Anti-Atlas (Álvaro et al., 2014a,c). By contrast, the Ediacaran Serie Negra Group of Ossa-Morena (590−545 Ma) displays oceanic environments with island-arc affinity, which are linked to fore- and back-arc basins (Ribeiro et al., 2003; Sánchez Lorda et al., 2013).

Other neighbouring, calk-alkaline, arc-related, acidic-dominated volcanosedimentary complexes related to the Pan-African and Cadomian orogenies, similar to those recorded at the top of the Olette Formation and within the Fabert and Finestrelles members, are represented by the Ouarzazate Supergroup of the Anti-Atlas in Morocco (ca. 615−548 Ma; Gasquet et al., 2005; Pouclet et al., 2007; Álvaro et al., 2014a; Blein et al., 2014), the Malcocinado Group of the Ossa-Morena Zone in SW Iberia (587−540 Ma; Sánchez-García et al., 2003, 2010), some reworked clasts lining the Narcea/Herrería contact in the Cantabrian Zone (ca. 575−560 Ma; Rubio-Ordóñez et al., 2015), and the Sériès Tuffs of the Axial Zone and the Rivernous and Layrac formations of the northern flank of the Montagne Noire in the Occitan Domain (ca. 542−539 Ma; Lescuyer and Cocherie, 1992; Álvaro et al., 2014b; Pouclet et al., 2016; Padel et al., in press). All these acidic activities are attributed to the arc-related final stage of the Pan-African (in the Anti-Atlas) and Cadomian (in SW Europe) orogenies. The diachronous character of the above-reported ages reflects a SW-NE trending of active subduction migrating from the Moroccan to the Ossa-Morena and Armorican, outer margins of Gondwana. Despite the lack of associated deformation, the inner peri-Gondwanan margins recorded a parallel SW-NE trending of calk-alkaline, acidic volcanism that finally reached (so delayed) the Pyrenean and Occitan Domains. Mafic volcanism is not yet recognized in the Cambrian of the Eastern Pyrenees, as a result of which, no volcanic products are representative of the Cambrian rifting conditions that characterize West Gondwana (see Álvaro et al., 2014a; Pouclet et al., 2016, and references within).

Throughout West Gondwana, the development of carbonate production across the Ediacaran−Cambrian transition is exclusively recorded in subduction-free basins, such as those recorded in the Central-Iberian Zone (*Cloudina*-bearing mounds and reefs; Cortijo et al., 2010), the northern Montagne Noire (Terreneuvian shelly phosphate-rich limestones of the Heraultia Beds; Devaere et al., 2013; Álvaro et al., 2014b) and the lateral equivalent, peritidal-dominated, Puig Sec Member of the Eastern Pyrenees (this work).

9. Conclusions

The volcanism embedded in the Ediacaran Canaveilles Group of the Eastern Pyrenees displays two distinct geochemical affinities: (i) the metabasites of the Nyer and Olette formations reflect the emplacement of a tholeiitic magmatism linked to Ediacaran extensional conditions; whereas (ii) the acidic and calk-alkaline magmatism recorded at the top of the

Olette Formation and in the Fabert and Finestrelles members (Pic de la Clape Formation) is representative of the Cadomian orogeny.

By comparison with similar magmatism recorded in neighbouring basins of West Gondwana (such as the Anti-Atlas, the Iberian Massif and the Montagne Noire), a distinct diachronism can be outlined following a SW-NE trending. Pan-African and Cadomian deformation is recorded in outer peri-Gondwanan margins (e.g. Anti-Atlas, Ossa-Morena, Cantabrian and West Asturian-Leonese Zones, and North- and Central-Armorican Domains), whereas it is absent in back-arc settings (Central Iberian Zone) and inner margins of the eastern Ibero-Armorican Arc (Montagne Noire and Pyrenees). Despite the absence of deformation, the latter inner margins have recorded, although delayed, a parallel SW-NE trending of Cadomian-related, calk-alkaline, acidic volcanism. The most representative is recognized in the Fabert and Finestrelles members cropping out in the Puigmal and Cap de Creus units of the Eastern Pyrenees. There, three volcanosedimentary edifices can be identified based on palaeotopography and distance from the sources. These are named, from near-vent to distal areas, Creus (ca. 577−558 Ma), Fabert-Tregurà-Finestrelles (ca. 559−552 Ma) and Pic de la Clape (ca. 542−532 Ma) edifices. The top of the palaeorelief formed by the two latter edifices recorded the nucleation and lateral migration of centres of carbonate production (Puig Sec Member), characterized by microbial carbonate productivity linked to synsedimentary fissuring (unstable substrates) and karstification. The presence of carbonate production across the Ediacaran–Cambrian transition is exclusively located in areas far from the Cadomian subduction suture and devoid of significant terrigenous input, such as those reported in the Eastern Pyrenees and the northern Montagne Noire (Marcou Formation).

10. References

Álvaro, J.J., Benziane, F., Thomas R., Walsh, G.J., Yazidi, A., 2014a. Neoproterozoic–Cambrian stratigraphic framework of the Anti-Atlas and Ouzellagh promontory (High Atlas), Morocco. J. Afr. Earth Sci. 98, 1–15.

Álvaro, J.J., Bauluz, B., Clausen, S., Devaere, L., Imaz, A.G., Monceret, E., Vizcaïno, D., 2014b. Stratigraphy of the Cambrian–Lower Ordovician volcanosedimentary complexes, northern Montagne Noire, France. Stratigraphy 11, 83–96.

Álvaro, J.J., Pouclet, A., Ezzouhairi, H., Soulaimani, A., Bouougri, E.H., Gil Imaz, A., Fekkak, A., 2014c. Early Neoproterozoic rift-related magmatism in the Anti-Atlas margin of the West African craton, Morocco. Precambr. Res. 255, 433−442.

Ballèvre, M., Le Goff, E., Hébert, R., 2001. The tectonothermal evolution of the Cadomian belt of northern Brittany, France: a Neoproterozoic volcanic arc. Tectonophysics 331, 19–43.

Bandrés, A., Eguíluz, L., Gil Ibarguchi, J.I., Palacios, T., 2002. Geodynamic evolution of a Cadomian arc region: the northern Ossa-Morena Zone, Iberian massif. Tectonophysics 352, 105–120.

Baudin, T., Autran, A., Guitard, G., Laumonier, B., 2008. Carte géologique de France (1/50 000). Feuille Arles-Sur-Tech (1100). BRGM, Orléans.

Blein, O., Baudin, T., Soulaimani, A., Cocherie, A., Chèvremont, P., Admou, H., Ouanaimi, H., Hafid, A., Razin, P., Bouadbelli, M., Roger, J., 2014. New geochemical, geochronological and structural constraints on the Ediacaran evolution of the south Sirwa, Agadir-Melloul and Iguerda inliers, Anti-Atlas, Morocco. J. Afr. Earth Sci. 98, 47–71.

Bowring, S.A., Schoene, B., Crowley, J.L., Ramezani, J., Conon, D.J., 2006. High-precision U–Pb zircon geochronology and the stratigraphic record: progress and promise. Geochronology: Emerging Opportunities, Paleontological Society Short Course. Paleontol. Soc. Pap. 11, 23–43.

Bull, K.F., McPhie, J., 2007. Fiamme textures in volcanic successions: Flaming issues of deformation and interpretation. J. Volcanol. Geotherm. Res. 164, 205–216.

Casas, J.M., Martí, J., Ayora, C., 1986. Importance du volcanisme dans la composition lithostratigraphique du Paléozoïque inférieur des Pyrénées Catalanes. C. R. Acad. Sci., Paris (sér. 2) 302 (19), 1193–1198.

Casas, J.M., Castiñeiras, P., Navidad, M., Liesa, M., Carreras, J., 2010. New insights into the Late Ordovician magmatism in the Eastern Pyrenees: U–Pb SHRIMP zircon data from the Canigó massif. Gondwana Res.17, 317–324.

Casas, J.M., Navidad, M., Castiñeiras, P., Liesa, M., Aguilar, C., Carreras, J., Hofmann, M., Gärtner, A., Linnemann, U., 2015. The Late Neoproterozoic magmatism in the Ediacaran series of the Eastern Pyrenees: new ages and isotope geochemistry. Int. J. Earth Sci. 104, 909–925.

Castiñeiras, P., Navidad, M., Liesa, M., Carreras, J., Casas, J.M., 2008. U–Pb zircon ages (SHRIMP) for Cadomian and Lower Ordovician magmatism in the Eastern Pyrenees: new insights in the pre–Variscan evolution of the northern Gondwana margin. Tectonophysics 461, 228–239.

Cavet, P., 1957. Le Paléozoïque de la zone axiale des Pyrénées orientales françaises entre le Roussillon et l'Andorre. Bull. Sér. Carte géol. Fr. 55, 303–518.

Cirés, J., Casas, J.M., Muñoz, J.A., Fleta, J., Barbera, M., 1995. Memoria explicativa del mapa geológico de España a escala 1:50.000. Hoja de Molló (n°218). ITGE, Madrid.

Cocherie, A., Baudin, T., Autran, A., Guerrot, C., Fanning, M., Laumonier, B., 2005. U–Pb zircon (ID–TIMS and SHRIMP) evidence for the early Ordovician intrusion of metagranites in the late Proterozoic Canaveilles Group of the Pyrenees and the Montagne Noire (France). Bull. Soc. géol. Fr. 176, 269–282.

Cortijo, I., Martí Mus, M., Jensen, S., Palacios, T., 2010. A new species of *Cloudina* from the terminal Ediacaran of Spain. Precambr. Res. 176, 1–10.

Devaere, L., Clausen, S., Steiner, M., Álvaro, J.J., Vachard, D., 2013. Chronostratigraphic and palaeogeographic significance of an early Cambrian microfauna from the Heraultia Limestone, northern Montagne Noire, France. Palaeont. Electr. 16.2.17A, 755–768.

Deloule, E., Alexandrov, P., Cheilletz, A., Laumonier, B., Barbey, P., 2002. In situ U–Pb zircon ages for Early Ordovician magmatism in the eastern Pyrenees, France: The Canigou orthogneisses. Int. J. Earth Sci. 91, 398–405.

Donzeau, M., Laumonier, B., Guitard, g., Autran, A., Llac, F., Baudin, T., Calvet, M., 2010. Carte géologique de France (1/50 000). Feuille Céret (1096). BRGM, Orléans.

Gasquet, D., Levresse, G., Cheilletz, A., Azizi-Samir, M.R., Mouttaqi, A., 2005. Contribution to a geodynamic reconstruction of the Anti-Atlas (Morocco) during Pan-African times with the emphasis on inversion tectonics and metallogenic activity in the Precambrian–Cambrian transition. Precambr. Res. 140, 157–182.

Guitard, G., 1970. Le métamorphisme hercynien mésozonal et les gneiss oeillés du massif du Canigou (Pyrénées orientales). Mém. BRGM 63, 1–353.

Guitard, G., Laffite, P., 1956. Sur l'importance et la nature des manifestations volcaniques dans le Paléozoïque inférieur des Pyrénées orientales. C. R. Acad. Sci., Paris 242, 2749–2752.

Irvine, I., Baragar, W.R., 1971. A guide to the chemical classification of the common volcanic rocks. Can. J. Earth Sci, 8, 523–548.

Keppie, J.D., Nance, R.D., Murphy, J.B., Dostal, J., 2003. Tethyan, Mediterranean, and Pacific analogues for the Neoproterozoic–Paleozoic birth and development of peri-Gondwanan terranes and their transfer to Laurentia and Laurussia. Tectonophysics 365, 195–219.

Kroner, A., Stern, R.J., 2004. Pan-African orogeny. Encyclopedia of Geology 1, 1–12.

Laumonier, B., Abad, A., Alonso, J.L., Baudelot, S., Bessière, G., Besson, M., Bouquet, C., Bourrouilh, R., Brula, P., Carreras, J., Centène, A., Courjault-Radé, R., Courtessole, R., Fauconnier, D., García-Sansegundo, Guitard, G., Moreno-Eiris, E., Perejón, A., Vizcaïno, D., 1996. Cambro–Ordovicien. In: Synthèse géologique et géophysique des Pyrénées. Tome 1: Cycle Hercynien (Barnolas, A., Chiron, J.C., eds.). BRGM-ITGE, Orléans-Madrid, 729 p.

Laumonier B., Autran, A., Barbey, P., Cheilletz, A., Baudin, T., Cocherie, A., Guerrot, C., 2004. Conséquences de l'absence de socle cadomien sur l'âge et la signification des séries pré–varisques (anté–Ordovicien supérieur) du sud de la France (Pyrénées, Montagne Noire). Bull. Soc. géol. Fr. 175, 105–117.

Laumonier, B., Calvet, M., Wiazemsky, M., Barbey, P., Marignac, C., Lambert, J., Lenoble, J.L., 2015. Notice explicative de la Carte géologique de la France (1/50.000). Feuille Céret (1096). BRGM, Orléans.

Laumonier, B., Le Bayon, B., Calvet, M., in press. Carte géologique de France (1/50 000). Feuille Prats-de-Mollo (1099). BRGM, Orléans.

Lescuyer, J.L., Cocherie, A., 1992. Datation sur monozircons des métadacites de Sériès. Arguments pour un âge protérozoïque terminal des "schistes X" de la Montagne Noire (Massif central français). C. R. Acad. Sci., Paris (sér. 2) 314, 1071–1077.

Liesa, M., Carreras, J., Castiñeiras, P., Casas, J.M., Navidad, M., Vila, M., 2011. U–Pb zircon of Ordovician magmatism in the Albera Massif (Eastern Pyrenees). Geol. Acta 9, 93–101.

Linnemann, U., Gerdes, A., Drost, K., Buschmann, B., 2007. The continuum between

Cadomian Orogenesis and opening of the Rheic Ocean: constraints from LA−ICP−MS U–Pb zircon dating and analysis of plate-tectonic setting (Saxo-Thuringian Zone, NE Bohemian massif, Germany). In: Linnemann, U., Nance, D., Kraft, P., Zulauf, G. (eds.), The Evolution of the Rheic Ocean: From Avalonian–Cadomian active margin to Alleghenian–Variscan collision. Geol. Soc. Am. Bull. 423, 61–96.

Linnemann, U., Pereira, F., Jeffries, T.E., Drost, K., Gerdes, A., 2008. The Cadomian Orogeny and the opening of the Rheic Ocean: the diacrony of geotectonic processes constrained by LA-ICP-MS U–Pb zircon dating (Ossa-Morena and Saxo-Thuringian Zones, Iberian and Bohemian Massifs). Tectonophysics 461, 21–43.

Linnemann, U., Gerdes, A., Hofmann, M., Marko, L., 2014. The Cadomian Orogen: Neoproterozoic to Early Cambrian crustal growth and orogenic zoning along the periphery of the West African Craton – Constraints from U–Pb zircon ages and Hf isotopes (Schwarzburg Antiform, Germany). Precambr. Res. 244, 236–278.

Ludwig, K.R., 2012. Users Manual for Isoplot/Ex rev. 3.75. Berkeley Geochronology Center, Spec. Publ. 5, 1–75.

Ludwig, K.R., Mundil, R., 2002. Extracting reliable U–Pb ages and errors from complex populations of zircons from Phanerozoic tuffs. Geochim. Cosmochim. Acta 66, A463.

Martínez, F.J., Iriondo, A., Dietsch, C., Aleinikoff, J.N., Peucat, J.J., Cirès, J., Reche, J., Capdevila, R., 2011. U–Pb SHRIMP-RG zircon ages and Nd signature of Lower Paleozoic rifting-related magmatism in the Variscan basement of the Eastern Pyrenees. Lithos 127, 10–23.

Murphy, J.B., Keppie, J.D., Dostal, J., Nance, R.D., 1999. Neoproterozoic–early Paleozoic evolution of Avalonia. In: Laurentia-Gondwana Connections before Pangea (Ramos, V.A., Duncan, K.J., eds.). Geol. Soc. Am., Spec. Pap. 336, 253–266.

Murphy, J.B., Pisarvesky, S.A., Nance, R.D., Keppie, J.D., 2004. Neoproterozoic–Early Paleozoic evolution of peri-Gondwana terranes: implications for Laurentia-Gondwana connections. Int. J. Earth Sci. 93, 659–682.

Nance, D.R., Murphy, J.B., Keppie, J.D., 2002. A Cordilleran model for the evolution of Avalonia. Tectonophysics 352, 11–31

Navidad, M., Carreras, J., 2002. El volcanismo de la base del Paleozoico Inferior del Canigó (Pirineos Orientales). Evidencias geoquímicas de la apertura de una cuenca continental. Geogaceta 32, 91–94.

Navidad, M., Liesa, M., Carreras, J., 1996. Magmatismo del Roc de Frausa (Pirineos

Orientales). Acta Geol. Hisp. 31 (4), 1–15.

Padel, M., Álvaro, J.J., Clausen, S., Guillot, F., Poujol, M., Chichorro, M., Monceret, E., Pereira, M.F., Vizcaïno, D., in press [article 3]. U–Pb laser ablation ICP–MS zircon dating across the Ediacaran–Cambrian transition of the Montagne Noire, southern France. C. R. Geosci.

Pearce, J.A., 1996. Sources and setting of granitic rocks. Episodes 19 (4), 120–125.

Pearce, J.A., 2008, Geochemical fingerprinting of oceanic basalts with applications to ophiolite classifi cation and the search for Archean oceanic crust. Lithos 100, 14–48.

Pearce, J.A., Harris, N.B.W., Tindle, A.G., 1984. Trace element discrimination diagrams for the tectonic interpretation of granitic rocks. J. Petrol. 25, 956–983.

Pereira, M.F., Chichorro, M., Solá, A.R., Silva, J.B., Sánchez-García, T., Bellido, F., 2011. Tracing the Cadomian magmatism with detrital/inherited zircon ages by in-situ U– Pb SHRIMP geochronology (Ossa-Morena Zone, SW Iberian Massif). Lithos 123, 204–217.

Pouclet, A., Aarab, A., Fekkak, A., Benharref, M., 2007. Geodynamic evolution of the northwestern Paleo-Gondwana margin in the Moroccan Atlas at the Precambrian–Cambrian boundary. In: Linnemann, U., Nance, R.D., Kraft, P., Zulauf, G. (eds.), The Evolution of the Rheic Ocean: From Avalonian–Cadomian Active Margin to Alleghenian–Variscan Collision. Geol. Soc. Am., Spec. Pap. 423, 27–60.

Pouclet, A., Álvaro, J.J., Bardintzeff, J.M., Gil Imaz, A, Monceret, E., Vizcaïno, D., 2016 . Cambrian–Early Ordovician volcanism across the South Armorican and Occitan Domains of the Variscan Belt in France: Continental break-up and rifting of the northern Gondwana margin. Geosci. Frontiers, doi: 10.1016/j.gsf.2016.03.002.

Ribeiro, M.L., Pereira, M.F., Solá, A.R., 2003. O ciclo Cadomiano na ZOM: Evidencias geoquímicas. Congr. Iber. Geoqu., Univ. Coimbra, Portugal, pp. 102−104.

Rubio Ordóñez, A., Gutiérrez-Alonso, G., Valverde-Vaquero, P., Cuesta-Fernández, A., Gallastegui, G., Gerdes, A., Cárdenes, V., 2015. Arc-related Ediacaran magmatism along the norhtern margin of Gondwana: geochronology and isotopic geochemistry from northern Iberia. Gondwana Res. 27, 216–227.

Sánchez Lorda, M.E., Sarrionandia, F., Abalos, B., Carracedo, M., Eguíluz, L., Gil Ibarguchi, J.L., 2013. Geochemistry and paleotectonic setting of Ediacaran metabasites from the Ossa-Morena Zone (SW Iberia). Int. J. Earth Sci., doi: 10.1007/s00531-013-0937-x.

Sánchez-García, T., Bellido, F., Quesada, C., 2003. Geodynamic setting and geochemical signatures of Cambrian–Ordovician rift-related igneous rocks (Ossa-Morena zone, SW

Iberia). Tectonophysics 365, 233–255.

Sánchez-García, T., Bellido, F., Pereira, M.F., Chichorro, M., Quesada, C., Pin, C., Silva, J.B., 2010. Rift-related volcanism predating the birth of the Rheic Ocean (Ossa-Morena zone, SW Iberia). Gondwana Res. 17, 392–407.

Sláma, J., J. Košler, 2012. Effects of sampling and mineral separation on accuracy of detrital zircon studies. Geochem. Geophys. Geosyst. 13, 1–17.

Spencer, C.J, Kirkland, C.L., Taylor, R.J.M., 2016. Strategies towards statistically robust interpretations of in situ U-Pb zircon geochronology. Geosci. Frontiers 7, 581–589.

Syme, E.C., 1998. Ore-Associated and Barren Rhyolites in the central Flin Flon Belt: Case Study of the Flin Flon Mine Sequence; Manitoba Energy and Mines, Open File Report OF98–9, 1–32.

Sun, S.S., McDonough, W.F. 1989. Chemical and isotopic systematics of oceanic basalts; implications for mantle composition and processes. In: Magmatism in the Ocean Basins (Saunders, A.D., Norry, M.J., eds.). Geol. Soc., London, Spec. Vol. 42, 429–448.

Vermeesch, P., 2004. How many grains are needed for a provenance study? Earth Planet. Sci. Lett. 224, 351–441.

Wendt, I., Carl, C., 1991. The statistical distribution of the mean squared weighted deviation. Chemical Geology Isotope Geoscience Section 86, 275–285.

Wood, D.A., 1980. The application of a Th–Hf–Ta diagram to problems of tectonomagmatic classification and to establishing the nature of crustal contamination of basaltic lavas of the British Tertiary volcanic province. Earth Planet. Sci. Lett. 50, 11–30.

11. Appendix

Appendix 1: Table1, geochemical analysis

	Basic and intermediate rocks (own data)					
Sample	**JM-100**	**JM-13**	**PIR-100**	**PIR-13**	**PYR-100**	**PC-6**
Fm/Mb	**NYER**	**NYER**	**NYER**	**NYER**	**NYER**	**Fabert**
Lithology	**Basalt**	**Basalt**	**Basalt**	**Basalt**	**Amphibolite**	**basanite**
SiO_2	**48.60**	**44.77**	**48.80**	**45.84**	**44.82**	**41.28**
Al_2O_3	**17.27**	**15.26**	**16.43**	**16.37**	**19.99**	**25.28**
FeO	**8.97**	**9.00**	**8.41**	**9.77**	**9.41**	**9.41**
MnO	**0.13**	**0.17**	**0.13**	**0.18**	**0.13**	**0.06**
MgO	**6.30**	**7.57**	**5.61**	**8.47**	**6.71**	**5.28**
CaO	**9.69**	**10.40**	**11.52**	**8.44**	**7.52**	**0.52**
Na_2O	**3.13**	**3.27**	**2.61**	**3.34**	**3.44**	**0.45**
K_2O	**0.35**	**0.04**	**0.51**	**0.05**	**0.47**	**7.32**
TiO_2	**1.21**	**0.96**	**1.20**	**1.03**	**1.07**	**1.88**
P_2O_5	**0.12**	**0.07**	**0.17**	**0.09**	**0.12**	**0.37**
LOI	**3.00**	**7.20**	**3.40**	**5.10**	**5.00**	**6.40**
Total	**98.77**	**98.71**	**98.79**	**98.68**	**98.68**	**98.25**
K	**2905.52**	**332.06**	**4233.76**	**415.07**	**3901.70**	**60766.88**
P	**523.62**	**305.45**	**741.80**	**392.72**	**523.62**	**1614.50**
Ti	**7252.43**	**5753.99**	**7192.49**	**6173.55**	**6413.30**	**11268.23**
Ba	**79.00**	**18.00**	**96.00**	**20.00**	**56.00**	**3980.00**
Cr	**314.73**	**225.78**	**294.20**	**253.15**	**225.78**	**116.31**
Cs	**0.30**	**0.10**	**0.50**	**0.10**	**1.30**	**4.10**
Hf	**2.10**	**2.30**	**2.10**	**2.40**	**2.30**	**11.70**
Nb	**5.80**	**4.60**	**5.30**	**4.60**	**5.60**	**22.10**
Ni	**56.00**	**110.00**	**56.00**	**124.00**	**118.00**	**37.70**
Rb	**7.70**	**0.50**	**12.20**	**0.40**	**20.50**	**178.60**
Sr	**330.40**	**308.00**	**365.00**	**347.70**	**305.90**	**89.80**
Sc	**39.00**	**24.00**	**37.00**	**26.00**	**20.00**	**34.00**
Ta	**0.30**	**0.20**	**0.40**	**0.30**	**0.30**	**1.50**
Th	**1.30**	**1.20**	**1.30**	**0.90**	**1.50**	**21.80**
U	**0.30**	**0.10**	**0.20**	**0.20**	**0.20**	**5.10**
V	**235.00**	**150.00**	**213.00**	**153.00**	**160.00**	**254.00**
Zn	**43.00**	**64.00**	**37.00**	**80.00**	**66.00**	**82.00**
Zr	**81.60**	**90.40**	**82.90**	**95.70**	**92.60**	**469.30**
La	**8.60**	**6.80**	**9.20**	**7.90**	**9.70**	**56.00**
Ce	**17.90**	**15.20**	**21.00**	**16.10**	**21.40**	**119.10**
Pr	**2.32**	**1.91**	**2.72**	**2.18**	**2.61**	**14.28**
Nd	**10.20**	**9.10**	**12.50**	**10.60**	**11.40**	**57.20**
Sm	**2.87**	**2.36**	**3.45**	**2.51**	**3.04**	**11.57**
Eu	**1.02**	**1.03**	**1.22**	**1.14**	**1.07**	**2.04**
Gd	**3.52**	**3.12**	**4.03**	**3.36**	**3.39**	**12.77**
Tb	**0.58**	**0.55**	**0.65**	**0.58**	**0.57**	**2.06**
Dy	**3.72**	**3.52**	**4.22**	**3.84**	**3.68**	**12.94**
Ho	**0.79**	**0.75**	**0.81**	**0.83**	**0.72**	**2.68**
Er	**2.13**	**2.20**	**2.46**	**2.30**	**1.98**	**7.36**
Tm	**0.31**	**0.33**	**0.33**	**0.33**	**0.29**	**1.15**
Yb	**1.86**	**2.02**	**2.07**	**2.17**	**1.74**	**7.16**
Lu	**0.30**	**0.32**	**0.30**	**0.33**	**0.26**	**1.10**
Y	**20.40**	**19.70**	**20.80**	**21.10**	**18.10**	**72.60**

	Acid and Intermediate (own data)										
Sample	**PC-2**	**PC-4**	**TR 10-1**	**TR 10-2**	**TR 10-3**	**FA 1**	**PC-5**	**LPT1**	**LPT2**	**PC-21**	**PC-22**
Fm/Mb	**Finestrelles**	**Finestrelles**	**Finestrelles**	**Finestrelles**	**Finestrelles**	**Fabert**	**Fabert**	**Olette top?**	**Olette top?**	**Olette top**	**Olette top**
Lithology	**Dacite**	**Dacite**	**Basaltic trachyandesite**	**Trachyandesite**	**Andesite**	**Dacite**	**Dacite**	**Dacite**	**Rhyolite**	**Rhyolite**	**Rhyolite**
SiO_2	**69.66**	**73.00**	**54.08**	**57.30**	**60.26**	**65.22**	**72.03**	**64.01**	**74.73**	**69.64**	**69.44**
Al_2O_3	**12.30**	**11.27**	**14.66**	**14.51**	**11.30**	**14.17**	**11.85**	**14.65**	**13.02**	**14.15**	**13.56**
FeO	**5.94**	**4.58**	**2.37**	**2.34**	**3.45**	**5.87**	**3.85**	**6.17**	**1.23**	**4.27**	**4.92**
MnO	**0.05**	**0.07**	**0.06**	**0.04**	**0.04**	**0.07**	**0.03**	**0.10**	**0.01**	**0.05**	**0.07**
MgO	**2.98**	**2.30**	**1.48**	**1.49**	**1.85**	**3.03**	**3.04**	**2.66**	**0.06**	**2.11**	**2.29**
CaO	**0.20**	**0.19**	**9.86**	**8.21**	**8.58**	**0.89**	**0.23**	**1.46**	**0.23**	**0.62**	**0.77**
Na_2O	**1.97**	**1.02**	**1.86**	**1.79**	**2.13**	**3.95**	**1.38**	**2.73**	**3.08**	**3.32**	**4.18**
K_2O	**1.87**	**2.53**	**4.23**	**4.28**	**2.52**	**2.41**	**2.74**	**3.50**	**6.07**	**2.11**	**1.05**
TiO_2	**0.85**	**0.74**	**1.00**	**0.92**	**0.66**	**1.03**	**0.79**	**1.01**	**0.15**	**0.84**	**0.77**
P_2O_5	**0.17**	**0.17**	**0.38**	**0.27**	**0.19**	**0.25**	**0.23**	**0.24**	**0.02**	**0.21**	**0.18**
LOI	**3.10**	**3.40**	**9.50**	**8.30**	**8.40**	**2.20**	**3.20**	**2.40**	**1.10**	**2.00**	**2.10**
Total	**99.09**	**99.27**	**99.48**	**99.45**	**99.38**	**99.09**	**99.37**	**98.93**	**99.70**	**99.32**	**99.33**
K	**15523.78**	**21002.76**	**35115.29**	**35530.36**	**20919.75**	**20006.58**	**22746.07**	**29055.20**	**50390.02**	**17516.14**	**8716.56**
P	**741.80**	**741.80**	**1658.13**	**1178.15**	**829.07**	**1090.88**	**1003.61**	**1047.24**	**87.27**	**916.34**	**785.43**
Ti	**5094.68**	**4435.37**	**5993.74**	**5514.24**	**3955.87**	**6173.55**	**4735.06**	**6053.68**	**899.06**	**5034.74**	**4615.18**
Ba	**496.00**	**1117.00**	**1366.00**	**1369.00**	**734.00**	**1236.00**	**845.00**	**1685.00**	**528.00**	**560.00**	**267.00**
Cr	**82.10**	**82.10**	**68.42**	**61.58**	**61.58**	**68.42**	**82.10**	**68.42**	**13.68**	**75.26**	**68.42**
Cs	**2.30**	**2.60**	**4.70**	**4.40**	**4.30**	**0.40**	**1.90**	**3.80**	**1.50**	**2.50**	**1.10**
Hf	**6.00**	**4.70**	**7.60**	**6.60**	**5.10**	**7.80**	**6.80**	**7.10**	**8.50**	**5.50**	**5.30**
Nb	**13.00**	**9.50**	**11.30**	**10.80**	**8.30**	**12.40**	**10.10**	**11.90**	**20.70**	**10.10**	**9.10**
Ni	**40.30**	**27.10**	**12.80**	**11.90**	**21.40**	**26.70**	**22.40**	**32.00**	**20.00**	**22.00**	**45.00**
Rb	**46.40**	**68.90**	**120.30**	**116.40**	**80.00**	**54.70**	**62.20**	**129.10**	**184.60**	**65.50**	**34.20**
Sr	**28.00**	**18.20**	**193.90**	**168.40**	**158.90**	**251.50**	**27.20**	**195.00**	**37.60**	**125.70**	**139.60**
Sc	**12.00**	**11.00**	**15.00**	**15.00**	**9.00**	**17.00**	**11.00**	**16.00**	**4.00**	**12.00**	**12.00**
Ta	**0.60**	**0.80**	**0.80**	**0.60**	**0.70**	**0.80**	**0.80**	**0.80**	**1.50**	**0.80**	**0.70**
Th	**10.90**	**8.80**	**12.40**	**10.50**	**8.70**	**11.90**	**10.00**	**12.70**	**22.70**	**6.70**	**6.50**
U	**3.00**	**2.10**	**3.90**	**2.80**	**2.10**	**3.40**	**2.00**	**3.40**	**5.20**	**1.90**	**1.80**
V	**101.00**	**89.00**	**117.00**	**118.00**	**72.00**	**110.00**	**92.00**	**123.00**	**8.00**	**103.00**	**92.00**
Zn	**94.00**	**162.00**	**20.00**	**20.00**	**47.00**	**85.00**	**61.00**	**106.00**	**14.00**	**56.00**	**148.00**
Zr	**240.30**	**183.30**	**295.80**	**262.60**	**180.70**	**291.10**	**261.00**	**255.20**	**252.20**	**190.10**	**181.10**
La	**32.20**	**28.30**	**17.20**	**12.60**	**21.40**	**37.10**	**36.10**	**27.80**	**57.80**	**13.60**	**14.90**
Ce	**70.80**	**54.30**	**45.60**	**29.10**	**51.90**	**79.50**	**69.70**	**67.30**	**116.50**	**25.00**	**31.70**
Pr	**9.09**	**6.00**	**5.58**	**3.55**	**5.48**	**8.97**	**8.35**	**6.66**	**13.19**	**3.70**	**4.24**
Nd	**37.00**	**23.40**	**24.40**	**17.00**	**22.20**	**34.90**	**31.90**	**28.50**	**48.40**	**16.00**	**17.40**
Sm	**9.32**	**5.31**	**5.64**	**3.17**	**4.53**	**7.76**	**6.93**	**6.07**	**10.17**	**3.85**	**4.39**
Eu	**1.53**	**0.95**	**0.79**	**0.55**	**0.74**	**1.42**	**1.31**	**1.05**	**0.73**	**1.02**	**0.95**
Gd	**9.07**	**4.78**	**5.28**	**3.35**	**4.02**	**7.29**	**6.69**	**6.11**	**9.89**	**4.08**	**4.44**
Tb	**1.44**	**0.72**	**0.88**	**0.54**	**0.66**	**1.18**	**1.11**	**0.99**	**1.60**	**0.67**	**0.68**
Dy	**7.87**	**4.24**	**4.97**	**3.07**	**3.75**	**7.00**	**6.40**	**6.43**	**10.26**	**4.24**	**4.18**
Ho	**1.57**	**0.87**	**1.19**	**0.71**	**0.69**	**1.47**	**1.29**	**1.28**	**2.05**	**0.81**	**0.82**
Er	**4.30**	**2.39**	**3.36**	**2.43**	**2.06**	**4.41**	**3.26**	**4.16**	**5.77**	**2.50**	**2.51**
Tm	**0.62**	**0.36**	**0.54**	**0.39**	**0.31**	**0.60**	**0.46**	**0.62**	**0.86**	**0.37**	**0.38**
Yb	**3.99**	**2.22**	**3.72**	**2.55**	**2.09**	**4.00**	**3.12**	**4.06**	**6.01**	**2.44**	**2.55**
Lu	**0.58**	**0.31**	**0.56**	**0.40**	**0.34**	**0.59**	**0.49**	**0.56**	**0.86**	**0.37**	**0.38**
Y	**44.50**	**22.30**	**31.50**	**19.40**	**20.40**	**39.60**	**34.80**	**34.30**	**56.80**	**22.40**	**23.80**

	Basic and intermediate rocks, ROC DE FRAUSA, (Navidad et al, 1996)										
Sample	**10LV**	**11LV**	**16LV**	**2MB**	**3MB**	**4MJ**	**5MJ**	**6MJ**	**7MJ**	**8MJ**	**9MJ**
Lithology	**Amphibolite**	**Amphibolite**	**Amphibolite**	**Amphibolite**	**Amphibolite**	**Amphibolite**	**Amphibolite**	**Amphibolite**	**Amphibolite**	**Amphibolite**	
SiO_2	**47.12**	**51.78**	**51.47**	**44.92**	**51.90**	**46.90**	**47.69**	**49.00**	**49.14**	**45.73**	**48.12**
Al_2O_3	**14.16**	**14.35**	**17.28**	**16.92**	**14.83**	**13.27**	**14.71**	**15.66**	**15.80**	**16.42**	**16.60**
FeO	**12.12**	**9.59**	**2.11**	**11.38**	**14.69**	**2.07**	**4.89**	**4.23**	**3.99**	**10.83**	**11.02**
MnO	**0.19**	**0.17**	**0.22**	**0.20**	**0.25**	**0.17**	**0.27**	**0.21**	**0.23**	**0.20**	**0.19**
MgO	**6.75**	**6.37**	**6.03**	**7.63**	**1.86**	**13.20**	**10.46**	**7.80**	**7.96**	**7.33**	**7.40**
CaO	**10.03**	**9.71**	**9.00**	**8.03**	**6.34**	**7.31**	**6.40**	**9.44**	**9.39**	**10.03**	**10.07**
Na_2O	**3.58**	**3.50**	**1.53**	**0.88**	**3.29**	**1.72**	**1.16**	**1.60**	**1.92**	**1.76**	**1.72**
K_2O	**0.32**	**0.44**	**0.68**	**2.08**	**1.35**	**0.51**	**1.36**	**0.36**	**0.48**	**0.69**	**0.80**
TiO_2	**2.70**	**1.08**	**1.62**	**2.06**	**1.56**	**1.13**	**1.22**	**1.46**	**1.22**	**1.27**	**1.28**
P_2O_5	**0.44**	**0.17**	**0.23**	**2.06**	**0.91**	**0.16**	**0.16**	**0.15**	**0.16**	**0.20**	**0.20**
LOI											
Total	**97.41**	**97.16**	**90.17**	**96.16**	**96.98**	**86.44**	**88.32**	**89.91**	**90.29**	**94.46**	**97.40**
K	**2656.48**	**3652.65**	**5645.01**	**17267.09**	**11207.01**	**4233.76**	**11290.02**	**2988.54**	**3984.71**	**5728.03**	**6641.19**
P	**1919.94**	**741.80**	**1003.61**	**8988.83**	**3970.79**	**698.16**	**698.16**	**654.53**	**698.16**	**872.70**	**872.70**
Ti	**16183.10**	**6473.24**	**9709.86**	**12347.11**	**9350.24**	**6772.93**	**7312.37**	**8750.86**	**7312.37**	**7612.05**	**7671.99**
Ba	**111.00**	**266.00**	**48.00**	**180.00**	**333.00**					**89.00**	**125.00**
Cr	**255.00**	**168.00**	**2.44**	**217.00**	**77.00**					**296.00**	**320.00**
Cs											
Hf											
Nb	**20.00**	**2.00**	**8.00**	**38.00**	**14.00**					**2.00**	**1.75**
Ni	**102.00**	**51.00**	**70.00**	**142.00**	**12.00**					**89.00**	**110.00**
Rb	**9.00**	**18.00**	**25.00**	**12.00**	**58.00**					**22.00**	**25.00**
Sr	**388.00**	**312.00**	**322.00**	**270.00**	**305.00**					**274.00**	**276.00**
Sc	**29.00**	**41.59**	**42.50**	**24.89**	**25.28**					**32.78**	**33.20**
Ta		**14.68**									
Th	**1.95**	**1.23**	**2.00**	**3.22**	**7.64**					**0.76**	**0.64**
U	**0.81**	**0.36**		**0.80**	**2.28**					**0.17**	**0.19**
V	**263.00**	**254.00**	**268.00**	**191.00**	**118.00**					**216.00**	**212.00**
Zn	**113.00**	**124.00**	**104.00**	**660.00**	**258.00**					**99.00**	**100.00**
Zr	**187.00**	**73.00**	**116.00**	**160.00**	**341.00**					**87.00**	**89.00**
La	**20.80**	**9.76**	**10.30**	**30.38**	**41.58**					**5.73**	**5.82**
Ce	**47.05**	**16.44**	**32.20**	**60.05**	**90.86**					**14.68**	**14.76**
Pr											
Nd	**26.82**	**10.52**	**15.79**	**27.88**	**52.10**					**10.07**	**10.21**
Sm	**6.79**	**3.41**	**4.76**	**6.17**	**13.39**					**3.23**	**3.23**
Eu	**2.25**	**1.47**	**1.57**	**2.03**	**3.45**					**1.11**	**1.15**
Gd	**5.89**	**3.40**	**5.16**	**5.30**	**12.58**					**3.32**	**3.19**
Tb											
Dy	**5.24**	**4.48**	**5.92**	**5.04**	**12.69**					**3.94**	**3.96**
Ho											
Er	**2.51**	**2.66**	**3.32**	**2.82**	**6.75**					**2.40**	**2.49**
Tm											
Yb	**2.14**	**2.64**	**3.08**	**2.80**	**6.32**					**2.39**	**2.36**
Lu	**0.31**	**0.42**	**0.42**	**0.43**	**0.94**					**0.36**	**0.36**
Y	**28.00**	**25.00**	**29.00**	**26.00**	**59.00**					**24.00**	**24.00**

	Acid and Intermediate, ROC DE FRAUSA, (Navidad et al, 1996)							
Sample	**12LV**	**13LV**	**14LV**	**15LV**	**17LV**	**18LV**	**19LV**	**1MB**
Lithology	**Amphibolite**	**Amphibolite**	**Amphibolite**	**Amphibolite**	**Granulé porphyroid**	**Granulé porphyroid**	**Granulé porphyroid**	**Amphibolite**
SiO_2	**52.23**	**53.93**	**53.07**	**52.50**	**70.09**	**73.00**	**63.04**	**52.87**
Al_2O_3	**13.67**	**14.75**	**14.21**	**14.00**	**14.51**	**14.30**	**15.21**	**14.91**
FeO	**1.22**	**1.91**	**3.29**	**2.94**	**2.69**	**1.58**	**6.58**	**13.71**
MnO	**0.21**	**0.19**	**0.28**	**0.09**	**0.04**	**0.01**	**0.07**	**0.28**
MgO	**8.90**	**14.97**	**4.17**	**3.98**	**0.72**	**1.50**	**2.57**	**1.79**
CaO	**9.23**	**7.47**	**6.27**	**6.50**	**2.50**	**1.23**	**2.56**	**6.19**
Na_2O	**2.80**	**3.12**	**0.63**	**3.40**	**4.15**	**2.90**	**3.58**	**3.52**
K_2O	**0.98**	**0.58**	**1.59**	**0.57**	**3.15**	**2.80**	**2.08**	**1.33**
TiO_2	**0.85**	**1.75**	**2.55**	**2.50**	**0.28**	**0.13**	**1.08**	**1.54**
P_2O_5	**0.07**	**0.29**	**0.32**	**0.46**	**0.10**	**0.10**	**0.35**	**1.54**
LOI								
Total	**90.16**	**98.96**	**86.38**	**86.94**	**98.23**	**97.55**	**97.12**	**97.68**
K	**8135.46**	**4814.86**	**13199.36**	**4731.85**	**26149.68**	**23244.16**	**17267.09**	**11040.98**
P	**305.45**	**1265.42**	**1396.32**	**2007.21**	**436.35**	**436.35**	**1527.23**	**6719.80**
Ti	**5094.68**	**10489.05**	**15284.04**	**14984.36**	**1678.25**	**779.19**	**6473.24**	**9230.36**
Ba				**343.00**	**860.00**	**68.00**		**363.00**
Cr				**20.00**	**15.00**		**84.00**	**78.00**
Cs								
Hf								
Nb				**9.00**	**2.00**	**17.00**	**15.00**	**14.00**
Ni				**23.00**	**13.00**	**10.00**	**25.00**	**10.00**
Rb				**19.00**	**103.00**	**301.00**	**64.00**	**60.00**
Sr				**126.00**	**265.00**	**32.00**	**259.00**	**304.00**
Sc				**47.50**	**4.08**		**21.00**	**24.78**
Ta				**16.44**				
Th				**2.00**	**11.91**		**11.00**	**7.71**
U					**3.36**			**2.33**
V				**590.00**	**31.00**	**5.00**	**135.00**	**104.00**
Zn				**132.00**	**51.00**	**89.00**	**88.00**	**236.00**
Zr				**195.00**	**110.00**	**94.00**	**271.00**	**338.00**
La				**15.43**	**36.05**		**38.03**	**40.69**
Ce				**42.00**	**74.21**		**84.31**	**91.50**
Pr								
Nd				**23.00**	**35.56**		**38.88**	**52.97**
Sm				**6.00**	**8.03**		**8.74**	**13.92**
Eu				**1.78**	**1.47**		**1.56**	**3.49**
Gd				**6.12**	**6.79**		**8.05**	**12.43**
Tb								
Dy				**6.83**	**6.91**		**8.31**	**12.34**
Ho								
Er				**3.74**	**3.92**		**4.60**	**6.92**
Tm								
Yb				**3.48**	**3.95**		**4.30**	**6.18**
Lu				**0.50**	**0.59**		**0.52**	**0.96**
Y				**38.00**	**7.00**	**21.00**	**44.00**	**60.00**

Appendix 2 : LA-ICPMS and SHRIMP U-Pb results for samples TG0701, TG0702, TG0703 and RF3 (data from Casas et al., 2015 and Castiñieras et al., 2008)

				ISOTOPIC RATIOS					AGES						
TG0701	**U ppm**	**Pb ppm**	**Th/U**	**207/235**	**err (2σ)**	**206/238**	**err (2σ)**	**rho**	**207/206**	**err (2σ)**	**206/238**	**err (2σ)**	**207/235**	**err (2σ)**	**conc**
b3	2	23	0.45	0.71	6.3	0.0899	3.60	0.57	507	113	555	19	545	27	109
b6	5	53	0.42	0.73	6.3	0.0904	3.90	0.62	555	107	558	21	558	27	101
a15	23	235	0.56	0.76	3.1	0.0908	2.30	0.72	626	47	561	12	574	14	90
a13	17	182	0.48	0.74	3.4	0.0910	2.30	0.69	571	53	561	13	563	15	98
a38	5	54	0.64	0.76	5.1	0.0925	3.20	0.63	578	87	570	18	572	23	99
a26	6	54	0.73	0.76	4.6	0.0931	2.60	0.56	578	83	574	14	575	20	99
a3	5	49	0.47	0.75	6.0	0.0932	4.10	0.68	533	96	574	23	566	26	108
b4	5	54	0.36	0.77	6.6	0.0938	3.60	0.54	588	121	578	20	580	30	98
a20	6	61	0.58	0.76	5.9	0.0939	3.20	0.54	566	108	578	17	576	26	102
a29	22	238	0.18	0.76	3.8	0.0941	3.10	0.82	561	47	580	17	576	17	103
b1	9	83	1.06	0.78	4.2	0.0955	3.20	0.76	575	60	588	18	585	19	102
b2	19	209	0.03	0.81	3.1	0.0963	2.10	0.66	642	50	593	12	603	14	92
a36	7	66	0.7	0.81	5.8	0.0971	3.50	0.60	629	99	597	20	604	27	95
b5	3	34	0.46	0.79	5.2	0.0973	3.30	0.62	567	89	598	19	592	24	106
b8	6	58	0.49	0.79	5.2	0.0974	3.20	0.61	563	90	599	18	592	24	106
a21	8	57	2.45	0.80	7.6	0.0975	3.50	0.47	585	145	600	20	597	35	102
a60	16	175	0.03	0.81	3.0	0.0979	2.10	0.69	603	48	602	12	602	14	100
a12	4	39	0.49	0.83	6.7	0.0980	3.40	0.50	652	125	603	19	613	31	92
a37	22	185	1.08	0.82	3.8	0.0989	3.30	0.86	597	42	608	19	606	18	102
a23	17	186	0.03	0.82	3.1	0.0991	2.20	0.70	599	49	609	13	607	14	102
a41	5	52	0.49	0.81	6.3	0.0997	3.50	0.55	561	115	613	21	602	29	109
a47	7	64	0.79	0.81	4.8	0.0999	3.20	0.65	566	80	614	18	604	22	108
a16	27	218	1.4	0.84	3.2	0.1007	2.70	0.82	623	40	619	16	620	15	99
a4	4	38	0.45	0.84	5.0	0.1013	3.20	0.65	609	82	622	19	619	23	102
b7	12	115	0.65	0.87	5.8	0.1016	3.10	0.53	669	105	624	18	633	28	93
a24	11	101	0.61	0.86	5.4	0.1024	3.20	0.58	624	95	628	19	627	26	101
a58	5	47	0.61	0.88	9.6	0.1029	3.70	0.38	682	190	631	22	642	47	93
a44	7	62	0.51	0.87	4.7	0.1032	3.20	0.68	640	74	633	19	635	22	99
a43	25	243	0.34	0.87	4.0	0.1053	3.40	0.85	592	46	645	21	634	19	109
a48	11	96	0.54	0.89	3.9	0.1060	3.00	0.77	623	54	650	19	644	19	104
a42	6	47	0.84	0.88	5.4	0.1065	3.20	0.59	596	93	652	20	640	26	109
a33	15	105	1.45	0.92	4.2	0.1101	3.30	0.78	625	57	673	21	662	21	108
a46	8	66	0.56	0.94	5.2	0.1118	3.10	0.60	645	89	683	20	674	26	106
a25	5	44	0.31	0.94	4.5	0.1123	3.30	0.73	633	67	686	22	674	23	108
a40	5	37	0.58	1.03	5.5	0.1179	3.30	0.59	714	94	718	22	717	29	101
a30	10	76	0.68	1.04	3.8	0.1208	3.00	0.79	686	50	735	21	723	20	107
a55	3	17	1.63	1.14	6.0	0.1268	3.50	0.58	773	102	770	26	771	33	100
a32	16	118	0.2	1.25	4.2	0.1384	3.50	0.82	792	50	835	27	824	24	105
a8	7	44	0.57	1.36	3.5	0.1445	2.20	0.62	876	57	870	18	872	21	99
a17	4	24	0.8	1.31	7.0	0.1445	4.20	0.61	797	117	870	35	850	41	109
a1	18	115	0.44	1.43	4.0	0.1540	3.10	0.79	852	51	923	27	903	24	108
a5	19	123	0.03	1.54	4.2	0.1623	3.40	0.81	894	51	969	31	947	26	108
a51	6	37	0.41	1.65	4.8	0.1669	3.50	0.73	978	67	995	32	989	31	102
a31	12	55	1.22	1.83	4.3	0.1823	3.10	0.73	1004	60	1079	31	1055	29	107
a6	2	12	0.59	1.90	7.1	0.1868	3.60	0.50	1032	125	1104	36	1080	49	107
a45	25	59	0.55	6.30	3.5	0.3834	3.10	0.88	1943	30	2092	55	2018	31	108
a59	14	34	0.57	6.76	4.4	0.3902	3.40	0.76	2039	51	2124	61	2081	40	104
a18	25	58	0.21	8.61	3.6	0.4064	3.40	0.95	2387	18	2199	64	2298	33	92
a2	31	50	1.64	9.70	3.3	0.4524	3.10	0.93	2408	20	2406	62	2407	31	100
a7	28	48	0.73	10.86	3.4	0.4965	3.10	0.91	2441	24	2599	66	2511	32	106
a9	22	38	0.47	12.76	4.3	0.5172	3.50	0.80	2643	43	2687	77	2662	42	102

				ISOTOPIC RATIOS					AGES						
TG0702	U ppm	Pb ppm	Th/U	207/235	err (2σ)	206/238	err (2σ)	rho	207/206	err (2σ)	206/238	err (2σ)	207/235	err (2σ)	conc
a21	200	18	0.43	0.71	4.9	0.0884	3.20	0.66	540	81	546	17	545	21	101
a58	84	8	0.58	0.73	4.1	0.0893	3.20	0.79	570	54	552	17	555	18	97
a11	209	20	0.51	0.73	4.2	0.0905	3.20	0.77	561	58	559	17	559	18	100
a23	97	10	0.73	0.73	5.7	0.0908	3.30	0.58	553	101	560	18	559	25	101
a59	46	4	0.47	0.77	4.9	0.0926	3.50	0.71	610	75	571	19	579	22	94
a37	59	6	0.49	0.75	4.4	0.0933	3.40	0.76	553	63	575	18	571	20	104
a44	67	7	0.69	0.79	5.9	0.0947	3.60	0.61	616	101	584	20	590	27	95
a6	61	7	1.12	0.78	5.4	0.0952	3.20	0.59	583	95	586	18	586	24	100
a39	104	12	1.14	0.78	4.4	0.0954	3.20	0.73	566	66	587	18	583	20	104
a55	147	16	1.04	0.81	3.7	0.0967	3.10	0.85	620	42	595	18	600	17	96
a19	94	9	0.32	0.79	4.9	0.0974	3.30	0.67	557	79	599	19	590	22	108
a36	144	14	0.44	0.80	4.4	0.0983	3.20	0.72	573	66	604	18	598	20	105
a28	54	5	0.35	0.84	5.0	0.0987	3.50	0.71	655	76	607	20	617	23	93
a57	22	2	0.51	0.93	5.3	0.0990	3.50	0.66	882	83	608	20	670	26	69
a13	228	25	0.77	0.82	4.2	0.0993	3.20	0.76	587	59	611	18	606	19	104
a10	36	4	0.74	0.82	5.0	0.0999	3.30	0.66	596	82	614	19	610	23	103
a40	131	14	0.52	0.87	4.2	0.1010	3.20	0.75	683	59	620	19	634	20	91
a9	32	4	0.84	0.82	5.7	0.1013	3.60	0.63	568	97	622	22	611	27	110
a43	273	30	0.75	0.85	3.9	0.1016	3.30	0.86	636	43	624	20	626	18	98
a1	229	26	0.79	0.85	3.9	0.1017	3.20	0.83	619	47	624	19	623	18	101
a5	166	18	0.64	0.86	4.9	0.1018	3.90	0.78	659	66	625	23	632	24	95
a30	84	9	0.72	0.83	5.5	0.1018	3.30	0.60	577	96	625	20	615	26	108
a29	169	19	0.94	0.86	4.1	0.1021	3.40	0.81	647	52	627	20	631	20	97
a27	138	16	0.82	0.88	4.3	0.1025	3.20	0.75	686	61	629	19	642	21	92
a24	79	8	0.46	0.84	5.3	0.1025	3.40	0.63	596	88	629	20	622	25	106
a14	59	7	0.84	0.98	5.8	0.1059	3.40	0.58	843	98	649	21	694	30	77
a2	51	6	0.78	0.90	5.4	0.1062	3.30	0.61	647	92	650	21	650	26	101
a42	57	6	0.47	0.88	5.5	0.1063	3.40	0.62	610	94	651	21	642	27	107
a4	214	23	0.32	0.90	4.0	0.1066	3.20	0.80	642	51	653	20	650	19	102
a41	91	10	0.55	0.89	4.9	0.1072	3.30	0.68	619	77	656	21	648	24	106
a8	115	14	0.75	0.93	4.3	0.1089	3.30	0.78	678	57	666	21	669	21	98
a16	124	13	0.3	0.92	4.4	0.1092	3.20	0.72	639	66	668	20	661	22	105
a56	47	6	0.85	0.93	4.3	0.1097	3.40	0.80	646	56	671	22	665	21	104
a45	59	7	0.58	0.91	4.5	0.1097	3.30	0.74	614	64	671	21	658	22	109
a60	8	1	0.87	0.93	6.0	0.1105	4.00	0.66	641	97	676	25	668	30	105
a33	35	5	1.43	1.04	5.8	0.1178	3.40	0.59	743	99	718	23	724	31	97
a22	73	11	1.18	1.10	4.8	0.1226	3.30	0.69	776	73	746	23	753	26	96
a15	70	10	0.7	1.12	4.4	0.1262	3.10	0.71	755	65	766	23	763	24	101
a38	127	18	0.94	1.14	4.6	0.1274	3.40	0.73	774	67	773	25	773	25	100
a48	23	4	1.71	1.19	6.4	0.1281	3.60	0.55	843	111	777	26	794	36	92
a7	90	12	0.43	1.15	4.1	0.1289	3.20	0.77	769	55	782	24	778	23	102
a54	51	8	1.05	1.19	4.5	0.1319	3.50	0.77	779	61	799	26	794	25	102
a47	21	4	1.6	1.20	5.8	0.1321	3.80	0.65	798	93	800	29	800	33	100
a3	91	13	0.62	1.21	4.5	0.1336	3.20	0.71	788	66	808	24	803	25	103
a52	95	15	1.26	1.23	3.7	0.1363	3.10	0.85	796	40	824	24	816	21	104
a51	23	3	0.71	1.25	5.5	0.1374	3.30	0.59	809	93	830	26	824	32	103
a18	42	7	1.1	1.25	5.4	0.1387	3.30	0.62	791	88	837	26	825	31	106
a53	31	5	0.41	1.35	5.0	0.1433	3.40	0.67	876	77	864	27	867	30	99
a17	33	5	0.61	1.38	5.2	0.1471	3.30	0.64	870	83	885	27	880	31	102
a25	59	10	1.22	1.41	5.1	0.1479	3.20	0.63	908	82	889	27	894	31	98
a31	349	61	1.18	1.43	3.7	0.1487	3.30	0.89	920	34	894	27	901	22	97
a35	173	31	0.85	1.50	3.8	0.1578	3.30	0.87	902	39	944	29	932	23	105
a26	159	26	0.48	1.52	3.9	0.1582	3.10	0.80	916	48	946	28	937	24	103
a12	196	36	0.7	1.69	3.6	0.1682	3.10	0.87	1009	36	1002	29	1004	23	99
a20	88	20	0.95	2.19	3.9	0.2032	3.20	0.82	1151	44	1192	35	1178	27	104
a46	98	26	1.38	2.34	3.7	0.2100	3.20	0.84	1220	40	1229	35	1225	27	101
a50	110	35	0.81	3.86	3.5	0.2820	3.30	0.92	1611	25	1602	46	1605	29	99
a32	214	76	1.03	4.38	3.7	0.3003	3.10	0.84	1726	36	1693	46	1708	31	98
a49	38	22	0.78	10.86	3.3	0.4871	3.20	0.96	2474	16	2558	68	2512	31	103
a34	65	39	1.16	11.02	3.4	0.4890	3.20	0.93	2492	21	2566	68	2525	32	103

				ISOTOPIC RATIOS					AGES						
TG0703	**U ppm**	**Pb ppm**	**Th/U**	**207/235**	**err (2σ)**	**206/238**	**err (2σ)**	**rho**	**207/206**	**err (2σ)**	**206/238**	**err (2σ)**	**207/235**	**err (2σ)**	**conc**
a29	66	8	0.61	1.08	11.8	0.1104	3.00	0.25	951	234	675	19	743	64	71
a30	38	4	0.45	0.83	7.1	0.0954	3.20	0.44	711	136	588	18	614	33	83
a1	321	29	0.74	0.69	4.5	0.0832	3.30	0.73	608	67	515	16	533	19	85
a23	38	4	0.48	0.75	6.3	0.0915	3.50	0.56	589	113	564	19	569	28	96
b18	99	10	0.58	0.75	4.2	0.0917	2.90	0.68	590	67	565	16	570	18	96
b6	159	16	0.75	0.75	5.5	0.0918	2.70	0.49	570	105	566	15	567	24	99
b15	288	29	0.61	0.75	3.7	0.0921	3.10	0.83	578	45	568	17	570	16	98
b7	130	12	0.41	0.75	4.3	0.0921	3.20	0.76	574	61	568	18	569	19	99
a2	123	12	0.53	0.74	4.0	0.0925	2.70	0.68	526	65	570	15	561	18	108
a15	137	12	0.23	0.75	4.3	0.0927	3.20	0.74	561	64	571	18	569	19	102
b25	126	13	0.92	0.76	4.3	0.0930	3.00	0.70	584	66	573	17	576	19	98
b3	273	26	0.5	0.76	3.7	0.0931	2.90	0.77	587	51	574	16	577	16	98
a8	59	6	0.54	0.77	4.4	0.0933	3.20	0.72	609	67	575	18	582	20	94
b17	47	5	0.55	0.75	6.2	0.0934	3.10	0.50	536	117	576	17	568	27	107
a7	105	10	0.39	0.76	4.3	0.0938	3.00	0.69	546	68	578	17	571	19	106
a6	556	58	0.81	0.77	3.2	0.0940	2.80	0.87	592	34	579	15	582	14	98
b14	70	7	0.71	0.75	5.7	0.0939	3.40	0.59	538	101	579	19	571	25	108
a26	88	8	0.37	0.75	4.7	0.0941	2.90	0.61	534	82	579	16	570	21	109
b4	50	5	0.49	0.79	5.9	0.0954	3.30	0.55	598	107	587	18	590	27	98
b23	132	12	0.25	0.78	3.9	0.0954	3.00	0.78	578	53	587	17	585	17	102
b22	59	6	0.42	0.81	5.2	0.0955	3.00	0.57	646	91	588	17	600	24	91
a9	145	14	0.32	0.80	4.3	0.0954	3.00	0.71	630	65	588	17	596	20	93
b30	33	3	0.45	0.80	4.7	0.0964	3.00	0.64	617	78	593	17	598	21	96
a25	64	6	0.23	0.82	5.4	0.0967	3.50	0.65	658	87	595	20	608	25	90
b26	112	12	0.81	0.80	3.7	0.0967	2.80	0.78	611	49	595	16	599	17	97
a12	146	17	1.38	0.80	3.5	0.0969	2.90	0.81	604	44	597	16	598	16	99
a16	63	6	0.59	0.78	4.7	0.0970	2.90	0.62	550	80	597	17	587	21	109
a5	40	4	0.43	0.82	7.0	0.0982	3.60	0.51	636	131	604	21	610	33	95
b1	178	18	0.47	0.81	3.8	0.0982	3.10	0.82	595	47	604	18	602	17	102
b29	66	7	0.53	0.80	5.6	0.0983	3.50	0.63	577	95	604	20	599	26	105
a13	210	31	2.65	0.80	4.4	0.0983	2.90	0.67	561	71	605	17	595	20	108
a22	54	5	0.47	0.81	4.6	0.0992	3.00	0.65	564	76	609	17	600	21	108
b24	99	10	0.49	0.83	5.1	0.0999	2.90	0.57	601	91	614	17	611	24	102
a4	186	23	1.42	0.83	3.5	0.1002	3.00	0.84	618	41	616	17	616	16	100
a17	296	28	0.09	0.84	3.1	0.1013	2.80	0.88	608	32	622	16	619	15	102
b21	115	12	0.42	0.85	4.6	0.1022	3.00	0.66	608	75	627	18	623	22	103
b5	50	5	0.57	0.87	5.2	0.1025	3.10	0.59	657	90	629	18	635	25	96
a10	56	6	0.35	0.91	5.3	0.1052	3.20	0.60	699	90	645	19	657	26	92
b20	63	7	0.23	0.92	4.5	0.1080	2.90	0.64	663	73	661	18	661	22	100
b19	66	7	0.34	0.95	4.6	0.1114	3.00	0.66	678	73	681	19	680	23	100
b13	54	7	0.89	0.93	5.4	0.1113	2.80	0.52	630	100	681	18	669	27	108
a28	33	4	0.76	0.94	5.7	0.1122	2.80	0.49	628	106	686	18	672	28	109
a19	86	12	0.57	1.12	4.3	0.1280	2.90	0.67	726	67	776	21	763	23	107
b28	97	12	0.24	1.16	4.2	0.1296	2.90	0.69	770	64	785	21	781	23	102
b8	216	28	0.38	1.15	3.4	0.1303	3.10	0.89	735	33	790	23	775	19	107
b2	112	19	1.22	1.30	4.1	0.1362	2.90	0.71	911	59	823	22	847	24	90
b12	14	2	0.5	1.23	7.5	0.1366	3.60	0.49	784	137	825	28	814	43	105
a21	47	7	0.69	1.24	5.5	0.1368	3.60	0.66	795	87	827	28	818	31	104
b11	157	25	0.61	1.41	3.4	0.1493	2.90	0.84	879	39	897	24	892	21	102
b16	84	13	0.53	1.41	3.5	0.1510	2.70	0.78	862	46	906	23	894	21	105
b10	121	20	0.75	1.47	3.9	0.1511	2.80	0.71	942	56	907	24	917	24	96
b9	221	38	0.79	1.49	3.2	0.1557	2.80	0.90	913	29	933	25	927	19	102
a24	169	28	0.4	1.64	3.4	0.1623	2.80	0.81	1024	41	970	25	987	22	95
a20	72	32	2.1	4.85	3.6	0.3209	3.00	0.85	1791	34	1794	48	1793	30	100
b27	35	12	0.56	5.46	5.5	0.3295	2.80	0.51	1959	85	1836	45	1894	48	94
a11	149	70	0.25	10.13	2.9	0.4447	2.70	0.92	2510	20	2372	53	2447	27	94
a27	43	7	1.06	1.34	3.8	0.1466	2.80	0.74	810	54	882	23	862	23	109
a3	54	5	0.45	0.73	5.5	0.0921	3.00	0.55	517	100	568	16	558	24	110
a18	45	5	0.35	0.81	6.8	0.1017	3.30	0.49	529	129	624	20	604	31	118
a14	49	5	0.4	0.72	5.0	0.0931	3.40	0.68	462	81	574	18	552	21	124

Appendix 3: LA-ICPMS U-Pb results for samples FIN 11, FA1, PC5 and PC11

				ISOTOPIC RATIOS					AGES						
FA1	Pb ppm	U ppm	Th/U	207/235	err (1σ)	206/238	err (1σ)	rho	207/206	err (1σ)	206/238	err (1σ)	207/235	err (1σ)	conc
ZR117	15.38	182.94	0.31	0.706	0.011	0.08336	0.00094	0.72	654.7	32.3	516.1	5.6	542.4	6.6	95.2
ZR133	9.20	108.89	0.28	0.704	0.011	0.08367	0.00093	0.72	641.7	32.3	518.0	5.5	541.4	6.5	95.7
ZR116	21.55	236.05	0.53	0.734	0.011	0.08476	0.00095	0.78	701.0	29.2	524.5	5.7	558.7	6.2	93.9
ZR184	13.81	156.26	0.39	0.719	0.010	0.08539	0.00099	0.84	641.6	27.6	528.2	5.9	550.0	5.9	96.0
ZR120	12.15	140.80	0.29	0.724	0.011	0.08618	0.00097	0.74	636.8	31.4	532.9	5.8	553.0	6.5	96.4
ZR200	21.20	227.70	0.51	0.733	0.009	0.08693	0.00099	0.89	646.1	25.1	537.4	5.9	558.6	5.5	96.2
ZR210	33.29	364.81	0.49	0.748	0.009	0.08730	0.00099	0.93	679.0	23.6	539.5	5.9	567.0	5.3	95.1
ZR202	10.50	114.93	0.43	0.757	0.010	0.08761	0.00100	0.86	697.9	25.9	541.4	5.9	572.4	5.8	94.6
ZR125	37.09	318.07	1.51	0.797	0.011	0.08794	0.00097	0.83	798.7	26.4	543.3	5.8	595.3	6.0	91.3
ZR223	20.05	180.73	1.07	0.777	0.011	0.08938	0.00102	0.83	711.1	27.2	551.9	6.0	584.0	6.1	94.5
ZR203	10.19	109.32	0.43	0.748	0.010	0.08953	0.00103	0.83	624.7	27.6	552.7	6.1	567.0	6.0	97.5
ZR185	8.81	95.97	0.35	0.756	0.010	0.08978	0.00104	0.85	642.1	27.0	554.3	6.1	571.7	6.0	97.0
ZR207	15.46	169.91	0.35	0.721	0.010	0.08992	0.00103	0.86	536.0	27.5	555.0	6.1	551.4	5.7	100.7
ZR126	10.98	109.46	0.73	0.760	0.011	0.08997	0.00100	0.80	647.5	28.6	555.4	5.9	573.8	6.1	96.8
ZR143	11.03	120.84	0.31	0.740	0.010	0.09007	0.00102	0.86	589.5	26.5	556.0	6.1	562.5	5.7	98.8
ZR165	11.57	125.15	0.38	0.737	0.010	0.09013	0.00104	0.84	577.6	27.7	556.3	6.1	560.5	5.9	99.3
ZR224	20.71	235.41	0.19	0.736	0.010	0.09016	0.00102	0.86	573.5	26.4	556.5	6.0	559.8	5.6	99.4
ZR208	13.41	147.26	0.33	0.740	0.010	0.09017	0.00103	0.88	585.0	25.8	556.6	6.1	562.1	5.6	99.0
ZR158	18.26	195.59	0.42	0.734	0.010	0.09023	0.00103	0.88	566.7	26.3	556.9	6.1	558.8	5.6	99.7
ZR217	13.54	138.66	0.55	0.739	0.010	0.09023	0.00103	0.84	581.8	27.5	556.9	6.1	561.8	5.9	99.1
ZR164	21.15	215.65	0.61	0.735	0.010	0.09024	0.00104	0.86	568.9	26.3	557.0	6.1	559.3	5.8	99.6
ZR162	9.96	109.47	0.34	0.738	0.012	0.09025	0.00105	0.73	579.1	32.9	557.0	6.2	561.3	6.9	99.2
ZR213	14.23	150.42	0.46	0.740	0.010	0.09024	0.00103	0.86	583.8	26.7	557.0	6.1	562.2	5.7	99.1
ZR180	9.09	99.59	0.32	0.737	0.011	0.09029	0.00105	0.79	574.7	30.0	557.3	6.2	560.7	6.4	99.4
ZR216	8.67	94.37	0.33	0.744	0.010	0.09031	0.00103	0.81	594.1	28.5	557.4	6.1	564.7	6.1	98.7
ZR205	9.31	99.25	0.41	0.749	0.011	0.09038	0.00104	0.81	607.1	28.7	557.8	6.2	567.5	6.2	98.3
ZR212	15.74	166.66	0.42	0.736	0.010	0.09044	0.00104	0.81	567.3	29.0	558.1	6.1	559.9	6.1	99.7
ZR141	19.62	191.01	0.77	0.741	0.009	0.09044	0.00102	0.91	582.5	24.5	558.2	6.0	562.9	5.4	99.2
ZR115	14.17	152.85	0.38	0.740	0.010	0.09047	0.00101	0.81	579.0	28.2	558.3	6.0	562.4	5.9	99.3
ZR150	12.48	132.73	0.41	0.726	0.010	0.09050	0.00103	0.86	535.0	27.3	558.5	6.1	553.9	5.7	100.8
ZR193	12.01	128.04	0.42	0.736	0.010	0.09053	0.00105	0.86	565.9	27.3	558.7	6.2	560.1	5.8	99.8
ZR195	11.78	126.72	0.38	0.737	0.010	0.09059	0.00105	0.86	566.2	27.3	559.0	6.2	560.4	5.8	99.8
ZR144	10.20	108.69	0.40	0.724	0.010	0.09065	0.00103	0.85	525.9	27.6	559.4	6.1	552.8	5.7	101.2
ZR174	12.90	136.06	0.43	0.729	0.010	0.09066	0.00104	0.85	542.7	27.2	559.5	6.2	556.1	5.8	100.6
ZR186	11.70	124.15	0.42	0.721	0.010	0.09076	0.00105	0.86	515.5	27.5	560.1	6.2	551.3	5.8	101.6
ZR159	9.65	104.06	0.37	0.731	0.010	0.09076	0.00104	0.83	545.7	27.8	560.1	6.2	557.2	5.9	100.5
ZR134	7.75	83.08	0.35	0.763	0.012	0.09082	0.00101	0.73	638.4	31.7	560.4	6.0	576.0	6.7	97.3
ZR190	20.60	231.22	0.22	0.734	0.010	0.09088	0.00105	0.88	551.3	26.0	560.7	6.2	558.8	5.6	100.3

ZR183	34.40	392.40	0.16	0.740	0.009	0.09087	0.00104	0.94	569.3	24.0	560.7	6.1	562.3	5.2	99.7
ZR181	13.79	144.54	0.45	0.735	0.010	0.09096	0.00104	0.88	553.5	25.7	561.2	6.2	559.6	5.6	100.3
ZR145	35.84	372.46	0.46	0.741	0.009	0.09100	0.00103	0.93	570.5	23.9	561.4	6.1	563.2	5.3	99.7
ZR201	18.08	188.81	0.49	0.727	0.010	0.09105	0.00104	0.87	525.6	26.7	561.7	6.2	554.7	5.6	101.3
ZR173	7.65	82.47	0.34	0.728	0.010	0.09108	0.00105	0.84	529.5	28.3	561.9	6.2	555.5	5.9	101.2
ZR218	12.79	134.55	0.44	0.720	0.010	0.09117	0.00104	0.82	501.1	28.7	562.4	6.2	550.5	5.9	102.2
ZR221	22.45	215.14	0.77	0.732	0.010	0.09115	0.00104	0.85	539.2	28.0	562.4	6.1	557.9	5.8	100.8
ZR129	8.23	90.74	0.27	0.743	0.012	0.09142	0.00103	0.71	564.7	33.4	563.9	6.1	564.1	6.9	100.0
ZR119	10.69	114.12	0.39	0.735	0.011	0.09143	0.00103	0.78	541.3	30.8	564.0	6.1	559.6	6.2	100.8
ZR131	13.92	143.15	0.48	0.766	0.011	0.09143	0.00101	0.79	632.4	29.1	564.0	6.0	577.7	6.2	97.6
ZR123	11.45	122.16	0.39	0.737	0.010	0.09149	0.00102	0.81	545.2	28.7	564.3	6.0	560.5	5.9	100.7
ZR142	7.07	76.62	0.31	0.731	0.010	0.09154	0.00104	0.81	527.0	28.9	564.6	6.2	557.2	6.0	101.3
ZR154	17.80	153.27	1.16	0.780	0.011	0.09231	0.00106	0.85	649.8	26.7	569.2	6.2	585.6	6.0	97.2
ZR177	15.42	159.06	0.44	0.757	0.010	0.09242	0.00106	0.91	581.6	24.9	569.8	6.3	572.1	5.5	99.6
ZR135	58.31	632.36	0.20	0.886	0.011	0.09276	0.00101	0.88	906.2	24.1	571.8	6.0	644.0	5.9	88.8
ZR168	11.57	120.72	0.42	0.761	0.010	0.09304	0.00107	0.85	578.8	27.1	573.5	6.3	574.5	6.0	99.8
ZR147	15.13	153.87	0.50	0.765	0.010	0.09307	0.00105	0.89	589.0	25.1	573.7	6.2	576.7	5.6	99.5
ZR166	20.10	221.08	0.23	0.767	0.010	0.09311	0.00107	0.89	594.3	25.5	573.9	6.3	578.0	5.7	99.3
ZR148	9.53	58.52	2.86	0.766	0.011	0.09314	0.00107	0.77	590.5	30.4	574.1	6.3	577.4	6.6	99.4
ZR161	13.47	138.77	0.43	0.784	0.012	0.09381	0.00109	0.79	624.7	29.6	578.0	6.4	587.5	6.6	98.4
ZR121	9.67	101.44	0.36	0.779	0.011	0.09415	0.00105	0.79	604.7	29.3	580.1	6.2	585.0	6.3	99.2
ZR182	17.68	173.66	0.51	0.790	0.010	0.09546	0.00110	0.88	605.4	25.8	587.8	6.5	591.3	5.9	99.4
ZR194	14.03	143.08	0.38	0.777	0.010	0.09616	0.00111	0.87	553.9	26.3	591.9	6.5	584.0	5.9	101.4
ZR140	15.44	147.34	0.50	0.820	0.011	0.09677	0.00106	0.79	656.5	28.8	595.5	6.2	608.3	6.4	97.9
ZR170	15.42	128.63	1.03	0.815	0.010	0.09815	0.00112	0.90	612.6	25.0	603.6	6.6	605.4	5.8	99.7
ZR215	2.52	23.30	0.64	0.823	0.016	0.09826	0.00116	0.61	630.4	40.4	604.2	6.8	609.7	8.9	99.1
ZR176	37.36	282.28	1.45	0.810	0.010	0.09900	0.00113	0.94	580.0	23.6	608.5	6.6	602.5	5.5	101.0
ZR220	21.08	196.43	0.52	0.844	0.011	0.09977	0.00113	0.88	650.7	25.4	613.1	6.6	621.1	6.0	98.7
ZR214	33.87	291.12	0.84	0.832	0.010	0.10018	0.00113	0.91	612.3	24.3	615.5	6.7	614.7	5.7	100.1
ZR225	8.97	93.85	0.08	0.877	0.012	0.10081	0.00115	0.83	712.6	27.3	619.1	6.7	639.5	6.5	96.8
ZR136	72.25	480.50	1.91	0.855	0.011	0.10120	0.00110	0.87	648.6	25.5	621.5	6.4	627.3	5.9	99.1
ZR151	33.79	291.76	0.70	0.852	0.010	0.10274	0.00116	0.93	608.0	23.6	630.4	6.8	625.5	5.6	100.8
ZR163	36.29	334.61	0.39	0.895	0.011	0.10549	0.00120	0.92	657.5	23.9	646.5	7.0	648.9	5.9	99.6
ZR219	72.91	521.36	1.02	1.045	0.013	0.11560	0.00130	0.92	793.1	23.4	705.2	7.5	726.5	6.4	97.1
ZR187	10.60	83.04	0.56	1.026	0.014	0.11697	0.00135	0.87	729.6	25.7	713.1	7.8	717.0	6.8	99.5
ZR179	12.58	84.31	1.10	1.042	0.014	0.12025	0.00138	0.87	703.0	25.7	732.0	8.0	724.9	6.8	101.0
ZR199	10.61	87.89	0.23	1.101	0.015	0.12216	0.00142	0.85	786.5	26.2	743.0	8.1	753.8	7.2	98.6
ZR152	16.16	113.47	0.73	1.142	0.015	0.12501	0.00142	0.89	814.1	24.3	759.3	8.2	773.3	6.9	98.2
ZR209	35.46	232.17	0.86	1.181	0.015	0.13052	0.00148	0.92	795.1	23.5	790.8	8.5	791.9	6.8	99.9
ZR189	17.08	100.73	1.24	1.194	0.016	0.13326	0.00154	0.87	774.2	25.7	806.4	8.8	797.9	7.4	101.1
ZR204	7.68	52.12	0.64	1.222	0.017	0.13426	0.00154	0.83	806.1	26.9	812.1	8.8	810.5	7.7	100.2
ZR139	57.04	410.94	0.23	1.305	0.017	0.13478	0.00147	0.85	934.9	25.3	815.1	8.3	847.8	7.4	96.1

ZR155	31.91	221.47	0.49	1.248	0.015	0.13513	0.00153	0.93	837.6	22.9	817.1	8.7	822.6	6.9	99.3
ZR160	46.89	315.38	0.55	1.278	0.016	0.13773	0.00157	0.94	847.4	22.8	831.8	8.9	836.0	6.9	99.5
ZR114	29.54	175.77	0.92	1.373	0.018	0.14170	0.00158	0.85	936.9	25.4	854.3	8.9	877.6	7.7	97.3
ZR132	57.79	380.21	0.46	1.385	0.017	0.14297	0.00156	0.89	936.7	23.8	861.4	8.8	882.7	7.2	97.6
ZR169	24.65	149.92	0.79	1.389	0.018	0.14444	0.00166	0.88	921.1	24.5	869.7	9.4	884.3	7.7	98.3
ZR167	63.33	354.68	0.93	1.481	0.018	0.15008	0.00172	0.92	974.5	22.8	901.4	9.6	922.8	7.5	97.7
ZR130	84.44	519.42	0.49	1.496	0.018	0.15270	0.00167	0.90	958.8	23.2	916.1	9.3	928.7	7.4	98.6
ZR127	25.28	122.87	1.39	1.539	0.020	0.15707	0.00173	0.86	959.4	24.8	940.5	9.7	946.1	7.9	99.4
ZR211	37.61	215.52	0.59	1.578	0.019	0.15942	0.00181	0.94	980.3	22.4	953.5	10.0	961.6	7.6	99.2
ZR197	18.95	96.69	1.05	1.582	0.021	0.16145	0.00186	0.89	959.0	24.1	964.8	10.3	963.0	8.1	100.2
ZR172	26.63	137.95	0.83	1.628	0.020	0.16482	0.00188	0.94	975.7	22.2	983.5	10.4	981.0	7.6	100.3
ZR157	26.73	153.46	0.38	1.675	0.020	0.16823	0.00191	0.93	991.6	22.4	1002.4	10.6	998.9	7.8	98.9
ZR113	159.35	819.71	0.88	1.687	0.020	0.16432	0.00181	0.92	1054.2	22.7	980.7	10.0	1003.7	7.7	95.2
ZR153	99.46	508.91	0.67	1.862	0.022	0.17336	0.00196	0.96	1144.5	20.8	1030.6	10.8	1067.7	7.7	96.5
ZR222	129.33	526.96	1.50	1.960	0.024	0.17833	0.00201	0.92	1189.9	22.0	1057.8	11.0	1101.8	8.2	92.6
ZR118	49.28	146.42	0.38	5.031	0.062	0.31140	0.00345	0.90	1913.9	20.6	1747.6	17.0	1824.6	10.4	95.3
ZR171	33.77	77.24	0.53	7.258	0.086	0.38526	0.00441	0.96	2185.3	18.5	2100.8	20.5	2143.7	10.6	98.1
ZR196	43.32	102.17	0.38	8.431	0.103	0.38454	0.00442	0.94	2445.4	18.5	2097.5	20.6	2278.5	11.1	93.2
ZR175	204.76	464.32	0.71	8.121	0.093	0.36841	0.00419	0.99	2454.6	17.2	2021.9	19.8	2244.6	10.4	91.4
ZR188	18.18	34.01	1.10	9.187	0.112	0.41252	0.00475	0.94	2471.9	18.5	2226.4	21.7	2356.8	11.2	95.3
ZR156	27.02	43.60	1.19	10.956	0.131	0.46747	0.00533	0.95	2557.6	18.0	2472.5	23.4	2519.4	11.1	98.1
ZR128	96.49	217.46	0.55	9.085	0.107	0.37663	0.00412	0.93	2605.8	18.3	2060.5	19.3	2346.6	10.8	90.1
ZR149	190.57	376.57	0.43	10.787	0.124	0.44655	0.00503	0.98	2608.1	17.1	2379.9	22.4	2504.9	10.7	95.0
ZR138	65.86	127.12	0.69	10.714	0.132	0.42682	0.00464	0.88	2671.9	19.5	2291.4	21.0	2498.7	11.5	93.5
ZR137	360.06	615.53	0.38	14.479	0.176	0.50532	0.00548	0.89	2888.8	18.7	2636.6	23.5	2781.6	11.5	96.3

				ISOTOPIC RATIOS					AGES						
PC5	Pb ppm	U ppm	Th/U	207/235	err (1σ)	206/238	err (1σ)	rho	207/206	err (1σ)	206/238	err (1σ)	207/235	err (1σ)	conc
ZR54	13.4	159.8	0.38	0.660	0.009	0.08045	0.00091	0.82	585.3	28.0	498.8	5.4	514.5	5.6	85.2
ZR24	9.5	112.6	0.32	0.669	0.012	0.08187	0.00098	0.66	577.0	38.0	507.3	5.8	520.1	7.4	87.9
ZR25	14.8	170.8	0.41	0.696	0.011	0.08239	0.00096	0.76	647.3	30.9	510.4	5.7	536.1	6.4	78.9
ZR23	12.1	137.0	0.46	0.688	0.010	0.08365	0.00097	0.81	590.7	28.9	517.9	5.8	531.5	6.0	87.7
ZR20	19.4	219.9	0.41	0.701	0.009	0.08514	0.00099	0.88	594.1	26.0	526.7	5.9	539.5	5.5	88.7
ZR6	14.7	165.8	0.42	0.754	0.011	0.08631	0.00103	0.84	721.3	27.1	533.7	6.1	570.6	6.2	74.0
ZR59	24.2	253.7	0.60	0.711	0.010	0.08654	0.00098	0.83	589.5	27.9	535.0	5.8	545.4	5.8	90.8
ZR29	10.8	117.8	0.43	0.728	0.011	0.08670	0.00100	0.79	636.7	29.4	536.0	5.9	555.6	6.2	84.2
ZR9	22.5	251.7	0.43	0.717	0.009	0.08705	0.00103	0.90	595.3	25.8	538.0	6.1	549.2	5.6	90.4
ZR22	9.5	106.1	0.34	0.707	0.010	0.08717	0.00102	0.79	560.3	29.9	538.8	6.0	542.9	6.2	96.2
ZR46	8.7	97.8	0.36	0.705	0.010	0.08718	0.00100	0.81	554.5	29.0	538.8	5.9	541.8	6.0	97.2
ZR18	13.8	150.3	0.47	0.718	0.010	0.08736	0.00102	0.86	590.6	26.8	539.9	6.0	549.7	5.8	91.4
ZR15	14.7	158.0	0.53	0.716	0.010	0.08742	0.00102	0.86	582.2	26.5	540.3	6.1	548.3	5.7	92.8
ZR32	9.5	108.0	0.35	0.721	0.010	0.08744	0.00102	0.82	594.9	28.9	540.4	6.0	551.0	6.1	90.8
ZR26	15.7	166.8	0.50	0.716	0.010	0.08755	0.00101	0.85	579.3	27.0	541.0	6.0	548.4	5.7	93.4
ZR16	13.8	148.3	0.53	0.715	0.010	0.08765	0.00103	0.85	574.4	27.3	541.6	6.1	547.9	5.8	94.3
ZR17	13.0	141.9	0.47	0.709	0.010	0.08767	0.00103	0.85	555.6	27.4	541.7	6.1	544.4	5.8	97.5
ZR19	12.2	134.0	0.39	0.734	0.010	0.08768	0.00102	0.85	628.1	26.9	541.8	6.1	558.7	5.9	86.3
ZR51	14.9	159.6	0.47	0.746	0.010	0.08775	0.00100	0.83	661.0	27.6	542.2	5.9	565.6	6.0	82.0
ZR14	9.7	106.5	0.42	0.719	0.010	0.08776	0.00103	0.83	581.3	27.9	542.3	6.1	549.8	6.0	93.3
ZR13	10.7	119.1	0.39	0.721	0.010	0.08778	0.00103	0.83	589.6	28.0	542.4	6.1	551.5	6.0	92.0
ZR55	9.7	105.3	0.39	0.720	0.010	0.08786	0.00100	0.80	582.3	29.2	542.9	5.9	550.4	6.1	93.2
ZR12	9.5	105.9	0.36	0.716	0.010	0.08806	0.00104	0.84	566.1	27.9	544.1	6.2	548.3	6.0	96.1
ZR57	8.3	90.7	0.36	0.736	0.011	0.08825	0.00100	0.78	620.0	29.5	545.2	5.9	559.8	6.2	87.9
ZR60	10.8	115.8	0.38	0.745	0.011	0.08845	0.00101	0.77	643.4	30.3	546.3	6.0	565.4	6.4	84.9
ZR35	9.0	101.1	0.32	0.732	0.010	0.08846	0.00103	0.82	604.1	28.4	546.4	6.1	557.7	6.1	90.4
ZR53	11.9	128.9	0.39	0.731	0.010	0.08859	0.00101	0.82	598.2	28.2	547.2	6.0	557.1	6.0	91.5
ZR8	10.5	116.7	0.40	0.742	0.010	0.08871	0.00105	0.86	627.5	26.8	547.9	6.2	563.5	6.0	87.3
ZR2	10.4	117.6	0.35	0.711	0.010	0.08875	0.00106	0.85	534.8	27.9	548.1	6.3	545.6	5.9	102.5
ZR49	22.1	227.9	0.56	0.746	0.010	0.08938	0.00102	0.88	623.5	25.8	551.8	6.0	566.0	5.6	88.5
ZR30	12.4	124.8	0.59	0.759	0.011	0.08953	0.00103	0.83	656.4	27.8	552.8	6.1	573.5	6.1	84.2
ZR42	8.7	95.0	0.36	0.723	0.010	0.08976	0.00103	0.83	545.3	27.8	554.1	6.1	552.4	5.9	101.6
ZR40	8.8	96.3	0.36	0.739	0.010	0.09021	0.00104	0.85	582.9	27.1	556.8	6.1	561.9	5.9	95.5
ZR27	33.0	328.4	0.66	0.757	0.010	0.09023	0.00103	0.88	633.0	25.4	556.9	6.1	572.1	5.7	88.0
ZR44	8.2	89.1	0.33	0.748	0.010	0.09031	0.00104	0.83	606.3	27.9	557.4	6.1	567.1	6.0	91.9
ZR36	8.0	88.1	0.36	0.739	0.010	0.09037	0.00104	0.84	578.8	27.2	557.7	6.2	561.8	5.9	96.4
ZR34	25.4	276.5	0.37	0.747	0.009	0.09049	0.00104	0.91	600.2	24.6	558.5	6.2	566.7	5.5	93.1
ZR38	7.8	85.7	0.33	0.752	0.010	0.09083	0.00105	0.85	604.8	27.2	560.4	6.2	569.3	6.0	92.7

ZR33	9.2	100.3	0.34	0.740	0.010	0.09087	0.00105	0.86	570.7	26.7	560.7	6.2	562.6	5.8	98.2
ZR43	22.5	246.0	0.25	0.756	0.010	0.09201	0.00105	0.89	588.3	25.2	567.4	6.2	571.6	5.6	96.4
ZR48	19.0	204.1	0.26	0.780	0.010	0.09306	0.00106	0.87	631.6	25.8	573.6	6.2	585.4	5.8	90.8
ZR39	7.3	74.7	0.28	0.800	0.013	0.09794	0.00115	0.72	576.3	33.5	602.3	6.8	596.8	7.3	104.5
ZR41	13.6	118.9	0.87	0.838	0.011	0.09886	0.00113	0.86	656.6	26.1	607.7	6.7	618.1	6.1	92.6
ZR45	10.4	91.4	0.37	0.931	0.013	0.10961	0.00125	0.84	660.6	26.9	670.5	7.3	668.2	6.6	101.5
ZR7	11.5	92.7	0.70	0.963	0.013	0.11156	0.00133	0.87	694.8	26.3	681.8	7.7	684.7	6.9	98.1
ZR56	15.5	127.9	0.41	1.035	0.014	0.11499	0.00130	0.83	783.8	27.0	701.6	7.5	721.4	7.1	89.5
ZR4	18.0	153.6	0.21	1.090	0.014	0.12152	0.00144	0.91	777.5	24.0	739.3	8.3	748.7	6.9	95.1
ZR3	46.9	327.2	0.77	1.160	0.015	0.12875	0.00153	0.95	786.1	22.8	780.7	8.7	782.0	6.8	99.3
ZR10	8.7	63.1	0.27	1.336	0.020	0.13946	0.00167	0.81	912.8	28.1	841.6	9.4	861.3	8.6	92.2
ZR50	56.1	334.5	0.30	1.618	0.020	0.16380	0.00186	0.90	976.1	23.5	977.8	10.3	977.2	7.9	100.2
ZR58	16.4	225.7	0.28	0.727	0.010	0.06707	0.00076	0.82	1162.6	25.9	418.5	4.6	554.7	5.9	75.4
ZR1	30.5	306.0	0.64	1.014	0.014	0.08708	0.00104	0.88	1304.3	23.3	538.3	6.2	711.1	6.9	75.7
ZR47	11.8	129.2	0.31	1.021	0.013	0.08273	0.00094	0.86	1415.4	23.2	512.4	5.6	714.5	6.7	71.7
ZR5	16.9	91.7	0.42	2.982	0.038	0.16701	0.00199	0.94	2091.5	19.6	995.6	11.0	1403.0	9.7	71.0
ZR11	9.6	69.8	0.71	1.955	0.026	0.10430	0.00123	0.89	2176.5	20.7	639.5	7.2	1100.2	8.9	58.1
ZR37	19.7	200.6	0.26	1.545	0.020	0.07741	0.00090	0.89	2285.5	20.6	480.6	5.4	948.7	8.1	50.7
ZR21	80.6	202.6	0.28	8.090	0.100	0.36709	0.00423	0.93	2454.0	18.8	2015.7	20.0	2241.1	11.2	89.9
ZR31	24.0	39.2	1.36	10.317	0.127	0.46028	0.00533	0.94	2482.7	18.6	2440.8	23.5	2463.6	11.4	99.1
ZR52	22.8	275.9	0.18	1.531	0.020	0.05787	0.00066	0.88	2758.4	19.7	362.6	4.0	942.8	7.9	38.5
ZR28	56.8	117.9	0.36	13.933	0.173	0.19447	0.00223	0.92	4297.9	16.7	1145.5	12.0	2745.1	11.8	41.7

				ISOTOPIC RATIOS					AGES						
FIN11	Pb ppm	U ppm	Th/U	207/235	err (1σ)	206/238	err (1σ)	rho	207/206	err (1σ)	206/238	err (1σ)	207/235	err (1σ)	conc
ZR103	13.86	151.29	0.48	0.718	0.009	0.08655	0.00099	0.88	609.0	25.6	535.1	5.9	549.3	5.5	97.4
ZR11	17.75	189.84	0.48	0.765	0.010	0.08816	0.00102	0.88	706.9	25.4	544.7	6.1	577.0	5.8	94.4
ZR36	15.013	146.282	0.84	0.724	0.010	0.08827	0.00101	0.87	584.3	26.0	545.3	6.0	552.8	5.6	98.6
ZR49	30.0624	313.245	0.51	0.737	0.009	0.08986	0.00102	0.91	583.9	24.3	554.7	6.1	560.4	5.3	99.0
ZR101	31.88	318.25	0.65	0.734	0.009	0.09014	0.00102	0.92	569.7	24.3	556.4	6.1	558.9	5.3	99.6
ZR28	15.7947	170.556	0.40	0.726	0.009	0.09037	0.00104	0.91	538.8	25.6	557.7	6.1	554.1	5.4	100.6
ZR37	112.244	1113.39	0.65	0.756	0.009	0.09102	0.00104	0.97	611.3	22.6	561.5	6.1	571.4	5.2	98.3
ZR40	25.9816	266.96	0.48	0.776	0.010	0.09177	0.00105	0.90	651.1	24.6	566.0	6.2	583.2	5.6	97.1
ZR90	13.01	125.20	0.67	0.781	0.010	0.09205	0.00105	0.89	657.9	25.1	567.7	6.2	586.0	5.7	96.9
ZR58	76.66	820.82	0.33	0.802	0.010	0.09206	0.00106	0.97	715.4	22.2	567.7	6.2	598.1	5.4	94.9
ZR21	37.61	404.54	0.29	0.764	0.009	0.09243	0.00106	0.93	601.6	23.9	569.9	6.3	576.3	5.4	98.9
ZR60	6.34	64.05	0.47	0.782	0.011	0.09417	0.00109	0.83	611.2	27.8	580.2	6.4	586.5	6.2	98.9
ZR75	23.90	220.51	0.70	0.786	0.010	0.09569	0.00109	0.91	587.8	24.6	589.1	6.4	588.8	5.6	100.1
ZR66	16.87	144.01	1.06	0.785	0.010	0.09583	0.00110	0.90	583.2	25.0	589.9	6.5	588.5	5.7	100.2
ZR44	26.7289	241.297	0.72	0.844	0.010	0.09722	0.00111	0.92	708.1	23.8	598.1	6.5	621.6	5.8	96.2
ZR81	27.99	260.43	0.60	0.819	0.010	0.09748	0.00111	0.91	636.7	24.5	599.6	6.5	607.4	5.7	98.7
ZR110	26.20	247.65	0.55	0.822	0.010	0.09775	0.00111	0.90	639.8	24.9	601.2	6.5	609.3	5.8	98.7
ZR42	77.3541	776.614	0.34	0.817	0.010	0.09776	0.00111	0.95	627.0	22.8	601.3	6.5	606.6	5.4	99.1
ZR4	101.61	898.54	0.81	0.821	0.010	0.09802	0.00113	0.97	631.7	22.4	602.8	6.7	608.8	5.4	99.0
ZR80	31.19	293.66	0.53	0.820	0.010	0.09844	0.00112	0.91	617.4	24.4	605.3	6.6	607.8	5.7	99.6
ZR13	20.25	183.79	0.67	0.833	0.010	0.09916	0.00115	0.92	637.1	24.1	609.5	6.7	615.3	5.8	99.1
ZR27	7.52812	63.5349	0.93	0.858	0.012	0.09918	0.00115	0.85	700.3	26.8	609.6	6.7	629.2	6.4	96.9
ZR64	18.48	156.51	0.98	0.810	0.011	0.09922	0.00114	0.86	574.5	26.5	609.8	6.7	602.3	6.1	101.2
ZR57	17.50	174.02	0.34	0.832	0.010	0.09933	0.00114	0.92	630.5	24.0	610.5	6.7	614.7	5.7	99.3
ZR59	18.68	184.55	0.34	0.842	0.011	0.09964	0.00115	0.92	648.8	24.1	612.3	6.7	620.1	5.8	98.7
ZR99	12.41	120.97	0.38	0.825	0.011	0.09969	0.00114	0.89	604.5	25.6	612.6	6.7	610.8	5.9	100.3
ZR111	12.24	122.74	0.26	0.848	0.011	0.10001	0.00114	0.86	658.1	26.2	614.4	6.7	623.8	6.2	98.5
ZR106	20.34	183.41	0.63	0.841	0.011	0.10024	0.00114	0.89	635.0	25.0	615.8	6.7	619.9	5.9	99.3
ZR84	14.69	142.10	0.40	0.826	0.010	0.10049	0.00114	0.90	590.2	24.8	617.3	6.7	611.5	5.8	100.9
ZR67	5.80	51.11	0.73	0.842	0.012	0.10052	0.00117	0.80	629.9	29.0	617.5	6.8	620.1	6.7	99.6
ZR17	22.24	218.80	0.28	0.855	0.011	0.10091	0.00117	0.90	654.1	25.0	619.8	6.8	627.1	6.1	98.8
ZR39	19.3796	193.446	0.24	0.866	0.011	0.10141	0.00116	0.91	672.5	24.1	622.7	6.8	633.5	5.9	98.3
ZR82	14.86	131.89	0.60	0.863	0.011	0.10179	0.00116	0.88	657.7	25.5	624.9	6.8	632.0	6.1	98.9
ZR3	36.68	333.90	0.54	0.858	0.010	0.10234	0.00119	0.95	633.1	23.2	628.1	6.9	629.2	5.7	99.8
ZR54	4.91	46.00	0.42	0.850	0.013	0.10378	0.00121	0.79	581.6	29.9	636.5	7.1	624.5	6.9	101.9
ZR102	69.74	683.57	0.17	0.909	0.011	0.10506	0.00119	0.95	701.0	22.9	644.0	6.9	656.7	5.8	98.1
ZR18	9.48	88.71	0.30	0.886	0.012	0.10593	0.00123	0.87	627.7	26.2	649.1	7.2	644.3	6.4	100.7
ZR50	50.264	415.145	0.70	0.918	0.011	0.10749	0.00122	0.92	672.5	23.9	658.2	7.1	661.4	6.0	99.5

ZR108	7.56	66.27	0.46	0.911	0.013	0.10835	0.00124	0.82	637.9	27.9	663.2	7.2	657.4	6.7	100.9
ZR87	6.90	57.75	0.63	0.931	0.013	0.10851	0.00125	0.84	681.3	27.2	664.1	7.2	668.0	6.7	99.4
ZR29	10.483	75.630 5	1.26	0.932	0.012	0.10930	0.00126	0.87	668.4	26.0	668.7	7.3	668.6	6.5	100.0
ZR100	15.07	110.75	1.03	0.952	0.012	0.11208	0.00128	0.89	661.6	25.2	684.8	7.4	679.4	6.4	100.8
ZR45	50.5643	437.42 7	0.28	1.006	0.012	0.11518	0.00131	0.94	719.6	23.0	702.8	7.6	706.7	6.2	99.4
ZR105	76.35	654.09	0.27	1.031	0.012	0.11654	0.00132	0.94	747.9	23.1	710.6	7.6	719.6	6.2	98.7
ZR69	37.86	313.58	0.35	1.034	0.013	0.11822	0.00135	0.94	723.5	22.9	720.3	7.8	721.1	6.2	99.9
ZR26	73.9022	576.79 8	0.52	1.060	0.013	0.11985	0.00137	0.97	747.4	22.0	729.7	7.9	734.0	6.2	99.4
ZR73	26.16	162.55	1.38	1.091	0.014	0.12005	0.00137	0.91	804.6	23.6	730.8	7.9	749.2	6.6	97.5
ZR2	13.30	96.73	0.75	1.075	0.014	0.12104	0.00141	0.89	755.4	24.7	736.5	8.1	741.2	6.9	99.4
ZR56	25.71	209.24	0.27	1.087	0.013	0.12351	0.00142	0.94	735.8	23.0	750.8	8.2	747.0	6.5	100.5
ZR95	19.76	130.81	0.98	1.134	0.014	0.12549	0.00143	0.92	791.8	23.7	762.1	8.2	769.7	6.7	99.0
ZR96	21.28	154.72	0.60	1.134	0.014	0.12559	0.00143	0.92	789.4	23.5	762.6	8.2	769.4	6.7	99.1
ZR53	56.8267	389.75 4	0.78	1.129	0.014	0.12566	0.00143	0.92	779.6	23.4	763.0	8.2	767.2	6.6	99.5
ZR89	42.06	312.57	0.51	1.142	0.014	0.12591	0.00143	0.96	800.5	22.3	764.5	8.2	773.7	6.4	98.8
ZR24	20.30	147.29	0.54	1.143	0.015	0.12668	0.00146	0.90	787.9	24.4	768.9	8.4	773.7	7.0	99.4
ZR93	12.36	85.21	0.75	1.149	0.015	0.12777	0.00146	0.87	782.3	25.4	775.1	8.4	776.9	7.1	99.8
ZR70	20.46	155.81	0.35	1.170	0.015	0.12782	0.00146	0.92	819.6	23.3	775.4	8.4	786.8	6.8	98.6
ZR12	23.21	129.03	1.66	1.177	0.015	0.12863	0.00149	0.92	817.4	23.5	780.0	8.5	789.7	6.9	98.8
ZR32	45.9727	386.42 9	0.02	1.151	0.014	0.12874	0.00147	0.96	769.2	22.2	780.7	8.4	777.6	6.5	100.4
ZR109	158.62	1192.4 7	0.33	1.250	0.015	0.12935	0.00146	0.93	930.8	22.5	784.2	8.4	823.3	6.8	95.3
ZR41	15.7174	103.25 1	0.88	1.183	0.015	0.12942	0.00148	0.90	815.6	24.1	784.5	8.5	792.6	7.0	99.0
ZR55	63.82	341.79	1.83	1.176	0.014	0.13001	0.00149	0.96	794.4	22.1	787.9	8.5	789.6	6.6	99.8
ZR94	20.84	150.06	0.50	1.191	0.015	0.13041	0.00148	0.92	814.9	23.3	790.2	8.5	796.6	6.8	99.2
ZR74	9.53	68.23	0.48	1.221	0.016	0.13066	0.00150	0.87	861.7	25.2	791.6	8.6	810.2	7.4	97.7
ZR88	26.55	198.29	0.37	1.189	0.014	0.13083	0.00149	0.95	803.4	22.6	792.6	8.5	795.4	6.6	99.6
ZR48	35.0345	224.16 7	0.91	1.183	0.015	0.13116	0.00149	0.92	788.1	23.4	794.5	8.5	792.8	6.8	100.2
ZR23	11.37	71.82	0.92	1.214	0.016	0.13213	0.00153	0.86	826.2	25.6	800.0	8.7	806.9	7.5	99.1
ZR22	8.19	57.96	0.36	1.287	0.017	0.13608	0.00158	0.86	887.5	25.6	822.4	9.0	840.1	7.7	97.9
ZR63	8.29	56.69	0.43	1.296	0.017	0.14010	0.00162	0.87	840.1	25.2	845.2	9.2	843.7	7.6	100.2
ZR46	23.9254	169.56 6	0.21	1.385	0.017	0.14169	0.00162	0.91	953.8	23.4	854.2	9.2	882.4	7.5	96.8
ZR83	55.86	351.73	0.62	1.343	0.016	0.14279	0.00162	0.93	874.9	22.9	860.4	9.2	864.4	7.1	99.5
ZR77	18.96	109.09	0.84	1.381	0.018	0.14750	0.00168	0.90	865.9	23.9	886.9	9.5	880.9	7.5	100.7
ZR97	35.14	230.72	0.33	1.446	0.018	0.14962	0.00170	0.93	931.1	22.6	898.8	9.5	908.2	7.3	99.0
ZR79	8.61	50.85	0.61	1.499	0.020	0.15288	0.00176	0.85	960.5	25.5	917.1	9.8	929.9	8.2	98.6
ZR76	13.13	76.13	0.48	1.586	0.020	0.16084	0.00184	0.89	971.9	23.9	961.4	10.2	964.5	8.0	99.7
ZR52	58.8951	357.50 9	0.30	1.598	0.019	0.16193	0.00184	0.93	973.9	22.4	967.5	10.2	969.4	7.6	99.8
ZR38	13.2328	67.370 3	1.01	1.605	0.021	0.16195	0.00186	0.89	983.1	23.9	967.6	10.3	972.3	8.1	99.5
ZR51	64.6305	381.69 9	0.39	1.603	0.019	0.16225	0.00185	0.94	976.1	22.2	969.3	10.2	971.3	7.6	99.8
ZR98	42.28	238.64	0.56	1.609	0.019	0.16304	0.00185	0.94	973.6	22.0	973.7	10.2	973.6	7.5	100.0
ZR62	27.20	146.06	0.59	1.700	0.021	0.17034	0.00196	0.95	997.4	21.9	1014.0	10.8	1008.7	7.8	100.5
ZR30	173.772	973.67 1	0.80	1.568	0.018	0.15371	0.00176	0.98	1041.5	20.8	921.7	9.8	957.7	7.3	92.0

ZR7	3.15	16.63	0.89	1.652	0.027	0.15993	0.00191	0.74	1066.3	30.7	956.4	10.6	990.2	10.2	92.9
ZR61	70.10	250.85	1.64	2.188	0.026	0.19992	0.00229	0.97	1181.7	20.7	1174.9	12.3	1177.2	8.3	99.6
ZR85	58.66	250.08	0.56	2.622	0.031	0.21353	0.00242	0.97	1405.4	19.9	1247.6	12.9	1306.8	8.6	93.0
ZR33	28.8346	242.003	0.32	1.381	0.017	0.10800	0.00124	0.96	1482.5	20.3	661.1	7.2	880.8	7.1	59.4
ZR25	42.8416	145.133	0.56	3.561	0.043	0.26648	0.00306	0.95	1565.8	20.3	1522.9	15.6	1540.9	9.6	98.4
ZR14	9.26	31.19	0.97	3.245	0.042	0.23650	0.00276	0.90	1615.3	21.8	1368.5	14.4	1468.0	10.1	90.9
ZR65	81.23	261.23	0.70	4.102	0.049	0.26685	0.00305	0.97	1823.9	19.0	1524.8	15.5	1654.7	9.7	90.7
ZR47	33.6951	67.2589	1.97	5.367	0.066	0.33097	0.00378	0.93	1920.3	19.8	1843.1	18.3	1879.6	10.5	97.9
ZR71	238.39	576.93	0.55	6.956	0.082	0.36349	0.00414	0.97	2212.4	18.1	1998.7	19.6	2105.8	10.5	95.2
ZR34	135.582	274.009	0.89	7.903	0.092	0.40645	0.00464	0.98	2239.9	17.8	2198.6	21.3	2220.0	10.5	99.0
ZR104	112.53	240.80	0.26	8.794	0.104	0.43894	0.00497	0.95	2291.6	18.3	2345.9	22.3	2316.9	10.8	101.1
FIN11-1 ZR1	177.784	460.398	0.28	7.474	0.091	0.35530	0.00400	0.92	2375.0	19.0	1959.9	19.0	2169.8	11.0	91.4
ZR43	39.2705	63.8723	1.68	9.278	0.111	0.42568	0.00487	0.95	2435.3	18.2	2286.2	22.0	2365.8	11.0	97.1
ZR68	97.56	180.61	0.59	10.279	0.121	0.46477	0.00531	0.97	2460.1	17.6	2460.6	23.4	2460.2	10.9	100.0
ZR5	256.92	507.30	0.34	10.296	0.121	0.46365	0.00535	0.98	2466.9	17.3	2455.6	23.6	2461.7	10.9	99.8
ZR19	38.16	73.82	0.37	10.336	0.125	0.46541	0.00537	0.95	2467.1	18.2	2463.4	23.6	2465.3	11.2	99.9
ZR91	70.21	127.07	1.09	9.564	0.111	0.42894	0.00486	0.97	2473.8	17.5	2300.9	21.9	2393.7	10.7	96.8
ZR72	43.87	77.97	0.92	10.098	0.120	0.44881	0.00513	0.96	2489.1	17.9	2389.9	22.8	2443.8	11.0	98.2
ZR9	115.17	213.84	0.79	10.027	0.119	0.44401	0.00512	0.98	2495.4	17.4	2368.6	22.9	2437.3	10.9	97.7
ZR31	87.9445	145.874	1.25	10.294	0.121	0.45168	0.00517	0.98	2510.8	17.4	2402.7	22.9	2461.6	10.8	98.0
ZR6	123.50	238.11	0.47	10.429	0.123	0.45625	0.00527	0.98	2515.8	17.3	2423.0	23.3	2473.7	10.9	98.3
ZR10	72.36	124.59	0.85	10.818	0.129	0.47231	0.00546	0.97	2519.1	17.5	2493.7	23.9	2507.6	11.1	99.5
ZR8	433.97	972.53	0.17	9.992	0.118	0.42161	0.00486	0.98	2576.3	17.2	2267.8	22.1	2434.0	10.9	94.5
ZR92	331.48	634.22	0.56	10.659	0.123	0.44161	0.00500	0.98	2606.7	17.2	2357.8	22.4	2493.8	10.8	95.7
ZR35	484.652	893.108	0.48	11.970	0.139	0.46999	0.00536	0.98	2695.9	17.0	2483.5	23.5	2602.1	10.9	96.5
ZR20	78.73	135.97	0.31	13.291	0.160	0.52039	0.00599	0.96	2700.5	17.6	2700.8	25.4	2700.5	11.4	100.0
ZR78	325.50	560.83	0.47	12.834	0.153	0.50017	0.00568	0.95	2708.2	17.6	2614.5	24.4	2667.6	11.2	98.5
ZR86	185.37	304.35	0.57	13.440	0.155	0.51949	0.00588	0.98	2721.8	16.9	2697.0	25.0	2711.1	10.9	99.6
ZR15	221.73	354.23	0.57	13.767	0.164	0.52848	0.00608	0.97	2733.1	17.2	2735.0	25.7	2733.8	11.3	100.0
ZR107	1066.85	1592.23	0.10	19.882	0.238	0.61002	0.00690	0.94	3095.9	17.2	3070.1	27.6	3085.6	11.6	99.7
ZR16	107.72	146.59	0.42	20.308	0.242	0.61999	0.00714	0.97	3103.9	16.8	3109.9	28.4	3106.1	11.5	100.1

				ISOTOPIC RATIOS					AGES						
PC11	Pb ppm	U ppm	Th/U	207/235	err (1σ)	206/238	err (1σ)	rho	207/206	err (1σ)	206/238	err (1σ)	207/235	err (1σ)	conc
ZR35	126.7	2553.6	0.10	0.432	0.005	0.05214	0.00061	0.95	608.9	23.4	327.6	3.8	364.9	3.8	89.8
ZR30	19.2	224.8	1.12	1.206	0.018	0.06706	0.00081	0.82	2103.4	23.8	418.4	4.9	803.1	8.2	52.1
ZR82	93.6	1236.1	0.25	0.634	0.008	0.07642	0.00090	0.96	609.7	23.1	474.7	5.4	498.5	4.8	95.2
ZR43	8.7	105.6	0.31	0.655	0.013	0.08022	0.00097	0.62	574.2	40.9	497.4	5.8	511.3	7.8	97.3
ZR44	13.4	155.6	0.40	0.662	0.011	0.08179	0.00097	0.71	555.4	34.7	506.8	5.8	515.7	6.7	98.3
ZR34	48.0	550.2	0.52	0.665	0.009	0.08227	0.00097	0.92	554.1	24.6	509.7	5.8	517.8	5.2	98.4
ZR58	34.3	422.8	0.08	0.824	0.011	0.08357	0.00101	0.90	971.3	24.0	517.4	6.0	610.0	6.2	84.8
ZR38	11.3	132.5	0.31	0.689	0.010	0.08460	0.00100	0.81	568.4	29.2	523.5	6.0	531.9	6.0	98.4
ZR17	18.8	208.5	0.44	0.773	0.011	0.08468	0.00101	0.82	813.8	28.0	524.0	6.0	581.6	6.5	90.1
ZR33	10.8	119.6	0.30	0.901	0.013	0.08473	0.00101	0.84	1125.0	25.9	524.3	6.0	652.4	6.9	80.4
ZR50	14.2	158.8	0.38	0.686	0.012	0.08491	0.00100	0.69	553.5	35.8	525.3	5.9	530.6	7.0	99.0
ZR47b	11.5	133.6	0.35	0.693	0.011	0.08497	0.00104	0.75	574.0	32.7	525.7	6.2	534.8	6.8	98.3
ZR94	16.0	177.3	0.41	0.696	0.009	0.08529	0.00098	0.87	572.6	26.5	527.6	5.8	536.1	5.5	98.4
ZR13	10.8	123.8	0.33	0.699	0.011	0.08547	0.00102	0.79	578.2	30.0	528.7	6.0	538.1	6.3	98.3
ZR57	10.9	126.9	0.33	0.698	0.011	0.08556	0.00104	0.77	574.4	31.4	529.2	6.2	537.8	6.6	98.4
ZR15	12.2	140.9	0.31	0.694	0.010	0.08566	0.00102	0.82	557.9	28.9	529.8	6.0	535.1	6.0	99.0
ZR42	11.5	130.8	0.32	0.702	0.010	0.08584	0.00101	0.79	580.0	30.1	530.9	6.0	540.2	6.2	98.3
ZR3	10.8	123.4	0.28	0.703	0.010	0.08694	0.00102	0.84	553.8	27.7	537.4	6.1	540.5	5.9	99.4
ZR98	15.7	165.7	0.48	0.711	0.010	0.08715	0.00100	0.86	574.6	27.1	538.6	5.9	545.5	5.7	98.7
ZR122	52.0	609.1	0.21	0.761	0.010	0.08718	0.00104	0.89	718.2	25.2	538.8	6.2	574.5	5.9	93.8
ZR62	8.9	94.7	0.65	0.705	0.010	0.08735	0.00106	0.83	549.6	28.7	539.8	6.3	541.7	6.2	99.6
ZR6	27.0	300.5	0.36	0.730	0.009	0.08736	0.00102	0.90	624.0	24.8	539.9	6.1	556.3	5.6	97.1
ZR46	39.3	401.3	0.63	0.718	0.010	0.08755	0.00101	0.83	584.1	27.9	541.0	6.0	549.3	5.9	98.5
ZR68	17.6	205.9	0.22	0.719	0.010	0.08792	0.00107	0.87	578.3	26.8	543.2	6.3	550.0	5.9	98.8
ZR50b	11.6	126.9	0.42	0.730	0.010	0.08832	0.00106	0.84	602.7	27.7	545.6	6.3	556.7	6.1	98.0
ZR37	8.9	99.8	0.33	0.721	0.011	0.08841	0.00105	0.81	574.0	29.5	546.1	6.2	551.5	6.3	99.0
ZR67	9.7	108.3	0.38	0.722	0.011	0.08888	0.00108	0.81	562.8	30.1	548.9	6.4	551.6	6.4	99.5
ZR32	9.5	95.0	0.77	0.741	0.012	0.08905	0.00108	0.75	617.1	32.4	549.9	6.4	563.1	7.0	97.7
ZR79	14.5	167.1	0.24	0.713	0.010	0.08909	0.00107	0.84	532.6	28.7	550.1	6.3	546.8	6.0	100.6
ZR22	26.5	307.3	0.15	0.734	0.010	0.08987	0.00107	0.85	575.7	27.4	554.8	6.3	558.8	6.0	99.3
ZR9	11.6	121.9	0.47	0.736	0.012	0.09025	0.00108	0.75	572.5	32.2	557.0	6.4	560.0	6.9	99.5
ZR48	11.9	121.8	0.50	0.737	0.011	0.09028	0.00105	0.77	574.1	31.0	557.2	6.2	560.5	6.5	99.4
ZR88	48.5	451.7	0.88	0.748	0.010	0.09084	0.00106	0.90	593.8	25.0	560.5	6.3	567.1	5.6	98.8
ZR46b	25.0	258.2	0.48	0.766	0.010	0.09207	0.00110	0.93	615.3	24.0	567.8	6.5	577.3	5.7	98.4
ZR63	46.7	486.5	0.48	0.758	0.010	0.09218	0.00111	0.93	589.9	24.2	568.4	6.5	572.7	5.7	99.2
ZR100	12.0	117.5	0.47	0.782	0.011	0.09425	0.00107	0.83	609.5	27.4	580.6	6.3	586.5	6.1	99.0
ZR45	23.0	225.9	0.48	0.794	0.011	0.09459	0.00110	0.83	635.8	28.0	582.6	6.5	593.5	6.3	98.2
ZR107	64.0	650.1	0.40	0.815	0.010	0.09488	0.00111	0.93	685.1	23.6	584.4	6.6	605.4	5.7	96.5

ZR110	104.2	984.6	0.68	0.805	0.010	0.09546	0.00112	0.95	646.5	23.3	587.7	6.6	599.9	5.6	98.0
ZR89	38.3	413.3	0.15	0.794	0.010	0.09547	0.00111	0.93	614.2	23.9	587.8	6.5	593.2	5.6	99.1
ZR56	55.5	465.2	1.20	0.825	0.010	0.09581	0.00115	0.95	689.1	23.3	589.8	6.8	610.7	5.8	96.6
ZR47	105.5	1078.0	0.25	0.806	0.011	0.09638	0.00111	0.84	626.8	27.3	593.2	6.5	600.1	6.2	98.9
ZR51	32.7	285.9	0.97	0.815	0.011	0.09657	0.00116	0.87	645.6	26.3	594.3	6.8	605.0	6.3	98.2
ZR7	14.7	143.7	0.45	0.813	0.011	0.09678	0.00114	0.87	636.9	26.4	595.5	6.7	604.1	6.2	98.6
ZR77	86.6	864.5	0.45	0.809	0.010	0.09755	0.00116	0.97	608.5	22.7	600.0	6.8	601.8	5.6	99.7
ZR75	16.2	145.2	0.86	0.818	0.011	0.09868	0.00118	0.90	607.1	25.3	606.7	6.9	606.7	6.1	100.0
ZR24	26.8	266.4	0.37	0.812	0.011	0.09870	0.00117	0.87	593.2	25.9	606.8	6.9	603.8	6.2	100.5
ZR49	19.1	191.4	0.18	0.853	0.012	0.09976	0.00116	0.80	675.6	29.3	613.0	6.8	626.4	6.8	97.9
ZR29	12.6	125.9	0.29	0.831	0.013	0.09990	0.00120	0.77	615.7	31.3	613.8	7.1	614.2	7.2	99.9
ZR93	19.9	172.7	0.73	0.850	0.011	0.10062	0.00116	0.89	650.2	25.5	618.0	6.8	624.9	6.1	98.9
ZR61	23.2	207.1	0.70	0.868	0.012	0.10163	0.00123	0.90	673.6	25.1	623.9	7.2	634.7	6.3	98.3
ZR45b	18.4	168.4	0.54	0.896	0.012	0.10180	0.00122	0.90	736.3	24.7	625.0	7.1	649.6	6.4	96.2
ZR55	35.0	331.3	0.42	0.861	0.011	0.10265	0.00123	0.93	634.6	24.0	629.9	7.2	630.9	6.1	99.8
ZR76	5.7	46.9	1.08	0.855	0.013	0.10285	0.00125	0.77	614.6	31.1	631.1	7.3	627.5	7.3	100.6
ZR83	3.1	28.4	0.48	0.951	0.017	0.10307	0.00125	0.69	835.0	34.5	632.4	7.3	678.5	8.7	93.2
ZR95	26.9	254.2	0.27	0.881	0.011	0.10341	0.00118	0.90	666.9	24.8	634.4	6.9	641.5	6.0	98.9
ZR28	47.9	453.1	0.37	0.868	0.012	0.10352	0.00123	0.88	633.3	25.8	635.0	7.2	634.5	6.3	100.1
ZR72	90.9	756.0	0.67	1.017	0.013	0.10418	0.00125	0.96	952.7	21.6	638.9	7.3	712.6	6.4	89.7
ZR49b	27.2	258.5	0.17	0.933	0.012	0.10864	0.00130	0.94	683.7	23.4	664.8	7.6	669.1	6.2	99.4
ZR109	16.6	152.1	0.28	0.948	0.014	0.10940	0.00130	0.81	703.7	28.5	669.3	7.6	677.2	7.2	98.8
ZR120	14.7	115.4	0.84	0.975	0.014	0.11081	0.00132	0.86	735.0	26.3	677.5	7.7	690.9	7.0	98.1
ZR12	21.3	159.9	0.80	1.053	0.016	0.11529	0.00138	0.77	815.2	30.0	703.4	8.0	730.6	8.1	96.3
ZR43b	7.8	59.9	0.68	1.012	0.015	0.11633	0.00140	0.84	710.8	27.5	709.4	8.1	709.7	7.4	100.0
ZR69	9.8	80.9	0.49	1.008	0.015	0.11650	0.00142	0.84	701.1	27.4	710.4	8.2	708.1	7.4	100.3
ZR73	25.0	170.6	1.32	1.076	0.016	0.11659	0.00142	0.80	835.3	28.7	710.9	8.2	741.5	8.0	95.9
ZR25	179.4	1338.9	0.82	1.043	0.014	0.11674	0.00138	0.91	768.9	24.2	711.8	8.0	725.6	6.8	98.1
ZR97	31.9	252.4	0.47	1.025	0.013	0.11679	0.00133	0.90	729.5	24.4	712.1	7.7	716.2	6.5	99.4
ZR21	57.7	408.9	0.98	1.063	0.015	0.11683	0.00139	0.86	806.9	26.1	712.3	8.0	735.5	7.3	96.8
ZR87	22.6	152.0	1.06	1.081	0.016	0.11808	0.00140	0.79	819.4	29.2	719.5	8.1	744.2	8.0	96.7
ZR14	12.2	95.0	0.51	1.086	0.015	0.11919	0.00141	0.85	808.4	26.4	725.9	8.1	746.4	7.4	97.3
ZR27	26.0	171.2	1.25	1.056	0.015	0.11958	0.00142	0.86	743.7	26.3	728.2	8.2	731.9	7.2	99.5
ZR4	39.0	261.1	1.09	1.080	0.014	0.11999	0.00140	0.91	783.2	23.9	730.5	8.1	743.5	6.8	98.3
ZR39	15.7	114.1	0.79	1.086	0.015	0.12066	0.00142	0.87	783.0	25.7	734.4	8.2	746.4	7.2	98.4
ZR54	18.0	114.3	1.38	1.104	0.016	0.12191	0.00148	0.84	796.3	27.3	741.5	8.5	755.2	7.7	98.2
ZR59	61.2	444.4	0.65	1.131	0.014	0.12600	0.00151	0.95	777.1	22.8	765.0	8.7	768.0	6.8	99.6
ZR5	57.7	423.6	0.53	1.147	0.014	0.12622	0.00148	0.93	803.5	23.1	766.3	8.4	775.8	6.8	98.8
ZR124	76.1	556.2	0.58	1.163	0.015	0.12767	0.00152	0.91	808.0	24.1	774.6	8.7	783.2	7.2	98.9
ZR90	42.8	291.5	0.76	1.169	0.015	0.12854	0.00149	0.93	805.8	23.1	779.5	8.5	786.3	6.8	99.1
ZR2	79.3	516.8	0.92	1.187	0.015	0.12891	0.00150	0.93	831.6	22.8	781.7	8.6	794.7	6.9	98.4
ZR115	25.2	169.6	0.82	1.190	0.016	0.12966	0.00154	0.90	824.3	24.4	785.9	8.8	795.9	7.3	98.7

ZR86	63.9	380.1	1.36	1.173	0.015	0.12970	0.00151	0.92	794.2	23.4	786.2	8.6	788.2	6.9	99.7
ZR121	15.7	107.8	0.76	1.175	0.016	0.13056	0.00156	0.86	783.9	26.2	791.1	8.9	789.2	7.6	100.2
ZR114	21.4	149.5	0.59	1.217	0.016	0.13240	0.00157	0.90	826.9	24.4	801.5	8.9	808.2	7.4	99.2
ZR64	11.1	74.5	0.70	1.254	0.018	0.13492	0.00164	0.86	851.1	26.1	815.9	9.3	825.3	8.0	98.9
ZR96	14.8	98.9	0.52	1.308	0.017	0.13595	0.00156	0.87	922.8	24.9	821.7	8.8	849.5	7.6	96.7
ZR70	8.9	63.0	0.40	1.257	0.019	0.13768	0.00169	0.80	812.9	29.1	831.5	9.6	826.4	8.7	100.6
ZR91	14.8	104.3	0.32	1.260	0.017	0.13777	0.00159	0.86	816.3	25.8	832.1	9.0	827.7	7.6	100.5
ZR8	16.3	107.2	0.57	1.273	0.019	0.13812	0.00164	0.81	833.1	27.9	834.0	9.3	833.7	8.3	100.0
ZR84	14.1	93.4	0.60	1.277	0.017	0.13829	0.00162	0.89	837.1	24.7	835.0	9.2	835.5	7.5	99.9
ZR105	17.8	117.6	0.61	1.288	0.017	0.13840	0.00163	0.90	853.3	24.3	835.6	9.2	840.4	7.5	99.4
ZR106	8.3	56.1	0.48	1.370	0.024	0.13900	0.00170	0.70	971.3	33.6	839.0	9.6	876.1	10.2	95.8
ZR1	25.9	175.3	0.45	1.300	0.017	0.13920	0.00163	0.91	860.9	23.6	840.1	9.2	845.8	7.4	99.3
ZR41	11.7	71.7	0.82	1.314	0.019	0.13923	0.00163	0.82	883.1	27.2	840.3	9.2	852.1	8.2	98.6
ZR53	27.3	162.1	1.00	1.320	0.017	0.14145	0.00170	0.91	858.8	23.8	852.8	9.6	854.4	7.6	99.8
ZR92	46.4	301.1	0.46	1.373	0.017	0.14324	0.00164	0.92	914.2	23.0	862.9	9.3	877.4	7.3	98.3
ZR31	31.3	195.5	0.70	1.391	0.018	0.14402	0.00171	0.94	930.1	22.8	867.4	9.6	885.2	7.5	98.0
ZR26	48.8	330.4	0.31	1.392	0.019	0.14599	0.00173	0.88	902.9	24.6	878.5	9.7	885.3	7.9	99.2
ZR78	51.9	350.9	0.32	1.418	0.018	0.14801	0.00176	0.96	913.4	21.9	889.8	9.9	896.5	7.4	99.3
ZR103	43.5	291.0	0.31	1.440	0.018	0.14968	0.00175	0.94	921.4	22.5	899.2	9.8	905.6	7.5	99.3
ZR108	64.5	457.2	0.01	1.472	0.018	0.15119	0.00177	0.95	946.2	22.1	907.6	9.9	918.9	7.5	98.8
ZR40	57.2	343.6	0.58	1.510	0.020	0.15235	0.00178	0.90	983.2	23.8	914.1	10.0	934.5	7.9	97.8
ZR119	19.3	100.3	1.28	1.492	0.020	0.15244	0.00181	0.88	956.6	24.7	914.6	10.2	927.0	8.3	98.7
ZR41b	19.3	113.8	0.68	1.481	0.019	0.15245	0.00182	0.93	941.5	23.0	914.7	10.2	922.5	7.8	99.2
ZR99	87.8	517.5	0.43	1.538	0.019	0.15644	0.00177	0.92	966.1	22.9	937.0	9.9	945.6	7.6	99.1
ZR36	76.1	470.4	0.38	1.551	0.019	0.15684	0.00184	0.94	978.1	22.4	939.2	10.3	950.8	7.7	98.8
ZR18	34.5	214.7	0.33	1.550	0.020	0.15770	0.00186	0.90	966.4	23.6	944.0	10.4	950.7	8.1	99.3
ZR130	38.2	238.7	0.23	1.611	0.022	0.16461	0.00197	0.88	956.9	24.4	982.3	10.9	974.5	8.5	100.8
ZR60	24.9	135.6	0.58	1.728	0.023	0.17042	0.00205	0.90	1029.4	23.5	1014.4	11.3	1019.1	8.6	99.0
ZR85	64.2	322.5	0.73	1.800	0.022	0.17638	0.00206	0.94	1041.8	22.1	1047.2	11.3	1045.4	8.1	100.3
ZR66	19.6	107.2	0.32	1.864	0.025	0.17961	0.00217	0.90	1075.9	23.4	1064.9	11.9	1068.4	8.9	99.3
ZR52	24.3	130.8	0.52	1.832	0.026	0.17382	0.00210	0.87	1106.9	24.8	1033.1	11.6	1057.0	9.2	95.5
ZR81	21.1	156.1	0.30	1.604	0.023	0.13288	0.00159	0.84	1372.4	25.0	804.3	9.0	971.6	8.9	70.8
ZR74	10.5	111.1	0.28	1.134	0.015	0.08771	0.00106	0.90	1503.5	22.4	542.0	6.3	769.6	7.2	51.2
ZR19	92.7	291.2	0.75	3.737	0.047	0.27547	0.00324	0.93	1594.2	20.8	1568.5	16.4	1579.4	10.2	99.1
ZR113	17.3	40.7	2.11	3.907	0.052	0.28516	0.00339	0.89	1612.5	22.1	1617.3	17.0	1615.1	10.8	100.2
ZR128	112.3	297.5	0.85	4.974	0.066	0.32548	0.00389	0.91	1813.3	21.0	1816.4	18.9	1814.9	11.2	100.1
ZR125	62.1	169.1	0.68	5.117	0.067	0.32677	0.00390	0.91	1857.4	20.8	1822.7	18.9	1838.9	11.1	99.0
ZR10	148.6	412.4	0.53	5.113	0.063	0.32459	0.00380	0.95	1868.2	19.3	1812.1	18.5	1838.3	10.4	98.4
ZR71	143.3	361.0	0.64	6.231	0.076	0.36409	0.00437	0.98	2016.4	18.3	2001.5	20.7	2008.8	10.7	99.6
ZR44b	11.4	93.0	0.42	1.764	0.025	0.09689	0.00118	0.86	2125.2	22.3	596.2	6.9	1032.2	9.1	48.6
ZR20	221.6	629.5	0.19	7.417	0.093	0.33873	0.00399	0.94	2443.3	18.6	1880.6	19.2	2163.1	11.3	88.5
ZR102	87.5	160.5	0.67	10.297	0.125	0.46389	0.00542	0.96	2466.3	17.9	2456.7	23.9	2461.8	11.3	99.8

ZR117	138.5	307.8	0.40	9.056	0.114	0.40793	0.00482	0.94	2466.4	18.4	2205.5	22.1	2343.7	11.5	95.0
ZR101	223.1	575.2	0.64	7.466	0.090	0.33368	0.00389	0.96	2479.8	17.8	1856.2	18.8	2169.0	10.8	87.5
ZR65	15.1	117.9	0.42	2.158	0.029	0.09620	0.00117	0.92	2483.9	19.5	592.1	6.9	1167.5	9.2	47.0
ZR126	230.6	433.0	0.55	10.580	0.138	0.47115	0.00562	0.92	2485.8	19.2	2488.6	24.6	2487.0	12.1	100.0
ZR23	124.6	242.1	0.84	9.442	0.122	0.41775	0.00494	0.92	2496.7	19.1	2250.3	22.5	2381.9	11.8	95.4
ZR116	168.6	314.3	0.61	10.542	0.132	0.46558	0.00549	0.94	2499.8	18.3	2464.1	24.2	2483.6	11.6	99.4
ZR123	24.1	43.0	0.77	10.682	0.141	0.47145	0.00564	0.91	2500.9	19.6	2489.9	24.7	2495.9	12.3	99.8
ZR42b	17.3	137.9	0.27	2.278	0.030	0.10016	0.00121	0.93	2507.3	19.2	615.4	7.1	1205.5	9.2	48.1
ZR112	15.1	21.8	1.53	11.484	0.150	0.49926	0.00596	0.91	2526.3	19.5	2610.6	25.6	2563.3	12.2	101.5
ZR129	294.8	548.8	0.71	10.591	0.139	0.45714	0.00546	0.91	2538.2	19.3	2426.9	24.2	2487.9	12.2	98.0
ZR48b	38.8	64.9	1.00	11.139	0.139	0.47495	0.00569	0.96	2558.8	17.9	2505.2	24.9	2534.8	11.6	99.1
ZR11	97.2	174.0	0.72	11.019	0.136	0.46368	0.00544	0.95	2580.7	18.0	2455.8	24.0	2524.7	11.5	97.8
ZR127	167.5	308.3	0.42	12.002	0.157	0.48891	0.00583	0.91	2634.9	19.0	2566.0	25.3	2604.6	12.3	98.9
ZR80	188.6	324.6	0.52	12.781	0.154	0.51117	0.00604	0.98	2665.4	17.1	2661.6	25.8	2663.7	11.4	99.9
ZR118	26.7	39.4	1.26	13.044	0.168	0.51087	0.00608	0.92	2700.1	18.7	2660.3	25.9	2682.9	12.1	99.4
ZR104	171.1	263.9	0.79	13.751	0.167	0.52814	0.00617	0.96	2732.2	17.4	2733.6	26.0	2732.7	11.5	100.0
ZR16	18.8	122.4	1.24	2.586	0.035	0.08778	0.00105	0.90	2933.3	19.5	542.4	6.2	1296.5	9.8	44.2
ZR111	483.9	619.4	0.56	22.330	0.275	0.64236	0.00755	0.96	3198.3	16.9	3198.3	29.6	3198.2	12.0	100.0

				ISOTOPIC RATIOS									AGES			
RF 3	**U (ppm)**	**Th (ppm)**	**$^{232}Th/^{238}U$**	**206/238**	**Err 1σ (%)**	**207/206**	**err 1σ (%)**	**207/235**	**err 1σ (%)**	**206/238**	**err 1σ (%)**	**Error corr.**	**206/238**	**err (1σ)**	**207/206**	**err (1σ)**
1.1	120	37	0.32	11.9	1.7	0.059	2.833	0.666	5.031	0.084	1.716	0.341	518	9	520	104
3.1	127	46	0.37	11.5	1.7	0.057	2.658	0.681	3.143	0.087	1.677	0.534	**537**	**9**	490	59
2.1	108	36	0.34	11.4	1.7	0.061	2.755	0.733	3.248	0.088	1.721	0.530	**539**	**9**	628	59
4.1	110	39	0.36	11.4	1.7	0.058	2.990	0.706	3.460	0.088	1.740	0.503	**542**	**9**	545	65
7.1	93	32	0.36	11.2	1.8	0.058	2.963	0.716	3.451	0.089	1.769	0.513	**550**	**10**	542	65
6.1	105	33	0.33	11.2	1.7	0.058	2.834	0.718	3.320	0.089	1.729	0.521	**551**	**9**	542	62
8.1	111	32	0.30	11.0	1.7	0.061	2.598	0.744	4.331	0.090	1.698	0.392	**558**	**9**	590	86
5.1	91	30	0.34	11.0	1.8	0.059	2.977	0.725	5.261	0.091	1.778	0.338	**562**	**10**	524	109
10.1	121	34	0.29	10.6	1.7	0.059	2.904	0.748	4.531	0.094	1.685	0.372	**581**	**10**	515	92
11.1	135	51	0.39	10.6	1.7	0.058	2.495	0.758	2.993	0.095	1.653	0.552	583	10	534	55
9.1	132	44	0.34	10.2	1.7	0.059	2.447	0.803	2.952	0.098	1.651	0.559	605	10	577	53

4 Datation U-Pb par LA-ICPMS de la transition Ediacarien-Cambrien de la Montagne Noire, France. [Article 3]

U–Pb laser ablation ICP-MS zircon dating across the Ediacaran–Cambrian transition of the Montagne Noire, southern France

Auteurs

Maxime Padel[1*]; J. Javier Álvaro[2]; Sébastien Clausen[1]; François Guillot[3]; Marc Poujol[4]; Martim Chichorro[5]; Eric Monceret[6]; M. Francisco Pereira[7]; Daniel Vizcaïno[8]

[1]UMR 8198 EEP CNRS, Université de Lille 1, Bâtiment SN5, Avenue Paul Langevin, 59655 Villeneuve d'Ascq Cedex, France, e-mails: maxime.padel@etudiant.univ-lille1.fr, sebastien.clausen@univ-lille1.fr

[2]Instituto de Geociencias (CSIC-UCM), Novais 12, 28040 Madrid, Spain, email: jj.alvaro@csic.es

[3] UMR 8187 LOG CNRS, Univ. Lille-Univ. Littotal Côte d'Opale, SN5 Sciences de la Terre, 59655 Villeneuve d'Ascq Cedex, France, e-mail: Francois.Guillot@univ-lille1.fr

[4]Géosciences Rennes, UMR 6118, Université de Rennes1, Campus de Beaulieu, 35042 Rennes, France, e-mail: marc.poujol@univ-rennes1.fr

[5]GEOBITEC/Departamento de Ciências da Terra, Universidade Nova de Lisboa, Portugal, e-mail: ma.chichorro@fct.unl.pt

[6]18 rue des Pins, 11570 Cazilhac, France, e-mail: eric.monceret@orange.fr

[7]IDL/Departamento de Geociências, ECT, Universidade de Évora, Portugal, e-mail: mpereira@uevora.pt

[8] 7 Jean-Baptise Chardin, Maquens, 11090 Carcassonne, France, e-mail: daniel.vizcaino@wanadoo.fr

[*]Corresponding author

Abstract.

U-Pb Laser Ablation-Inductively Coupled Plasma-Mass Spectrometry was used for dating zircon grains extracted from four sedimentary and volcanosedimentary rocks of the Montagne Noire encompassing the presumed Ediacaran-Cambrian boundary interval. Magmatic zircon from two samples from the basal and middle part of the Rivernous Formation (a rhyolitic tuff) were deposited at 542.5±1 Ma and 537.1±2.5 Ma bracketing the

541 Ma age presently admitted as Ediacaran-Cambrian boundary. In addition, a sandstone from the underlying Rivernous Formation containing mostly euhedral zircon grains, suggesting proximal magmatic sources, yields Neoproterozoic dates ranging from 574 Ma to 1 Ga, and subsidiary older dates from 1.25 to 2.75 Ga. Another sandstone from the overlying Marcory Formation yielded mostly rounded zircon grains probably issued from more remote areas, with a large spectrum dominated by Neoproterozoic dates as well as older ages up to 3.2 Ga. A comparison of both sandstones suggests a significant change in provenance, changing from a restricted source area during the Ediacaran to a much larger source domain during the Cambrian Epoch 2 that recorded contributions from different cratons of Gondwana.

1. Introduction

The pre–Variscan succession of the Montagne Noire crops out as a fold and thrust complex divided into two sedimentary-dominated, northern and southern flanks fringing an essentially metamorphic, Axial Zone (Gèze, 1949; Arthaud, 1970). Several tectonic models have been proposed for the Montagne Noire and are still subject of debate (Faure and Cottereau, 1988; Van Den Driessche and Brun, 1992; Brun and Van Den Driessche, 1994; Mattauer et al., 1996; Soula et al., 2001; Charles et al., 2009; Fréville et al., 2016; Poujol et al., in press). The Precambrian–Cambrian boundary has traditionally been tentatively located in the lowermost formation exposed in the southern Montagne Noire, namely the Marcory Formation (Álvaro et al., 1998). However, recent reviews of the northern successions challenged the former stratigraphic chart (Devaere et al., 2013; Álvaro et al., 2014b) and established a lower stratigraphic position for the Volcanosedimentary successions of the Grandmont, Rivernous and Layrac formations, exclusively exposed in the northern Montagne Noire. The only previous radiometric data from the Rivernous Formation (Fm) yielded an Ordovician age, ranging from 473±19 Ma to 443±40 (Rb/Sr method; Demange, 1982), which was subsequently ruled out by biostratigraphic ages yielded by acritarch-bearing, laterally equivalent deposits (the so-called “Schistes X”) from the Axial Zone (Fournier-Vinas and Debat, 1970). There, the “Schistes X” are capped by the Sériès Tuff (“Sériès” is a village name) tentatively correlated with the Rivernous Fm. The Sériès Tuff was dated at 545±15 Ma by Pb-evaporation on zircon from a metadacite (Lescuyer and Cocherie, 1992). Some scarce zircon crystals were sampled in a garnet-grade Cambrian meta-siltstone from the southern Montagne Noire, giving a maximum depositional age of 556 Ma based only on a single zircon

(Gebauer et al., 1989). This age attribution may look disputable, given the more recent statistical guidelines for provenance studies (see below) and also taking into account the marked metamorphic character of this rock. In fact, in a previous paper, Gebauer and Grünenfelder (1977) admitted that about 80 % of the primitive radiogenic Pb might have been lost due to Phanerozoic thermal events. In order to improve the stratigraphic framework of the Neoproterozoic–Cambrian boundary interval, and the lithostratigraphic nomenclatural links between the Axial Zone and the northern and southern flanks of the Montagne Noire, zircon grains were sampled from the Rivernous, Grandmont and Marcory formations and dated by *in situ* LA-ICP-MS U–Pb analysis. Our results place new constraints upon the paleogeographic affinities of the different tectonostratigraphic units that form the Montagne Noire, as well as on the detrital provenance of the Ediacaran-Cambrian sediments preserved in neighbouring tectonostratigraphic areas.

2. Geological and stratigraphic setting

Located in the southern part of the French Massif Central (Fig. 1A), the Montagne Noire represents a segment of the external, southwestern component of the Variscan Belt in Europe (Demange, 1998; Roger et al., 2004; Poujol et al., in press). As summarized above, this ENE-WSW striking range is divided into three tectonic units: a central metamorphic dome, the so-called Axial Zone, fringed by its northern and southern flanks (Gèze 1949; Demange, 1985).

The Axial Zone is essentially composed of micaschist, minor marble, paragneiss and migmatized orthogneiss (Gèze, 1949). The protolith age of the orthogneiss and its relationship with the metasedimentary rocks have been disputed. Some authors interpreted the orthogneiss as a granitic Precambrian basement (Demange, 1975, 1998), whereas others considered it as Paleozoic intrusions (Bard and Loueyit, 1978). Recent conventional (ID-TIMS), SHRIMP and LA-ICP-MS U–Pb datings of various orthogneiss samples (Roger et al., 2004; Cocherie et al., 2005; Pitra et al., 2012) suggests that the granitic protolith was emplaced during the Ordovician.

The southern and northern sedimentary-dominated flanks of the Axial Zone are a fold-and-thrust complex of nappes (Fig.1). The Precambrian–Cambrian boundary interval, only reported in the northern Montagne Noire (Álvaro et al., 2014b), comprises four formations, from bottom to top, the Grandmont, Rivernous, Layrac and Marcou formations (Fig. 2). The

Grandmont Fm, about 700 m thick, consists of grey to black shales with subsidiary sandstone interbeds (Fig. 2).

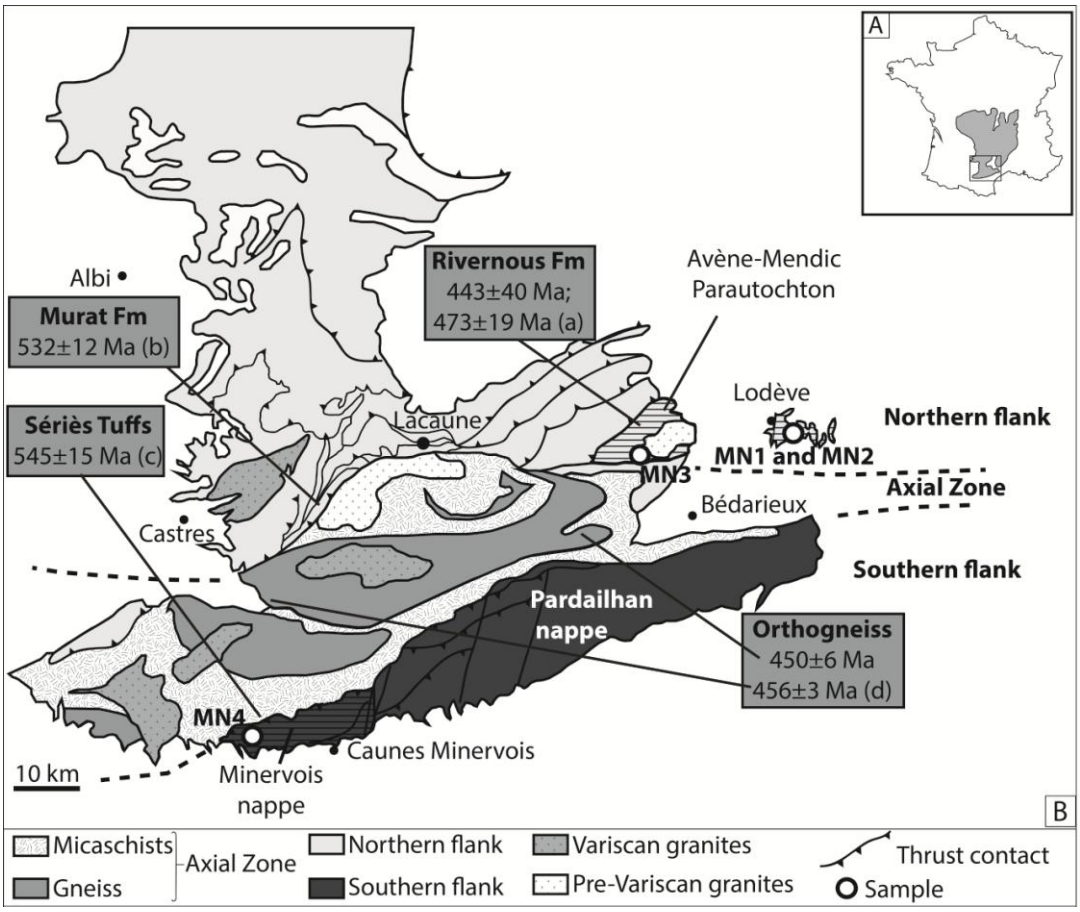

Fig. 1 : Simplified geological map of the Montagne Noire; modified from Devaere et al. (2014). A, Location of the French Massif Central (grey) and Montagne Noire (rectangle) in France. B, Structural units and previous radiometric ages (a) Demange, 1982 (Rb/Sr) discarded by our results (see text); (b) Ducrot et al., 1979 (U–Pb) in Demange et al., 1995; and (c) Lescuyer and Cocherie, 1992 (U–Pb); (d) Roger et al.,2004.

The Rivernous Fm, up to 200 m thick, comprises slightly metamorphosed rhyolitic tuffs that include rare breccia and shale interbeds (Fig. 2). Both formations crop out in the Avène-Mendic parautochthon, which includes the Lodévois inlier and the Lacaune thrust slice (Murat, Fig.1B). In the Lacaune unit, a lateral equivalent of the Rivernous Fm (locally named Murat Fm), with base and top truncated by faults, was dated at 532±12 Ma (U-Pb on zircon; Ducrot et al., 1979; Demange et al., 1995). In the Avène-Mendic parautochthon (Fig.1), the rhyolitic paleorelief formed by the Rivernous Fm (up to about 300 m high, after Álvaro et al., 2014b) is unconformably onlapped by the volcanosedimentary conglomerates and sandstones of the Layrac Fm (Fig. 2). The Layrac Fm is itself overlain by the carbonate-dominated

Marcou Fm, about 400 m thick and assigned to the Cambrian Stage 2 by recent biostratigraphic studies (Fig. 2, Devaere et al., 2013).

The above-reported formations are not exposed in the southern Montagne Noire, where the oldest outcrop is represented by the up to 1000 m-thick Marcory Fm (Fig. 2), a monotonous alternation of sandstones and shales with subordinate carbonate nodules and layers. The upper part of the Marcory Fm has been assigned to the Cambrian Stage 2–3 transition due to the occurrence of the ichnogenera Psammichnites and Taphrelmintopsis (Álvaro and Vizcaïno, 1999), and the oldest trilobites found in the Montagne Noire, i.e. *Blayacina miqueli* (Cobbold, 1935; Geyer, 1992). The Marcory Fm, although absent in the Avène-Mendic parautochthon, is exposed in other thrust slices and nappes of the northern Montagne Noire.

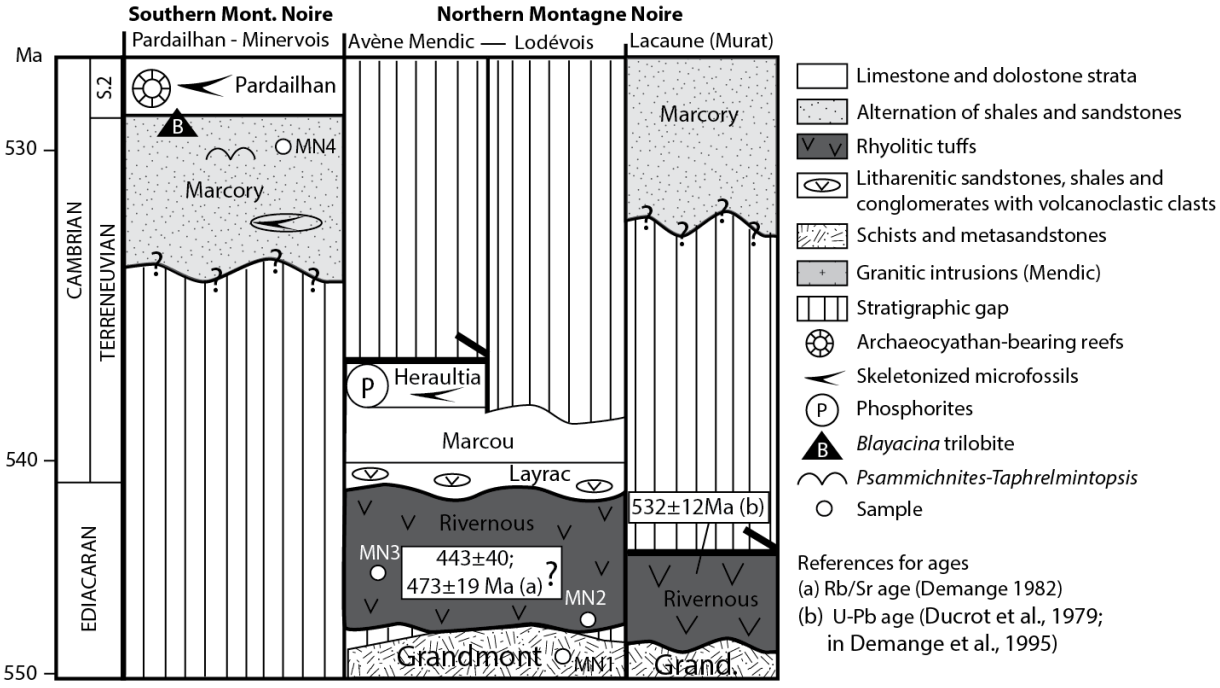

Fig. 2 : Upper Ediacaran–Cambrian Series 2 stratigraphic chart of the southern and northern Montagne Noire; modified from Álvaro et al. (2014b).

3. Material and methods

3.1 Material

The Grandmont and Rivernous formations have been sampled at their stratotype, along the Rivernous rivulet (about 4 km to the East of Lodève): a sandstone from the base of the exposed Grandmont Fm (sample MN1), and a rhyolitic tuff from the base of the Rivernous Fm (sample MN2). The Rivernous Fm was also sampled at its middle part near the

Col du Layrac (sample MN3). MN1 to MN3 samples belong to the so-called Avène-Mendic parauthochton. In order to investigate the provenance of the Marcory Fm, a sandstone (sample MN4) was also selected from the *Psammichnites gigas*-bearing level in the southern Montagne Noire (Álvaro and Vizcaïno, 1999), along the Orbiel river section of the Minervois nappe (Fig. 2).

3.2 Samples preparation

Zircon separation from fresh samples started with rock grinding using a steel crusher. The resulting powders were sieved in the range 50–250 µm. Grains were separated first using heavy liquid (sodium heteropolytungstates 2.85 $g.cm^{-3}$ density), then using Frantz magnetic separator. Following Slama and Košler (2012), the selected grains were obtained from random hand-picking under binocular microscope whatever their size, shape, or color in order to avoid any operator bias. They were finally set in an epoxy resin puck and polished to expose their core.

3.3 LA-ICP-MS *in situ* U-Pb dating

To identify internal growth textures and morphologies, zircon grains were imaged by scanning electron microscope (SEM) to get cathodoluminescence and back-scattered electron imaging (“Laboratoire d'Océanologie et de Géosciences”, Univ.Lille).

In situ U–Pb age of zircon were determined at the Géosciences Rennes laboratory by LA-ICP-MS using an ICP-MS Agilent 7700x coupled with an ESI laser Excimer system producing a wave-length of 193 nm (NWR193UC), with ablation spot diameters of 25 µm, energy pulse of $7J.cm^{-2}$ and repetition rates of 5 Hz. Ablations were operated on both grain rims and cores. Where necessary, distinct domains from a zircon grain were analyzed to compare their ages. The resulting ablated material was mixed in a He, N and Ar gas mixture before being carried into the plasma source of the ICP-MS. Each analysis took 80 s and consisted of a first ≈ 20 s background measurement followed by ≈ 60 s ablation with the measurement of ^{204}(Hg+Pb), ^{206}Pb, ^{207}Pb, ^{208}Pb, ^{232}Th, and ^{238}U, and a ≈ 15 s wash out delay before the next acquisition. Data were collected in batch of 43 analyses divided in 3 sets of 10 unknowns, bracketed by 2 measurements of the GJ-1 primary zircon standard (Jackson et al., 2004) to correct for U–Pb and Th–Pb laser-induced fractionation and for instrumental mass discrimination, followed by one analysis of the Plesovice secondary zircon standard (Slama et al., 2008) in order to check the precision and accuracy of the measurements. During the course of this study, the Plesovice zircon standard yielded a Concordia age of 336.8±0.67 Ma

(N=32). The operating conditions for the LA-ICP-MS equipment can be found in supplementary data Table 1. For more information on the acquisition protocol, see Manzotti et al. (2015).

Data treatment was performed with the GLITTER software (Van Achterberg et al., 2001) and plotted using the Isoplot 3.75 software (Ludwig, 2012) in both Wetherill and Tera-Wasserburg Concordia diagrams. For rhyolitic tuffs, the ages were calculated using the TuffZirc Age algorithm (Ludwig and Mundil, 2002) together with the Sambridge and Compston (1994) algorithm. For the sandstones, age distribution curves with probability density plot were obtained using the density plotter freeware proposed by Vermeesch (2004). For dates > 1Ga, we reported the $^{207}Pb/^{206}Pb$ dates and for dates <1 Ga we used the $^{206}Pb/^{238}U$ dates. Analysis out of the [90%-110%] concordance interval, calculated with $100x(^{207}Pb/^{235}U$ age)/($^{207}Pb/^{206}Pb$ age) for dates> 1Ga (Meinhold et al., 2011) and $100x(^{206}Pb/^{238}U$ age)/($^{207}Pb/^{235}U$ age) for dates <1Ga, were rejected((Faure and Mensing, 2005 and Talavera et al., 2012). Age of the youngest zircon population is derived from a cluster of at least 3 analyses from 3 different grains overlapping in age at 2σ (standard deviation) as proposed by Dickinson and Gehrels (2009) to ensure a statistically robust estimate of the maximum depositional ages. Percentages of concordance, isotopic ratios and ages with 1σ errors, as well as U and Pb concentrations are provided in the supplementary data Table 2.

In sedimentary rock samples (MN1 and MN4), about 110 grains were analyzed in order to get the best representation of the detrital zircon populations. For tuffs (MN2 and MN3) about 50 grains were analyzed, following Bowring et al. (2006) suggestions, to give a robust estimate of the best age for the related volcanic event(s).

4. Results

4.1 Grandmont Formation (MN1)

Zircons from the sample MN1, a medium-grained sandstone, are mostly in the 100-250 µm range, euhedral, facetted, rarely sub-rounded, colorless and generally well zoned (Fig.3A). 107 of the 114 MN1 analyses were concordant [90–110%], among which, 94% are Neoproterozoic (101 grains), 3% Mesoproterozoic (3 grains), 2% Paleoproterozoic (2 grains) and 1 grain (1%) is Archean in age (Fig. 5B). In the interval ranging from 500 to 1100 Ma, the probability curve shows a dominant Ediacaran group within the cluster 550–850 Ma that displays a main peak around 605 Ma and a secondary one around 635 Ma (Fig. 5B). In this same cluster, 4 subsidiary peaks are identified around 690 Ma, 760 Ma, 805 Ma and 835 Ma.

The Tonian-aged zircon grains are characterized by one peak around 906 Ma, in an 890–920 Ma cluster and another peak around 1Ga in the 950–1050 Ma cluster. The four youngest and concordant zircon grains from this group ranging from 567.2±6.12 Ma to 579.5±6.28 Ma, yield an average date of 574±6 Ma (95% conf., Fig. 4E).

4.2 Rivernous Formation (MN2 and MN3)

Samples MN2 and MN3 are both rhyolitic tuffs. Accordingly, zircon grains from samples MN2 and MN3 are euhedral, clear and colorless. Rarely cored, internal structures highlighted by the CL-imaging show clear magmatic zoning (Fig. 3C and 3D).

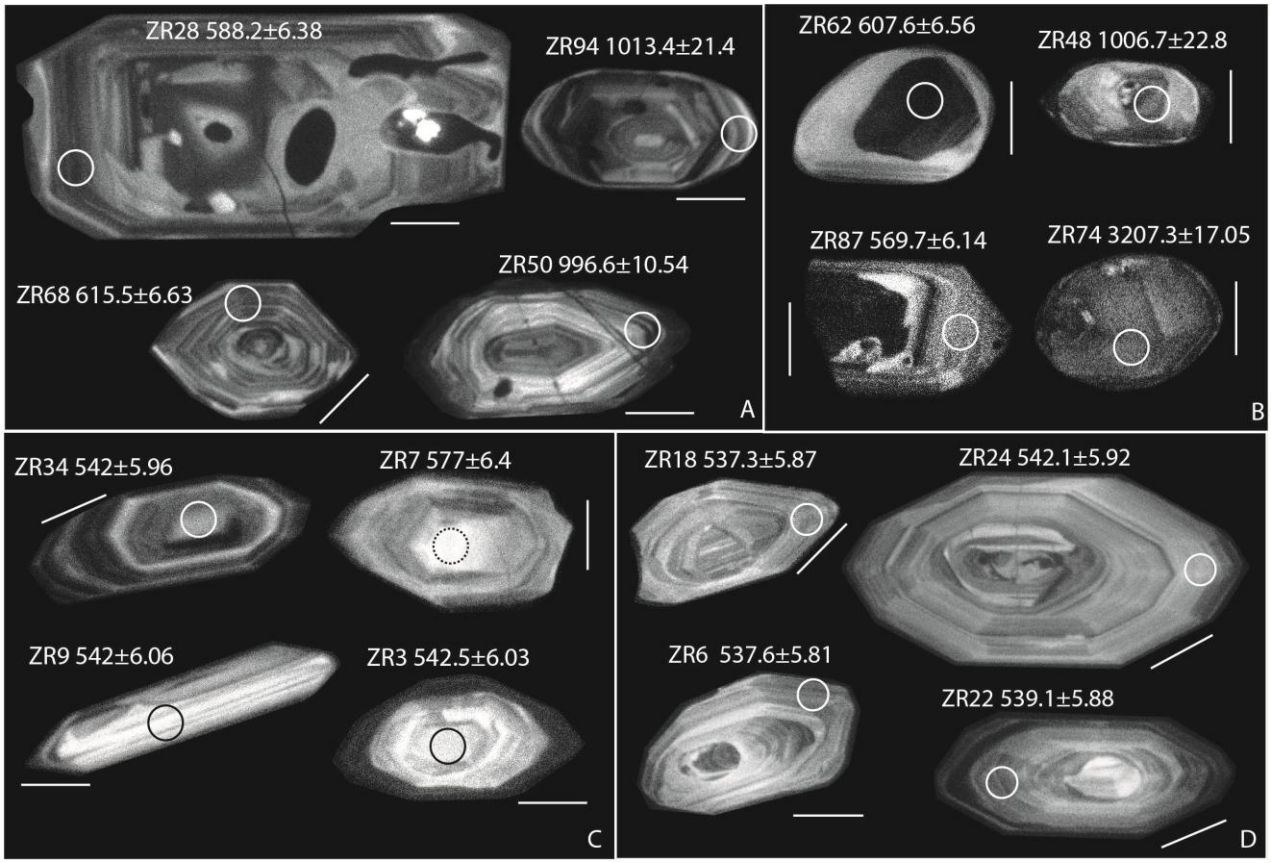

Fig. 3 : Example of CL-imaging for analyzed zircon. A: sample MN1, B: sample MN4, C: sample MN2, D: sample MN3. Scale bars are 50 µm. Zircon numbers (ZRxx) and dates are in supplementary tables.

In sample MN2, 59 zircon grains were analyzed, among which, 50 gave concordant dates [90–110% as defined above]. Seven of the 50 analyses were rejected due to possible lead loss. Thus the youngest and main population from this sample represent 65% of these 43 zircon grains with individual $^{206}Pb/^{238}U$ dates ranging from 534.8±6.01 Ma to 546±6.02 Ma. The second group represents 23% of the total population, and gives $^{206}Pb/^{238}U$ dates ranging

from 576.9±6.3 Ma to 600.8±6.7 Ma (Fig. 5A). Finally, 5 inherited core grains were dated at 651.6±7.2 Ma, 661.8±7.1 Ma, 662±3 7.1 Ma, 685.8±7.6 Ma and 704.7±7.6 Ma.

Looking at the youngest population, the TuffZirc Age algorithm returned a date of 542.5 +0.7/-0.6 Ma while the Sambridge and Compston algorithm yielded a comparable date of 541.9 ± 2.3 Ma (Fig. 4A and 4C). Therefore, choosing between those two within error identical results, we conclude that this rhyolitic tuff was emplaced 542.5 +0.7/-0.6 Ma.

In sample MN3, 58 zircon grains were analyzed, among which 52 yielded concordant results [90-110%]: 2 composite grains with cores (Zr 1 and Zr 27) yielding U–Pb dates of 1837.7±19.1 Ma and 583.1±6.37 Ma respectively. The youngest zircon population suggested by the Sambridge and Compston approach for sample MN3 returned a date around 524 Ma (Fig.4B), which is poorly constrained, by only one concordant zircon among seven somewhat discordant data points (on a Concordia plot, see suppl. data). Therefore, this date is interpreted as geologically meaningless as it could be linked to a possible lead loss.

Keeping only a group comprising three concordant data points (grey bars in Fig. 4B), the TuffZirc Age algorithm yielded a date of 537.35 +2.35/-1.25 Ma while the Sambridge and Compston approach returned a comparable date of 537.1 ± 2.5 Ma. This second rhyolitic sample was therefore emplaced 537.1 ± 2.5 Ma ago (2σ) (Fig. 4B an 4D)

4.3 Marcory Formation (MN4)

Sample MN4 is a fine-grained and mature sandstone. Accordingly, its zircon crystals are mostly anhedral, rounded to subrounded, often broken and rarely bi-pyramidal, largely in the 50-100 µm size range. They are colorless to yellowish, though the biggest zircon grains are reddish in color. In the analyzed fraction, 104 of the 112 MN4 analyses were concordant [90–110%], among which 87% are Neoproterozoic (90 grains), 4% Mesoproterozoic (4 grains), 5% Paleoproterozoic (6 grains), 2% Neoarchean (2 grains), one grain is Mesoarchean and the oldest one is Paleoarchean in age at 3.2 Ga (Fig. 5A).

The probability density curve (Vermeesch, 2004) shows a dominant Ediacaran group (clustered across 550–850 Ma) with a main peak around 614 Ma and a secondary peak around 575 Ma (Fig. 5A). In this same cluster, 6 other peaks are identified around 651 Ma, 678 Ma, 700 Ma, 737 Ma, 800 Ma and 850 Ma. The Tonian-aged zircon grains are characterized by one peak around 900 Ma in an 890–920 Ma cluster and another distinctive peak around 1Ga in the 950–1050 Ma cluster. The three youngest dates obtained from this sample that are concordant yield an average date of 602.5±7.3 Ma (Fig.4F).

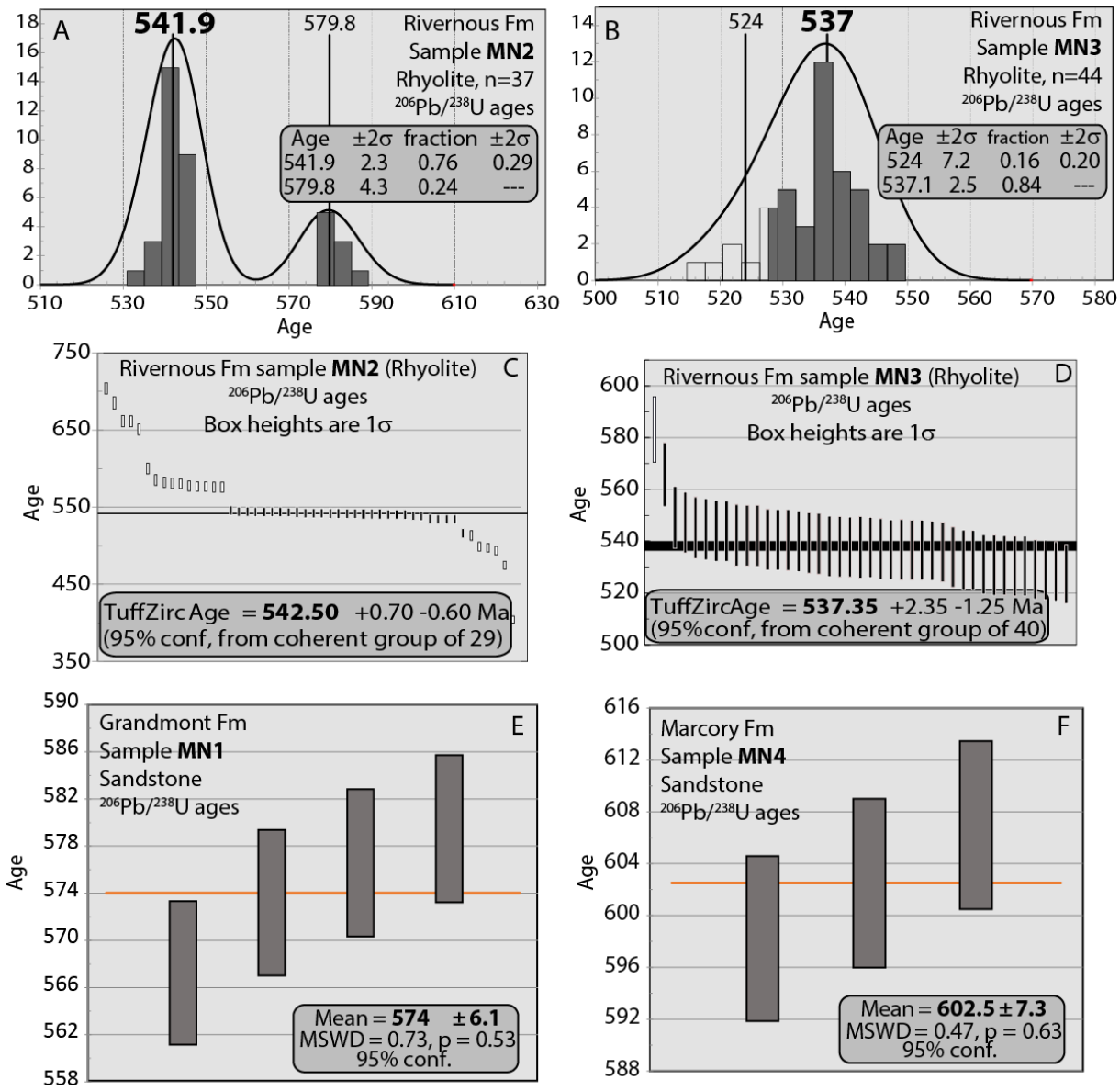

Fig. 4 : LA-ICP-MS results for all samples using $^{206}Pb/^{238}U$ ages. Diagram A: mixture analysis for sample MN2 using Sambridge and Compston (1994) approach; the age 579.8±4.3 Ma is considered as inherited age. Diagram B: mixture analysis for sample MN3 using Sambridge and Compston (1994) approach; the age 524±7.2 Ma is considered as geologically meaningless, due to lead loss. Diagrams C and D: data point age distribution for samples MN2 and MN3, resp., using TuffZirc Age (Ludwig and Mundil, 2002); chosen emplacement age for the rhyolitic tuffs of the Rivernous Fm are: 542.5+0.7/-0.6 Ma (2 σ) for sample MN2 and 537.3+2.35/-1.25 Ma (2 σ) for sample MN3. Diagrams E and F: average age calculated for the youngest concordant zircon population of Grandmont and Marcory Fm (sample MN1 and MN4), derived from a cluster of at least 3 analyses from 3 different grains overlapping in age at 2 σ (standard deviation) as proposed by Dickinson and Gehrels (2009).

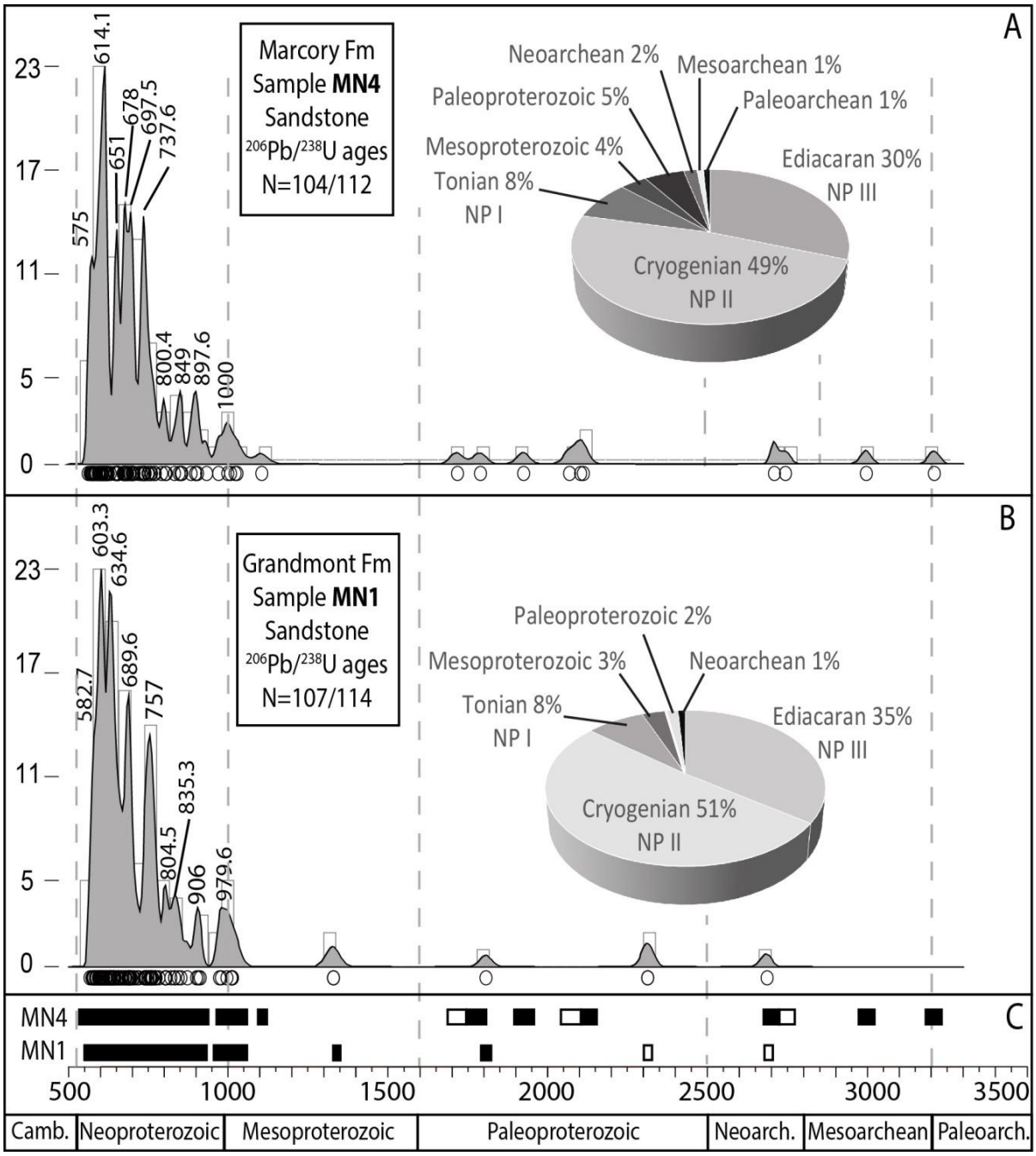

Fig. 5 : Frequency and probability density plots of detrital zircon grains in the range 500-3300 Ma for samples MN1 (B) and MN4 (A). Age groups of each sample are presented in a pie diagram. Section C shows a comparison of age groups where white boxes represent dates from inherited core and black boxes relate to dates from zoned rims.

5. Discussion

5.1 The Rivernous volcanic activity marking the Precambrian-Cambrian boundary interval

The two dates (537.1 ± 2.5 Ma and 542.5 +0.7/-0.6 M) obtained from the Rivernous rhyolitic tuffs are much older than previously estimated (473±19 Ma and 443±40 Ma;

Demange, 1982). These results allow us to confidently identify the Precambrian–Cambrian boundary (541 Ma, Gradstein et al., 2012) in the basal succession of the Montagne Noire. By comparison with the previously determined age of the Sériès Tuffs from the Axial Zone (545±15 Ma; Lescuyer and Cocherie, 1992) and the Rivernous (former Murat) Fm in the Lacaune thrust slice of the northern flank (532±12 Ma, intercept superior; Demange et al., 1995 and references therein; Figs. 1–2), these results support the lateral equivalence of the Sériès volcanic episode (Axial Zone) and Rivernous rhyolitic tuff deposition (northern flank), as already suggested (Pouclet et al., 2016).

In other Variscan units of the Ibero-Armorican Arc, some plutonic bodies have recently been dated around 540 Ma by LA-ICPMS (Fig. 7): the Arc-de-Fix and Ardéchois augen gneisses in the Massif Central, with respective Concordia age of 541.8 ± 3.1 and 542.5 ± 3.1 Ma (Couzinié et al., this issue), as well as the Laparan orthogneiss in the Central Pyrenees with a Concordia age of 545±3 Ma (Mezger and Gerdes, 2016). All these plutonic and volcanic events, overlapping in age within error, should be linked to a common episode associated with the voluminous magmatic and anatectic Cadomian events reported for West Gondwana, among others, by Linnemann et al. (2007, 2008). According to these authors, the numerous plutonic and volcanic to volcanosedimentary complexes identified in the Ossa-Morena, Saxo-Thuringian and Anti-Atlas zones (Álvaro et al., 2014a; Blein et al., 2014) can result from a slab breakoff of a southward subducted oceanic plate ending with the Cadomian cycle at about 545–540 Ma. The end of the Pan-African/Cadomian cycle led to the onset of a Cambrian magmatic cycle (Fig. 7), related to the rifting of the North Gondwana margin (Álvaro et al., 2014; Pouclet et al., 2016).

5.2 Age and potential provenances of the Grandmont and Marcory formations

Depositional ages. The youngest group of concordant zircon grains from the Grandmont Fm (sample MN1) yield an average date of 574±6 Ma which is interpreted here as its maximum depositional age (i.e. late Ediacaran ; Fig. 4E). This result is coherent with the stratigraphic framework proposed by Álvaro et al. (2014b) and the Neoproterozoic age based on acritarchs reported from the “Schistes X” Fm of the Axial Zone (Fournier-Vinas and Debat, 1970). As a result, this maximum age of deposition supports their correlation between the Grandmont and “Schistes X” formations (Álvaro et al., 2014b).

The average date calculated from the youngest group of concordant data for the Marcory Fm at 602.5±7.3 Ma (Fig.4F) might be considered as a maximum depositional age.

However, it is far from the real depositional age, as mentioned above. Indeed, this sample was selected from the *Psammichnites gigas*-bearing level (Fig. 2), and consequently must be assigned to the Cambrian Stage 2–3 transition, i.e. less than 521 Ma-old.

Source of the pre- ca.1Ga detrital zircon grains. The age spectra obtained for the samples from the Marcory (MN4) and Grandmont (MN1) formations are somewhat similar, but display some differences. Although each individual singleton-date should be treated with caution, the distributions of pre-1Ga ages are plainly distinct (Figs. 5-6).

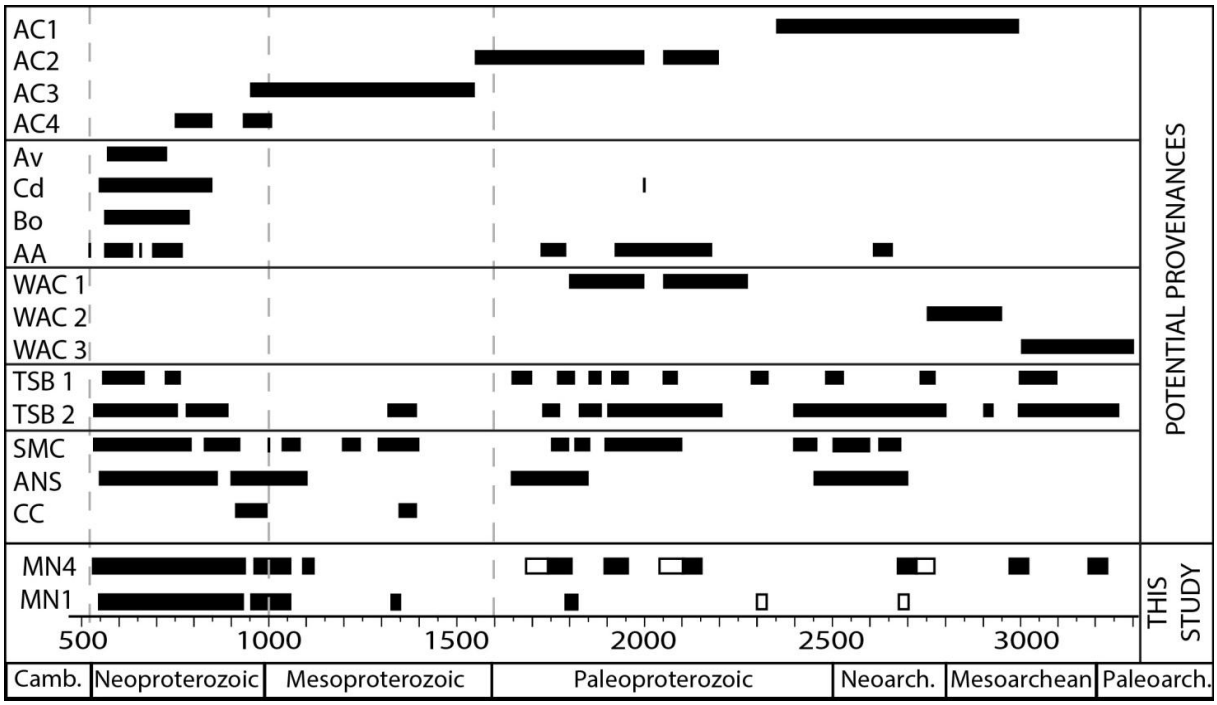

Fig. 6 : Potential sources for samples MN1 and MN4 (modified after Drost et al., 2011; Linnemann et al., 2011; Pereira et al., 2012 a,b; Tack et al., 2001, 2010). AC1: Siderian event of Amazonian craton; AC2: Rhyacian, Orosirian and Statherian events of Amazonian craton; AC3: San Ignacio and Sunsas events of Amazonian craton; AC4: eastern margin of Amazonian craton; Av: Avalonia; Cd: Cadomia; Bo: Bohemian massif; AA: Anti-Atlas; WAC1: Eburnean event of West African craton; WAC2: Liberian event of West African craton; WAC3: Leonian event of West African craton; TSB1: Trans-Saharan belt, Benin-Nigerian shield; TSB2: Trans-Saharan belt, Tuareg shield; SMC: Saharan metacraton; ANS: Arabian-Nubian shield; CC: Congo craton.

As mentioned above, zircon grains from the Marcory Fm (sample MN4) are much smaller and definitely more rounded (Fig. 3) than those from the Grandmont Fm (sample MN1), suggesting a long distance of transport for the former grains. We have separated data from inherited cores (white boxes in Fig. 5), meaningless regarding the source age, from data from zoned magmatic rims (black boxes, Fig. 5) that represent most probably the age of the source-rock. From this respect, the oldest zircon rim from the Grandmont Fm (MN1) is only

Late Paleoproterozoic (1806±19 Ma), and only two grain rims are older than 1Ga. By contrast, the presence of several Archean zircon rims in MN4 points to a major change in the source areas. MN1 zircon grains could possibly be derived, ultimately, from the Amazonian craton (Rhyacian, Orosirian and Statherian events), more probably from the Eburnean West African craton, or from the Saharan metacraton (Fig. 6). By contrast, eight pre-1Ga zircon rims from sample MN4 form a Paleoproterozoic group (cluster ranging from 2109 ±19 Ma to 1787±20 Ma) and an Archean group. Those groups fit much better with an African source comprising Eburnean areas plus Archean West African Craton (Fig.6).

However, we should not exclude that the availability of zircon to erosion and transport from either primary crystalline or recycled sources requires that the zircon-bearing rocks be exposed at the appropriate time, and recycling from older sedimentary deposits may constitute a more significant source than from primary crystalline rocks.

Sources of the Stenian-Tonian detrital zircons. The cluster pointing to the Stenian–Tonian transition (950 to 1100 Ma) in samples MN1 and MN4 could share a common origin (Fig. 5). One should expect an Amazonian craton affinity (Linnemann et al., 2011) with detrital sources related to the San Ignacio and Sunsas events and on its eastern margin (Pereira et al., 2012). However, many studies on sandstones from Lower Paleozoic peri-Gondwanan exposures around the Mediterranean region (e.g., Israel, Jordan, Libya, Pyrenees, Sardinia, Greece and Sicily) rule out an Amazonian provenance and suggest instead an eastern to southeastern African origin (Altumi et al., 2013; Avigad et al., 2003; Avigad et al., 2012; Margalef et al., in press; Meinhold et al., 2011; Meinhold et al., 2013; Williams et al., 2012; Kydonakis et al., 2014). Therefore, the Arabian-Nubian shield, the Saharan metacraton, possibly the western edge of the Congo craton (Tack et al., 2001) as well as its eastern part recording the “Kibaran Event” (Tack et al., 2010) and the Irumide belt (Meinhold et al., 2011), fit well as potential sources for Mesoproterozoic and Stenian–Tonian zircon grains. These zircon-forming events occurred simultaneously with the assembly of the supercontinent Rodinia (Grenvillian orogeny). Different hypotheses have been advanced to explain this input of Mesoproterozoic and Stenian–Tonian zircon crystals (Altumi et al., 2013), including: (i) the transport of large amounts of sediment through Neoproterozoic glaciers following an original S-N transect, later reworked and deposited (Avigad et al., 2003); and (ii) a source region linked to the Transgondwanan supermountain range resulting from the East African-Antarctic Orogen and formed during the protracted late Neoproterozoic docking of East and West

Gondwana (Williams et al., 2012), involving the development of a super-fan system (Squire et al., 2006, Kydonakis et al., 2014).

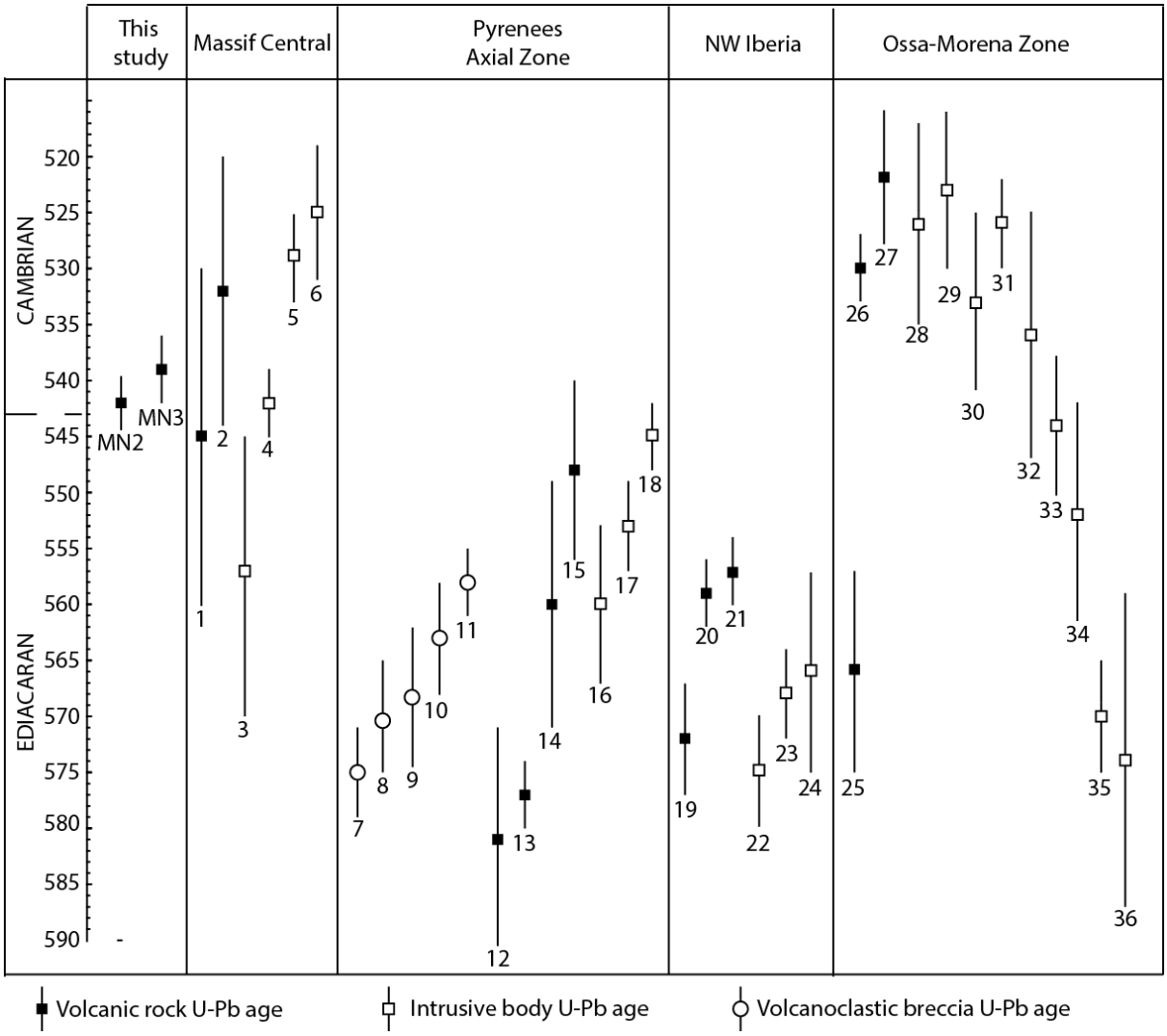

Fig. 7 : Rivernous Fm U–Pb ages, MN2 and MN3, compared with regional magmatic ages in the Massif Central and Pyrenean massifs and in the Iberian domain across the Ediacaran–Cambrian transition. Massif Central : 1 – Sériès metadacite, 545±15 Ma(1); 2 – Murat Fm, 532±12 Ma(2) ; 3 - Caplongue granodiorite, 557±12 Ma (3); 4 – Arc-de-Fix and Ardéchois augen 541.8 ± 3.1 and 542.5 ± 3.1 Ma (4); 5 – Li14, Moulin du Chambon orthogneiss, 529±4Ma(3); 6 – Vergonzac orthogneiss, 525±6 Ma(3). Pyrenees Axial Zone : 7 – TG03, Tregurà volcanoclastic breccia, 575±4 Ma(5); 8 – TG01, Tregurà volcanoclastic breccia, 570±5 Ma(5); 9 - TG02, Tregurà volcanoclastic breccia, 568±6 Ma(5); 10 – CC0807, Cap de Creus volcanoclastic breccia 563±5 Ma(5); 11 – CC0808, Cap de Creus volcanoclastic breccia, 558±3Ma(5) ; 12 – GRA1, Mas des Sitges metarhyolithic tuff, 581±10 Ma(6); 13 – CC0801, 577±3 Ma(5); 14 – CC0502, Cap de Creus metatuff 560±11 Ma(7); 15 – RF3 Mas Blanc metarhyolithic tuff, 548±8 Ma(7); 16 – RF4, Mas Blanc gneiss, 560±7Ma(7); 17 – CC0507, Port gneiss 553±4 Ma(6); 18 – LOG, Laparan gneiss, 545±3 Ma(8). NW Iberia : 19 – PEN552, Allande group dacitic tuff, 572±5 Ma (9) ; 20 – NWIb, 559±3 Ma(10); 21 – CQ39 Cudillero rhyolite, 557±2.7 Ma(9) ; 22 – PEN151, Escrita diorite, 575±5 Ma(9) ; 23 – Lomes tonalite, 568±4 Ma(9) ; 24 – La Cueta granodiorite, 566±9 Ma(9). Ossa-Morena Zone : 25 – La Cardenchosilla amphibolite, 566±9 Ma(11); 26 – Bodonal porphyroid, 530±3 Ma(11); 27 – Escoural felsic gneiss, 522±5 Ma(11); 27 -

Alcaçovas felsic gneiss, 526±9 Ma(11); 29 – Mina afortunada granitoids and migmatites, 523±7 Ma(11); 30 – Monestério granitoids and migmatites, 533±8 Ma(11); 31 –Barquete granite, 526±4 Ma(11); 32 – Monteagudo gabbro, 536±11 Ma(11); 33 – Mosquil tonalite 544±6 Ma(11); 34 – Ahillones granite, 552±10 Ma(11) ; 35 – Mouriscas gneiss, 570±5 Ma(11) ; 36 – Vale de Serena-Zalamea granodiorite, 573±14 Ma(11). Reference numbers : (1) Lescuyer and Cocherie 1992 ; (2) Ducrot et al., in Demange et al., 1995 ; (3) Melleton et al., 2010 and therein references ; (4) Couzinié et al., this issue ; (5) Casas et al., 2015 ; (6) Cocherie et al., 2005 ; (7) Castiñeiras et al., 2008 ; (8) Mezgher et al., 2016 ; (9) Rubio-Ordoñez et al., 2015 ; (10) Gutiérrez-Alonso et al., 2004 ; (11) Pereira et al., 2011 and references therein.

Sources of Neoproterozoic detrital zircons. Neoproterozoic grains display similar age distributions in the Grandmont and Marcory formations: a main Neoproterozoic population of zircon grains (with one predominant Ediacaran group) followed by five similar peaks across the Tonian–Cryogenian interval (Fig.5). Potential sources for these detrital zircons are located in the eastern (Saharan metacraton, Arabian-Nubian shield) and western (Trans-Saharan belt, Pan-African suture of the Anti-Atlas, early and late Cadomian arcs, and Avalonian Arc) area of the North-Gondwana margin(Fig.6). The probability density curve of the Marcory Fm, as well as the shape and roundness of its zircon grains, implies more remote origins for them than for the Grandmont Fm ones. Therefore, a comparison of the morphological and age differences of these zircon grains suggests an evolution of the depositional basin and it sourcing from a narrow basin being infilled by the Grandmont Fm, probably a back-arc basin resulting from the Panafrican/Cadomian orogeny, to a more evolved and opened basin infilled by the Marcory Formation, represents a more evolved and widespread basin with wider potential source areas, developed during the break-up West Gondwana.

A composite zircon grain of the Grandmont sandstone (sample MN 1; ZR 49) demonstrates that crust with ca. 586 Ma old rocks became recycled during magmatism at ca. 567 Ma, and underlines the existence of two distinct Ediacaran magmatic events in the source area.

One should expect to identify the Ediacaran Rivernous volcanic event as reworked zircon grains in the overlying Cambrian Marcory Fm. However, this is not the case. A rapid burial of the Rivernous volcanosedimentary paleorelief, related to high rates of sedimentation and available accommodation space due to active thermal subsidence, has been proposed for Furongian to Early Ordovician times in West Gondwana (Linnemann et al., 2011; Pereira et al., 2012) and the late Neoproterozoic-to-early Cambrian in the ANS (Avigad and Gvirtzman, 2009) or post-Cadomian rifting extension (Pouclet et al., 2016; Von Raumer and Stampfli,

2008), which should preclude reworking of the Rivernous from distal (northern) to proximal areas (southern Montagne Noire).

6. Conclusions

The Ediacaran–Cambrian boundary has been confidently identified within error, based on U–Pb zircon dating, into the Rivernous Fm of the northern Montagne Noire (Fig.8). The Rivernous volcanic event is indicated to be the lateral equivalent of the Sériès Tuff of the Axial Zone. This fits well with a latest Ediacaran depositional age (ca. 574 Ma) estimated with detrital zircon U-Pb geochronology for the underlying Grandmont Fm. The latter should be considered as a time-stratigraphic equivalent of the acritarch-bearing "Schist X" Fm of the Axial Zone.

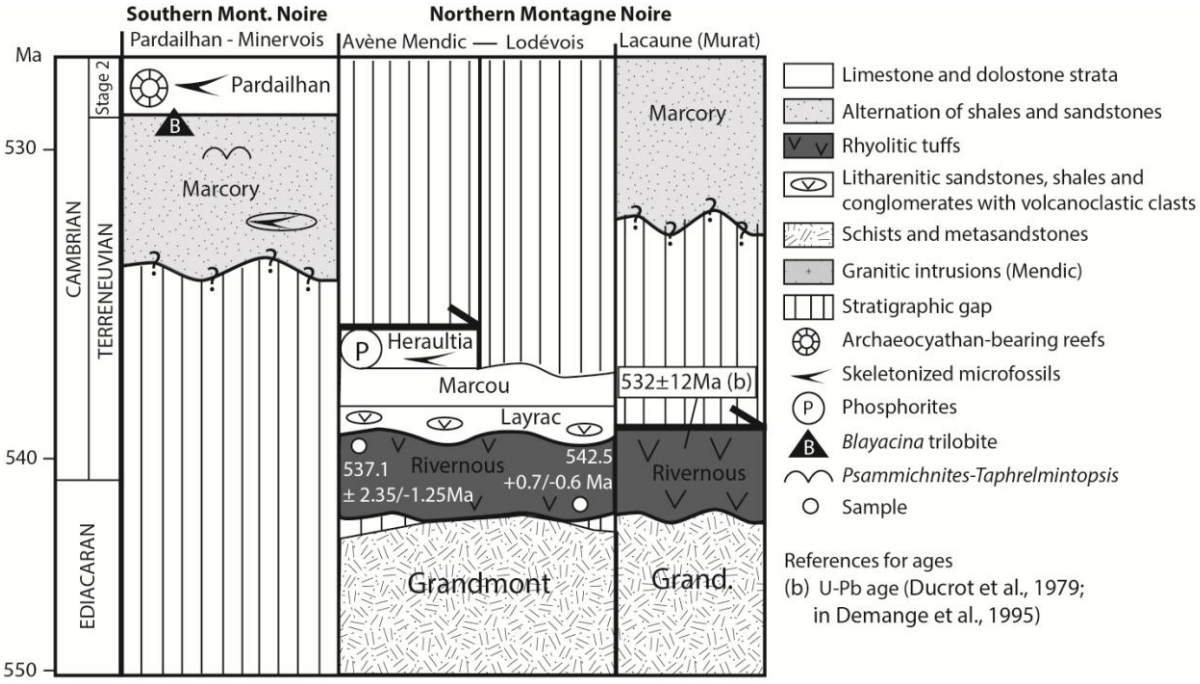

Fig. 8 : Updated stratigraphy of the Ediacaran-Cambrian transition in the Montagne Noire with new U-Pb ages.

U-Pb analysis of the detrital zircons from the Ediacaran Grandmont Fm and the Cambrian Series 2 Marcory Fm suggests a change over time in the sourcing. The Ediacaran sediments were deposited in a narrow back-arc basin far from the influence of far cratonic sources, whereas Cambrian Series 2 detrital sediments were derived from mature source rocks involving the denudation of different Gondwanan cratons.

Acknowledgements

The authors thank constructive criticism made by O. Blein and B. Laumonier, and founding from the RGF program of the French Geological Survey (BRGM). This paper is a contribution to project CGL2013-48877-P from Spanish MINECO.

7. References

Altumi, M.M., Elicki, O., Linnemann, U., Hofmann, M., Sagawe, A., Gärtner, A., 2013. U–Pb LA-ICP-MS detrital zircon ages from the Cambrian of Al Qarqaf Arch, central-western Libya: Provenance of the West Gondwanan sand sea at the dawn of the early Palaeozoic. J. Afr. Earth Sci. 79, 74-97.

Álvaro, J.J., Vizcaïno, D., 1999. Biostratigraphic significance and environmental setting of the trace fossil Psammichnites in the Lower Cambrian of the Montagne Noire (France). Bull. Soc. géol. Fr. 170, 821-828.

Álvaro, J.J., Courjault-Radé, P., Chauvel, J.J., Dabard, M.P., Debrenne, F., Feist, R., Pillola, G.L., Vennin, E., Vizcaïno, D., 1998. Nouveau découpage stratigraphique des séries cambriennes des nappes de Pardailhan et du Minervois (versant sud de la Montagne Noire, France). Géol. France 1998 (2), 3-12.

Álvaro, J.J., Benziane, F., Thomas R., Walsh, G.J., Yazidi, A., 2014a. Neoproterozoic–Cambrian stratigraphic framework of the Anti-Atlas and Ouzellagh promontory (High Atlas), Morocco. J. Afr. Earth Sci. 98, 1-15.

Álvaro, J.J., Baulus, B., Clausen, S., Devaere, L., Imaz, A.G., Monceret, E., Vizcaïno, D., 2014b. Sratigraphy of the Cambrian-Lower Ordovician volcanosedimentary complexes, northern Montagne Noire, France. Stratigraphy 11, 83-96.

Álvaro, J.J., Colmenar, J., Monceret, E., Pouclet, A., Vizcaïno, D. (2015). Late Ordovician (post–Sardic) rifting branches in the North Gondwanan Montagne Noire and Mouthoumet massifs of southern France. Tectonophysics, http://dx.doi.org/10.1016/j.tecto.2015.11.031

Arthaud, F., 1970. Etude tectonique et microtectonique comparée de deux domaines hercyniens : les nappes de la Montagne Noire (France) et l'anticlinorium de l'Iglesiente (Sardaigne). PhD, Université de Montpellier. Pub. USTELA, Montpellier, Série Géol. Struct. 1, 175 p.

Avigad, D., Gerde, A., Morag, N., Bechstädt, T., 2012. Coupled U–Pb–Hf of detrital zircons of Cambrian sandstones from Morocco and Sardinia: Implications for provenance and Precambrian crustal evolution of North Africa. Gondwana Res. 21, 690-703.

Avigad, D., Gvirtzman, Z., 2009. Late Neoproterozoic rise and fall of the northernArabian–Nubian shield: the role of lithospheric mantle delamination and sub-sequent thermal subsidence. Tectonophysics 477, 217–228.

Avigad, D., Kolodner, K., McWilliams, M., Persing, H.M., Weissbrod, T., 2003. Origin of northern Gondwana Cambrian sandstone as revealed by SHRIMP dating of detrital zircons. Geology 31, 227-230.

Ballèvre, M., Bosse, V., Ducassou, C., Pitra, P., 2009. Palaeozoic history of the Armorican Massif: Models for the tectonic evolution of the suture zones. C. R. Geosci. 341, 174-201.

Bard, J.-P., Loueyit, G., 1978. Sur l'origine des gneiss oeillés de l'Espinouse dans la zone axiale de la Montagne noire (Massif central) ; conséquences tectoniques. Bull. Soc. géol. Fr. 20, 751–772.

Blein, O., Baudin, T., Soulaimani, A., Cocherie, A., Chèvremont, P., Admou, H., Ouanaimi, H., Hafid, A., Razin, P., Bouadbelli, M., Roger, J., 2014. New geochemical, geochronological and structural constraints on the Ediacaran evolution of the south Sirwa, Agadir-Melloul and Iguerda inliers, Anti-Atlas, Morocco. J. Afr. Earth Sci. 98, 47-71.

Brun, J.-P., Van Den Driessche, J., 1994. Extensional gneiss dome and detachment fault systems: structure and kinematics. Bull. Soc. géol. Fr. 165, 519–530.

Bowring, S.A., Schoene, B., Crowley, J.L., Ramezani, J., Conon, D.J., 2006. High-precision U-Pb zircon geochronology and the stratigraphic record: progress and promise. Geochronology: Emerging Opportunities, Paleontological Society Short Course. Paleontol. Soc. Pap. 11, 23-43.

Casas, J. M., Navidad, M., Castiñeiras, P., Liesa, M., Aguilar, C., Carreras, J., Hofmann, M., Gärtner, A., Linnemann, U., 2015. The Late Neoproterozoic magmatism in the Ediacaran series of the Eastern Pyrenees: new ages and isotope geochemistry. Int. J. Earth Sci. 104, 909-925.

Castiñeiras, P., Navidad, M., Liesa, M., Carreras, J., Casas, J.M., 2008. U-Pb zircon ages (SHRIMP) for Cadomian and Lower Ordovician magmatism in the Eastern Pyrenees: new insights in the pre-Variscan evolution of the northern Gondwana margin. Tectonophysics 461, 228-239.

Charles, N., Faure, M., Chen, Y., 2009. The Montagne Noire migmatitic dome emplacement (French Massif Central): new insights from petrofabric and AMS studies. J. Struct. Geol. 31, 1423–1440.

Cobbold, E.S., 1935. Lower Cambrian faunas from Hérault, France. Ann. Mag. Nat. Hist. (ser. O), 16, 25-48.

Cocherie, A., Baudin, T., Autran, A., Guerrot, C., Fanning, M., Laumonier, B., 2005. U-Pb zircon (ID-TIMS and SHRIMP) evidence for the early Ordovician intrusion of metagranites in the late Proterozoic Canaveilles Group of the Pyrenees and the Montagne Noire (France). Bull. Soc. géol. Fr. 176, 269-282.

Couzinié, S., et al., this issue.

Demange, M., 1975. Style pennique de la zone axiale de la Montagne noire entre Saint-Pons et Murat-sur-Vèbre (Massif central), Bull. BRGM, 2e série I (2), 91-139.

Demange, M., 1982. Etude géologique du massif de l'Agout, Montagne Noire. PhD, Univ. Paris VI.

Demange, M., 1985. The eclogite-facies rocks of the Montagne Noire, France. Chem. Geol. 50, 173- 188.

Demange, M., 1998. Contribution au problème de la formation des dômes de la Zone Axiale de la Montagne Noire : analyse géométrique des plissements superposés dans les séries métasédimentaires de l'enveloppe. Implications pour tout modèle géodynamique. Géol. France 4, 3-56.

Demange, M., Guérangé-Lozes, J., Guérangé, B., 1995. Notice explicative, Carte géol. France (1/50 000), feuille Lacaune (987). Orléans: BRGM, 153 p.

Devaere, L., Clausen, S., Steiner, M., Álvaro, J.J., Vachard, D., 2013. Chronostratigraphic and palaeogeographic significance of an early Cambrian microfauna from the Heraultia Limestone, northern Montagne Noire, France. Palaeont. Electr. 16.2.17A, 755-768 p.

Dickinson, W.R., Gehrels, G.E., 2009. Use of U–Pb ages of detrital zircons to infer maximum depositional ages of strata: a test against a Colorado Plateau Mesozoic database. Earth Planet. Sci. Lett. 288, 115–125.

Drost, K., Gerdes, A., Jeffries, T., Linnemann, U., Storey, C., 2011. Provenance of Neoproterozoic and early Paleozoic silicicastic rocks of the Tepla-Barrandian unit (Bohemian Massif): Evidence from U-Pb detrital zircon ages. Gondwana Res. 19, 213-231.

Ducrot, J., Lancelot, J.-R., Reille, J.-L., 1979. Datation en Montagne noire d'un témoin d'une phase majeure d'amincissement crustal caractéristique de l'Europe prévarisque. Bull. Soc. géol. Fr. 21, 501-505.

Faure, M., Cottereau, N., 1988. Données cinématiques sur la mise en place du dôme migmatitique carbonifère moyen de la zone axiale de la Montagne Noire (Massif Central, France). C. R. Acad. Sci., Paris Série II 307, 1787–1794.

Faure, G., Mensing, T.M. (2005) Isotopes: principles and applications. Wiley, Hoboken, p 897.

Fournier-Vinas, C., Debat, P., 1970. Présence de micro-organismes dans les terrains métamorphiques précambriens (schistes X) de l'Ouest de la Montagne Noire. Bull. Soc. géol. Fr. 12, 351-355.

Fréville, K., Cenki-Tok, B., Trap, P., Rabin, M., Leyreloup, A., Régnier, J.-L., Whitney, D.L., 2016. Thermal interaction of middle and upper crust during gneiss dome formation : example from the Montagne Noire (French Massif Central). J. Metam. Geol. 34, 447-462.

Gebauer, D., Grünenfelder, M., 1977. U-Pb systematics of detrital zircons from some unmetamorphosed to slightly metamorphosed sediments of Central Europe. Contrib. Mineral. Petrol. 65, 29-37.

Gebauer, D., Williams, I.S., Compston, W., Grünenfelder, M., 1989. The development of the Central European Continental crust since the Early Archaean based on conventional and ion-microprobe dating of up to 3.84 b.y. old detrital zircons. Tectonophysics, 157, 81-96

Geyer, G, 1992. A re-evaluation of Blayacina Cobbold, 1932 and Thoralaspis Hupé, 1953 (Trilobita: Redlichiida). Paleont. Z. 66, 99-113.

Gèze, B., 1949. Etude géologique de la Montagne Noire et des Cévennes méridionales. Mém. Soc. Géol. France 62, 1-215.

Gradstein, F.M., Ogg, J.G., Schmitz, M.D., Ogg, G.M., eds, 2012. The Geological Time Scale 2012, Amsterdam, Elsevier, 2 vols., 1144 p.

Gutiérrez-Alonso, G., Fernández-Suárez, J., Jeffries, T.E., 2004. Age and setting of the Upper Neoproterozoic Narcea Antiform volcanic rocks (NW Iberia). Geogaceta 35, 78-82.

Jackson, S.E., Pearson, N.J., Griffin W.L., Belousova, E.A., 2004. The application of laser-ablation-inductively coupled plasma-mass spectrometry to in situ U-Pb zircon geochronology. Chem. Geol. 211, 47-69.

Kydonakis, K., Kostopoulos, D., Poujol, M., Brun, J.-P., Papanikolaou, D. et Paquette, J.-L. (2014). The dispersal of the Gondwana Super-fan System in the eastern Mediterranean : New insights from detrital zircon geochronology. Gondwana Research, 25, 1230-1241.

Lescuyer, J.L., Cocherie, A., 1992. Datation sur monozircons des metadacites de Sériès. Arguments pour un âge protérozoïque terminal des "schistes X" de la Montagne Noire (Massif Central français). C. R. Acad. Sci., Paris Série II 314, 1071-1077.

Linnemann, U., Gerdes, A., Drost, K., Buschmann, B., 2007. The continuum between Cadomian Orogenesis and opening of the Rheic Ocean: constraints from LA-ICP-MS U–Pb zircon dating and analysis of plate-tectonic setting (Saxo-Thuringian Zone, NE Bohemian massif, Germany). In: Linnemann, U., Nance, D., Kraft, P., Zulauf, G. (Eds.), The Evolution of the Rheic Ocean: from Avalonian-Cadomian active margin to Alleghenian-Variscan collision. Geol. Soc. Am. Bull. 423, 61-96.

Linnemann, U., Pereira, F., Jeffries, T.E., Drost, K., Gerdes, A., 2008. The Cadomian Orogeny and the opening of the Rheic Ocean: the diacrony of geotectonic processes constrained by LA-ICP-MS U–Pb zircon dating (Ossa-Morena and Saxo-Thuringian Zones, Iberian and Bohemian Massifs). Tectonophysics 461, 21-43.

Linnemann, U., Ouzegane, K., Drareni, A., Hofmann, M., Becker, S., Gärtner, A., Sagawe, A., 2011. Sands of West Gondwana: an archive of secular magmatism and plate interactions—a case study from the Cambro-Ordovician section of the Tassili Ouan Ahaggar (Algerian Sahara) using U–Pb LA-ICP-MS detrital zircon ages. Lithos 123, 188-203.

Ludwig, K.R., 2012. Users Manual for Isoplot/Ex rev. 3.75. Berkeley Geochronology Center, Spec. Publ. 5, 1-75.

Ludwig, K.R., and Mundil, R., 2002. Extracting reliable U-Pb ages and errors from complex populations of zircons from Phanerozoic tuffs. Geochim. Cosmochim. Acta 66, A463.

Manzotti, P., Poujol, M., Ballèvre, M. (2015). Detrital zircon in blueschist-facies metaconglomerates: implications for the Early Permian palaeo-topography of the Western Alps. Int. J. Earth Sci. 104, 703-731.

Margalef, A., Castiñeiras, P., Casas, J.M., Navidad, M., Montserrat, L., Linnemann, U., Hofmann, M., Gärtner, A. (in press). Detrital zircons from the Ordovician rocks of the Pyrenees: Geochronological constraints and provenance, Tectonophysics, doi:10.1016/j.tecto.2016.03.015.

Mattauer, M., Laurent, P., Matte, P., 1996. Plissement Hercynien synschisteux postnappe et étirement subhorizontal dans le versant sud de la Montagne Noire (sud du Massif Central, France). C. R. Acad. Sci., Paris Série IIa 322, 309–315.

Meinhold, G., Morton, A.C., Avigad, D., 2013. New insights into peri-Gondwana paleogeography and the Gondwana super-fan system from detrital zircon U–Pb ages. Gondwana Res. 23, 661-665.

Meinhold, G., Morton, A.C., Fanning, C.M., Frei, D., Howard, J.P., Phillips, R.J., Strogen, D., Whitham, A.G., 2011. Evidence from detrital zircons for recycling of Mesoproterozoic and Neoproterozoic crust recorded in Paleozoic and Mesozoic sandstones of southern Libya. Earth Planet. Sci. Lett. 312, 164-175.

Melleton, J., Cocherie, A., Faure, M., Rossi, P., 2010. Precambrian protoliths and Early Paleozoic magmatism in the Massif Central : U-Pb data and the North Gondwana connection in the west European Variscan Belt. Gondwana Res. 17, 13-25.

Mezger, J.E., Gerdes A., 2016. Early Variscan (Visean) granites int the core of central Pyrenean gneiss domes: implications from laser ablation U-Pb and Th-Pb studies. Gondwana Res. 29, 181-198.

Pereira, M.F., Chichorro, M., Solá, A.R., Silva, J.B., Sánchez-García, T., Bellido, F., 2011. Tracing the Cadomian magmatism with detrital/inherited zircon ages by in-situ U– Pb SHRIMP geochronology (Ossa-Morena Zone, SW Iberian Massif). Lithos 123, 204-217.

Pereira, M.F., Solá, A.R., Chichorro, M., Lope, L., Gerdes, A., Silva, J.B., 2012. North-Gondwana assembly, break-up and paleogeography: U–Pb isotope evidence from detrital and igneous zircons of Ediacaran and Cambrian rocks of SW Iberia. Gondwana Res. 22, 866-881.

Pereira, M.F., El Houicha, M., Chichorro, M., Armstrong, R., Jouharib, A. El Attarib, A. Ennih, N., Silva, J.B., 2015. Evidence of a Paleoproterozoic basement in the Moroccan VariscanBelt (Rehamna Massif, Western Meseta). Precambrian Research 268, 61–73.

Pitra, P., Poujol, M., Van Den Driessche, J., Poilvet, J.C. and Paquette, J.L. (2012). Early Permian extensional shearing of an Ordovician granite: the Saint-Eutrope "C/S-like" orthogneiss (Montagne Noire, French Massif Central). Comptes Rendus Geosciences, 344, 377–384.

Pouclet, A., Álvaro, J.J., Bardintzeff, J.-M., Gil Imaz, A, Monceret, E., Vizcaïno, D. 2016. Cambrian–Early Ordovician volcanism across the South Armorican and Occitan Domains of the Variscan Belt in France: Continental break-up and rifting of the northern Gondwana margin. Geosci. Frontiers, doi: 10.1016/j.gsf.2016.03.002.

Poujol, M., Pitra, P., Van Den Driessche, J., Ruffet, G., Paquette, J-L, Poilvet, J-C. (in press). Two-stage partial melting during the Variscan extensional tectonics (Montagne Noire, France). Intern. J. Earth Sciences. DOI : 10.1007/s00531-016-1369-1

Roger, F., Respault, J.P., Brunel, M., Matte, P., Paquette, J.L., 2004. Première datation U- Pb des orthogneiss œillés de la zone axiale de la Montagne Noire (Sud du Massif-Central) : nouveaux témoins du magmatisme ordovicien dans la chaine varisque. C. R. Geosci. 336, 19-28.

Rubio-Ordóñez, A., Gutiérrez-Alonso, G., Valverde-Vaquero, P., Cuesta, A., Gallastegui, G., Gerdes, A., Cárdenes, V., 2015. Arc-related Ediacaran magmatism along the northern margin of Gondwana: Geochronology and isotopic geochemistry from northern Iberia. Gondwana Res. 27, 216–227.

Sambridge, M.S., Compston, W., 1994. Mixture modelling of multi-component data sets with application to ion-probe zircon ages. Earth Planet. Sci. Lett. 128, 373-390.

Sláma, J., J. Košler, 2012. Effects of sampling and mineral separation on accuracy of detrital zircon studies. Geochem. Geophys. Geosyst. 13, 1-17.

Sláma, J., Košler, J., Condon, D.J., Crowley, J.L., Gerdes, A., Hanchar, J.M., Horstwood, M.S.A., Morris, G.A., Nasdala, L., Norberg, N., Schaltegger, U., Schoene, B., Tubrett, M.N., Whitehouse, M.J., 2008. Plešovice zircon — a new natural reference material for U–Pb and Hf isotopic microanalysis. Chem. Geol. 249, 1-35.

Soula, J.-C., Debat, P., Brusset, S., Bessière, G., Christophoul, F., Deramond, J., 2001. Thrust-related, diapiric and extensional doming in a frontal orogenic wedge: example of the Montagne Noire, southern French Hercynian belt. J. Struct. Geol. 23, 1677–1699.

Squire, R.J., Campbell, I.H., Allen, C.M., Wilson, C.J.L., 2006. Did the Transgondwana Supermontin trigger the explosive radiation of animals on Earth? Earth Planet. Sci. Lett. 250, 116-133.

Tack, L., Wingate, M.T.D., De Waele, B., Meert, J., Belousova, E., Griffin, B., Tahon, A., M. Fernandez-Alonso, A., 2010. The 1375Ma “Kibaran event” in Central Africa: Prominent emplacement of bimodal magmatism under extensional regime. Precambr. Res. 180, 63-84.

Tack, L., Wingate, M.T.D., Liégeois, J.P., Fernández-Alonso, M., Deblond, A., 2001. An Early Neoproterozoic magmatism (1000–910 Ma) of the Zadinian and Mayumbian Groups (Bas-Congo): onset of Rodinia rifting at the western edge of the Congo craton. Precambr. Res. 110, 277-306.

Talavera, C., Montero, P., Martínez Poyatos, D., Williams, I.S. (2012). Ediacaran to Lower Ordovician age for rocks ascribed to the Schist-Graywacke Complex (Iberian Massif, Spain): evidence from detrital zircon SHRIMP U–Pb geochronology. Gondwana Research, 22, 928–942.

Van Achterbergh, E., Ryan, C.G., Jackson, S.E., Griffin, W.L., 2001. Data reduction software for LA-ICP-MS: appendix. In: Sylvester P.J. (Ed.), Laser Ablation-ICP-mass spectrometry in the Earth Sciences: principles and applications, MAC Short Courses Series, Ottawa, Ontario, Canada 29, 239-243.

Van Den Driessche, J., Brun, J.-P., 1992. Tectonic evolution of the Montagne Noire (French Massif Central): a model of extensional dome. Geodin. Acta 5, 85–99.

Vermeesch, P., 2004. How many grains are needed for a provenance study? Earth Planet. Sci. Lett. 224, 351-441.

Von Raumer, J.F., Stampfli, G.M., 2008. The birth of the Rheic Ocean — Early Palaeozoic subsidence patterns and subsequent tectonic plate scenarios. Tectonophysics 461, 9-20.

Williams, I.S., Fiannacca, P., Cirrincione, R., Pezzino, A., 2012. Peri-Gondwanan origin and early geodynamic history of NE Sicily: a zircon tale from the basement of the Peloritani Mountains. Gondwana Res. 22, 855-865.

8. Appendix

Appendix 1: Operating conditions for the LA-ICP-MS equipment

Laboratory & Sample Preparation	
Laboratory name	Géosciences Rennes, UMR CNRS 6118, Rennes, France
Sample type/mineral	zircon
Sample preparation	Conventional mineral separation, 1 inch resin mount, 1µm polish to finish
Imaging	(CL) imaging using a Quanta 200 SEM with centaurus detector at the Laboratoire Magmas d'océanologie et de geosciences, Université de Lille 1 (Lille, France).
Laser ablation system	
Make, Model & type	ESI NWR193UC, Excimer
Ablation cell	ESI NWR TwoVol2
Laser wavelength	193 nm
Pulse width	< 5 ns
Fluence	7 J/cm-2
Repetition rate	5 Hz
Spot size	25 µm
Sampling mode / pattern	Single spot
Carrier gas	100% He, Ar make-up gas and N2 (3 ml/mn) combined using in-house smoothing device
Background collection	20 seconds
Ablation duration	60 seconds
Wash-out delay	15 seconds
Cell carrier gas flow (He)	0.75 l/min
ICP-MS Instrument	
Make, Model & type	Agilent 7700x, Q-ICP-MS
Sample introduction	Via conventional tubing
RF power	1350W
Sampler, skimmer cones	Ni
Extraction lenses	X type
Make-up gas flow (Ar)	0.85 l/min
Detection system	Single collector secondary electron multiplier
Data acquisition protocol	Time-resolved analysis
Scanning mode	Peak hopping, one point per peak
Detector mode	Pulse counting, dead time correction applied, and analog mode when signal intensity > ~ 10^6 cps
Masses measured	^{204}(Hg + Pb), ^{206}Pb, ^{207}Pb, ^{208}Pb, ^{232}Th, ^{238}U
Integration time per peak	10-30 ms
Sensitivity / Efficiency	20000 cps/ppm Pb (50µm, 10Hz)
Data Processing	
Gas blank	20 seconds on-peak
Calibration strategy	GJ1 zircon standard used as primary reference material, Plešovice used as secondary reference material (quality control)
Reference Material info	GJ1 (Jackson et al., 2004) Plešovice (Slama et al., 2008)
Data processing package used	GLITTER ® (van Achterbergh et al., 2001)
Quality control / Validation	Plešovice: concordia age = 336.8 ± 0.67 Ma (N=32; MSWD=0.084)

Appendix 2: LA-ICPMS U-Pb results for samples MN1 MN2 MN3 and MN4

				ISOTOPIC RATIOS					AGES						
MN1	Pb ppm	U ppm	Th/U	207/235	err (1σ)	206/238	err (1σ)	rho	207/206	err (1σ)	206/238	err (1σ)	207/235	err (1σ)	conc
ZR56	36.7	445.0	0.1	0.715	0.009	0.0849	0.0010	0.9	642.2	23.8	525.3	5.7	547.7	5.2	95.9
ZR33	76.9	810.6	0.7	0.776	0.009	0.0866	0.0010	1.0	774.1	22.3	535.5	5.8	583.3	5.3	91.8
ZR82	59.0	683.9	0.1	0.779	0.009	0.0910	0.0010	1.0	677.6	22.3	561.4	6.1	584.9	5.2	96.0
ZR49	45.7	428.1	0.9	0.757	0.009	0.0920	0.0010	1.0	591.3	23.2	567.2	6.1	572.0	5.2	99.2
ZR80	80.0	802.9	0.5	0.767	0.009	0.0930	0.0011	0.9	595.3	24.7	573.2	6.2	577.8	5.4	99.2
ZR58	7.0	70.6	0.5	0.776	0.011	0.0936	0.0011	0.8	608.7	28.0	576.6	6.3	583.1	6.2	98.9
ZR97	11.6	119.2	0.4	0.777	0.010	0.0941	0.0011	0.9	600.2	26.1	579.5	6.3	583.7	5.8	99.3
ZR32	20.2	211.8	0.3	0.793	0.010	0.0941	0.0011	0.9	645.3	24.5	579.6	6.3	593.1	5.6	97.7
ZR29	17.6	184.7	0.3	0.785	0.010	0.0948	0.0011	0.9	606.3	24.4	584.0	6.3	588.5	5.6	99.2
ZR90	22.0	214.4	0.6	0.808	0.010	0.0951	0.0011	0.9	661.8	24.3	585.8	6.3	601.6	5.6	97.4
ZR109	22.1	172.2	1.5	0.805	0.010	0.0953	0.0011	0.9	648.9	24.4	586.8	6.3	599.7	5.6	97.8
ZR28	20.2	212.9	0.3	0.793	0.010	0.0955	0.0011	0.9	610.5	24.1	588.2	6.4	592.8	5.5	99.2
ZR101	7.4	70.8	0.6	0.819	0.012	0.0962	0.0011	0.8	665.1	28.3	592.1	6.5	607.4	6.4	97.5
ZR7	33.0	326.9	0.4	0.831	0.010	0.0968	0.0011	0.9	683.1	24.0	595.6	6.5	614.1	5.7	97.0
ZR110	36.2	315.4	0.9	0.807	0.010	0.0970	0.0011	0.9	615.2	23.7	597.0	6.4	600.8	5.4	99.4
ZR35	25.3	259.8	0.3	0.803	0.010	0.0975	0.0011	0.9	593.9	23.9	599.5	6.5	598.2	5.5	100.2
ZR111	9.3	84.4	0.8	0.812	0.011	0.0976	0.0011	0.8	614.4	27.0	600.4	6.4	603.3	6.1	99.5
ZR2	8.5	78.5	0.7	0.823	0.011	0.0977	0.0011	0.8	642.0	27.0	601.0	6.6	609.6	6.2	98.6
ZR5	28.4	213.7	1.6	0.800	0.010	0.0978	0.0011	0.9	579.7	24.5	601.6	6.5	597.0	5.6	100.8
ZR49	23.5	216.1	0.7	0.823	0.011	0.0981	0.0011	0.9	635.3	25.0	603.0	6.6	609.8	5.9	98.9
ZR59	47.7	418.4	0.8	0.829	0.010	0.0982	0.0011	0.9	648.3	23.2	603.6	6.5	613.1	5.5	98.5
ZR69	12.0	107.6	0.8	0.815	0.011	0.0985	0.0011	0.9	604.0	26.3	605.5	6.6	605.1	6.0	100.1
ZR84	15.7	118.2	1.5	0.824	0.011	0.0986	0.0011	0.9	627.2	25.4	605.9	6.6	610.4	5.9	99.3
ZR53	52.1	526.3	0.3	0.824	0.010	0.0987	0.0011	1.0	624.0	22.8	606.5	6.5	610.1	5.4	99.4
ZR34	49.7	464.4	0.6	0.815	0.010	0.0987	0.0011	0.9	600.3	23.2	606.9	6.6	605.5	5.5	100.2
ZR42	26.1	251.4	0.5	0.854	0.011	0.0994	0.0011	0.9	684.6	24.3	610.8	6.6	626.6	5.9	97.5
ZR103	11.3	106.5	0.5	0.869	0.013	0.1002	0.0012	0.8	707.1	29.4	615.4	6.7	635.3	6.9	96.9
ZR68	30.3	273.4	0.6	0.885	0.011	0.1002	0.0011	0.9	745.0	23.5	615.5	6.6	643.9	5.8	95.6
ZR107	34.6	293.7	0.9	0.859	0.011	0.1003	0.0011	0.9	676.7	24.6	616.3	6.6	629.3	5.9	97.9
ZR47	37.4	340.6	0.6	0.827	0.010	0.1004	0.0011	0.9	593.9	24.2	616.6	6.7	611.7	5.7	100.8
ZR71	8.2	80.7	0.3	0.851	0.013	0.1007	0.0012	0.8	649.7	29.8	618.6	6.8	625.2	6.9	98.9
ZR6	29.1	234.4	1.1	0.865	0.011	0.1019	0.0012	0.9	659.4	23.9	625.7	6.8	633.0	5.8	98.8
ZR67	18.0	152.5	0.8	0.842	0.011	0.1020	0.0012	0.9	599.6	25.4	626.2	6.8	620.4	5.9	100.9
ZR112	11.8	116.8	0.2	0.879	0.011	0.1025	0.0012	0.9	682.2	25.8	629.0	6.7	640.7	6.2	98.2
ZR46	45.0	205.1	4.6	0.854	0.011	0.1028	0.0012	0.9	614.6	26.4	630.5	6.9	627.0	6.2	100.6
ZR87	6.3	59.5	0.4	0.885	0.013	0.1028	0.0012	0.8	689.3	28.3	630.8	6.9	643.6	6.8	98.0
ZR48	126.9	1248.5	0.2	0.909	0.011	0.1030	0.0012	0.9	742.4	23.0	631.9	6.9	656.5	5.9	96.3
ZR63	13.5	109.7	1.0	0.854	0.011	0.1031	0.0012	0.9	607.9	25.8	632.3	6.8	626.9	6.1	100.9

ZR102	13.3	128.1	0.3	0.856	0.011	0.1033	0.0012	0.9	607.2	25.7	633.5	6.8	627.7	6.0	100.9
ZR8	24.4	197.4	1.0	0.873	0.011	0.1033	0.0012	0.9	648.0	25.2	633.9	6.9	636.9	6.1	99.5
ZR15	17.2	150.6	0.7	0.883	0.011	0.1034	0.0012	0.9	673.1	25.2	634.3	6.9	642.8	6.1	98.7
ZR79	5.1	47.9	0.4	0.928	0.014	0.1042	0.0012	0.8	762.1	29.9	638.7	7.0	666.5	7.3	95.8
ZR23	17.3	157.0	0.5	0.873	0.011	0.1044	0.0012	0.9	625.5	24.5	640.3	6.9	637.0	5.9	100.5
ZR76	32.1	298.7	0.4	0.917	0.012	0.1045	0.0012	0.9	730.0	25.8	640.7	7.0	660.8	6.4	97.0
ZR44	20.4	165.4	1.0	0.874	0.011	0.1046	0.0012	0.9	626.4	25.0	641.1	7.0	637.8	6.0	100.5
ZR38	46.1	399.3	0.6	0.887	0.011	0.1052	0.0012	0.9	644.5	23.3	645.0	7.0	644.9	5.8	100.0
ZR65	8.8	83.5	0.3	0.885	0.012	0.1053	0.0012	0.8	638.5	28.4	645.5	7.0	643.9	6.7	100.2
ZR3	45.6	423.9	0.4	0.893	0.011	0.1054	0.0012	0.9	654.2	23.1	646.0	7.0	647.8	5.7	99.7
ZR91	28.1	250.9	0.5	0.926	0.011	0.1065	0.0012	0.9	710.8	23.2	652.5	7.0	665.7	5.9	98.0
ZR95	42.6	422.0	0.1	0.925	0.011	0.1069	0.0012	0.9	701.1	22.7	654.6	7.0	665.1	5.8	98.4
ZR83	23.3	222.4	0.2	0.912	0.011	0.1070	0.0012	0.9	668.1	23.5	655.3	7.1	658.1	5.9	99.6
ZR26	28.7	260.7	0.4	0.910	0.011	0.1079	0.0012	0.9	644.0	23.3	660.7	7.1	656.9	5.8	100.6
ZR66	47.5	432.1	0.3	0.924	0.011	0.1085	0.0012	0.9	667.3	23.7	663.8	7.1	664.5	5.9	99.9
ZR89	21.6	201.8	0.2	0.910	0.011	0.1086	0.0012	0.9	630.8	23.7	664.5	7.1	656.8	5.9	101.2
ZR37	26.5	201.8	1.0	0.933	0.013	0.1096	0.0013	0.9	665.1	26.6	670.5	7.3	669.2	6.6	100.2
ZR40	7.3	63.9	0.4	0.945	0.013	0.1106	0.0013	0.8	674.6	27.6	676.0	7.4	675.6	6.9	100.1
ZR45	27.0	247.3	0.3	0.952	0.012	0.1106	0.0013	0.9	688.1	24.1	676.3	7.3	678.9	6.2	99.6
ZR61	12.2	116.6	0.1	0.961	0.012	0.1112	0.0013	0.9	696.0	24.9	679.9	7.3	683.6	6.3	99.5
ZR93	18.6	174.7	0.1	0.965	0.012	0.1121	0.0013	0.9	690.0	23.8	685.0	7.3	686.1	6.1	99.8
ZR99	14.2	112.5	0.7	0.976	0.013	0.1125	0.0013	0.9	705.4	25.4	687.3	7.4	691.5	6.5	99.4
ZR20	13.9	114.5	0.5	1.002	0.013	0.1127	0.0013	0.9	756.8	25.8	688.6	7.4	704.7	6.7	97.7
ZR10	15.6	132.4	0.5	0.963	0.012	0.1130	0.0013	0.9	667.4	24.9	689.9	7.4	684.6	6.3	100.8
ZR52	21.7	186.3	0.4	0.968	0.012	0.1132	0.0013	0.9	676.2	23.6	691.3	7.4	687.7	6.1	100.5
ZR12	27.5	240.9	0.3	0.985	0.012	0.1133	0.0013	0.9	710.0	23.8	691.8	7.4	696.0	6.2	99.4
ZR51	31.3	263.7	0.4	0.980	0.012	0.1134	0.0013	0.9	697.1	23.0	692.4	7.4	693.4	6.0	99.9
ZR70	16.8	133.8	0.7	0.992	0.013	0.1135	0.0013	0.9	721.4	24.7	693.0	7.5	699.7	6.4	99.0
ZR11	14.3	123.2	0.4	0.971	0.013	0.1141	0.0013	0.9	665.1	25.7	696.4	7.5	689.0	6.5	101.1
ZR98	63.4	554.4	0.3	0.994	0.012	0.1150	0.0013	0.9	697.4	22.8	701.6	7.5	700.5	6.0	100.2
ZR75	17.6	149.3	0.3	1.013	0.013	0.1157	0.0013	0.9	727.0	24.9	705.5	7.6	710.6	6.6	99.3
ZR78	4.9	39.7	0.4	1.035	0.016	0.1172	0.0014	0.8	744.4	30.1	714.4	7.8	721.6	7.8	99.0
ZR16	33.4	257.0	0.6	1.049	0.013	0.1183	0.0013	0.9	752.7	23.8	720.8	7.7	728.6	6.5	98.9
ZR96	107.9	842.6	0.5	1.114	0.013	0.1211	0.0014	1.0	828.3	22.0	737.0	7.8	759.9	6.3	97.0
ZR108	25.5	203.0	0.4	1.066	0.013	0.1214	0.0014	0.9	730.8	24.1	738.8	7.9	736.7	6.5	100.3
ZR24	57.4	481.9	0.2	1.207	0.014	0.1221	0.0014	1.0	976.9	21.6	742.9	7.9	803.8	6.6	92.4
ZR18	32.7	262.5	0.3	1.108	0.014	0.1223	0.0014	0.9	797.5	23.6	743.6	8.0	757.1	6.6	98.2
ZR72	11.4	94.2	0.2	1.073	0.014	0.1231	0.0014	0.9	716.1	25.8	748.3	8.0	740.3	6.9	101.1
ZR54	59.7	456.3	0.5	1.118	0.013	0.1232	0.0014	1.0	800.8	22.2	748.7	7.9	761.9	6.3	98.3
ZR113	14.6	113.9	0.4	1.089	0.014	0.1242	0.0014	0.9	729.0	24.5	754.4	8.0	748.0	6.6	100.9
ZR55	9.4	73.6	0.4	1.132	0.016	0.1245	0.0014	0.8	804.6	28.5	756.3	8.2	768.6	7.8	98.4
ZR9	26.5	205.9	0.4	1.115	0.014	0.1246	0.0014	0.9	771.9	23.4	757.1	8.1	760.8	6.6	99.5

ZR1	20.2	164.9	0.2	1.128	0.014	0.1249	0.0014	0.9	789.7	23.3	758.9	8.1	766.7	6.6	99.0
ZR25	43.3	318.0	0.6	1.107	0.013	0.1252	0.0014	1.0	746.7	22.5	760.3	8.1	756.8	6.3	100.5
ZR81	23.8	179.6	0.5	1.119	0.014	0.1255	0.0014	0.9	763.4	23.0	762.1	8.1	762.4	6.5	100.0
ZR14	10.7	81.1	0.4	1.117	0.015	0.1257	0.0014	0.9	755.9	25.8	763.3	8.2	761.4	7.1	100.2
ZR41	29.5	242.4	0.1	1.154	0.014	0.1271	0.0015	0.9	802.5	23.3	771.1	8.3	779.1	6.7	99.0
ZR22	27.9	187.4	0.9	1.153	0.014	0.1272	0.0014	0.9	799.5	24.0	771.8	8.3	778.9	6.8	99.1
ZR39	16.9	133.1	0.3	1.136	0.014	0.1276	0.0015	0.9	760.5	24.0	774.0	8.3	770.5	6.8	100.5
ZR85	18.2	134.4	0.5	1.153	0.014	0.1291	0.0015	0.9	767.7	23.5	782.5	8.3	778.6	6.7	100.5
ZR62	26.9	172.7	0.9	1.235	0.015	0.1327	0.0015	0.9	854.3	23.7	803.1	8.5	816.8	7.0	98.3
ZR4	23.6	171.0	0.4	1.218	0.015	0.1329	0.0015	0.9	822.3	23.3	804.3	8.6	809.0	6.9	99.4
ZR17	6.1	45.8	0.3	1.248	0.018	0.1329	0.0015	0.8	872.0	27.4	804.5	8.7	822.5	8.0	97.8
ZR30	45.0	289.9	0.7	1.320	0.016	0.1355	0.0015	0.9	947.0	21.8	819.3	8.7	854.5	6.9	95.9
ZR77	33.8	255.5	0.1	1.262	0.016	0.1378	0.0016	0.9	820.3	23.5	832.2	8.8	828.9	7.0	100.4
ZR73	18.5	119.3	0.7	1.322	0.017	0.1379	0.0016	0.9	914.3	24.0	833.0	8.9	855.4	7.4	97.4
ZR88	46.4	323.5	0.4	1.307	0.015	0.1398	0.0016	1.0	863.3	21.9	843.4	8.9	848.9	6.8	99.4
ZR104	31.4	184.2	1.0	1.307	0.016	0.1412	0.0016	0.9	842.1	23.3	851.6	9.0	848.9	7.0	100.3
ZR13	42.6	269.0	0.6	1.406	0.017	0.1450	0.0016	0.9	937.8	22.7	873.1	9.2	891.5	7.3	97.9
ZR60	47.4	324.7	0.2	1.433	0.017	0.1499	0.0017	1.0	909.0	21.8	900.5	9.5	902.9	7.0	99.7
ZR19	121.5	754.6	0.5	1.462	0.018	0.1509	0.0017	0.9	937.2	22.5	905.9	9.6	914.9	7.3	99.0
ZR57	62.2	390.4	0.4	1.470	0.017	0.1521	0.0017	1.0	931.4	21.6	912.9	9.6	918.2	7.1	99.4
ZR86	35.0	211.2	0.3	1.604	0.019	0.1630	0.0018	0.9	968.7	21.9	973.5	10.2	971.9	7.5	100.2
ZR43	40.7	250.9	0.2	1.695	0.021	0.1639	0.0019	0.9	1069.0	22.0	978.3	10.3	1006.6	7.8	97.2
ZR50	35.1	199.7	0.5	1.644	0.020	0.1672	0.0019	0.9	966.8	22.9	996.6	10.5	987.2	7.8	101.0
ZR100	37.1	193.3	1.2	1.541	0.019	0.1535	0.0017	0.9	1009.1	23.4	920.4	9.7	946.8	7.7	93.8
ZR94	60.4	358.8	0.5	1.536	0.018	0.1527	0.0017	1.0	1013.4	21.4	916.0	9.6	945.0	7.2	93.3
ZR105	26.4	108.7	0.5	2.619	0.032	0.2220	0.0025	0.9	1328.5	21.6	1292.3	13.2	1305.9	9.0	98.3
ZR21	103.7	260.2	1.0	4.949	0.057	0.3251	0.0037	1.0	1806.4	18.7	1814.5	17.9	1810.6	9.8	100.2
ZR74	362.1	881.9	0.3	7.652	0.091	0.3774	0.0043	0.9	2312.1	18.4	2064.1	19.9	2191.0	10.7	94.8
ZR27	77.7	120.7	1.0	12.728	0.148	0.5037	0.0057	1.0	2683.0	17.2	2629.5	24.4	2659.7	10.9	99.1

				ISOTOPIC RATIOS					AGES						
MN2	Pb ppm	U ppm	Th/U	207/235	err (1σ)	206/238	err (1σ)	rho	207/206	err (1σ)	206/238	err (1σ)	207/235	err (1σ)	conc
ZR58	17.1	277.8	0.1	0.540	0.007	0.0649	0.0008	1.2	619.2	26.3	405.2	4.5	438.7	4.7	92.4
ZR21	30.6	427.4	0.1	0.619	0.008	0.0766	0.0009	1.1	553.7	24.5	475.7	5.4	489.3	4.9	97.2
ZR16	14.7	161.4	0.7	0.714	0.009	0.0798	0.0009	1.2	773.0	24.9	494.7	5.6	547.3	5.6	90.4
ZR45	22.7	292.3	0.1	0.710	0.009	0.0803	0.0009	1.1	746.0	24.0	498.1	5.5	544.9	5.3	91.4
ZR36	13.4	153.9	0.5	0.715	0.009	0.0806	0.0009	1.2	750.8	25.0	500.0	5.5	547.5	5.4	91.3
ZR25	50.6	570.4	0.6	0.693	0.009	0.0830	0.0010	1.1	621.7	24.1	514.1	5.8	534.3	5.3	96.2
ZR35	25.0	313.2	0.1	0.678	0.008	0.0835	0.0009	1.2	560.8	24.8	517.2	5.6	525.3	5.1	98.5
ZR19	24.2	296.1	0.1	0.714	0.009	0.0865	0.0010	1.2	598.3	24.7	534.8	6.0	546.9	5.4	97.8
ZR1	44.8	555.1	0.0	0.698	0.008	0.0865	0.0010	1.1	549.5	23.1	535.0	5.9	537.7	5.0	99.5
ZR41	25.5	295.3	0.3	0.725	0.009	0.0866	0.0010	1.1	628.6	24.4	535.3	5.8	553.4	5.3	96.7
ZR57	23.7	245.9	0.7	0.736	0.010	0.0866	0.0010	1.2	661.3	25.4	535.6	5.9	560.1	5.6	95.6
ZR42	22.3	272.1	0.1	0.701	0.009	0.0873	0.0010	1.2	537.5	26.4	539.7	5.9	539.3	5.4	100.1
ZR32	18.4	217.0	0.1	0.725	0.009	0.0873	0.0010	1.1	612.5	24.7	539.8	5.9	553.9	5.3	97.5
ZR24	17.5	208.8	0.2	0.708	0.010	0.0876	0.0010	1.2	555.1	26.2	541.1	6.1	543.8	5.7	99.5
ZR33	20.9	244.2	0.2	0.698	0.009	0.0877	0.0010	1.2	520.4	26.1	541.8	5.9	537.7	5.4	100.8
ZR49	32.7	399.8	0.1	0.710	0.009	0.0877	0.0010	1.1	556.1	24.7	541.9	5.9	544.6	5.3	99.5
ZR9	21.3	250.2	0.2	0.692	0.009	0.0877	0.0010	1.2	498.5	25.6	542.0	6.1	533.8	5.3	101.5
ZR22	16.7	198.3	0.2	0.696	0.009	0.0877	0.0010	1.2	512.4	25.8	542.0	6.1	536.4	5.5	101.0
ZR34	14.9	177.0	0.1	0.698	0.010	0.0877	0.0010	1.4	518.0	30.7	542.0	6.0	537.4	6.2	100.9
ZR44	34.0	403.7	0.2	0.709	0.009	0.0878	0.0010	1.1	551.6	24.6	542.3	5.9	544.0	5.2	99.7
ZR3	22.7	272.8	0.1	0.708	0.009	0.0878	0.0010	1.1	547.6	24.1	542.5	6.0	543.4	5.2	99.8
ZR18	19.4	233.5	0.1	0.710	0.009	0.0878	0.0010	1.2	553.1	25.0	542.6	6.1	544.5	5.4	99.7
ZR28	24.0	255.8	0.6	0.718	0.010	0.0879	0.0010	1.2	577.5	25.9	542.8	6.1	549.5	5.7	98.8
ZR13	23.7	286.3	0.1	0.702	0.009	0.0879	0.0010	1.1	526.0	24.8	543.1	6.1	539.8	5.3	100.6
ZR37	23.8	246.4	0.6	0.706	0.010	0.0879	0.0010	1.4	539.4	30.8	543.2	6.0	542.5	6.2	100.1
ZR55	14.6	166.5	0.3	0.713	0.010	0.0879	0.0010	1.3	560.9	27.1	543.2	6.0	546.6	5.7	99.4
ZR38	40.7	494.3	0.1	0.704	0.009	0.0881	0.0010	1.1	529.3	24.3	544.2	5.9	541.4	5.1	100.5
ZR20	15.4	174.3	0.3	0.713	0.010	0.0881	0.0010	1.2	556.7	26.1	544.2	6.1	546.5	5.7	99.6
ZR56	55.1	602.2	0.4	0.720	0.009	0.0881	0.0010	1.2	577.4	25.9	544.3	6.0	550.7	5.6	98.8
ZR52	28.0	324.9	0.2	0.712	0.009	0.0881	0.0010	1.2	552.3	25.3	544.5	6.0	545.9	5.4	99.7
ZR54	27.8	269.1	0.9	0.710	0.009	0.0882	0.0010	1.2	544.4	25.6	544.8	6.0	544.7	5.4	100.0
ZR43	32.0	375.9	0.2	0.715	0.009	0.0882	0.0010	1.1	559.1	24.2	544.9	5.9	547.6	5.2	99.5
ZR48	21.1	253.6	0.1	0.717	0.009	0.0882	0.0010	1.2	564.2	26.1	545.1	6.0	548.7	5.5	99.3
ZR31	22.8	268.1	0.1	0.728	0.009	0.0883	0.0010	1.1	597.7	24.5	545.5	5.9	555.6	5.3	98.2
ZR59	42.4	518.6	0.0	0.748	0.010	0.0886	0.0010	1.2	648.5	25.5	546.9	6.0	567.0	5.7	96.5
ZR53	31.4	357.3	0.1	0.788	0.010	0.0936	0.0011	1.2	642.5	24.7	576.9	6.3	590.3	5.7	97.7
ZR7	34.1	364.3	0.2	0.771	0.009	0.0936	0.0011	1.1	594.1	23.5	577.0	6.4	580.4	5.4	99.4
ZR46	17.5	199.4	0.1	0.751	0.010	0.0937	0.0011	1.2	536.0	26.0	577.2	6.3	569.0	5.6	101.4

ZR8	16.4	161.8	0.6	0.762	0.010	0.0937	0.0011	1.2	567.1	25.7	577.6	6.4	575.4	5.7	100.4
ZR14	18.4	203.2	0.2	0.753	0.010	0.0938	0.0011	1.2	536.8	25.5	578.2	6.5	569.9	5.6	101.5
ZR29	19.2	214.7	0.1	0.768	0.010	0.0944	0.0011	1.2	569.6	25.5	581.3	6.6	578.9	5.9	100.4
ZR26	31.2	341.1	0.2	0.785	0.010	0.0944	0.0011	1.2	615.6	25.1	581.4	6.5	588.4	5.9	98.8
ZR2	50.3	533.8	0.2	0.778	0.009	0.0947	0.0011	1.1	590.5	22.9	583.2	6.5	584.6	5.3	99.8
ZR10	42.0	463.4	0.1	0.776	0.010	0.0952	0.0011	1.1	572.7	23.6	586.2	6.5	583.4	5.5	100.5
ZR27	40.4	407.6	0.3	0.809	0.010	0.0977	0.0012	1.1	605.9	24.5	600.8	6.7	601.8	5.8	99.8
ZR5	100.5	990.3	0.1	0.923	0.011	0.1064	0.0012	1.0	706.4	22.1	651.6	7.2	663.9	5.8	98.1
ZR30	31.1	275.9	0.3	0.925	0.011	0.1081	0.0012	1.1	676.4	23.9	661.8	7.1	665.0	6.0	99.5
ZR39	38.1	348.7	0.3	0.932	0.011	0.1082	0.0012	1.1	691.2	23.4	662.3	7.1	668.8	5.9	99.0
ZR11	35.3	322.4	0.1	0.980	0.012	0.1122	0.0013	1.1	720.5	23.5	685.8	7.6	693.9	6.3	98.8
ZR50	32.1	284.4	0.2	0.999	0.013	0.1155	0.0013	1.1	700.1	24.4	704.7	7.6	703.5	6.4	100.2

				ISOTOPIC RATIOS					AGES						
MN3	Pb ppm	U ppm	Th/U	207/235	err (1σ)	206/238	err (1σ)	rho	207/206	err (1σ)	206/238	err (1σ)	207/235	err (1σ)	conc
ZR46	51.0	653.6	0.07	0.682	0.008	0.0831	0.001	0.9	585.8	23.5	514.6	5.6	527.9	5.0	97.5
ZR14	45.8	585.2	0.05	0.679	0.008	0.0835	0.001	0.9	567.1	24.4	516.8	5.6	526.1	5.1	98.2
ZR28	45.0	577.7	0.05	0.677	0.008	0.0837	0.001	0.9	557.2	24.1	517.9	5.7	525.2	5.0	98.6
ZR9	22.5	282.6	0.09	0.673	0.008	0.0843	0.001	0.9	523.5	25.1	522.0	5.7	522.3	5.1	99.9
ZR49	12.9	161.7	0.11	0.687	0.009	0.0846	0.001	0.9	564.6	25.2	523.3	5.7	531.0	5.2	98.5
ZR12	23.9	298.7	0.09	0.684	0.009	0.0847	0.001	0.9	551.3	25.5	523.9	5.7	529.0	5.3	99.0
ZR41	35.3	441.3	0.07	0.696	0.009	0.0852	0.001	0.9	575.6	24.2	527.0	5.7	536.1	5.1	98.3
ZR10	17.9	213.9	0.22	0.684	0.009	0.0854	0.001	0.9	535.3	25.9	528.0	5.7	529.5	5.2	99.7
ZR44	32.5	403.4	0.07	0.709	0.009	0.0854	0.001	0.9	610.8	24.1	528.5	5.8	544.2	5.2	97.1
ZR40	41.5	517.2	0.07	0.713	0.009	0.0855	0.001	0.9	621.8	23.6	528.7	5.8	546.5	5.1	96.7
ZR48	20.9	258.1	0.10	0.697	0.009	0.0857	0.001	0.9	566.4	24.4	530.1	5.8	536.9	5.2	98.7
ZR53	15.7	188.4	0.21	0.695	0.009	0.0857	0.001	0.9	559.9	24.8	530.1	5.8	535.7	5.2	99.0
ZR32	17.4	215.1	0.09	0.706	0.009	0.0858	0.001	0.9	593.4	24.7	530.4	5.8	542.4	5.3	97.8
ZR47	25.7	319.7	0.08	0.695	0.008	0.0858	0.001	0.9	560.0	23.9	530.4	5.8	536.0	5.1	99.0
ZR4	15.0	180.3	0.15	0.710	0.009	0.0858	0.001	0.9	604.6	25.0	530.7	5.7	544.8	5.3	97.4
ZR55	38.3	476.8	0.06	0.697	0.008	0.0861	0.001	0.9	557.2	23.8	532.4	5.8	537.0	5.1	99.1
ZR52	12.9	147.4	0.38	0.706	0.009	0.0861	0.001	0.9	585.6	25.5	532.5	5.8	542.6	5.4	98.1
ZR50	25.7	315.8	0.08	0.722	0.009	0.0863	0.001	0.9	627.6	23.5	533.6	5.8	551.7	5.2	96.7
ZR3	15.8	190.6	0.12	0.699	0.009	0.0866	0.001	0.9	550.3	25.3	535.6	5.8	538.4	5.3	99.5
ZR7	29.2	351.2	0.13	0.711	0.009	0.0867	0.001	0.9	585.0	24.0	536.1	5.8	545.5	5.1	98.3
ZR42	18.1	219.8	0.09	0.720	0.009	0.0868	0.001	0.9	609.6	25.3	536.3	5.9	550.4	5.4	97.4
ZR5	14.3	173.4	0.11	0.698	0.009	0.0868	0.001	0.9	543.3	25.1	536.4	5.8	537.7	5.2	99.8
ZR2	23.1	283.4	0.06	0.703	0.008	0.0868	0.001	0.9	557.6	23.9	536.5	5.8	540.5	5.1	99.3
ZR29	16.0	193.6	0.12	0.700	0.009	0.0868	0.001	0.9	549.8	24.8	536.5	5.9	538.9	5.2	99.6
ZR31	20.8	250.4	0.14	0.708	0.009	0.0868	0.001	0.9	571.6	24.6	536.8	5.9	543.4	5.2	98.8
ZR18	18.6	225.9	0.12	0.709	0.009	0.0869	0.001	0.9	571.8	23.5	537.3	5.9	543.9	5.2	98.8
ZR37	14.8	176.6	0.15	0.715	0.011	0.0869	0.001	0.8	589.8	30.4	537.4	6.0	547.4	6.3	98.2
ZR6	19.0	226.8	0.16	0.700	0.009	0.0870	0.001	0.9	544.1	24.6	537.6	5.8	538.8	5.2	99.8
ZR43	19.4	235.2	0.10	0.708	0.009	0.0870	0.001	0.9	567.3	25.6	537.7	5.9	543.3	5.3	99.0
ZR33	58.2	717.7	0.05	0.702	0.008	0.0870	0.001	0.9	549.3	23.8	537.8	5.9	540.0	5.1	99.6
ZR39	15.9	187.5	0.20	0.697	0.009	0.0872	0.001	0.9	528.0	26.0	538.8	5.9	536.7	5.3	100.4
ZR22	21.6	261.9	0.11	0.702	0.009	0.0872	0.001	0.9	544.9	24.3	539.1	5.9	540.2	5.2	99.8
ZR35	12.7	144.2	0.33	0.699	0.009	0.0873	0.001	0.9	531.9	26.3	539.7	5.9	538.2	5.4	100.3
ZR11	13.4	163.4	0.07	0.697	0.009	0.0874	0.001	0.9	523.5	26.3	540.3	5.9	537.1	5.4	100.6
ZR17	21.3	261.1	0.07	0.702	0.009	0.0874	0.001	0.9	537.3	24.5	540.3	5.9	539.8	5.1	100.1
ZR26	19.6	235.5	0.12	0.717	0.009	0.0874	0.001	0.9	585.5	24.2	540.4	5.9	549.1	5.2	98.4
ZR25	17.3	206.8	0.14	0.701	0.009	0.0877	0.001	0.9	528.2	26.0	541.8	5.9	539.2	5.4	100.5
ZR13	18.7	223.9	0.12	0.699	0.009	0.0877	0.001	0.9	522.7	25.7	541.9	5.9	538.2	5.3	100.7

ZR24	13.9	164.3	0.18	0.711	0.009	0.0877	0.001	0.9	560.1	24.9	542.1	5.9	545.5	5.3	99.4
ZR38	23.5	282.4	0.09	0.720	0.009	0.0880	0.001	0.9	578.7	24.4	543.7	5.9	550.5	5.3	98.8
ZR51	33.0	401.0	0.07	0.712	0.009	0.0880	0.001	0.9	556.3	23.4	543.7	5.9	546.1	5.0	99.6
ZR21	24.9	301.2	0.07	0.732	0.009	0.0881	0.001	0.9	612.9	23.4	544.4	5.9	557.7	5.2	97.6
ZR30	10.4	124.5	0.09	0.729	0.009	0.0882	0.001	0.9	602.7	25.5	545.0	6.0	556.2	5.5	98.0
ZR3	17.1	201.9	0.13	0.712	0.009	0.0886	0.001	0.9	541.4	25.3	547.1	5.9	546.0	5.2	100.2
ZR15	6.9	77.8	0.29	0.706	0.010	0.0889	0.001	0.8	514.7	29.7	549.1	6.0	542.5	6.0	101.2
ZR27	13.2	150.8	0.14	0.751	0.010	0.0917	0.001	0.9	581.7	25.4	565.6	6.2	568.7	5.6	99.5
ZR20	10.9	115.4	0.30	0.789	0.010	0.0947	0.001	0.9	618.9	25.4	583.1	6.4	590.5	5.8	98.7
ZR1	43.9	121.8	0.62	4.950	0.058	0.3196	0.004	1.0	1837.7	19.1	1787.7	17.5	1810.8	9.9	98.5

				ISOTOPIC RATIOS					AGES						
MN4	Pb ppm	U ppm	Th/U	207/235	err (1σ)	206/238	err (1σ)	rho	207/206	err (1σ)	206/238	err (1σ)	207/235	err (1σ)	conc
ZR1	21.6	194.5	0.27	0.947	0.012	0.1107	0.001	0.9	677.4	25.9	676.7	7.3	676.8	6.5	100.1
ZR56	20.8	215.2	0.48	0.747	0.009	0.0910	0.001	0.9	587.8	24.4	561.2	6.1	566.4	5.4	104.7
ZR54	69.1	606.5	1.12	0.778	0.009	0.0923	0.001	1.0	646.4	22.8	568.8	6.1	584.5	5.2	113.6
ZR87	35.7	377.2	0.36	0.798	0.010	0.0924	0.001	0.9	695.8	23.7	569.7	6.1	595.6	5.5	122.1
ZR23	96.6	943.8	0.62	0.773	0.009	0.0929	0.001	0.9	617.3	23.2	572.3	6.1	581.4	5.2	107.9
ZR15	14.1	144.2	0.47	0.769	0.010	0.0930	0.001	0.9	602.8	25.6	573.4	6.2	579.3	5.6	105.1
ZR95	101.2	882.0	1.05	0.790	0.009	0.0936	0.001	0.9	648.2	22.9	576.7	6.3	591.4	5.4	97.5
ZR63	24.6	220.1	0.91	0.791	0.010	0.0942	0.001	0.9	635.7	25.0	580.4	6.3	591.7	5.7	98.1
ZR108	12.4	110.1	1.01	0.786	0.011	0.0945	0.001	0.8	615.7	27.9	582.3	6.5	589.1	6.3	98.8
ZR109	31.3	285.2	0.89	0.794	0.010	0.0952	0.001	0.9	621.3	25.1	586.0	6.5	593.2	5.8	98.8
ZR93	10.4	100.9	0.58	0.803	0.011	0.0956	0.001	0.9	636.9	26.6	588.3	6.4	598.4	6.1	98.3
ZR30	55.2	449.3	1.19	0.900	0.011	0.0962	0.001	0.9	865.7	23.5	592.0	6.3	652.0	5.9	90.8
ZR60	17.4	155.1	0.82	0.809	0.011	0.0966	0.001	0.9	630.4	25.8	594.5	6.4	602.0	5.9	98.8
ZR69	22.9	234.7	0.29	0.808	0.010	0.0970	0.001	0.9	617.8	24.5	596.9	6.5	601.2	5.7	99.3
ZR85	22.9	217.8	0.52	0.822	0.010	0.0972	0.001	0.9	653.6	24.0	597.7	6.4	609.4	5.6	98.1
ZR24	53.6	523.2	0.47	0.804	0.010	0.0972	0.001	0.9	602.4	23.9	598.2	6.4	599.1	5.5	99.8
ZR8	6.0	50.0	1.08	0.804	0.012	0.0980	0.001	0.8	586.9	30.8	602.5	6.5	599.2	6.8	100.6
ZR68	11.0	107.9	0.42	0.832	0.011	0.0983	0.001	0.9	654.1	26.3	604.2	6.6	614.7	6.1	98.3
ZR53	42.4	386.0	0.65	0.822	0.010	0.0987	0.001	0.9	616.5	23.2	607.0	6.5	608.9	5.4	99.7
ZR77	37.3	386.9	0.22	0.828	0.010	0.0988	0.001	0.9	633.2	24.8	607.1	6.6	612.6	5.8	99.1
ZR62	19.0	157.4	1.04	0.830	0.010	0.0988	0.001	0.9	634.9	24.8	607.6	6.6	613.4	5.8	99.1
ZR81	51.3	399.2	1.32	0.836	0.011	0.0990	0.001	0.9	647.5	24.6	608.6	6.6	616.9	5.8	98.7
ZR4	8.1	73.2	0.65	0.845	0.012	0.0997	0.001	0.8	657.3	27.7	612.6	6.6	622.2	6.4	98.5
ZR76	21.7	208.4	0.43	0.842	0.011	0.0999	0.001	0.9	645.2	25.2	613.7	6.7	620.4	6.0	98.9
ZR13	12.3	117.4	0.42	0.867	0.011	0.0999	0.001	0.9	706.2	25.5	614.0	6.6	634.0	6.1	96.8
ZR19	33.9	331.6	0.36	0.830	0.010	0.1002	0.001	0.9	605.4	23.8	615.6	6.6	613.4	5.6	100.4
ZR41	50.5	537.4	0.43	0.830	0.010	0.1007	0.001	0.9	597.0	23.2	618.3	6.7	613.7	5.5	100.7
ZR44	6.4	68.2	0.58	0.833	0.012	0.1007	0.001	0.8	603.5	28.6	618.5	6.8	615.2	6.5	100.5
ZR25	14.8	147.2	0.30	0.854	0.011	0.1007	0.001	0.9	656.6	25.5	618.7	6.6	626.8	6.0	98.7
ZR110	74.7	776.9	0.22	0.865	0.011	0.1007	0.001	0.9	683.6	23.9	618.7	6.8	632.8	5.9	97.8
ZR72	11.8	114.2	0.37	0.847	0.011	0.1010	0.001	0.9	633.9	26.3	620.0	6.8	623.0	6.2	99.5
ZR75	34.7	314.1	0.58	0.859	0.011	0.1012	0.001	0.9	660.1	24.4	621.4	6.7	629.8	5.9	98.7
ZR49	30.4	318.9	0.49	0.855	0.011	0.1016	0.001	0.9	641.3	24.5	623.7	6.7	627.5	5.8	99.4
ZR46	23.9	247.2	1.02	0.871	0.011	0.1029	0.001	0.9	652.5	24.5	631.4	6.8	636.0	5.9	99.3
ZR26	34.7	256.5	1.25	0.952	0.012	0.1053	0.001	0.9	792.5	23.8	645.5	6.9	679.1	6.1	95.1
ZR90	27.7	254.5	0.35	0.920	0.011	0.1061	0.001	0.9	705.2	23.4	649.8	7.0	662.3	5.9	98.1
ZR6	14.6	135.1	0.33	0.893	0.011	0.1063	0.001	0.9	636.3	25.0	651.3	6.9	647.9	6.0	100.5
ZR39	35.1	352.6	0.53	0.882	0.011	0.1066	0.001	0.9	604.3	23.4	653.1	7.0	642.2	5.7	101.7

ZR16	45.0	414.6	0.33	0.940	0.011	0.1067	0.001	0.9	739.4	22.9	653.4	6.9	673.0	5.8	97.1
ZR21	27.7	241.4	0.54	0.909	0.011	0.1067	0.001	0.9	667.4	24.0	653.4	7.0	656.5	5.9	99.5
ZR32	13.5	109.0	0.81	0.947	0.013	0.1067	0.001	0.8	752.6	26.4	653.7	7.0	676.3	6.6	96.7
ZR47	16.8	166.2	0.77	0.994	0.013	0.1072	0.001	0.9	845.4	24.3	656.5	7.1	700.7	6.4	93.7
ZR112	40.6	374.2	0.29	0.951	0.012	0.1099	0.001	0.9	700.6	24.4	672.0	7.4	678.6	6.4	99.0
ZR11	23.3	186.0	0.74	0.952	0.012	0.1101	0.001	0.9	698.8	23.8	673.2	7.2	679.1	6.0	99.1
ZR103	30.1	239.1	0.84	0.972	0.012	0.1101	0.001	0.9	742.4	24.3	673.4	7.4	689.5	6.4	97.7
ZR52	17.8	171.6	0.63	0.938	0.012	0.1106	0.001	0.9	656.8	25.6	676.1	7.3	671.6	6.4	100.7
ZR34	23.2	224.4	0.48	0.940	0.011	0.1107	0.001	0.9	658.2	23.6	677.0	7.3	672.6	6.0	100.7
ZR86	15.9	94.3	2.04	0.969	0.013	0.1109	0.001	0.9	719.1	25.5	678.2	7.3	687.7	6.5	98.6
ZR78	60.6	532.5	0.35	0.977	0.012	0.1118	0.001	0.9	721.6	23.8	683.2	7.4	692.1	6.2	98.7
ZR111	78.5	711.9	0.52	0.993	0.013	0.1119	0.001	0.9	753.4	23.7	684.0	7.5	700.3	6.4	97.7
ZR57	41.0	331.8	0.58	0.979	0.012	0.1124	0.001	0.9	716.0	22.9	686.4	7.3	693.3	6.0	99.0
ZR59	58.4	398.6	1.32	0.997	0.012	0.1130	0.001	0.9	740.3	23.5	690.4	7.4	702.2	6.2	98.3
ZR82	30.0	255.1	0.39	0.998	0.013	0.1139	0.001	0.9	726.7	24.8	695.2	7.5	702.6	6.5	98.9
ZR7	65.4	510.7	0.69	0.992	0.011	0.1146	0.001	1.0	701.3	22.4	699.1	7.4	699.5	5.9	99.9
ZR88	19.0	147.8	0.66	1.016	0.013	0.1146	0.001	0.9	752.6	24.0	699.4	7.5	712.1	6.4	98.2
ZR18	27.1	214.9	0.61	0.995	0.012	0.1146	0.001	0.9	707.0	23.7	699.6	7.4	701.3	6.2	99.8
ZR61	134.2	1173.4	0.26	1.009	0.013	0.1148	0.001	0.9	734.8	24.2	700.3	7.5	708.5	6.4	98.8
ZR40	18.2	169.4	0.70	0.989	0.012	0.1148	0.001	0.9	691.7	24.2	700.4	7.5	698.2	6.3	100.3
ZR89	10.2	77.1	0.75	1.033	0.014	0.1150	0.001	0.9	779.7	26.0	701.8	7.6	720.5	6.9	97.4
ZR27	7.9	65.3	0.37	1.076	0.015	0.1158	0.001	0.8	850.0	27.4	706.4	7.6	741.7	7.4	95.2
ZR79	30.4	244.8	0.47	1.045	0.013	0.1182	0.001	0.9	746.2	24.4	720.3	7.8	726.6	6.6	99.1
ZR97	40.3	306.4	0.60	1.071	0.013	0.1198	0.001	0.9	769.6	23.2	729.5	7.9	739.3	6.4	98.7
ZR31	15.1	128.8	0.20	1.070	0.014	0.1198	0.001	0.9	767.1	25.7	729.6	7.8	738.8	6.9	98.8
ZR17	33.0	265.3	0.38	1.055	0.013	0.1206	0.001	0.9	722.4	23.4	734.0	7.8	731.1	6.3	100.4
ZR12	18.9	138.4	0.71	1.063	0.013	0.1211	0.001	0.9	730.2	24.2	736.8	7.8	735.1	6.5	100.2
ZR37	9.3	81.6	0.32	1.064	0.014	0.1212	0.001	0.9	732.2	25.7	737.2	8.0	735.9	6.9	100.2
ZR20	29.2	236.3	0.35	1.068	0.013	0.1212	0.001	0.9	739.1	23.9	737.4	7.8	737.8	6.4	99.9
ZR9	24.9	189.0	0.56	1.067	0.013	0.1213	0.001	0.9	735.5	23.4	738.2	7.8	737.5	6.3	100.1
ZR10	34.9	247.9	0.82	1.067	0.013	0.1216	0.001	0.9	729.3	23.0	739.6	7.8	737.0	6.2	100.4
ZR55	5.2	36.9	0.67	1.159	0.017	0.1217	0.001	0.8	901.1	29.5	740.5	8.1	781.6	8.2	94.7
ZR100	32.6	221.0	0.99	1.140	0.014	0.1231	0.001	0.9	843.2	23.3	748.4	8.1	772.5	6.7	96.9
ZR38	16.3	141.5	0.25	1.088	0.014	0.1234	0.001	0.9	740.0	24.0	749.9	8.1	747.3	6.6	100.3
ZR101	75.9	510.1	1.02	1.152	0.014	0.1244	0.001	0.9	842.6	22.6	756.0	8.2	778.2	6.6	97.1
ZR91	4.6	33.9	0.48	1.176	0.018	0.1252	0.001	0.8	872.7	29.5	760.4	8.3	789.4	8.3	96.3
ZR98	131.9	1006.1	0.38	1.197	0.014	0.1268	0.001	1.0	884.6	22.0	769.3	8.3	799.4	6.6	96.2
ZR66	8.3	65.1	0.27	1.155	0.016	0.1273	0.001	0.8	799.4	26.3	772.5	8.3	779.4	7.4	99.1
ZR71	10.5	75.2	0.50	1.207	0.016	0.1307	0.001	0.9	837.4	25.8	792.1	8.5	804.0	7.4	98.5
ZR43	39.0	313.2	0.40	1.202	0.015	0.1325	0.002	0.9	799.6	23.0	802.2	8.5	801.4	6.7	100.1
ZR70	18.7	134.9	0.40	1.241	0.016	0.1330	0.002	0.9	858.7	23.9	804.9	8.6	819.3	7.1	98.2
ZR5	48.2	332.2	0.47	1.254	0.015	0.1375	0.002	1.0	811.5	22.1	830.3	8.7	825.1	6.6	100.6

ZR33	25.4	193.5	0.27	1.270	0.015	0.1404	0.002	0.9	793.1	22.8	847.0	9.0	832.2	6.9	101.8
ZR3	41.9	272.7	0.55	1.312	0.015	0.1412	0.002	0.9	850.2	22.3	851.6	8.9	851.1	6.8	100.1
ZR36	12.9	96.6	0.57	1.305	0.017	0.1416	0.002	0.9	833.6	24.0	853.6	9.1	848.0	7.3	100.7
ZR64	45.4	282.9	0.60	1.389	0.017	0.1469	0.002	0.9	885.8	22.5	883.6	9.3	884.2	7.1	99.9
ZR14	65.1	406.8	0.50	1.437	0.017	0.1494	0.002	1.0	922.3	21.8	897.4	9.4	904.5	7.0	99.2
ZR67	60.8	411.1	0.21	1.434	0.017	0.1496	0.002	0.9	914.7	22.2	898.9	9.5	903.4	7.2	99.5
ZR104	43.4	280.3	0.40	1.460	0.018	0.1506	0.002	0.9	938.0	22.9	904.1	9.7	913.9	7.5	98.9
ZR80	80.3	488.6	0.47	1.531	0.019	0.1554	0.002	0.9	971.5	22.8	930.9	9.9	943.0	7.6	98.7
ZR28	17.5	106.1	0.33	1.611	0.020	0.1625	0.002	0.9	983.8	23.9	970.5	10.1	974.5	8.0	99.6
ZR50	32.5	205.3	0.50	1.631	0.020	0.1673	0.002	0.9	949.7	23.3	996.9	10.5	982.2	7.8	101.5
ZR48	32.6	202.6	1.19	1.705	0.021	0.1700	0.002	0.9	1006.7	22.8	1012.2	10.6	1010.4	7.9	100.4
ZR99	31.6	198.2	0.34	1.569	0.019	0.1555	0.002	0.9	1019.8	22.3	931.6	9.9	958.1	7.6	93.9
ZR106	14.6	84.6	0.22	1.792	0.025	0.1768	0.002	0.8	1027.4	25.3	1049.7	11.3	1042.4	8.9	101.5
ZR35	27.1	174.0	1.20	1.734	0.021	0.1647	0.002	0.9	1104.1	21.6	982.9	10.4	1021.1	7.7	92.5
ZR102	36.2	111.8	0.57	4.278	0.053	0.2953	0.003	0.9	1715.8	20.2	1667.9	16.9	1689.1	10.1	98.4
ZR29	60.8	157.5	0.92	4.812	0.058	0.3193	0.004	0.9	1787.8	20.2	1786.4	17.5	1786.9	10.2	99.9
ZR45	94.9	282.8	0.67	5.524	0.066	0.3400	0.004	0.9	1923.9	19.2	1886.7	18.5	1904.4	10.2	99.0
ZR96	199.5	521.2	0.49	6.039	0.071	0.3431	0.004	1.0	2066.4	18.5	1901.4	18.7	1981.4	10.3	95.9
ZR65	31.8	71.4	0.63	6.953	0.083	0.3871	0.004	0.9	2101.6	18.9	2109.5	20.4	2105.4	10.6	100.2
ZR107	99.2	214.9	0.91	6.962	0.086	0.3859	0.004	0.9	2109.8	19.2	2103.5	20.7	2106.6	11.0	99.8
ZR22	93.5	159.7	0.37	13.376	0.156	0.5223	0.006	1.0	2705.0	17.5	2708.9	24.7	2706.5	11.0	100.1
ZR92	65.0	113.5	0.44	13.019	0.152	0.4975	0.006	1.0	2740.6	17.2	2603.2	24.2	2681.1	11.0	97.8
ZR83	100.0	150.5	0.45	17.112	0.196	0.5593	0.006	1.0	2994.8	16.6	2863.6	25.9	2941.1	11.0	98.2
ZR74	239.6	307.1	0.57	22.175	0.266	0.6343	0.007	0.9	3207.3	17.1	3166.6	28.4	3191.4	11.7	99.5

5 Evolution de la provenance sédimentaire au cours du Cambrian-Ordovicien Inférieur le long de la marge occidentale péri-gondwanienne. [Article 4]

Cambrian–Lower Ordovician sedimentary provenance shifts in Northwest Gondwana

Maxime Padel[1*], Sébastien Clausen[1], Marc Poujol[2] and J. Javier Álvaro[3]

[1]UMR 8198 EEP CNRS, Université de Lille 1, Bâtiment SN5, Avenue Paul Langevin, 59655 Villeneuve d'Ascq Cedex, France, maxime.padel@etudiant.univ-lille1.fr and sebastien.clausen@univ-lille1.fr

[2]Géosciences Rennes, UMR 6118, Université de Rennes1, Campus de Beaulieu, 35042 Rennes, France, marc.poujol@univ-rennes1.fr

[3]Instituto de Geociencias (CSIC-UCM), Novais 12, 28040 Madrid, Spain, jj.alvaro@csic.es

** Corresponding author*

Abstract

Detrital zircons from Cambrian–Lower Ordovician sediments of Northwest Gondwana are studied herein in order to assess the influence, across space and time, of different craton sources. Age distribution curves from new data obtained through LA-ICPMS U–Pb zircon dating from Cambrian sandstones sampled in the Pyrenees are compared to other available data from Morocco, the Iberian Peninsula, South France and Sardinia. Kolmogorov–Smirnov (K–S) test and crystallization age (CA) - depositional age (CA-DA) diagrams are applied herein to compare the zircon source populations and assess their possible correlation with the arc/rift geodynamic evolution recorded throughout this margin of Gondwana. During the Terreneuvian, zircon population allows distinction of (i) a southwestermost edge (Atlas and Ossa-Morena Rifts) mostly influenced by Panafrican and Atlasian sources (ca. 0.63–0.54), (ii) a northeasternmost edge (Sardinia) recording the influence of the Saharan Metacraton and the Arabian Nubian Shield, with an important Stenian–Tonian cluster (ca 1.2–0.9 Ga), and (iii) an intermediate palaeogeographic transect, where lies the Central-Iberian Zone, the Montagne Noire and the Pyrenees, sharing parent populations and a progressive influence of both sources. According to this gradual modification of zircon population percentages, the Cambrian Pyrenean Basin should be located between the Montagne Noire (Occitan Domain) and Sardinia. This trend of zircon compositions gradually disappeared from Cambrian Epoch 2 to Early Ordovician times, reflecting a distinct geodynamic evolution in Northwest

Gondwana. The Atlas and Ossa-Morena Rifts show a rapid post-Panafrican/Cadomian shift to extensional conditions, with an arc/rift turnover across the Ediacaran-Cambrian transition. In this context, sediment supply of recently built Panafrican, Cadomian and Atlasian orogenic sources influenced the zircon age distribution curves of Terreneuvian deposits. During later Cambrian and Ordovician times, the relative influence of different cratons tended to balance, leading to a more spread age distribution curve, characteristic of extensional settings evolving from rift to drift (passive margin) conditions.

Keywords: orogeny, palaeogeography, Pyrenees, rift, zircon.

1. Introduction

U–Pb dating of detrital zircon has become one of the main methods for direct age-determination of craton sources and magmatic rocks. Although the analysis of reworked detrital zircons does not provide absolute ages of hosting material, a broad estimate of the maximum depositional age of strata is available. This method constitutes a powerful tool to (i) characterize continental, crustal growth episodes, (ii) decipher detrital sources, and (iii) constrain the palaeogeographic and geodynamic evolution of continental margins (Gehrels, 2014 and references therein).

During the two last decades, the analysis of zircon provenance has been regularly applied to identify the different sources of the Neoproterozoic–Lower Palaeozoic detrital successions from Northwest Gondwana in order to determine their palaeogeographic affinities and their proximity to orogens (e.g., Gutiérrez-Alonso et al., 2003; Drost et al., 2011; Meinhold et al., 2011, 2013; Avigad et al., 2012; Altumi et al., 2013; Pastor-Galán et al., 2013; Fernández-Suárez et al., 2014; Shaw et al., 2014; Margalef et al., 2015; Padel et al., in press [article 3]).

Among these orogenic events, the Neoproterozoic Panafrican (Anti-Atlas, 790–560 Ma), Cadomian (e.g., Armorican Massif, Ossa-Morena and Bohemian Massif, 850–550 Ma) and Avalonian (e.g., Newfoundland, New England and Nova Scotia Cape Breton, 730–570 Ma) events have received a particular attention as they record a major shift from an overall convergent setting to a new extensional setting which ended close to the Ediacaran–Cambrian boundary (590–540 Ma; Murphy et al., 1999; Ballèvre et al., 2001; Nance et al., 2002; Linnemann et al., 2007; Stampfi et al., 2013; Blein et al., 2014a and b).

In NW Gondwana (including the Moroccan Anti-Atlas, the Iberian Peninsula, south France and Sardinia), evidence of this arc/rift geodynamic turnover is preserved in relatively scattered exposures of the European Variscan Belt (Fig. 1). In southwestern Europe, the Variscan Ibero-Armorican Arc contains two branches: (i) a southwestern branch represented by the Iberian Massif, and (ii) a northeastern branch that includes the Armorican Massif, the South Armorican Domain (southwestern Britany and Vendée), the northern Massif Central, the Occitan Domain (Albigeois, Montagne Noire, Mouthoumet, and Cévennes part of the southern Massif Central) and its lateral prolongation into Corsica and Sardinia, and the Pyrenean Domain. A main difference between both branches is the onset of a Cadomian gap (commonly associated with angular discordance), recording the transition from convergence to rifting referred to above, and a Sardic gap in the latter (Casas and Fernández, 2007; Álvaro et al., 2015). Although the Pyrenees share strong Ediacaran–Cambrian stratigraphic similarities with the Cantabrian Zone, the Montagne Noire and SW Sardinia, its Cambrian palaeogeographic setting remains still uncertain (Laumonier et al., 1996, 2004; Ballèvre et al., 2009; Álvaro et al., 2014a; Pouclet et al., 2016). As a result, the palaeogeographic position of the Pyrenees is often questioned or even omitted in many Ediacaran–Early Palaeozoic palaeogeographic reconstructions of Gondwana (e.g., Murphy et al., 2004; Nance et al., 2008).

This study has been aimed at assessing the evolution, across space and time, of the influence of the different sediment sources across Cambrian–Early Ordovician times in NW Gondwana. It focuses on successions from Anti-Atlas (Morocco), the Ossa-Morena and Central-Iberian Zones (Spain), the Pyrenees (France/Spain border), the Montagne Noire (France) and Sardinia (Italy). We expect this comparison will illustrate the SW-NE variations in sediment sources along the northwestern Gondwana margin (Fig. 2). To fill the existing gap in zircon data from the Pyrenees, we present below the first study of detrital zircon from Cambrian sandstones from the Pyrenees. The obtained curves of age repartition of zircons, used as source-proxies of studied sediments, are then compared with previous analyses.

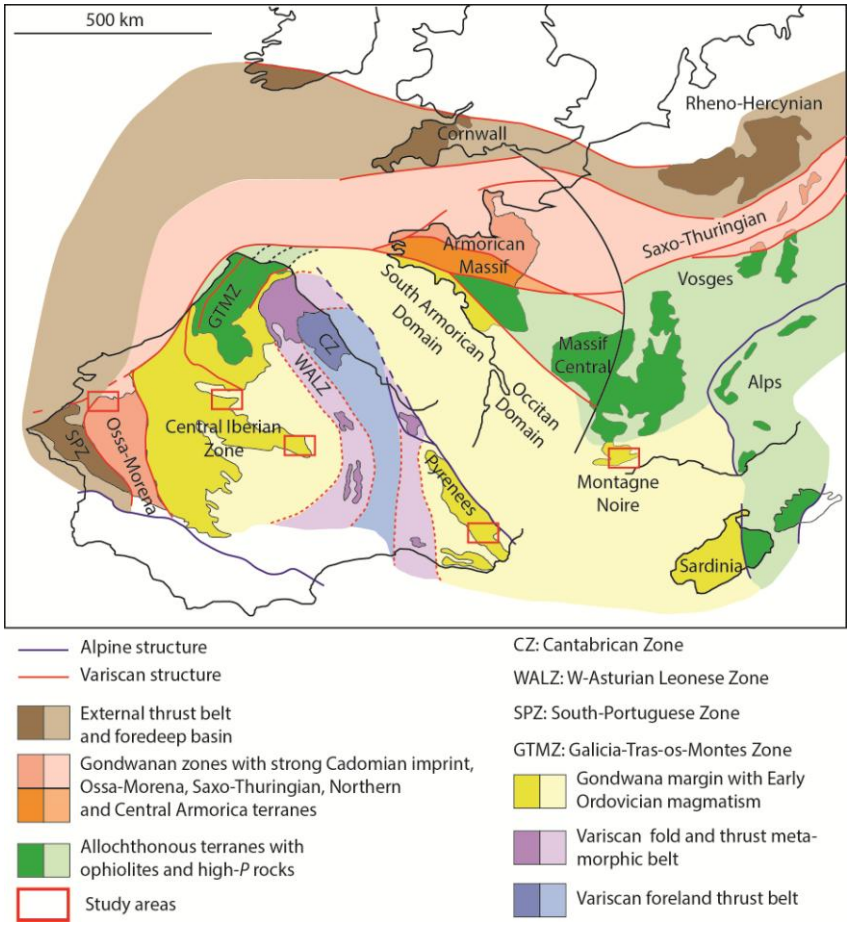

Fig. 1 : Geological sketch of the Variscan Belt in southwestern Europe with tectonostratigraphic domains including Cambrian–Ordovician exposures from peri-Gondwana; modified after Matte (1986), Ballèvre et al. (2009), Martínez-Catalán (2012) and Pouclet et al. (2016). Red squares represent the study areas.

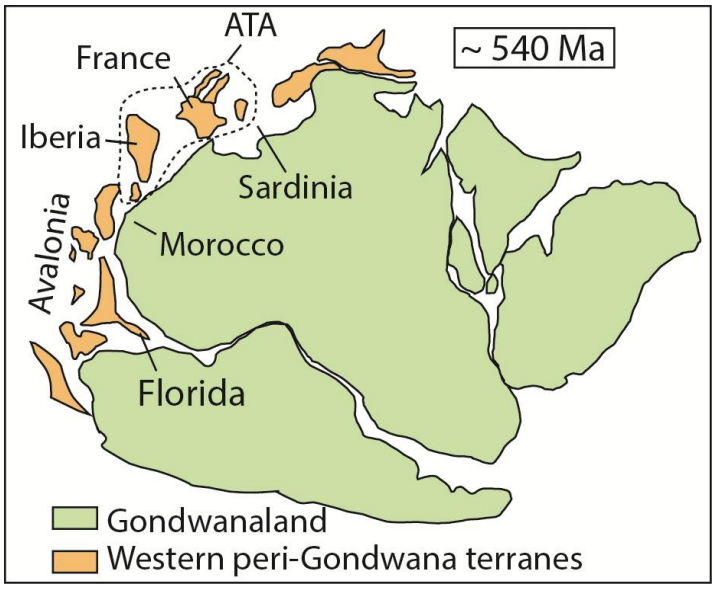

Fig. 2 : Palaeogeographic sketch of Northwestern Gondwana and setting of platforms and basins reported herein: France, Iberia, Sardinia and Morocco; modified after Torsvik and Cocks (2013); ATA: Amoricain Terrane Assemblage.

2. Geological setting and stratigraphy of the Pyrenees

The Pyrenean Belt formed as an intracontinental fold and thrust belt during Late Cretaceous to Early Neogene collision between the Iberian microplate and the southern edge of the European plate (Lagabriele et al., 2010). The belt is divided into three E-W morphostructural units (Barnolas et al., 1996) (Fig. 3B). The Axial Zone mostly consists of Ordovician and Variscan granitic intrusions (including distinct migmatised orthogneiss aureoles) emplaced in a thick Cambro–Ordovician sedimentary succession that was consequently affected by various metamorphic grades (Fig. 3C). The Axial Zone is bounded by the North- and South-Pyrenean Thrusts (Laumonier et al., 2015) (Fig. 3B), subsequently flanked by post–Variscan-dominated series.

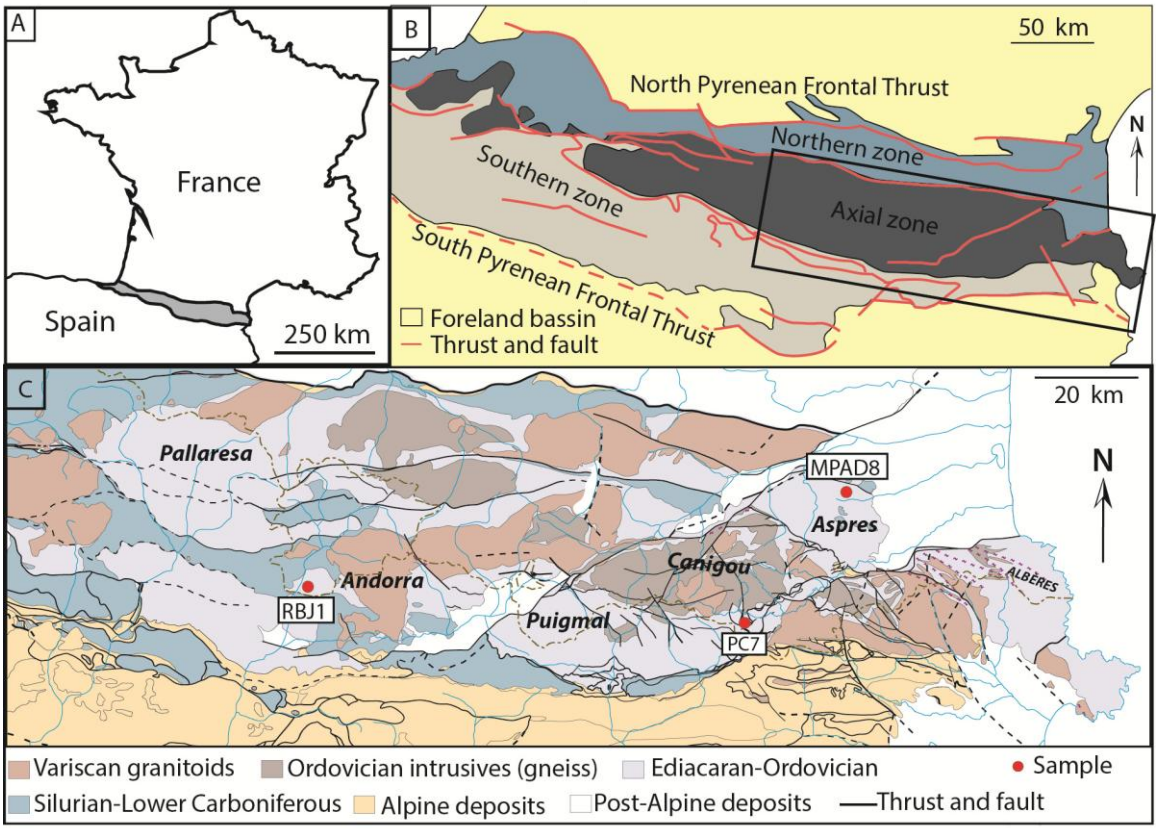

Fig. 3 : A. Location of the Pyrenees (in grey). B. Structural domains of the Pyrenees. C. Geological map of the eastern Pyrenees (squared in B) with setting of studied samples.

Pre–Variscan rocks mostly crop out in the central and eastern Axial Zone, from Pallaresa to the Mediterranean sea (Fig. 3C). There, the pre–Variscan succession is subdivided into the Canaveilles and Jujols groups (Laumonier et al., 1996, 2004; Fig. 4). The

Ediacaran Canaveilles Group, 2–3 km thick, is a monotonous shale-to-schist succession, locally punctuated by rhyolites, volcanosedimentary breccias, marbles and sandstones. The presence/absence of carbonate interbeds allows distinction between the (lower) Nyers and the (upper) Olette formations (Padel et al., in prep a [article 1]). The latter is capped, in the Puigmal tectonostratigraphic unit, by a volcanosedimentary complex up to 500 m in thickness, named Pic de la Clape Formation and composed, from bottom to top, of rhyolites (Fabert Member), acidic-dominated ignimbrites and volcanosedimentary breccias (Finestrelles Member) and massive-to-bedded limestones and marbles (Puig Sec Member; Padel et al., in prep a [article 1]). The overlying Cambrian–Lower Ordovician Jujols Group has an estimated thickness of 3–4 km and comprises, in ascending order, the schist-dominated Err Formation (~1500 m thick), the massive-to-bedded carbonate Valcebollère Formation (200 to 300 m thick), and the homogeneous schistose Serdinya Formation irregularly punctuated by fine-grained sandy interbeds (~2000 m thick).

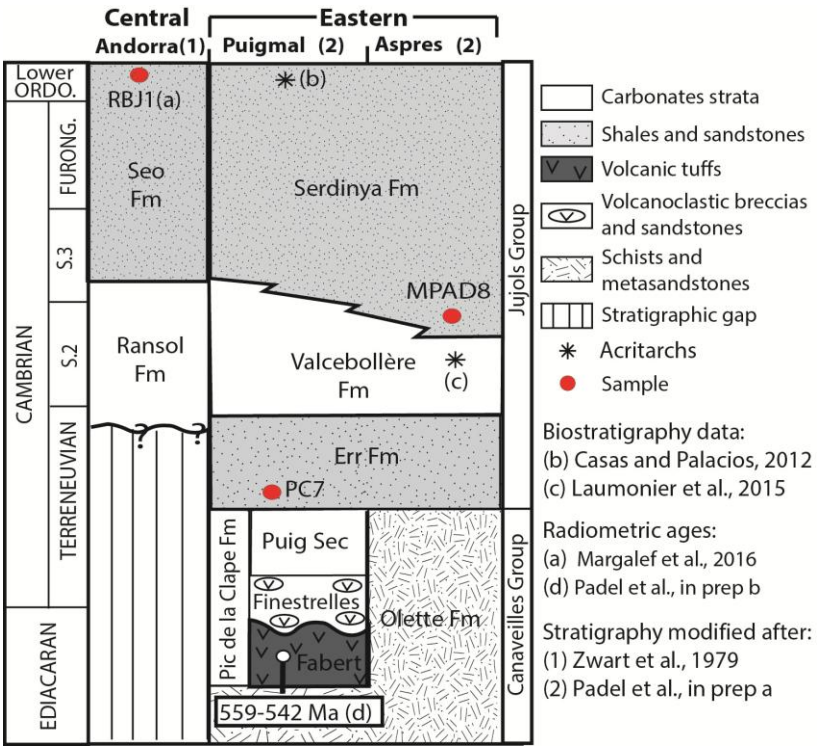

Fig. 4 : Ediacaran–Lower Ordovician stratigraphic chart of the central and eastern Pyrenees (after Zwart et al., 1979; Padel et al., in prep a [article 1]) with setting of studied samples (red circles).

3. Material and methods

Two fine- to medium-grained sandstones were sampled in the Pyrenean Axial Zone for U–Pb detrital zircon analyses (Figs. 3-4): (i) PC7 comes from the Terreneuvian Err Formation of the Puigmal Unit; and (ii) MPAD8 from the lowermost Serdinya Formation (encompassing the Cambrian Series 2–3 transition) of the Aspres Unit. Results of the U–Pb detrital zircon analyses performed by Margalef et al. (2015) on sample RBJ1, a Lower Ordovician sandstone from the Seo Formation in the Andorre Unit (Figs. 3-4), are included herein. These data from the Pyrenees have been compared with previous analyses from Cambro–Ordovician detrital zircons sampled in neighbouring basins in order to check source changes in a W-E transect along the northwestern Gondwana margin (Figs. 2, 5), including data from the Moroccan Anti-Atlas (Avigad et al., 2012), the Ossa-Morena Zone (Pereira et al., 2012) and the Central-Iberian Zone (Spain; Fernández-Suárez et al., 2014; Shaw et al., 2014) of the Iberian Peninsula, the Montagne Noire of South France (Padel et al., in press [article 3]) and SW Sardinia (Italy; Avigad et al., 2012). The deposition age of the previously analysed samples follows the relative up-cited references (Fig. 6 and 7).

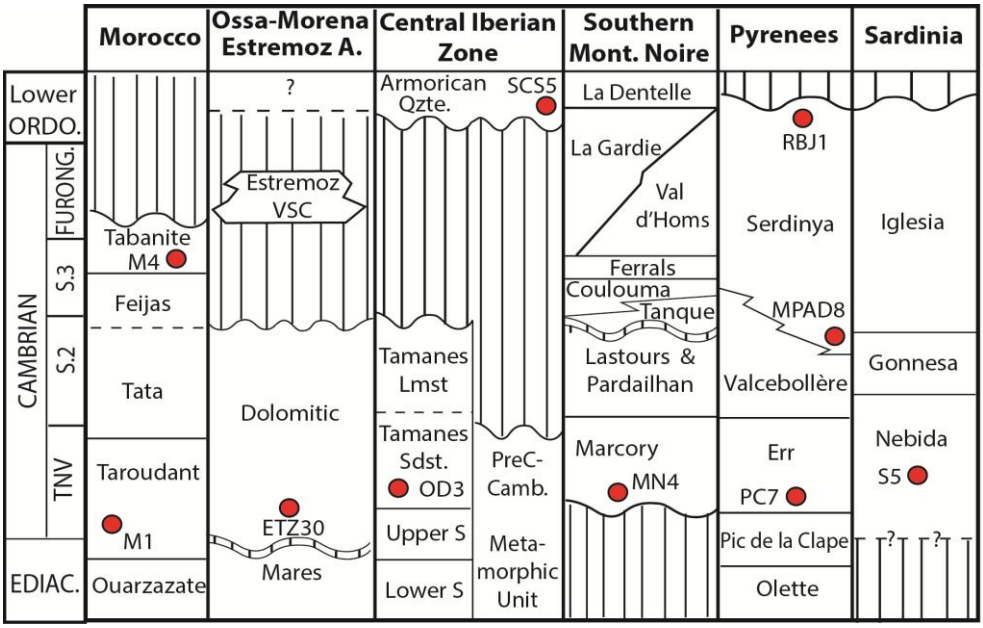

Fig. 5 : Schematic Ediacaran–Lower Ordovician stratigraphic chart showing setting and correlation of samples included in this study: M1, M4 (Morocco) from Avigad et al. (2012); ETZ30 (Ossa-Morena) from Pereira et al. (2015); OD3 and SCS5 (Central-Iberian Zone) from Fernández-Suárez et al. (2014) and Shaw et al. (2014), respectively; MN4 (Montagne Noire) from Padel et al. (in press, [article 3]); S5 (Sardinia) from Avigad et al. (2012); PC7, ALN1, RBJ1 (Pyrenees), see Fig. 3.; S: Series, Qtze: Quartzite, VSC: volcanosedimentary complex, Estremoz A: Estremoz Anticline; Sdst: sandstone, Lmst: limestone.

The U–Pb analytical method used for new samples of the Cambrian Pyrenean succession is summarized below (for further details, see Padel et al., in press [article 3]). Acquisition protocols used in previous analyses are not detailed herein (see up-cited references). From these, only raw data were included herein and, as newly acquired data were subsequently treated using the methodology introduced below (new and previous raw data are provided as supplementary data files). Sedimentary sources are identified according to the methodology reported by Avigad et al., (2003, 2012), Linnemann et al. (2011), Drost et al. (2012) and Pereira et al. (2012).

3.1 U–Pb analytical method

The zircon grains from the Pyrenees analysed herein were randomly hand-picked under binocular microscope after grinding of fresh rocks followed by heavy liquid and magnetic separation. They were included in epoxy resin and then polished in order to expose both core and rim. Internal growth textures and morphologies of zircon were revealed using cathodoluminescence and back-scattered electron imaging under scanning electron microscope (SEM) at the "Laboratoire Océanologie et Géoscience" of the University of Lille 1. U–Pb In situ analysis of single grains were determined at the Géosciences Rennes laboratory by Laser ablation coupled with plasma source mass spectrometry (LA-ICP-MS), using ablation spot diameters of 25 µm, energy pulse of 7J.cm^{-2} and repetition rates of 5 Hz. U–Pb zircon analysis were bracketed with GJ-1 and Plesovice zircons to correct eventual Th-Pb laser induced fractionation and instrumental mass discrimination, and to control the precision and accuracy of the measurements (Jackson et al., 2004; Salma et al., 2008). The Plesovice standard has yielded a Concordia age of 336.7 ±0.75 Ma

3.2 U–Pb data treatment: comparison of sources and tectonic settings

Concordia analysis is made using the Isoplot 3.75 software (Ludwig, 2012) and plotted in an inverse Terra-Wasserburg diagram to control possible outliers. Probability density plots are built using density plotter (Vermeesch, 2004). $^{207}Pb/^{206}Pb$ ages are used for U–Pb analysis giving an age older than 1000 Ma whereas $^{206}Pb/^{238}U$ ages are preferred for U–Pb analysis yielding an age younger than 1000 Ma. Only analysis included in the calculated [90–110] concordance interval (Faure and Mensing, 2005; Meinhold et al., 2011; Talavera et al., 2012) are considered for data treatment.

The Kolmogorov–Smirnov (K-S) test is used herein to determine if studied siliciclastic sediments of similar age were supplied from the same sources (revealed by spike on age

distribution of zircons) along the Gondwana margin (Figs. 8–9). The K-S test is a non-parametric probabilistic test to compare age distributions of detrital zircons from different samples and to discriminate potential statistic differences between each other (Guynn and Gehrels, 2010). The K-S test compares the cumulative probability curves, or cumulative distribution functions (CDF) of different zircon populations and evaluate the probability (P) that they might be different (Guynn and Gehrels, 2010). For a K-S test with a 95% confidence level, as used herein, a P-value lower than 0.05, means that the compared populations are significantly different.

Sedimentary basins can be classified according to their lithospheric basement, their position with respect to the plate boundary (intracratonic vs plate margin), and their background plate motion (convergent, collisional, divergent or transform; Allen and Allen, 2005). The type of basin and relative tectonic settings can be deciphered from the sediment record, following the methodology proposed by Cawood et al. (2012) based on detrital zircon analysis. Cawood et al. (2012) provided a comparative CA-DA diagram, where the cumulative distribution function of zircon age (CDF) is illustrated according to the differences between the crystallization age (CA) and the depositional age (DA) of the detrital zircons. This empirical model considers that convergent settings between plates induce large proportion of detrital zircons with narrow unimodal age distribution curves, produced by early magmatic arcs close in space and time to the depositional basin (e.g., fore-arc, back-arc, intra-arc and foreland cordillera basins). On the contrary, collisional, extensional and intracratonic settings (passive margin, rift and foreland basins) would induce a relatively late incorporation of detrital zircons with plurimodal age distributions (compared to their crystallization age) through possibly multiple reworking. On this basis, it is considered that an extensional tectonic setting can be deduced from detrital zircon analyses if CA-DA > 150 Ma at 5% of the CDF (step1). If step 1 is not reached, a CA-DA < 100 Ma at 30% of the CDF points to a convergent tectonic setting (magmatic arc-related basin; step 2). This method is applied here for the first time to the previously listed samples in order to decipher the tectonic evolution along NW Gondwana through space and through time, during Cambrian–Early Ordovician times.

4. New data from the Pyrenean samples

In sample PC7, 105 of the 115 analysis were considered as concordant [90–110%]. The three youngest dates, considered as affected by possible lead loss, were not included

either in the age distribution curves or in the CA-DA diagram. PC7 displays a predominant upper Stenian–Ediacaran group (77%) with a Stenian–Tonian group around 13% (Fig.6).

In sample MPAD8, 103 of 107 analyses are considered as concordant [90–110%], but the 5 youngest of these former do not overlie the Concordia line and are excluded either in the age distribution curves or in the CA-DA diagram. 57 % of the detrital zircon from sample MPAD8 belongs in the upper Stenian–Ediacaran group, 16% are part of a Stenian–Tonian cluster, where other Proterozoic zircon represent 14 % of the population and 13 % are Archean (Fig. 7).

5. Discussion

5.1 West-east trend of Terreneuvian sedimentary sources

The above-reported K-S test allows us to differentiate three Terreneuvian (earliest Cambrian) palaeogeographic settings based on their zircon sources (Figs. 8–9). Zircon populations of the Anti-Atlas and the Ossa-Morena Zone, the westernmost domains of the margin, are relatively similar and distinctive from all others. As a result, they are considered to have been supplied from similar sources. The three intermediate domains (the central and northern Iberian Massif zones, the Montagne Noire and the Pyrenees) cannot be differentiated from each other based on their zircon populations. Finally, the zircon populations from Sardinia differ significantly from all the remaining western domains. As a consequence, a west-east differentiation of zircon sources can be diagnosed on the northwestern Gondwana margin during Terreneuvian times, with a western source edge mainly feeding the Anti-Atlas and Ossa-Morena rifts, an eastern source edge represented by Sardinia, and an intermediate area comprising the Pyrenees, the Montagne Noire and the central and northern Iberian Massif zones.

Several Archaean–Palaeoproterozoic zircon populations are identified in all lower Cambrian samples. Even if they can represent up to about 25% of recovered grains in total, variations in their relative proportion along the margin is high and do not seem to reflect any distinct trend. In addition, each population consists of very small number of grains. Although a West-African Craton source has often been involved to explain Archaean to Palaeoproterozoic zircon populations in lower Cambrian successions (Avigad et al., 2012 for Morocco and Sardinia; Pereira et al., 2014 for Ossa-Morena; Fernández-Suárez et al., 2014 for the central and northern Iberian Massif zones; Padel et al., in press [article 3] for Montagne Noire), a Moroccan source cannot be excluded for recovered Palaeoproterozoic

populations from the Anti-Atlas, as suggested by Linnemann et al (2011) for Cambro–Ordovician sediments from Algerian Sahara.

Such a Moroccan source may be consequently assumed to have influenced deposits along the whole margin, but in indeterminable proportions. These interpretations are mostly based on the closeness of targeted and suggested sources, and influence of other sources (such as the Arabian Nubian Shield, Saharan Metacraton and Trans-Saharan Belt) cannot be ruled out for most studied areas. Indeed, Neoarchaean populations of zircons, which cannot be related to the West-African Craton, are more abundant in Sardinia and the Pyrenees and demonstrate the influence of the Arabian Nubian Shield, the Saharan Metacraton and the Trans-Saharan Belt; on the contrary, these populations are absent in Morocco. Even if Archaean to Palaeoproterozoic populations can represent up to about 25% of the whole recovered zircons, each population consists of very small number of grains. Their proportions along the margin are highly variable and do not seem to reflect any clear palaeogeographic trend, as suggested above. On the contrary, this trend may be partly explained by differentiated supply from younger sources.

The Amazonian craton has been considered as a potential source for some exotic Palaeoproterozoic and Mesoproterozoic zircons sampled in the Northwestern Gondwana margin and, even assumed to have potentially influenced all observed zircon populations (see Fernández-Suárez et al., 1999, 2000; Linnemann et al., 2011). Involvement of an Amazonian source in earlier studies might have relied on the absence of then known Gondwana sources for zircons of about 1 Ga (Fernández-Suárez et al., 2014) which have been clearly identified by now (Avigad et al., 2012; Be'eri-Shlevin et al., 2012). Following Fernández-Suárez et al. (2014), the absence of 1.2–1.6 Ga zircons in different deposits from northwestern Gondwana is considered herein to discard the Amazonian craton as a possible significant source. Therefore, although it is impossible to definitely rule out an Amazonian origin of some recovered zircons, its influence is considered herein as minor, subordinate to other potential sources, and is accordingly not reported in Figures 6 and 7.

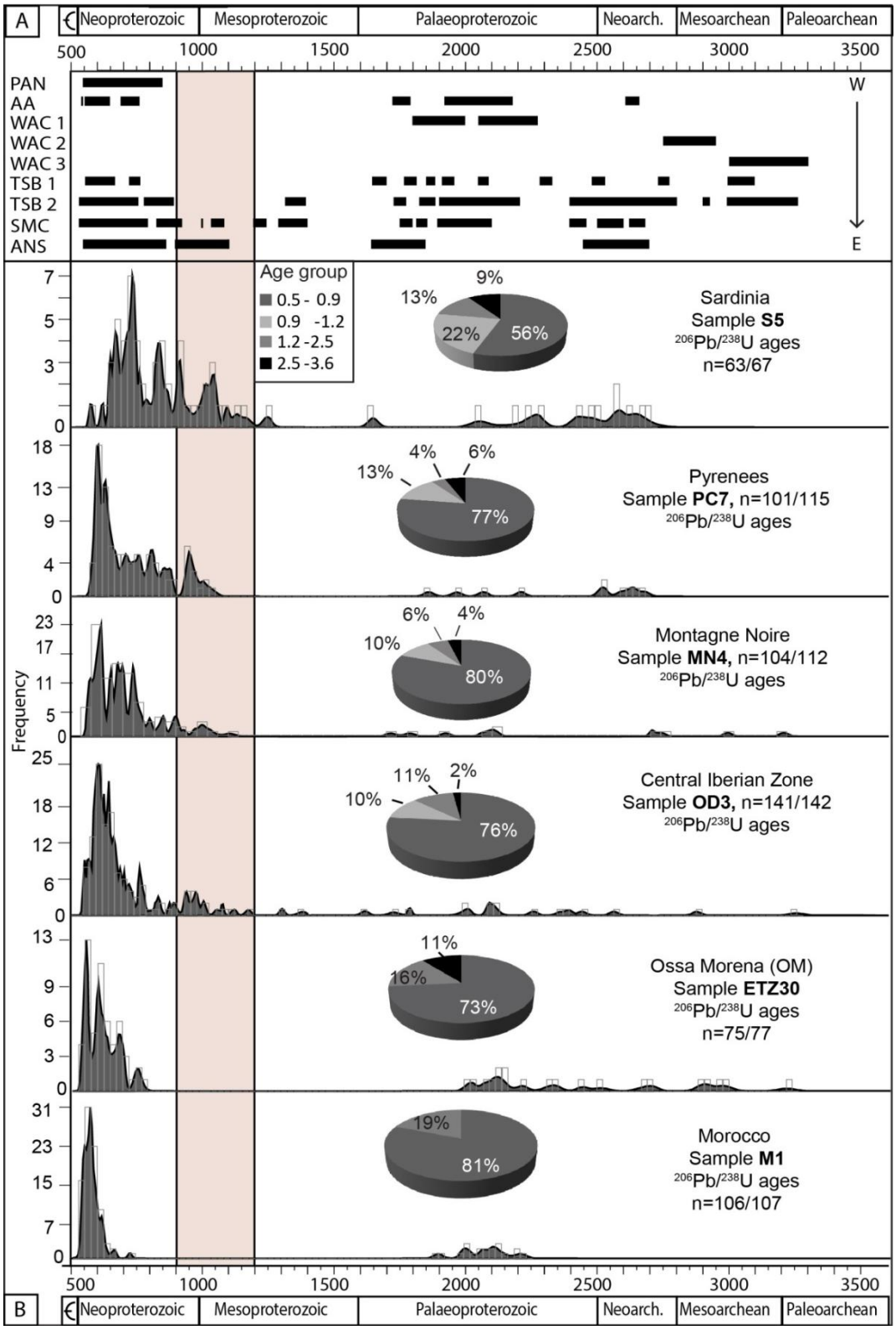

Fig. 6 : A. Potential 3500–500 Ma zircon sources of detrital zircon populations (B) found in Terreneuvian successions from Northwest Gondwana. B. Age distribution curve and age repartition of detrital zircons from Terreneuvian samples (for stratigraphic setting, see Figs. 4–5); n=number of zircons considered for analyses/total number of zircons (see supplementary data); modified from Drost et al. (2011), Linnemann et al. (2011), Pereira et al. (2012) based on data from Avigad et al. (2012). PAN: Panafrican magmatic arcs; AA: Anti-Atlas; WAC1: Eburnean event of West African craton;

WAC2: Liberian event of West African craton; WAC3: Leonan event of West African craton; TSB1: Trans-Saharan belt, Benin-Nigerian shield; TSB2: Trans-Saharan belt, Tuareg shield; SMC: Saharan metacraton; ANS: Arabian-Nubian shield.

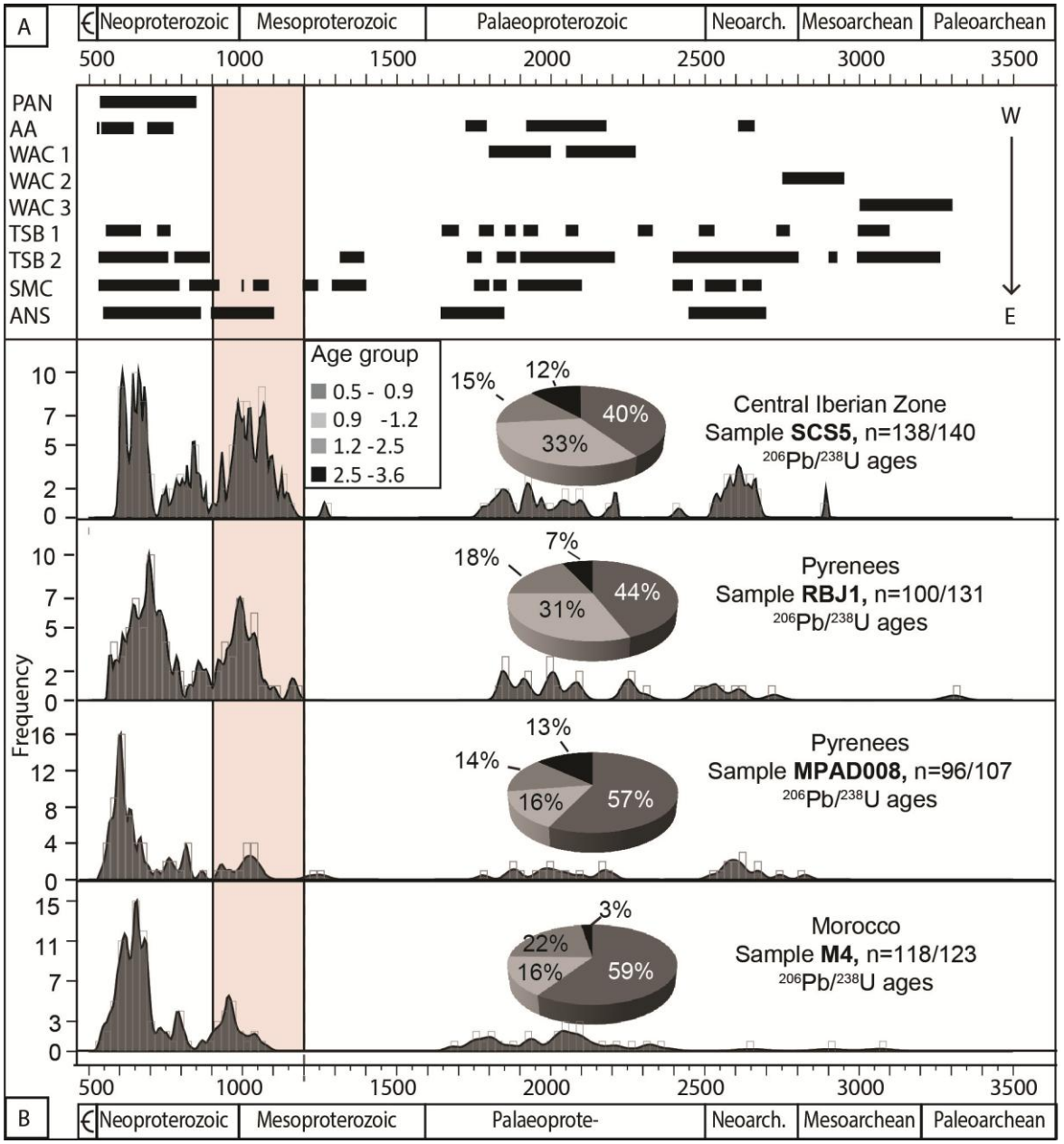

Fig. 7 : A. Potential 3500–500 Ma zircon sources of detrital zircon populations recovered from Cambrian Series 2–Lower Ordovician successions of Northwest Gondwana. B. Age distribution curve and age repartition of detrital zircons (for stratigraphic setting, see Figs. 4–5); abbreviations as in Figure 6.

	M1	ETZ30	OD3	MN4	PC7	S5
M1		**0.743**	0.000	0.000	0.000	0.000
ETZ30	**0.743**		0.000	0.000	0.000	0.000
OD3	0.000	0.000		**0.331**	**0.135**	0.000
MN4	0.000	0.000	**0.331**		**0.404**	0.000
PC7	0.000	0.000	**0.135**	**0.404**		0.001
S5	0.000	0.000	0.000	0.000	0.001	

Fig. 8 : Results of K-S test displayed by Terreneuvian samples (for abbreviations and stratigraphic details, see Figures 5–6). Light grey boxes identify samples with probable identical parent populations of zircons with a 95% confidence level.

	M4	SCS5	MPAD8	RBJ1
M4		**1.000**	**1.000**	**0.304**
SCS5	**1.000**		**0.990**	**0.719**
MPAD8	**1.000**	**0.990**		**0.317**
RBJ1	**0.304**	**0.719**	**0.317**	

Fig. 9 : Results of K-S test shown by Cambrian Series 2 see Figures 5–6 Lower Ordovician samples (for abbreviations and stratigraphic details, see Figures 5–6). Light grey boxes identify samples with probable identical parent populations of zircons with a 95% confidence level.

Lower Cambrian sediments from Ossa-Morena and Morocco are characterized by a predominant cluster of zircons at ca. 0.63–0.54 Ga, which represents 73–81% of the analyzed zircons. Avigad et al. (2012) proposed a major influence of the upper Ediacaran volcanic event represented by the Ouarzazate Supergroup (the so-called Ediacaran Atlasian Chain of Pouclet et al., 2008) emplaced during the last stages of the Panafrican orogeny (Álvaro et al., 2014b), as the Atlasian source of the observed predominant cluster in lower Cambrian sediments from the Moroccan Anti-Atlas. Although Pereira et al. (2012) suggested that 0.7–0.54 Ga zircons from Ossa-Morena (sample ETZ30) could be derived from the Cadomian Arc, the more recently described Atlasian source (Blein et al., 2014a, 2014b) might more precisely fit with the observed ca. 0.63–0.54 spike in age distribution of zircons from both Morocco and Ossa-Morena, where older Panafrican zircons (0.95–0.65 Ga) are not recovered. In the intermediate area (central and northern Iberian Massif zones, Montagne Noire and Pyrenees), a 76–80% of zircons form a 0.9–0.5 Ga cluster (Fig. 6), which is also observed in Sardinia but formed by only 56% of the analyzed zircons. In the intermediate to eastern parts of the margin, the youngest populations of zircons are less important than in Morocco and Ossa-Morena, or even absent (Pyrenees). In these areas, either a western (Panafrican or Atlasian) or eastern (Trans-Saharian Belt, Arabian-Nubian Shield, Saharan Metacraton) sources can be invoked for zircons aged from 0.54 Ga to 0.95 Ga, so a western influence

cannot be ruled out. However, the presence of 0.9-0.8Ga zircons demonstrates the influence of eastern sources, which are absent in the successions of Morocco and Ossa-Morena. The slight increase in 0.9–0.8 Ga zircons from the central and northern Iberian Massif zonesto Pyrenean sediments suggests as well an eastward increase in eastern supplies (Trans-Saharian Belt, Arabian-Nubian Shield, Saharan Metacraton), whereas a parallel decrease in younger 0.63–0.54 Ga zircons may reflect a lowering influence of Moroccan sources along the early–Cambrian Gondwana margin.

A distinct SW-NE trend in sourcing is better constrained in proportion of zircons which originated in the 1.2-0.9 Ga period (i.e. coeval to the Grenville orogeny elsewhere; Figs. 6–7, 10). These are generally associated with the Arabian-Nubian Shield, which was exhumed thanks to the suture of Panafrican orogenic events (Caby, 2003; Liégeois et al., 2003; Kroner and Stern, 2005), and or the Saharan Metacraton (Avigad et al., 2003; Fernández-Suárez et al., 2014; Shaw et al., 2014; Padel et al., in press [article 3]). Such zircons are absent in lower Cambrian siliciclastics of Morocco and Ossa-Morena and show a distinct progressive increase in proportion from the central and northern Iberian Massif zones (11%) to Sardinia (22%; Figs. 6, 10). Fernández-Suárez et al. (2014) further noticed that sample OD3 (Central-Iberian Zone) revealed a zircon age distribution similar to lower Cambrian samples from the northwestern part of the Arabian-Nubian Shield (Israel and Jordan). The influence of both the eastern Arabian-Nubian Shield and the Saharan metacraton increases eastward along the northwestern Gondwana margin.

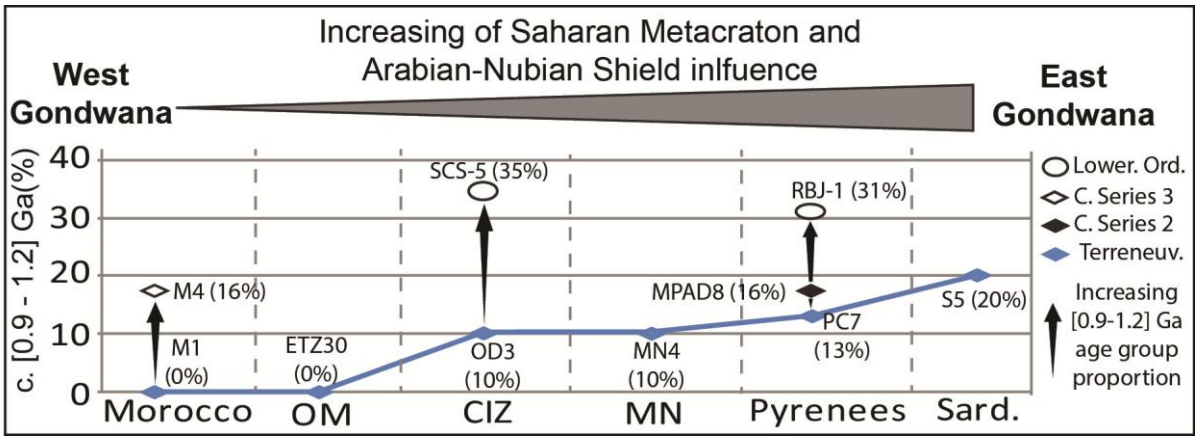

Fig. 10 : E-W transect of Northwest Gondwana showing an increasing influence of Stenian–Tonian sources from the Saharan Metacraton and the Arabian-Nubian Shield on Cambro–Ordovician sediments; C.: Cambrian; CIZ: Central-Iberian Zone, OM: Ossa-Morena Zone, Ord.; Ordovician; Sard.: SW Sardinia, Terreneuv.: Terreneuvian.

5.2 Cambrian evolution of sources and related tectonic settings

Analyses of detrital zircons from Cambrian Series 2–Lower Ordovician sandstones from Northwest Gondwana are limited in number. In total, only four analyses were taken into account herein, including two focusing on Lower Ordovician samples (Fig. 5). Terreneuvian and earlier sediment sources are interpreted in a same way. Temporal trends in sedimentary sources are tentatively interpreted herein based on K-S test on zircon populations and CA-DA diagrams.

It is noticeable that none of the considered samples reveals significantly different zircon populations using the K-S Test (Fig. 8), arguing for a homogenization of sediment sources along Northwest Gondwana from Cambrian Epoch 2 to Early Ordovician times. The proportion of Stenian–Tonian zircons, which best illustrates the latter tendencies, increases upsection in all analysed successions. In particular, sources from the Arabian Nubian Shield and the Saharan Metacraton, which did not influence the Moroccan Atlas rift during the Terreneuvian, provided up to 16 % of inherited grains during the Cambrian Epoch 3. Nevertheless, Avigad et al. (2012) argued the Stenian–Tonian zircons from Sardinia and Morocco are petrologically different, implying two different 1.2-0.9 Ga sources could still have been feeding the western and eastern parts of NW Gondwana.

The end of the Terreneuvian SW-NE trend described above is interpreted herein to reflect, with some delay, a shift in tectonic settings. Amalgamation of the Gondwana supercontinent (Stern, 1994; Ballèvre et al., 2001; Meert, 2003; Kroner and Stern, 2005; Von Raumer and Stampfi, 2008 et al., 2008; Murphy et al., 2013; Stampfi et al., 2013; Linnemann et al., 2014; Blein et al., 2014a,b) is recorded in the studied area by the Panafrican orogen, which ended up at about 540 Ma (close to the Ediacaran–Cambrian boundary). During the Early Palaeozoic, the tectonic setting of Northwest Gondawana changed drastically from convergent to extensional conditions (Linnemann et al., 2007, 2008; Pouclet et al., 2016), marking the beginning of the rifting phase associated with the opening of the Rheic Ocean (Ballèvre et al., 2001; Linnemann et al., 2007, 2008; Pereira et al. 2012; Stampfi et al., 2013; Pouclet et al., 2016). These tectonic settings are variably reflected by the CA-DA diagram (Cawood et al., 2012), according to which (Fig. 11), Terreneuvian sandstones from Morocco (M1), the Ossa-Morena (ETZ30) and Central Iberian zones (OD3), the Montagne Noire (MN4), and Cambrian Series 3 sandstones of Morocco (M4) mimic those deposited in convergent settings (so influenced by magmatic activities in an active margin domain), while Terreneuvian–Cambrian Series 3 samples from the Pyrenees and Sardinia are similar to those

deposited in a foreland basin associated with collisional setting. This definitely contrasts and mismatches the geological evidence indicating extensional settings with rifting initiation along the margin (Cocozza and Gandin, 1990; Ugidos et al., 2003; Linnemann et al., 2007, 2008; Von Raumer and Stampfi, 2008; Álvaro et al., 2015,b; Pouclet et al., 2016). However, this apparent mismatch between Cawood et al.'s (2012) CA-DA model and the geological evidence is interpreted herein as a result of two major controls on zircon population deposited in an early extensional setting, which were not integrated in the Cawood et al.'s model: time-lap since the last convergent setting (last sources and fastness in shifting from convergent to extensional setting; see discussion in Cawood et al., 2012) and physical distance to these sources. This effect of "closeness of a recent source" on the CA-DA diagram and its interpretation is well illustrated by the studied lower Cambrian samples.

The rapid post–Panafrican shift to extensional conditions and the close distance to the major, late Neoproterozoic Panafrican and Atlasian sources explain their still predominant influence on the Terreneuvian sediments (major spike in zircon age distributions), along with reduced CA-DA value, in Morocco and Ossa-Morena successions, deposited in active rifting systems. However, the influence of these sources quickly fall with the distance to the sedimentary basin, resulting in a more flattened and stretched age distribution of recovered zircons with a more balanced influence of relatively distant sources of various ages, and a higher CA-DA value.

In our case study, the easternmost basins (Pyrenees and Sardinia) are not located close to any source inherited from the late Mesoproterozoic to Neoproterozoic orogens, so that Panafrican or Atlasian orogens (to the southwest), and Arabian-Nubian Shield and Sahara metacraton (to the Northeast) have a more balanced influence on the sediment composition, increasing the relative CA-DA value. As a result, the lower Cambrian sediments from Sardinia and the Pyrenees are misinterpreted as deposited under collisional settings. Intermediate palaeogeographic areas (Montagne Noire and Central-Iberian Zone) revealed intermediate CA-DA values and zircon age distribution curves. With time, the effect of closeness of a recent source further decreases. In the present case, the different major Mesoproterozoic to Proterozoic sources tend to enlarge their target to more distant basins, again stretching the zircon age curve repartition and increasing the CA-DA value in the relative siliciclastic successions (M4, MPAD8). Only the later, Lower Ordovician sandstones of the Pyrenees (RBJ1) and the Central-Iberian Zone (SCS5), deposited in "post-transitional" extensional

settings (Shaw et al., 2014; Margalef et al., 2015; Pouclet et al., 2016), are associated in CA-DA accordingly.

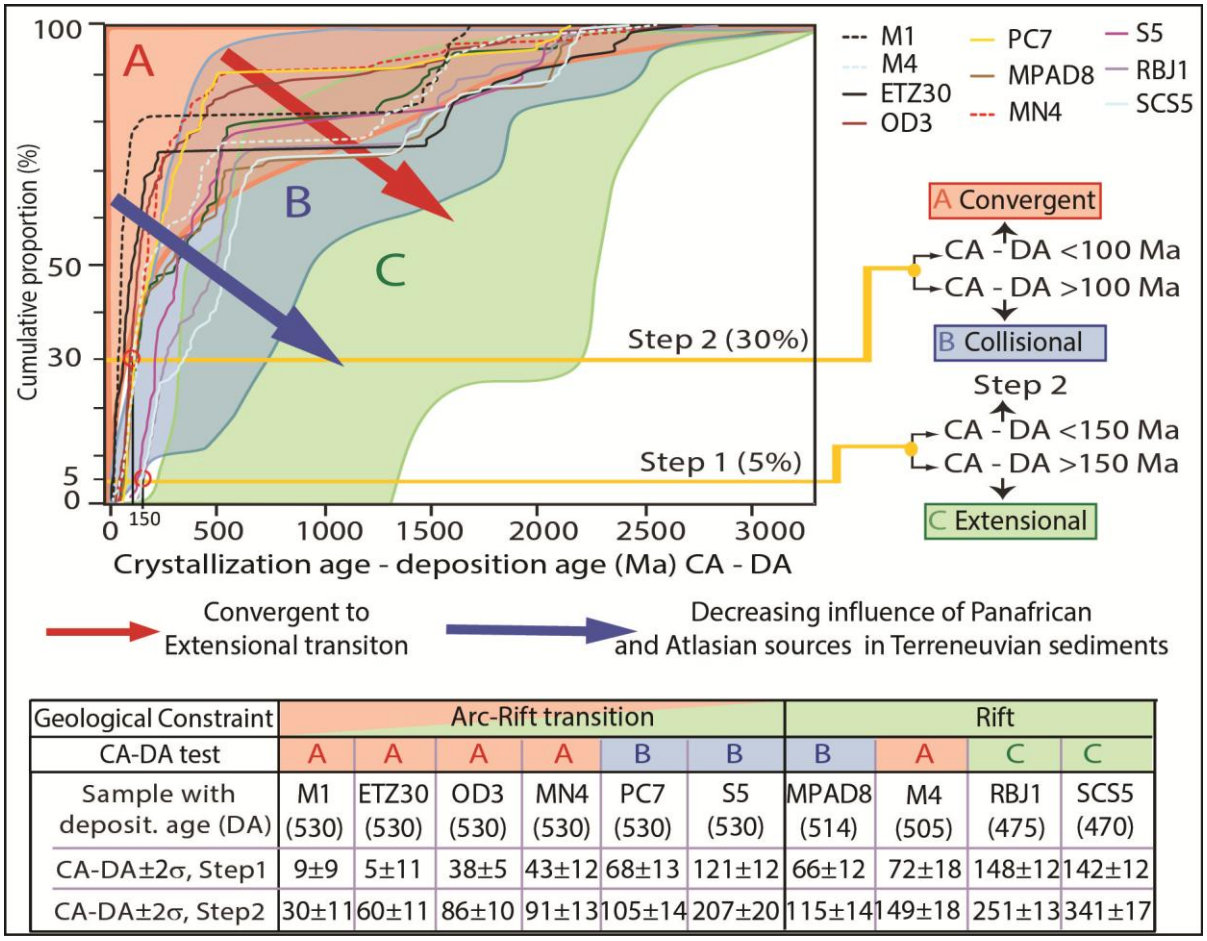

Geological Constraint	Arc-Rift transition						Rift			
CA-DA test	A	A	A	A	B	B	B	A	C	C
Sample with deposit. age (DA)	M1 (530)	ETZ30 (530)	OD3 (530)	MN4 (530)	PC7 (530)	S5 (530)	MPAD8 (514)	M4 (505)	RBJ1 (475)	SCS5 (470)
CA-DA±2σ, Step1	9±9	5±11	38±5	43±12	68±13	121±12	66±12	72±18	148±12	142±12
CA-DA±2σ, Step2	30±11	60±11	86±10	91±13	105±14	207±20	115±14	149±18	251±13	341±17

Fig. 11 : CA-DA diagrams (after Cawood et al., 2012) illustrating the interpreted tectonic setting and depositional basin for Terreneuvian–Lower Ordovician samples from Northwestern Gondwana; see text for abbreviations of samples.

In conclusion, CA-DA diagrams are interpreted herein to reveal the eastward decreasing influence of Panafrican or Atlasian Neoproterozoic sources on Terreneuvian successions deposited along the Northwestern Gondwana margin in favour of sources from Mesoproterozoic to Neoproterozoic Arabian-Nubian Shield and Sahara Metacraton, in a context of relatively brief transition from convergent to extensional settings. This transition from fast, post-collisional orogenic establishment of extensional settings with rifting initiation close to the inherited sediment sources, to more stabilised, later Cambrian–Ordovician settings along a passive margin with migration and expansion of rifting conditions to the Occitan Domain and South Armorican domain (Pouclet et al., 2016) are also reflected in the CAD-DA diagrams.

6. Conclusions

Age distribution of detrital zircons, their comparison using K-S test and, for the first time, variations of CA-DA diagrams through time and space are used herein to analyse the Cambrian-Lower Ordovician variation in sediment sources along Northwest Gondwana. During the Terreneuvian, the zircon age distribution curves of different siliciclastic successions illustrating a SW-NE transect reflects the distinction of three Terreneuvian areas based on a K-S test on zircon age distribution curves: a southwestern edge (comprising the Moroccan Anti-Atlas and the Iberian Ossa-Morena Rifts), a central transitional area (grouping the central and northern Iberian Massif zones, the Montagne Noire and the Pyrenees), and an eastern edge (represented by Sardinia). A SW-NE trend in relative influence of major sediment sources is distinctively identified: the Panafrican-Atlasian sources predominate throughout the westernmost successions, whereas the influence of the Arabian-Nubian Shield and Sahara Metacraton sources increases eastward. Such Terreneuvian trend tends to disappear from Cambrian Epoch 2 to Early Ordovician. This tendency reflects the evolution of tectonic settings with a fast post–Panafrican shift to extensional and rifting conditions development under strong westward influence of still young Panafrican and Atlasian sources. Subsequently, the relative influence of the different sources on the margin sedimentation tends to balance, giving cohorts of inherited zircons more characteristic of extensional rifting to passive margin settings. Although the palaeogeographic position of the Pyrenean domain during Early Palaeozoic times cannot be definitely assessed, the analysis of zircon populations from Cambrian–Ordovician successions suggests highest affinities with Montagne Noire and Sardinia, between which it may have been positioned.

Acknowledgements

Founding for this research was yielded by RGF program of the French Geological Survey (BRGM). This paper is a contribution to project CGL2013-48877-P from Spanish MINECO. François Guillot, Olivier Blein and Cesar Witt are warmly thanked by geodynamic discussions.

7. References

Allen, P.A., Allen, J.R., 2005. Blackwell Scientific Publications, Cambridge, 451 pp.

Altumi, M.M., Elicki, O., Linnemann, U., Hofmann, M., Sagawe, A., Gärtner, A., 2013. U–Pb LA-ICP-MS detrital zircon ages from the Cambrian of Al Qarqaf Arch, central-western Libya: Provenance of the West Gondwanan sand sea at the dawn of the early Palaeozoic. J. Afr. Earth Sci. 79, 74-97.

Álvaro, J.J., Vizcaïno, D., 1999. Biostratigraphic significance and environmental setting of the trace fossil *Psammichnites* in the Lower Cambrian of the Montagne Noire (France). Bull. Soc. géol. Fr. 170, 821–828.

Álvaro, J.J., Bauluz, B., Clausen, S., Devaere, L., Imaz, A.G., Monceret, E., Vizcaïno, D., 2014a. Stratigraphy of the Cambrian-Lower Ordovician volcanosedimentary complexes in the northern Montagne Noire, France. Stratigraphy 11, 83–96.

Álvaro, J.J., Benziane, F., Thomas R., Walsh, G.J., Yazidi, A., 2014b. Neoproterozoic–Cambrian stratigraphic framework of the Anti-Atlas and Ouzellagh promontory (High Atlas), Morocco. J. Afr. Earth Sci. 98, 1-15.

Álvaro, J.J., Colmenar, J., Monceret, E., Pouclet, A., Vizcaïno, D., 2015. Late Ordovician (post–Sardic) rifting branches in the North Gondwanan Montagne Noire and Mouthoumet massifs of southern France. Tectonophysics 681, 111–123.

Atwater, 1970. Implication of plate tectonics for the Cenozoic tectonic evolution of western North America. Geol. Soc. Am. Bull. 81, 3513–3536.

Avigad, D., Gerde, A., Morag, N., Bechstädt, T., 2012. Coupled U–Pb–Hf of detrital zircons of Cambrian sandstones from Morocco and Sardinia: Implications for provenance and Precambrian crustal evolution of North Africa. Gondwana Res. 21, 690–703.

Ballèvre, M., Le Goff, E., Hébert, R., 2001. The tectonothermal evolution of the Cadomian belt of northern Britany, France: a Neoproterozoic volcanic arc. Tectonophysics 331, 19–43.

Ballèvre, M., Bosse, V., Ducassou, C., Pitra, P., 2009. Palaeozoic history of the Armorican Massif: Models for the tectonic evolution of the suture zones. C. R. Geosci. 341, 174–201.

Barnolas, A., Chiron, J.C., 1996. Synthèse géologique et géophysique des Pyrénées. Tome 1: Cycle hercynien. BRGM-ITGE, Orléans-Madrid, 729 p.

Blein, O., Baudin, T., Soulaimani, A., Cocherie, A., Chèvremont, P., Admou, H., Ouanaimi, H., Hafid, A., Razin, P., Bouadbelli, M., Roger, J., 2014a. New geochemical, geochronological and structural constraints on the Ediacaran evolution of the south Sirwa, Agadir-Melloul and Iguerda inliers, Anti-Atlas, Morocco. J. Afr. Earth Sci. 98, 47–71.

Blein, O., Baudin, T., Chèvremont, Ph., Soulaimani, A., Admou, H., Gasquet, D., Cocherie, A., Egal, E., Youbi, N., Razin, Ph., Bouabdelli, M., Gombert, Ph., 2014b. Geochronological constraints on the polycyclic magmatism in the Bou Azzer-El Graara inlier (Anti-Atlas, Morocco). J. Afr.Earth Sci. 99, 287–306.

Caby, R., 2003. Terrane assembly and geodynamic evolution of central-western Hoggar: a synthesis. J. Afr. Earth Sci. 37, 133–159.

Casas, J.M., Castiñeiras, P., Navidad, M., Liesa, M., Carreras, J., 2010. New insights into the Late Ordovician magmatism in the Eastern Pyrenees: U–Pb SHRIMP zircon data from the Canigó massif. Gondwana Res. 17, 317–324.

Casas, J. M., Navidad, M., Castiñeiras, P., Liesa, M., Aguilar, C., Carreras, J., Hofman, M., Gärtner, A., & Linnemann, U., 2015. The Late Neoproterozoic magmatism in the Ediacaran series of the Eastern Pyrenees: new ages and isotope geochemistry. Int. J. Earth Sci. 104, 909–925.

Casas, J.M., Fernández, O., 2007. On the Upper Ordovician unconformity in the Pyrenees: New evidence from the La Cerdanya area. Geol. Acta 5, 193–198.

Castiñeiras, P., Navidad, M., Liesa, M., Carreras, J., Casas, J.M., 2008. U–Pb zircon ages (SHRIMP) for Cadomian and Lower Ordovician magmatism in the Eastern Pyrenees: new insights in the pre-Variscan evolution of the northern Gondwana margin. Tectonophysics 46, 228–239.

Cavet, P., 1957. Le Paléozoïque de la zone axiale des Pyrénées orientales françaises entre le Roussillon et l'Andorre. Bull. Ser. Carte géol. Fr. 55, 303–518.

Cocherie, A., Baudin, T., Autran, A., Guerrot, C., Fanning, M., Laumonier, B., 2005. U–Pb zircon (ID-TIMS and SHRIMP) evidence for the early Ordovician intrusion of metagranites in the late Proterozoic Canaveilles Group of the Pyrenees and the Montagne Noire (France). Bull. Soc. géol. Fr. 176, 269–282.

Cawood, P.A., Hawkesworth, C.J., Dhuime, B., 2012. Detrital zircon record and tectonic setting. Geology 40, 875–878.

Deloule, E., Alexandrov, P., Cheilletz, A., Laumonier, B., Barbey, P., 2002. In situ U–Pb zircon ages for Early Ordovician magmatism in the eastern Pyrenees, France : The canigou orthogneisses. Int. J. Earth Sci. 91, 398–405.

Díaz Fernández, R., Martínez Catalán, J.R., Gerdes, A., Abati J., Arenas, R., Fernández-Suárez, J., 2010. U–Pb ages of detrital zircons from the Basal allochthonous units of NW

Iberia: Provenance and paleoposition on the northern margin of Gondwana during the Neoproterozoic and Paleozoic. Gondwana Res. 18, 385–399.

Dickinson, W.R., 1981. Plate tectonics and the continental margin of California, in Ernst, W.G., ed., The geotectonic development of California, Rubey volume 1: Englewood Cliffs, New Jersey, Prentice-Hall, 1-28.

Dickinson, W.R., Gehrels, G.E., 2009. Use of U–Pb ages of detrital zircons to infer maximum depositional ages of strata: a test against a Colorado Plateau Mesozoic database. Earth Planet. Sci. Lett. 288, 115–125.

Drost, K., Gerdes, A., Jeffries, T., Linnemann, U., Storey, C., 2011. Provenance of Neoproterozoic and early Paleozoic silicicastic rocks of the Tepla-Barrandian unit (Bohemian Massif): Evidence from U–Pb detrital zircon ages. Gondwana Res. 19, 213–231.

Faure, G., Mensing, T.M., 2005. Isotopes: principles and applications. Wiley, Hoboken, 897 p.

Fernández-Suárez, J., Gutiérrez-Alonso, G., Jenner, G. A., Tubrett, M.N., 2000. New ideas on the Proterozoic-Early Palaeozoic evolution of NW Iberia: insights from U–Pb detrital zircon ages. Precambr. Res. 102, 185–206.

Fernández-Suárez, J., Gutiérrez-Alonso, G., Pastor-Galán, D., Hofmann, M., Murphy, J. B., Linnemann, U., 2014. The Ediacaran–Early Cambrian detrital zircon record of NW Iberia: possible sources and paleogeographic constraints. Int. J. Earth Sci. 103, 1335–1357.

Gehrels, G., 2014. Detrital zircon U-Pb geochronology applied to tectonics. Annu. Rev. Earth Planet. Sci. 42, 127-149.

Gutiérrez-Alonso, G., Fernández-Suarez, J., Jeffries, T.E., Jenner, G.A., Tubrett, M.N., Cox, R., Jackson, S.E., 2003. Terrane accretion and dispersal in the northern Gondwana margin. An Early Paleozoic analogue of a long-lived active Margin. Tectonophysics 365, 221–232

Gutiérrez-Alonso, G., Fernández-Suarez, J., Pastor-Galán, D., Johnston, S.T., Linnemann, U., Hofmann, M., Shaw, J., Colmenero, J.R., Hernández, P., 2015. Significance of detrital zircons in Siluro–Devonian rocks from Iberia. J. Geol. Soc. 172, 309–322.

Guynn, J., and Gehrels, G., 2010, Comparison of detrital zircon age distributions using the K-S test. https://sites.google.com/a/laserchron.org/laserchron/

Jackson, S.E., Pearson, N.J., Griffin, W.L., Belousova, E.A., 2004. The application of laser-ablation-inductively coupled plasma-mass spectrometry to in situ U-Pb zircon geochronology. Chem. Geol. 211, 47–69.

Kroner, A., Stern, R.J., 2005. Pan-African orogeny. Encyclopedia of Geology 1, 1–12.

Laumonier et al., 1996. Cambro–Ordovicien. In: Synthèse géologique et géophysique des Pyrénées. Tome 1: Cycle hercynien (Barnolas, A., Chiron, J.C., eds.). BRGM-ITGE, Orléans-Madrid, 729 p.

Laumonier, B., 1998. Les Pyrénées centrales et orientales au début du Paléozoïque (Cambrien s.l.) : évolution paléogéographique et géodynamique. Geodin. Acta 11, 1–11.

Laumonier, B., Guitard, G., 1986. Le Paléozoïque inférieur de la moitié orientale de la Zone Axiale des Pyrénées. Essai de synthèse. C. R. Acad. Sci. (sér. 2), 302, 473–478.

Laumonier B., Autran, A., Barbey, P., Cheilletz, A., Baudin, T., Cocherie, A., Guerrot, C., 2004. Conséquences de l'absence de socle cadomien sur l'âge et la signification des séries pré-varisques (anté–Ordovicien supérieur) du sud de la France (Pyrénées, Montagne Noire). Bull. Soc. géol. France 175, 105–117.

Laumonier, B., Calvet, M., Wiazemsky, M., Barbey, P., Marignac, C., Lambert, J., Lenoble, J.L., 2015. Notice explicative Carte géologique de la France (1/50.000), feuille Céret (1096). Orléans, BRGM.

Liégeois, J.P., Latouche, L., Boughara, M., Navez, J., Guiraud, M., 2003. The LATEA metacraton (Central Hoggar, Tuareg shield,Algeria): behaviour of an old passive margin during the Pan-African orogeny. J. Afr. Earth Sci. 37, 161–190.

Liesa, M., Carreras, J., Castiñeiras, P., Casas, J.M., Navidad, M., Vila, M., 2011. U–Pb zircon of Ordovician magmatism in the Albera Massif (Eastern Pyrenees). Geol. Acta 9, 93–101.

Linnemann, U., Gerdes, A., Drost, K., Buschmann, B., 2007. The continuum between Cadomian Orogenesis and opening of the Rheic Ocean: constraints from LA-ICP-MS U–Pb zircon dating and analysis of plate-tectonic setting (Saxo-Thuringian Zone, NE Bohemian massif, Germany). In: The Evolution of the Rheic Ocean: from Avalonian–Cadomian active margin to Alleghenian–Variscan collision (Linnemann, U., Nance, D., Kraft, P., Zulauf, G., eds.). Geol. Soc. Am. Bull. 423, 61–96.

Linnemann, U., Pereira, F., Jeffries, T.E., Drost, K., Gerdes, A., 2008. The Cadomian Orogeny and the opening of the Rheic Ocean: the diacrony of geotectonic processes constrained by LA-ICP-MS U–Pb zircon dating (Ossa-Morena and Saxo-Thuringian Zones, Iberian and Bohemian Massifs). Tectonophysics 461, 21–43.

Linnemann, U., Gerdes, A., Hofmann, M., Marko, L., 2014. The Cadomian Orogen: Neoproterozoic to Early Cambrian crustal growth and orogenic zoning along the periphery of the West African Craton–Constraints from U–Pb zircon ages and Hf isotopes (Schwarzburg Antiform, Germany). Precambr. Res. 244, 236–278.

Llopis Lladó, N., 1965. Sur le Paléozoïque inférieur de l'Andorre. Bull. Soc. géol. Fr. 7, 652–659.

Ludwig, K.R., 2012. Users Manual for Isoplot/Ex rev. 3.75. Berkeley Geochronology Center, Spec. Publ. 5, 1–75.

Manzotti, P., Poujol, M., Ballèvre, M., 2015. Detrital zircon in blueschist-facies metaconglomerates: implications for the Early Permian palaeo-topography of the Western Alps. Int. J. Earth Sci. 104, 703–731.

Margalef, A., Castiñeiras, P., Casas, J.M., Navidad, M., Montserrat, L., Linnemann, U., Hofmann, M., Gärtner, A. (2016). Detrital zircons from the Ordovician rocks of the Pyrenees: Geochronological constraints and provenance. Tectonophysics, 681, 124-134

Martínez, F.J., Iriondo, A., Dietsch, C., Aleinikoff, J.N., Peucat, J.J., Cirès, J., Reche, J., Capdevila, R., 2011. U–Pb SHRIMP-RG zircon ages and Nd signature of lower Paleozoic rifting-related magmatism in the Variscan basement of the Eastern Pyrenees. Lithos 127, 10–23.

Martínez-Catalán, 2012. The Central Iberian arc, an orocline centered in the Iberian Massif and some implications for the Variscan belt. Int J Earth Sci., 101, 1299–1314.

Meinhold, G., Morton, A.C., Fanning, C.M., Frei, D., Howard, J.P., Phillips, R.J., Strogen, D., Whitham, A.G., 2011. Evidence from detrital zircons for recycling of Mesoproterozoic and Neoproterozoic crust recorded in Paleozoic and Mesozoic sandstones of southern Libya. Earth Planet. Sci. Lett. 312, 164–175.

Meinhold, G., Morton, A.C., Avigad, D., 2013. New insights into peri-Gondwana paleogeography and the Gondwana super-fan system from detrital zircon U–Pb ages. Gondwana Res. 23, 661–665.

Meert, J.G., 2003. A synopsis of events related to the assembly of eastern Gondwana. Tectonophysics 362, 1–40.

Murphy, J.B., Keppie, J.D., Dostal, J., Nance, R.D., 1999. Neoproterozoic–early Paleozoic evolution of Avalonia. Geol. Soc. Am., Spec. Pap. 336, 253–266.

Murphy, J.B., Pisarvesky, S.A., Nance, R.D., Keppie, J.D., 2004. Neoproterozoic–Early Paleozoic evolution of peri-Gondwana terranes: implications for Laurentia-Gondwana connections. Int. J. Earth Sci. 93, 659-682.

Murphy, J.B., Pisarvesky, S.A., Nance, R.D., 2013. Potential geodynamic relationships between the development of peripheral orogens along the northern margin of Gondwana and the amalgamation of West Gondwana. Miner. Petrol 107, 635–650.

Nance, D.R., Murphy, J.B., Keppie, J.D., 2002. A Cordilleran model for the evolution of Avalonia. Tectonophysics 352, 11–31

Nance, R.D., Murphy, J.B., Strachan, R.B., Keppie, J.D., Gutiérrez-Alonso, G., Fernández-Suárez, J., Quesada, C., Linnemann, U., D'lemos, R., Pisarevsky, S.A., 2008. Neoproterozoic–early Palaeozoic Tectonostratigraphy and palaeogeography of the peri-Gondwanan terranes: Amazonian v. West African connections. From Ennih, N., Liégeois, J.-P., (eds), The Boundaries of the West African Craton. Geological Society, London, Special Publications, 297, 345–383.

Nance, R.D., Murphy, J.B., Santosh, M., 2014. The supercontinent cycle: a retrospective essay. Gondwana Res. 25, 4–29.

Padel, M., Álvaro, J.J., Clausen, S., Guillot, F., Poujol, M., Chichorro, M., Monceret, E., Pereira, M.F., Vizcaïno, D., in press [article 3]. U–Pb laser ablation ICP-MS zircon dating across the Ediacaran–Cambrian transition of the Montagne Noire, southern France. C. R. Geosci.

Padel, M., Clausen, S., Álvaro, J.J., Laumonier, B., in prep a [article 1]. Stratigraphic review of the Ediacaran-Lower Ordovician (pre-Sardic) volcanosedimentary framework in the Eastern Pyrenees, France and Spain.

Padel, M., Álvaro, J.J., Sánchez-García, T., Clausen, S., Poujol, M., Laumonier, B., Guillot, F., in prep b [article 2]. Cadomian volcanosedimentary complexes across the Ediacaran-Cambrian transition of the Eastern Pyrenees, France and Spain.

Pastor-Galán, D., Gutiérrez-Alonso, G., Fernández-Suarez, J., Murphy, J.B., Nieto, F., 2013. Tectonic evolution of NW Iberia during the Paleozoic inferred from the geochemical record of detrital rocks in the Cantabrian Zone. Lithos, 182–183, 211–228.

Pereira, M.F., Solá, A.R., Chichorro, M., Lope, L., Gerdes, A., Silva, J.B., 2012. North-Gondwana assembly, break-up and paleogeography: U–Pb isotope evidence from detrital and igneous zircons of Ediacaran and Cambrian rocks of SW Iberia. Gondwana Res. 22, 866–881.

Pouclet, A., Álvaro, J.J., Bardintzeff, J.-M., Gil Imaz, A, Monceret, E., Vizcaïno, D. 2016. Cambrian–Early Ordovician volcanism across the South Armorican and Occitan Domains of the Variscan Belt in France: Continental break-up and rifting of the northern Gondwana margin. Geosci. Frontiers, doi: 10.1016/j.gsf.2016.03.002.

Robert, N.M.W., 2012. Increased loss of continental crust during supercontinent amalgamation. Gondwana Res. 21, 994–1000.

Shaw, J., Gutiérrez-Alonso, G., Johnston, S.T., Galán, D.P., 2014. Provenance variability along the Early Ordovician north Gondwana margin: Paleogeographic and tectonic implications of U–Pb detrital zircon ages from the Armorican Quartzite of the Iberian Variscan belt. Geol. Soc. Am. Bull. 126, 702–719.

Sláma, J., Košler, J., Condon, D.J., Crowley, J.L., Gerdes, A., Hanchar, J.M., Horstwood, M.S.A., Morris, G.A., Nasdala, L., Norberg, N., Schaltegger, U., Schoene, B., Tubrett, M.N., Whitehouse, M.J., 2008. Plešovice zircon – a new natural reference material for U–Pb and Hf isotopic microanalysis. Chem. Geol. 249, 1–35.

Squire, R.J., Campbell, I.H., Allen, C.M., Wilson, C.J.L., 2006. Did the Transgondwana Supermontin trigger the explosive radiation of animals on Earth? Earth Planet. Sci. Lett. 250, 116–133.

Stampfi, G.M., Hochard, C., Vérard, C., Wilhem, C., Von Raumer, J., 2013. The formation of Pangea. Tectonophysics 593, 1–19.

Stern, R.J., 1994. Arc Assembly and continental collision in the neoproterozoic east African orogen: implication for the Consolidation of Gondwana. Ann. Rev. Earth Planet. Sci. 22, 319–351.

Talavera, C., Montero, P., Martínez Poyatos, D., Williams, I.S. 2012. Ediacaran to Lower Ordovician age for rocks ascribed to the Schist-Graywacke Complex (Iberian Massif, Spain): evidence from detrital zircon SHRIMP U–Pb geochronology. Gondwana Res. 22, 928–942.

Torsvik, T.H., Cocks, L.R.M., 2013. Gondwana from top to base in space and time. Gondwana Res., 24, 999-1030.

Vermeesch, P., 2004. How many grains are needed for a provenance study? Earth Planet. Sci. Lett. 224, 351–441.

Von Raumer, J., Stampfi, G.M., 2008. The birth of the Rheic ocean – Early Paleozoic subsidence patterns and subsequent tectonic plate scenarios. Tectonophysics 461, 9–20.

Zwart, H.J., 1979. The geology of the central Pyrenees. Leidse Geol. Medded. 50, 1–74.

8. Appendix

Appendix 1: LA-ICPMS U-Pb results for samples MPAD8 and PC7

				ISOTOPIC RATIOS					AGES						
mpad8	Pb ppm	U ppm	Th/U	207/235	err	206/238	err	rho	207/206		206/238		207/235	err	conc
ZR101	100.8	1035.1	0.9	0.666	0.008	0.0820	0.0009	0.91	564.7	24.5	508.1	5.4	518.4	4.9	98.0
ZR111	24.0	267.7	0.6	0.726	0.009	0.0834	0.0009	0.86	712.2	25.7	516.4	5.5	554.1	5.5	93.2
ZR46	35.6	385.8	0.6	0.708	0.009	0.0852	0.0009	0.87	612.0	25.6	527.2	5.6	543.4	5.3	97.0
ZR42	21.2	266.8	0.0	0.711	0.009	0.0856	0.0010	0.85	612.8	26.7	529.5	5.7	545.4	5.5	97.1
ZR36	84.3	873.5	0.7	0.754	0.009	0.0876	0.0010	0.94	689.9	23.2	541.4	5.8	570.8	5.2	94.8
ZR48	92.0	912.1	0.7	0.743	0.009	0.0901	0.0010	0.93	597.7	23.8	556.2	5.9	564.4	5.1	98.5
ZR4	22.6	190.8	1.3	0.764	0.011	0.0907	0.0010	0.81	642.4	28.4	559.6	6.1	576.2	6.2	97.1
ZR107	34.7	359.7	0.5	0.759	0.009	0.0920	0.0010	0.88	598.1	25.1	567.4	6.0	573.5	5.4	98.9
ZR108	29.4	327.4	0.2	0.752	0.009	0.0928	0.0010	0.88	559.9	25.6	571.8	6.0	569.4	5.5	100.4
ZR52	38.0	293.9	1.6	0.749	0.009	0.0928	0.0010	0.87	549.9	26.0	572.0	6.0	567.5	5.5	100.8
ZR7	22.8	199.3	1.1	0.782	0.011	0.0931	0.0011	0.82	638.7	27.8	573.6	6.2	586.8	6.2	97.8
ZR78	94.9	780.2	1.4	0.788	0.009	0.0942	0.0010	0.92	629.3	24.0	580.2	6.0	590.2	5.3	98.3
ZR28	158.0	1768.8	0.1	0.825	0.010	0.0946	0.0011	0.90	716.8	24.4	582.7	6.2	610.8	5.7	95.4
ZR47	38.6	355.1	0.7	0.809	0.010	0.0950	0.0011	0.91	667.2	24.3	584.8	6.2	602.0	5.5	97.1
ZR37	24.9	272.3	0.1	0.796	0.010	0.0958	0.0011	0.92	612.0	24.2	589.9	6.3	594.5	5.5	99.2
ZR95	121.7	1362.0	0.0	0.827	0.010	0.0963	0.0011	0.94	684.7	23.0	592.6	6.2	612.0	5.4	96.8
ZR24	28.6	216.2	1.3	0.888	0.012	0.0964	0.0011	0.84	831.5	26.4	593.2	6.4	645.1	6.5	92.0
ZR72	97.4	971.3	0.4	0.817	0.009	0.0968	0.0011	0.94	646.7	23.2	595.6	6.1	606.3	5.3	98.2
ZR54	25.8	214.4	1.0	0.815	0.011	0.0970	0.0011	0.85	638.5	26.6	596.7	6.3	605.4	5.9	98.6
ZR20	12.9	124.2	0.5	0.809	0.011	0.0975	0.0011	0.82	611.1	27.8	599.6	6.5	601.9	6.2	99.6
ZR25	22.4	199.2	0.7	0.955	0.013	0.0977	0.0011	0.84	955.9	25.6	600.7	6.5	680.8	6.6	88.2
ZR76	153.7	1399.8	0.7	0.830	0.010	0.0978	0.0011	0.93	659.8	23.3	601.4	6.2	613.8	5.3	98.0
ZR32	11.3	83.2	1.6	0.812	0.012	0.0979	0.0011	0.78	609.0	29.6	601.9	6.5	603.4	6.6	99.8
ZR45	18.6	161.3	0.9	0.817	0.011	0.0979	0.0011	0.85	622.4	26.4	602.3	6.4	606.5	5.9	99.3
ZR57	83.3	754.7	0.6	0.850	0.010	0.0980	0.0011	0.90	706.7	24.2	602.4	6.3	624.7	5.6	96.4
ZR59	28.9	267.1	0.6	0.845	0.011	0.0985	0.0011	0.83	681.2	27.1	605.5	6.4	621.7	6.2	97.4
ZR43	33.4	314.5	0.5	0.824	0.010	0.0985	0.0011	0.90	626.3	24.6	605.8	6.4	610.1	5.6	99.3
ZR12	19.0	180.4	0.5	0.879	0.012	0.0985	0.0011	0.81	765.5	27.9	605.8	6.6	640.6	6.7	94.6
ZR31	21.9	170.4	0.9	0.810	0.011	0.0986	0.0011	0.85	588.8	27.0	606.3	6.5	602.5	6.0	100.6
ZR2	23.6	214.4	0.7	0.822	0.010	0.0987	0.0011	0.89	618.3	25.1	606.8	6.5	609.2	5.8	99.6
ZR16	54.8	542.2	0.3	0.847	0.011	0.0992	0.0011	0.89	673.1	24.7	609.4	6.5	623.0	5.8	97.8
ZR92	16.5	157.8	0.4	0.825	0.011	0.0996	0.0011	0.84	607.0	26.8	612.1	6.4	610.9	6.0	100.2
ZR3	18.4	146.2	1.2	0.857	0.011	0.1004	0.0011	0.87	670.3	25.8	616.8	6.7	628.4	6.1	98.2
ZR14	16.8	129.0	1.3	0.844	0.011	0.1006	0.0011	0.85	635.5	26.9	617.9	6.7	621.6	6.2	99.4
ZR8	98.8	978.8	0.3	0.882	0.011	0.1009	0.0011	0.94	722.0	23.0	619.5	6.6	641.9	5.7	96.5
ZR40	10.5	78.9	1.3	0.869	0.014	0.1011	0.0012	0.69	687.3	34.1	620.7	6.8	635.2	7.8	97.7
ZR33	32.8	317.6	0.3	0.864	0.011	0.1025	0.0012	0.90	644.7	24.8	629.1	6.7	632.5	5.9	99.5
ZR68	118.4	1214.4	0.1	0.880	0.010	0.1033	0.0011	0.95	668.6	22.7	633.4	6.5	641.1	5.4	98.8
ZR79	30.7	264.2	0.7	0.870	0.011	0.1035	0.0011	0.87	639.4	25.6	634.6	6.6	635.6	5.9	99.8
ZR22	17.1	167.9	0.2	0.889	0.012	0.1039	0.0012	0.84	675.7	26.9	637.3	6.8	645.8	6.4	98.7
ZR64	12.9	121.1	0.4	0.894	0.012	0.1043	0.0011	0.84	681.2	26.5	639.2	6.6	648.5	6.2	98.6
ZR58	5.4	38.5	1.4	0.873	0.015	0.1043	0.0012	0.65	628.2	36.6	639.7	6.9	637.1	8.2	100.4
ZR50	38.8	377.3	0.1	0.933	0.012	0.1051	0.0012	0.89	754.6	24.4	644.0	6.8	669.0	6.0	96.3
ZR66	35.2	304.8	0.6	0.901	0.011	0.1058	0.0011	0.90	665.6	24.1	648.3	6.7	652.2	5.7	99.4
ZR35	31.7	237.3	1.2	0.894	0.011	0.1063	0.0012	0.89	638.3	25.2	651.2	7.0	648.3	6.1	100.4
ZR83	40.3	368.4	0.3	0.924	0.011	0.1085	0.0012	0.88	667.3	24.9	663.8	6.9	664.5	6.0	99.9
ZR94	79.2	692.1	0.4	0.942	0.011	0.1093	0.0012	0.94	691.6	22.8	668.8	6.9	674.0	5.7	99.2
ZR84	26.5	217.4	0.7	0.950	0.012	0.1094	0.0012	0.85	707.9	25.9	669.0	6.9	677.9	6.3	98.7
ZR69	22.6	191.4	0.5	0.947	0.012	0.1097	0.0012	0.88	695.1	24.8	670.9	6.9	676.4	6.1	99.2
ZR23	45.4	419.2	0.1	0.973	0.012	0.1123	0.0013	0.90	703.0	24.5	686.0	7.3	689.9	6.3	99.4
ZR96	28.1	240.1	0.3	0.981	0.012	0.1143	0.0013	0.91	683.3	24.1	697.4	7.3	694.0	6.1	100.5
ZR29	9.0	68.0	0.6	1.088	0.023	0.1188	0.0014	0.57	821.1	43.3	723.4	8.3	747.6	11.2	96.8
ZR26	5.6	36.9	1.0	1.149	0.019	0.1232	0.0014	0.71	857.7	32.6	749.0	8.2	776.8	8.9	96.4
ZR10	12.3	101.0	0.2	1.140	0.015	0.1256	0.0014	0.85	801.6	26.1	762.8	8.2	772.6	7.2	98.7
ZR81	6.5	49.8	0.4	1.135	0.018	0.1263	0.0014	0.72	780.9	31.7	766.5	8.0	770.1	8.4	99.5
ZR39	98.7	755.6	0.3	1.225	0.014	0.1289	0.0014	0.94	897.5	22.4	781.4	8.2	812.1	6.6	96.2
ZR44	45.9	332.1	0.4	1.233	0.015	0.1328	0.0015	0.92	848.4	23.2	803.7	8.4	815.7	6.8	98.5
ZR11	8.5	58.4	0.5	1.246	0.018	0.1349	0.0015	0.78	837.5	28.8	815.6	8.8	821.4	8.2	99.3
ZR60	8.7	59.8	0.5	1.253	0.018	0.1353	0.0015	0.77	843.4	28.8	817.8	8.5	824.6	8.1	99.2
ZR27	21.7	142.8	0.7	1.244	0.016	0.1357	0.0015	0.86	821.8	25.5	820.2	8.7	820.6	7.4	100.0
ZR85	91.9	665.7	0.3	1.264	0.015	0.1366	0.0015	0.90	841.4	23.6	825.5	8.4	829.7	6.8	99.5
ZR21	49.5	337.7	0.3	1.381	0.017	0.1443	0.0016	0.92	911.0	23.0	868.8	9.1	880.7	7.2	98.6
ZR34	34.2	186.1	0.9	1.498	0.018	0.1548	0.0017	0.93	934.0	22.6	927.7	9.7	929.5	7.3	99.8
ZR103	55.8	320.1	0.6	1.534	0.018	0.1562	0.0017	0.92	965.1	22.5	935.3	9.6	944.2	7.3	99.1
ZR41	59.7	345.0	0.5	1.594	0.019	0.1605	0.0018	0.93	987.6	22.3	959.4	9.9	967.9	7.5	99.1
ZR89	270.3	1659.8	0.7	1.434	0.017	0.1433	0.0016	0.90	1002.8	23.1	863.3	8.8	903.3	7.2	90.1
ZR102	46.3	307.1	0.4	1.402	0.017	0.1399	0.0015	0.89	1004.8	23.4	844.2	8.7	889.7	7.3	88.5
ZR38	55.3	297.2	1.0	1.562	0.019	0.1555	0.0017	0.93	1009.0	22.3	932.0	9.7	955.1	7.4	94.7
ZR30	56.1	336.9	0.2	1.664	0.021	0.1656	0.0019	0.90	1010.7	23.2	987.6	10.3	994.7	7.9	98.4
ZR18	26.8	153.1	0.7	1.581	0.020	0.1569	0.0018	0.88	1017.4	24.2	939.2	9.9	962.8	8.0	94.6

ZR73	23.2	125.7	0.8	1.618	0.021	0.1599	0.0018	0.86	1025.8	24.6	956.1	9.7	977.4	8.0	95.3
ZR70	31.0	138.9	1.2	1.766	0.021	0.1737	0.0019	0.90	1035.0	22.9	1032.2	10.4	1033.0	7.9	99.9
ZR106	31.5	147.0	1.2	1.698	0.021	0.1669	0.0018	0.90	1036.9	23.2	994.8	10.2	1007.9	7.9	97.2
ZR61	26.1	149.5	0.9	1.479	0.021	0.1453	0.0016	0.78	1037.3	27.7	874.4	9.0	921.8	8.6	88.9
ZR90	80.0	428.7	0.4	1.812	0.022	0.1772	0.0019	0.89	1047.1	23.4	1051.4	10.6	1049.9	8.0	100.3
ZR75	45.6	211.8	1.1	1.786	0.021	0.1741	0.0019	0.91	1051.9	22.6	1034.8	10.4	1040.2	7.8	98.9
ZR80	11.1	92.9	0.9	1.019	0.015	0.0994	0.0011	0.74	1051.9	29.7	610.6	6.5	713.4	7.8	67.8
ZR93	25.5	128.2	0.6	1.990	0.025	0.1782	0.0020	0.88	1222.4	23.0	1056.9	10.7	1112.3	8.4	91.0
ZR6	43.3	211.0	0.2	2.367	0.029	0.2075	0.0023	0.92	1263.1	21.9	1215.5	12.5	1232.7	8.8	97.6
ZR65	282.5	742.0	1.0	4.608	0.052	0.3068	0.0033	0.96	1782.0	19.1	1724.7	16.3	1750.7	9.3	98.5
ZR109	68.4	177.5	0.9	4.973	0.059	0.3155	0.0035	0.93	1869.7	19.8	1767.5	17.0	1814.8	10.0	97.1
ZR100	16.6	35.6	1.5	5.354	0.066	0.3376	0.0037	0.90	1880.6	20.9	1875.1	18.0	1877.6	10.6	99.8
ZR55	442.7	1570.8	0.5	4.095	0.048	0.2561	0.0028	0.93	1895.0	19.8	1470.0	14.3	1653.3	9.6	87.2
ZR104	353.7	840.6	1.0	5.641	0.065	0.3405	0.0037	0.95	1958.5	19.0	1889.3	18.0	1922.4	9.9	98.2
ZR74	86.4	238.3	0.5	5.424	0.063	0.3241	0.0035	0.93	1976.6	19.5	1809.9	17.1	1888.7	10.0	95.6
ZR71	106.7	236.8	1.0	6.151	0.070	0.3640	0.0039	0.94	1993.8	19.0	2001.2	18.6	1997.5	10.0	100.2
ZR5	138.7	422.3	0.1	5.570	0.065	0.3270	0.0037	0.96	2008.1	18.7	1823.9	17.8	1911.4	10.0	95.2
ZR62	82.1	208.0	0.4	6.317	0.071	0.3653	0.0039	0.96	2034.9	18.6	2007.1	18.6	2020.8	9.9	99.3
ZR19	53.7	126.1	0.8	6.211	0.074	0.3546	0.0040	0.94	2057.6	19.1	1956.6	18.9	2006.1	10.4	97.5
ZR15	126.5	300.3	0.5	6.879	0.081	0.3829	0.0043	0.96	2102.1	18.7	2090.0	20.0	2096.0	10.4	99.7
ZR98	320.0	879.4	0.2	6.516	0.074	0.3500	0.0038	0.96	2164.6	18.2	1934.6	18.3	2048.1	10.0	94.6
ZR88	60.0	131.8	0.5	7.563	0.092	0.4030	0.0044	0.90	2178.4	19.9	2182.9	20.1	2180.5	10.9	100.1
ZR110	70.7	164.3	0.3	7.617	0.090	0.4007	0.0044	0.93	2200.7	19.0	2172.4	20.3	2186.9	10.6	99.4
ZR99	45.3	108.6	0.4	8.437	0.100	0.3673	0.0041	0.93	2524.1	18.5	2016.5	19.1	2279.2	10.7	90.3
ZR112	40.3	103.6	0.6	7.426	0.092	0.3221	0.0036	0.90	2530.0	19.6	1800.1	17.5	2164.1	11.1	85.5
ZR9	117.6	210.6	1.1	10.022	0.117	0.4265	0.0048	0.96	2562.0	17.7	2289.9	21.7	2436.8	10.8	95.1
ZR63	435.3	1038.0	0.0	9.744	0.108	0.4121	0.0044	0.97	2572.6	17.3	2224.4	20.3	2410.9	10.2	93.7
ZR51	246.0	442.3	0.6	11.308	0.131	0.4756	0.0052	0.95	2581.8	17.9	2507.9	22.8	2548.9	10.8	98.7
ZR77	207.4	393.7	0.5	10.985	0.126	0.4597	0.0050	0.94	2590.2	17.9	2438.1	21.9	2521.9	10.7	97.4
ZR105	471.2	979.8	0.6	9.759	0.112	0.4060	0.0045	0.95	2599.7	17.7	2196.8	20.4	2412.3	10.6	92.8
ZR53	70.2	120.9	0.8	11.220	0.133	0.4628	0.0051	0.93	2614.1	18.4	2451.9	22.4	2541.6	11.0	97.2
ZR82	140.9	249.5	0.7	11.321	0.133	0.4648	0.0050	0.92	2621.9	18.3	2460.6	22.2	2549.9	11.0	97.3
ZR56	301.4	719.1	0.1	9.670	0.114	0.3963	0.0043	0.93	2625.1	18.4	2151.8	20.0	2403.9	10.8	91.6
ZR86	45.3	78.5	0.7	12.084	0.146	0.4811	0.0053	0.90	2672.9	18.9	2532.0	22.8	2611.0	11.3	97.7
ZR97	225.8	396.0	1.1	10.950	0.124	0.4349	0.0048	0.96	2677.0	17.3	2327.7	21.4	2518.9	10.6	94.1
ZR91	106.7	183.6	0.7	12.450	0.141	0.4739	0.0052	0.97	2747.0	17.2	2500.7	22.6	2639.0	10.6	94.8
ZR49	88.7	171.7	0.1	13.302	0.155	0.4819	0.0053	0.95	2827.8	17.6	2535.7	23.1	2701.3	11.0	95.5

				ISOTOPIC RATIOS					AGES						
PC7	Pb ppm	U ppm	Th/U	207/235	err	206/238	err	rho	207/206		206/238		207/235	err	conc
ZR16	19.4	206.0	0.7	0.704	0.009	0.0851	0.0010	0.90	603.6	25.1	526.5	5.7	541.1	5.3	97.3
ZR20	39.1	444.1	0.4	0.708	0.010	0.0853	0.0010	0.84	611.4	27.4	527.5	5.8	543.5	5.8	97.1
ZR23	94.0	922.3	0.9	0.714	0.009	0.0869	0.0010	0.94	590.9	23.6	536.9	5.8	547.3	5.1	98.1
ZR56	19.2	208.9	0.2	0.821	0.012	0.0938	0.0011	0.77	723.7	30.0	578.0	6.4	608.4	6.9	95.0
ZR3	17.2	175.5	0.4	0.796	0.010	0.0942	0.0011	0.90	650.4	24.8	580.4	6.2	594.8	5.6	97.6
ZR54	33.8	352.3	0.3	0.792	0.010	0.0954	0.0011	0.93	611.8	23.8	587.5	6.4	592.5	5.5	99.2
ZR41	11.5	106.7	0.8	0.797	0.012	0.0956	0.0011	0.77	620.6	30.5	588.5	6.5	595.1	6.8	98.9
ZR74	58.4	591.2	0.4	0.821	0.010	0.0966	0.0011	0.92	662.0	23.7	594.7	6.5	608.8	5.7	97.7
ZR107	33.6	277.1	1.2	0.826	0.010	0.0971	0.0011	0.94	664.4	23.3	597.2	6.5	611.4	5.6	97.7
ZR77	35.1	365.1	0.3	0.806	0.010	0.0973	0.0011	0.95	607.8	23.2	598.6	6.6	600.4	5.5	99.7
ZR32	7.9	67.4	1.0	0.809	0.012	0.0974	0.0011	0.75	613.6	31.5	598.9	6.6	601.9	7.0	99.5
ZR52	16.7	173.5	0.2	0.826	0.012	0.0975	0.0011	0.83	655.5	27.9	599.5	6.6	611.3	6.4	98.1
ZR18	32.1	318.8	0.4	0.811	0.010	0.0977	0.0011	0.95	610.3	23.1	601.1	6.5	603.0	5.4	99.7
ZR27	23.7	214.8	0.8	0.811	0.010	0.0977	0.0011	0.92	610.3	24.4	601.1	6.5	603.0	5.6	99.7
ZR35	22.8	225.5	0.4	0.813	0.010	0.0978	0.0011	0.93	615.4	24.0	601.4	6.5	604.3	5.6	99.5
ZR61	12.2	108.6	0.8	0.816	0.011	0.0978	0.0011	0.84	623.3	27.0	601.5	6.6	606.1	6.2	99.2
ZR8	21.2	216.3	0.3	0.828	0.012	0.0979	0.0011	0.82	652.2	28.0	602.0	6.5	612.6	6.4	98.3
ZR12	49.5	547.0	0.0	0.841	0.011	0.0986	0.0011	0.86	671.0	26.0	605.9	6.5	619.8	6.1	97.8
ZR38	13.1	121.4	0.6	0.808	0.010	0.0988	0.0011	0.88	580.3	25.8	607.3	6.6	601.5	5.9	101.0
ZR72	9.5	94.1	0.4	0.836	0.011	0.0991	0.0011	0.84	646.9	27.1	609.2	6.7	617.2	6.3	98.7
ZR101	17.3	166.8	0.4	0.826	0.011	0.0991	0.0011	0.88	619.4	25.6	609.3	6.6	611.4	6.0	99.7
ZR110	20.4	189.3	0.6	0.853	0.011	0.0992	0.0011	0.90	688.4	24.7	609.6	6.6	626.5	5.9	97.3
ZR51	35.9	374.5	0.1	0.841	0.010	0.0995	0.0011	0.95	651.3	23.0	611.2	6.6	619.7	5.5	98.6
ZR113	7.5	55.8	1.6	0.837	0.012	0.0998	0.0012	0.81	632.0	28.8	613.3	6.7	617.3	6.6	99.4
ZR5	9.6	97.3	0.2	0.837	0.011	0.1005	0.0011	0.85	617.3	26.6	617.4	6.6	617.4	6.1	100.0
ZR13	14.2	118.4	1.0	0.843	0.011	0.1007	0.0011	0.85	629.5	26.8	618.7	6.7	620.9	6.2	99.6
ZR1	4.6	40.2	0.7	0.833	0.013	0.1014	0.0012	0.74	586.6	31.9	622.8	6.8	615.0	7.1	101.3
ZR68	9.2	79.3	0.8	0.868	0.012	0.1021	0.0012	0.84	662.5	27.4	626.7	6.9	634.5	6.5	98.8
ZR75	8.9	86.5	0.4	0.873	0.012	0.1023	0.0012	0.84	671.6	27.1	627.7	6.9	637.3	6.5	98.5
ZR66	31.5	296.7	0.4	0.941	0.012	0.1024	0.0012	0.90	827.2	24.0	628.4	6.8	673.4	6.2	93.3
ZR94	28.4	277.1	0.3	0.876	0.011	0.1026	0.0012	0.93	672.8	23.6	629.6	6.8	639.1	5.8	98.5
ZR79	58.3	577.3	0.3	0.863	0.010	0.1027	0.0012	0.97	637.4	22.5	630.2	6.9	631.7	5.6	99.8
ZR19	38.0	390.4	0.1	0.867	0.011	0.1035	0.0012	0.92	629.9	24.0	634.8	6.9	633.7	5.8	100.2
ZR25	44.9	429.2	0.3	0.893	0.011	0.1035	0.0012	0.95	693.2	22.9	635.0	6.8	647.9	5.7	98.0
ZR43	19.2	177.7	0.5	0.863	0.011	0.1035	0.0012	0.91	620.9	24.7	635.0	6.9	631.9	5.9	100.5
ZR69	29.2	270.6	0.4	0.881	0.011	0.1037	0.0012	0.91	659.6	24.4	636.2	6.9	641.3	6.0	99.2
ZR33	14.0	131.2	0.3	1.001	0.014	0.1041	0.0012	0.84	921.6	25.8	638.1	7.0	704.2	6.9	90.6
ZR71	51.5	462.6	0.5	0.903	0.011	0.1047	0.0012	0.93	693.6	23.5	641.7	7.0	653.3	5.9	98.2
ZR91	21.6	162.9	1.0	0.883	0.011	0.1048	0.0012	0.91	645.4	24.6	642.2	7.0	642.9	6.0	99.9
ZR55	17.5	153.3	0.6	0.900	0.011	0.1052	0.0012	0.89	676.0	24.8	644.7	7.0	651.6	6.1	98.9
ZR90	13.4	118.2	0.5	0.926	0.012	0.1060	0.0012	0.86	721.0	26.1	649.3	7.1	665.5	6.5	97.6
ZR86	28.6	219.9	1.1	0.965	0.012	0.1067	0.0012	0.92	793.9	23.4	653.8	7.1	686.1	6.2	95.3
ZR7	61.6	559.7	0.4	0.929	0.011	0.1069	0.0012	0.93	710.4	23.6	654.5	7.0	667.1	5.9	98.1
ZR102	71.2	709.4	0.0	0.923	0.011	0.1071	0.0012	0.93	691.9	23.3	655.6	7.1	663.8	5.9	98.8
ZR11	14.5	125.5	0.6	0.932	0.013	0.1078	0.0012	0.79	698.3	29.1	660.2	7.2	668.8	7.1	98.7
ZR50	31.2	297.6	0.1	0.950	0.012	0.1093	0.0012	0.92	709.5	23.7	668.6	7.2	677.9	6.1	98.6
ZR34	37.4	350.8	0.2	0.945	0.011	0.1095	0.0012	0.94	694.9	23.2	669.8	7.2	675.5	6.0	99.2
ZR64	11.9	100.3	0.6	0.991	0.013	0.1102	0.0013	0.85	782.0	26.0	674.0	7.3	699.4	6.8	96.4
ZR14	12.1	103.5	0.5	0.955	0.014	0.1108	0.0013	0.80	691.7	28.9	677.5	7.4	680.7	7.1	99.5
ZR53	18.2	159.6	0.3	0.963	0.012	0.1130	0.0013	0.92	668.3	23.8	690.2	7.4	685.0	6.1	100.8
ZR37	15.5	129.5	0.5	0.999	0.013	0.1136	0.0013	0.88	733.7	25.3	693.6	7.5	703.1	6.6	98.6
ZR80	8.0	67.7	0.4	1.031	0.014	0.1150	0.0013	0.85	776.0	26.3	701.7	7.7	719.6	7.0	97.5
ZR109	17.2	154.1	0.2	1.004	0.012	0.1163	0.0013	0.92	697.0	23.8	709.0	7.6	706.1	6.3	100.4
ZR10	60.2	555.2	0.0	1.036	0.013	0.1165	0.0013	0.93	757.9	23.4	710.3	7.6	721.8	6.3	98.4
ZR17	40.2	337.0	0.3	1.062	0.013	0.1172	0.0013	0.94	798.4	22.9	714.2	7.7	734.8	6.3	97.2
ZR45	27.6	234.4	0.3	1.025	0.013	0.1183	0.0014	0.92	704.0	23.9	720.8	7.8	716.6	6.4	100.6
ZR96	13.3	102.4	0.6	1.090	0.014	0.1190	0.0014	0.88	820.9	24.7	724.8	7.8	748.6	6.9	96.8
ZR42	9.7	64.3	1.2	1.082	0.016	0.1208	0.0014	0.80	772.7	28.4	735.1	8.0	744.4	7.6	98.8
ZR67	20.0	157.9	0.5	1.069	0.014	0.1210	0.0014	0.89	746.0	24.5	736.0	8.0	738.4	6.7	99.7
ZR15	23.4	191.6	0.3	1.090	0.015	0.1223	0.0014	0.84	762.4	26.5	743.7	8.0	748.4	7.2	99.4
ZR106	25.5	198.2	0.5	1.096	0.013	0.1232	0.0014	0.94	760.4	22.9	748.6	8.0	751.5	6.4	99.6
ZR93	33.6	254.4	0.4	1.231	0.015	0.1247	0.0014	0.92	974.8	22.7	757.3	8.2	814.6	6.9	93.0
ZR49	18.2	135.8	0.5	1.155	0.014	0.1251	0.0014	0.92	836.4	23.2	759.8	8.1	779.4	6.7	97.5
ZR26	16.3	122.7	0.5	1.113	0.015	0.1255	0.0014	0.87	753.3	25.5	761.8	8.2	759.6	7.0	100.3
ZR24	32.8	249.2	0.4	1.136	0.013	0.1268	0.0014	0.95	773.3	22.5	769.8	8.2	770.6	6.4	99.9
ZR58	12.3	78.4	1.1	1.131	0.015	0.1269	0.0015	0.87	761.8	25.3	770.4	8.3	768.1	7.1	100.3
ZR85	16.9	119.8	0.6	1.179	0.015	0.1298	0.0015	0.91	801.6	23.7	787.0	8.5	790.7	6.9	99.5
ZR99	15.4	111.2	0.5	1.193	0.015	0.1305	0.0015	0.89	815.1	24.4	790.9	8.5	797.2	7.1	99.2
ZR2	41.5	280.1	0.7	1.221	0.015	0.1326	0.0015	0.94	831.6	22.6	802.9	8.4	810.4	6.6	99.1
ZR78	43.3	326.8	0.3	1.201	0.014	0.1329	0.0015	0.96	791.8	22.3	804.3	8.7	801.0	6.6	100.4
ZR40	18.7	141.2	0.3	1.226	0.016	0.1331	0.0015	0.90	832.6	24.2	805.5	8.6	812.7	7.1	99.1
ZR108	30.6	222.4	0.4	1.225	0.015	0.1341	0.0015	0.94	814.4	22.8	811.0	8.6	811.8	6.8	99.9
ZR44	32.2	202.0	0.8	1.262	0.016	0.1349	0.0015	0.92	864.4	23.5	815.7	8.7	828.8	7.1	98.4
ZR65	9.2	66.3	0.4	1.247	0.017	0.1350	0.0016	0.86	836.9	25.7	816.5	8.8	821.9	7.6	99.3
ZR97	10.7	76.2	0.3	1.264	0.017	0.1370	0.0016	0.87	835.8	25.2	827.4	8.9	829.6	7.5	99.7
ZR95	33.8	226.7	0.5	1.281	0.016	0.1384	0.0016	0.94	841.9	22.8	835.5	8.9	837.2	6.9	99.8

ZR9	10.8	73.2	0.4	1.352	0.018	0.1411	0.0016	0.86	914.1	25.3	850.6	9.0	868.3	7.7	98.0
ZR82	31.8	195.1	0.8	1.314	0.016	0.1418	0.0016	0.94	843.7	22.4	855.0	9.2	851.8	7.0	100.4
ZR92	86.8	599.0	0.3	1.353	0.016	0.1421	0.0016	0.96	900.8	21.8	856.6	9.1	869.0	6.9	98.6
ZR83	94.0	627.2	0.4	1.412	0.017	0.1447	0.0017	0.97	951.2	21.3	871.2	9.3	894.0	7.0	97.4
ZR62	31.4	219.0	0.2	1.376	0.017	0.1451	0.0017	0.92	892.5	23.2	873.5	9.3	878.8	7.3	99.4
ZR4	25.9	177.7	0.2	1.401	0.017	0.1470	0.0016	0.92	902.4	22.8	884.1	9.2	889.3	7.2	99.4
ZR31	49.8	303.7	0.7	1.429	0.017	0.1472	0.0017	0.96	939.6	21.7	885.4	9.4	901.0	7.1	98.3
ZR39	31.4	196.9	0.3	1.512	0.019	0.1567	0.0018	0.93	927.2	22.8	938.6	9.9	935.2	7.5	100.4
ZR28	64.3	345.9	0.9	1.532	0.018	0.1572	0.0018	0.97	948.6	21.5	941.3	9.9	943.4	7.2	99.8
ZR105	89.1	394.5	1.8	1.580	0.019	0.1586	0.0018	0.93	992.9	22.4	949.1	10.0	962.3	7.6	98.6
ZR104	46.1	261.0	0.6	1.557	0.019	0.1594	0.0018	0.93	954.2	22.7	953.1	10.1	953.4	7.6	100.0
ZR70	43.8	218.8	1.2	1.582	0.019	0.1595	0.0018	0.93	984.5	22.5	954.2	10.1	963.3	7.7	99.1
ZR76	61.9	363.3	0.5	1.578	0.019	0.1597	0.0018	0.97	977.3	21.3	954.9	10.2	961.6	7.4	99.3
ZR6	58.6	348.1	0.4	1.599	0.019	0.1608	0.0018	0.93	989.2	22.3	961.3	10.0	969.7	7.5	99.1
ZR47	46.1	247.4	0.7	1.612	0.019	0.1633	0.0018	0.94	974.5	22.1	975.0	10.2	974.8	7.5	100.0
ZR111	28.7	168.9	0.4	1.615	0.019	0.1633	0.0019	0.94	977.8	22.2	975.1	10.3	975.9	7.6	99.9
ZR89	28.0	153.0	0.6	1.676	0.021	0.1681	0.0019	0.92	994.7	23.1	1001.5	10.6	999.3	8.0	100.2
ZR115	27.0	134.3	1.0	1.682	0.021	0.1674	0.0019	0.90	1009.8	23.5	998.0	10.5	1001.6	8.1	99.2
ZR114	44.3	247.1	0.4	1.739	0.021	0.1723	0.0020	0.95	1019.3	21.7	1024.8	10.7	1022.9	7.7	100.4
ZR112	16.2	96.4	0.6	1.557	0.024	0.1538	0.0018	0.76	1026.4	29.1	922.1	10.0	953.3	9.5	92.9
ZR29	28.2	162.2	0.7	1.590	0.020	0.1565	0.0018	0.92	1033.2	22.6	937.3	9.9	966.3	7.7	93.5
ZR81	11.5	93.6	0.9	1.062	0.015	0.1014	0.0012	0.81	1095.1	26.7	622.4	6.9	734.8	7.5	67.1
ZR59	41.2	190.1	1.3	1.952	0.023	0.1661	0.0019	0.94	1321.1	21.0	990.4	10.4	1099.0	8.1	83.2
ZR88	16.9	108.2	0.2	2.063	0.025	0.1416	0.0016	0.93	1726.3	20.2	853.5	9.2	1136.6	8.4	65.8
ZR22	83.7	318.7	0.4	3.649	0.042	0.2448	0.0028	0.98	1768.5	18.8	1411.3	14.3	1560.4	9.2	88.2
ZR73	39.6	283.6	0.5	1.861	0.024	0.1187	0.0014	0.90	1860.3	21.1	722.8	7.9	1067.3	8.5	57.4
ZR46	52.7	141.9	0.7	5.056	0.059	0.3222	0.0036	0.97	1861.6	18.7	1800.3	17.7	1828.8	9.8	98.2
ZR21	162.9	562.7	0.3	4.570	0.052	0.2753	0.0031	0.99	1962.4	18.2	1567.6	15.7	1743.8	9.6	88.9
ZR57	74.3	202.1	0.5	5.514	0.066	0.3311	0.0038	0.95	1968.3	19.1	1843.5	18.2	1902.8	10.3	96.7
ZR87	604.6	2849.8	0.2	3.531	0.041	0.2012	0.0023	0.98	2060.8	18.2	1181.8	12.3	1534.1	9.2	74.4
ZR60	230.1	696.5	0.1	5.744	0.067	0.3258	0.0037	0.97	2069.2	18.4	1817.8	18.0	1938.0	10.1	93.7
ZR30	336.8	911.0	0.2	6.889	0.080	0.3599	0.0041	0.98	2212.8	18.0	1981.8	19.3	2097.3	10.3	94.8
ZR103	313.5	1277.5	1.2	3.707	0.045	0.1850	0.0021	0.94	2292.1	18.9	1094.1	11.4	1572.9	9.7	68.6
ZR36	178.2	406.6	0.1	9.683	0.113	0.4223	0.0048	0.97	2521.1	17.6	2270.7	21.7	2405.1	10.8	95.4
ZR84	120.2	254.9	0.6	9.293	0.108	0.4042	0.0046	0.98	2525.2	17.3	2188.5	21.2	2367.3	10.7	93.7
ZR48	176.5	388.8	0.2	10.240	0.117	0.4278	0.0048	0.98	2593.0	17.0	2295.8	21.7	2456.7	10.6	94.7
ZR98	173.8	271.6	1.4	11.629	0.138	0.4743	0.0054	0.96	2632.9	17.7	2502.3	23.5	2575.0	11.1	97.8
ZR100	97.6	120.6	2.3	12.429	0.148	0.5047	0.0057	0.95	2640.2	17.8	2633.9	24.6	2637.4	11.2	99.9
ZR63	76.9	138.8	0.5	12.283	0.145	0.4859	0.0055	0.96	2683.6	17.5	2552.7	24.0	2626.3	11.1	97.9

Appendix 2: Results of the CA-DA diagram

MPAD8 (DA~514 Ma)				PC7 (DA~530 Ma)			
Ages (Ma)	Err (2s)	CA-DA	C. Prop. (%)	Ages (Ma)	Err (2s)	CA-DA	C. Prop. (%)
567	12	53	1	588	13	58	1
572	12	58	2	589	13	59	2
572	12	58	3	595	13	65	3
574	12	60	4	597	13	67	4
580	12	66	5	599	13	69	5
583	12	69	6	599	13	69	6
585	12	71	7	600	13	70	7
590	13	76	8	601	13	71	8
593	12	79	9	601	13	71	9
593	13	79	10	601	13	71	10
596	12	82	11	602	13	72	11
597	13	83	13	602	13	72	12
600	13	86	14	606	13	76	13
601	12	87	15	607	13	77	14
602	13	88	16	609	13	79	15
602	13	88	17	609	13	79	16
602	13	88	18	610	13	80	17
606	13	92	19	611	13	81	18
606	13	92	20	613	13	83	19
606	13	92	21	617	13	87	20
606	13	92	22	619	13	89	21
607	13	93	23	623	14	93	22
609	13	95	24	627	14	97	23
612	13	98	25	628	14	98	24
617	13	103	26	628	14	98	25
618	13	104	27	630	14	100	26
620	13	106	28	630	14	100	27
621	14	107	29	635	14	105	28
629	13	115	30	635	14	105	29
633	13	119	31	635	14	105	30
635	13	121	32	636	14	106	31
637	14	123	33	638	14	108	32
639	13	125	34	642	14	112	33
640	14	126	35	642	14	112	34
644	14	130	36	645	14	115	35
648	13	134	38	649	14	119	36
651	14	137	39	654	14	124	37

664	14	150	40	655	14	125	38
669	14	155	41	656	14	126	39
669	14	155	42	660	14	130	40
671	14	157	43	669	14	139	41
686	15	172	44	670	14	140	42
697	15	183	45	674	15	144	43
723	17	209	46	678	15	148	44
749	16	235	47	690	15	160	45
763	16	249	48	694	15	164	46
767	16	253	49	702	15	172	47
781	16	267	50	709	15	179	48
804	17	290	51	710	15	180	49
816	18	302	52	714	15	184	50
818	17	304	53	721	16	191	50
820	17	306	54	725	16	195	51
826	17	312	55	735	16	205	52
869	18	355	56	736	16	206	53
928	19	414	57	744	16	214	54
935	19	421	58	749	16	219	55
959	20	445	59	757	16	227	56
1003	46	489	60	760	16	230	57
1009	45	495	61	762	16	232	58
1011	46	497	62	770	16	240	59
1017	48	503	64	770	17	240	60
1026	49	512	65	787	17	257	61
1035	46	521	66	791	17	261	62
1037	46	523	67	803	17	273	63
1037	55	523	68	804	17	274	64
1047	47	533	69	806	17	276	65
1052	45	538	70	811	17	281	66
1222	46	708	71	816	17	286	67
1263	44	749	72	817	18	287	68
1782	38	1268	73	827	18	297	69
1870	40	1356	74	836	18	306	70
1881	42	1367	75	851	18	321	71
1895	40	1381	76	855	18	325	72
1959	38	1445	77	857	18	327	73
1977	39	1463	78	871	19	341	74
1994	38	1480	79	874	19	344	75
2008	37	1494	80	884	18	354	76
2035	37	1521	81	885	19	355	77
2058	38	1544	82	939	20	409	78

2102	37	1588	83	941	20	411	79
2165	36	1651	84	949	20	419	80
2178	40	1664	85	953	20	423	81
2201	38	1687	86	954	20	424	82
2524	37	2010	88	955	20	425	83
2562	35	2048	89	961	20	431	84
2573	35	2059	90	975	20	445	85
2582	36	2068	91	975	21	445	86
2590	36	2076	92	1002	21	472	87
2600	35	2086	93	1010	47	480	88
2614	37	2100	94	1019	43	489	89
2622	37	2108	95	1033	45	503	90
2625	37	2111	96	1862	37	1332	91
2673	38	2159	97	1968	38	1438	92
2677	35	2163	98	2069	37	1539	93
2747	34	2233	99	2213	36	1683	94
2828	35	2314	100	2521	35	1991	95
				2525	35	1995	96
				2593	34	2063	97
				2633	35	2103	98
				2640	36	2110	99
				2684	35	2154	100

RBJ1 (DA~475 Ma)				MN4 (DA~530 Ma)			
Ages (Ma)	Err (2s)	CA-DA	C. Prop. (%)	Ages (Ma)	Err (2s)	CA-DA	C. Prop. (%)
595	12	120	1	561	12	31	1
605	14	130	2	569	12	39	2
612	12	137	3	570	12	40	3
613	11	138	4	572	12	42	4
623	12	148	5	573	12	43	5
628	14	153	6	577	13	47	6
632	12	157	7	580	13	50	7
640	14	165	8	582	13	52	8
641	13	166	9	586	13	56	9
647	11	172	10	588	13	58	10
649	14	174	11	592	13	62	11
653	12	178	12	595	13	65	12
655	12	180	13	597	13	67	13
663	12	188	14	598	13	68	13
667	14	192	15	598	13	68	14
667	13	192	16	603	13	73	15
676	12	201	17	604	13	74	16
678	12	203	18	607	13	77	17
680	16	205	19	607	13	77	18
687	12	212	20	608	13	78	19
687	13	212	21	609	13	79	20
694	14	219	22	613	13	83	21
695	11	220	23	614	13	84	22
699	13	224	24	614	13	84	23
704	13	229	26	616	13	86	24
707	14	232	27	618	13	88	25
714	18	239	28	619	14	89	26
717	17	242	29	619	13	89	27
726	13	251	30	619	14	89	28
727	15	252	31	620	14	90	29
737	32	262	32	621	13	91	30
739	16	264	33	624	13	94	31
754	14	279	34	631	14	101	32
765	14	290	35	646	14	116	33
780	19	305	36	650	14	120	34
788	15	313	37	651	14	121	35
793	15	318	38	653	14	123	36

831	18	356	39	653	14	123	37
856	16	381	40	653	14	123	38
857	17	382	41	654	14	124	38
870	16	395	42	657	14	127	39
882	14	407	43	672	15	142	40
894	15	419	44	673	14	143	41
919	16	444	45	673	15	143	42
924	18	449	46	676	15	146	43
935	20	460	47	677	15	147	44
943	26	468	48	677	15	147	45
953	18	478	49	678	15	148	46
954	16	479	50	683	15	153	47
970	18	495	51	684	15	154	48
970	19	495	52	686	15	156	49
976	25	501	53	690	15	160	50
982	23	507	54	695	15	165	51
983	16	508	55	699	15	169	52
988	17	513	56	699	15	169	53
991	25	516	57	700	15	170	54
994	18	519	58	700	15	170	55
996	20	521	59	700	15	170	56
997	20	522	60	702	15	172	57
1004	19	529	61	706	15	176	58
1010	22	535	62	720	16	190	59
1011	18	536	63	730	16	200	60
1016	25	541	64	730	16	200	61
1031	29	556	65	734	16	204	62
1031	20	556	66	737	16	207	62
1033	25	558	67	737	16	207	63
1036	25	561	68	737	16	207	64
1044	19	569	69	738	16	208	65
1047	20	572	70	740	16	210	66
1056	19	581	71	741	16	211	67
1077	16	602	72	748	16	218	68
1103	21	628	73	750	16	220	69
1161	21	686	74	756	16	226	70
1841	27	1366	76	760	17	230	71
1846	35	1371	77	769	17	239	72
1856	34	1381	78	773	17	243	73
1864	39	1389	79	792	17	262	74
1901	32	1426	80	802	17	272	75
1916	26	1441	81	805	17	275	76

1933	31	1458	82	830	17	300	77
2000	46	1525	83	847	18	317	78
2001	42	1526	84	852	18	322	79
2001	32	1526	85	854	18	324	80
2017	27	1542	86	884	19	354	81
2063	40	1588	87	897	19	367	82
2085	35	1610	88	899	19	369	83
2096	38	1621	89	904	19	374	84
2235	36	1760	90	931	20	401	85
2258	34	1783	91	971	20	441	86
2304	47	1829	92	997	21	467	87
2478	45	2003	93	1007	46	477	88
2500	50	2025	94	1020	45	490	88
2533	43	2058	95	1027	51	497	89
2541	40	2066	96	1104	43	574	90
2601	60	2126	97	1716	40	1186	91
2615	42	2140	98	1788	40	1258	92
2727	53	2252	99	1924	38	1394	93
3311	62	2836	100	2066	37	1536	94
				2102	38	1572	95
				2110	38	1580	96
				2707	22	2177	97
				2741	34	2211	98
				2995	33	2465	99
				3207	34	2677	100

M1 (DA~530 Ma)				M4 (DA~505 Ma)			
Ages (Ma)	Err (2s)	CA-DA	C. Prop. (%)	Ages (Ma)	Err (2s)	CA-DA	C. Prop. (%)
532	10	2	1	545.0	19	40.0	1
537	10	7	2	549.0	19	44.0	2
538	9	8	3	560.0	17	55.0	3
539	11	9	4	573.0	19	68.0	3
539	9	9	5	575.0	15	70.0	4
540	10	10	6	577.0	28	72.0	5
540	39	10	7	588.0	26	83.0	6
542	11	12	8	591.0	16	86.0	7
542	12	12	8	596.0	19	91.0	8
542	10	12	9	596.0	15	91.0	8
543	10	13	10	597.0	17	92.0	9
544	10	14	11	601.0	14	96.0	10
546	11	16	12	605.0	22	100.0	11
546	12	16	13	609.0	13	104.0	12
547	10	17	14	612.0	14	107.0	13
547	11	17	15	613.0	33	108.0	14
548	9	18	16	614.0	15	109.0	14
549	9	19	17	616.0	18	111.0	15
549	10	19	18	617.0	15	112.0	16
550	10	20	19	620.0	21	115.0	17
550	11	20	20	621.0	25	116.0	18
555	9	25	21	622.0	18	117.0	19
556	11	26	22	623.0	14	118.0	19
557	15	27	23	629.0	16	124.0	20
557	11	27	24	630.0	21	125.0	21
557	9	27	25	630.0	17	125.0	22
558	10	28	25	634.0	17	129.0	23
558	10	28	26	636.0	20	131.0	24
558	9	28	27	641.0	20	136.0	25
559	13	29	28	644.0	19	139.0	25
559	12	29	29	652.0	19	147.0	26
560	11	30	30	652.0	17	147.0	27
561	10	31	31	653.0	16	148.0	28
562	9	32	32	653.0	15	148.0	29
566	11	36	33	654.0	18	149.0	30
567	12	37	34	654.0	23	140.0	31
567	12	37	35	654.0	18	140.0	31

567	11	37	36	655.0	20	141.0	32
568	11	38	37	657.0	16	143.0	33
569	11	39	38	657.0	15	143.0	34
570	10	40	39	660.0	15	146.0	35
570	10	40	40	661.0	16	147.0	36
570	11	40	41	663.0	16	149.0	36
570	10	40	42	666.0	19	152.0	37
571	17	41	42	674.0	17	160.0	38
571	10	41	43	676.0	16	162.0	39
571	10	41	44	677.0	18	163.0	40
574	11	44	45	680.0	18	166.0	41
574	10	44	46	681.0	18	167.0	42
574	11	44	47	681.0	18	167.0	42
574	13	44	48	687.0	19	173.0	43
575	12	45	49	688.0	19	174.0	44
575	10	45	50	688.0	22	174.0	45
575	11	45	51	691.0	20	177.0	46
575	9	45	52	691.0	23	177.0	47
576	21	46	53	691.0	16	177.0	47
578	11	48	54	696.0	18	182.0	48
578	11	48	55	697.0	20	183.0	49
579	13	49	56	711.0	24	197.0	50
579	13	49	57	727.0	24	213.0	51
580	13	50	58	733.0	16	219.0	52
585	12	55	58	749.0	20	235.0	53
585	11	55	59	759.0	19	245.0	53
586	10	56	60	786.0	19	272.0	54
586	10	56	61	789.0	22	275.0	55
589	10	59	62	791.0	19	277.0	56
590	11	60	63	792.0	18	278.0	57
591	11	61	64	809.0	18	295.0	58
592	9	62	65	820.0	31	306.0	58
593	13	63	66	869.0	19	355.0	59
597	9	67	67	900.0	25	386.0	60
598	11	68	68	913.0	32	399.0	61
601	15	71	69	917.0	34	403.0	62
606	15	76	70	927.0	25	413.0	63
606	11	76	71	942.0	32	428.0	64
606	11	76	72	948.0	25	434.0	64
611	10	81	73	952.0	21	438.0	65
615	11	85	74	953.0	23	439.0	66

615	13	85	75	963.0	50	449.0	67
616	11	86	75	963.0	24	449.0	68
621	15	91	76	964.0	25	450.0	69
624	17	94	77	965.0	28	451.0	69
632	14	102	78	968.0	23	454.0	70
653	14	123	79	995.0	25	481.0	71
664	12	134	80	998.0	30	484.0	72
720	14	190	81	1019.0	23	505.0	73
1925	22	1395	82	1042.0	24	528.0	74
1946	19	1416	83	1042.0	26	528.0	75
2001	19	1471	84	1074.0	31	560.0	75
2005	18	1475	85	1684.0	45	1170.0	76
2025	18	1495	86	1748.0	50	1234.0	77
2034	16	1504	87	1752.0	42	1238.0	78
2037	16	1507	88	1784.0	58	1270.0	79
2039	17	1509	89	1802.0	47	1288.0	80
2067	23	1537	90	1806.0	49	1292.0	81
2069	14	1539	91	1823.0	50	1309.0	81
2069	17	1539	92	1871.0	42	1357.0	82
2084	20	1554	92	1934.0	47	1420.0	83
2089	17	1559	93	1935.0	53	1421.0	84
2090	18	1560	94	1942.0	43	1428.0	85
2132	21	1602	95	2000.0	45	1486.0	86
2136	22	1606	96	2029.0	45	1515.0	86
2163	18	1633	97	2030.0	50	1516.0	87
2176	29	1646	98	2038.0	49	1524.0	88
2232	21	1702	99	2051.0	47	1537.0	89
2235	36	1705	100	2059.0	50	1545.0	90
				2092.0	45	1578.0	91
				2095.0	56	1581.0	92
				2096.0	56	1582.0	92
				2117.0	58	1603.0	93
				2157.0	52	1643.0	94
				2210.0	46	1696.0	95
				2270.0	94	1756.0	96
				2322.0	45	1808.0	97
				2370.0	77	1856.0	97
				2653.0	101	2139.0	98
				2903.0	105	2389.0	99
				3070.0	93	2556.0	100

OD3 (DA~530 Ma)				SCS5 (DA~470Ma)			
Ages (Ma)	Err (2s)	CA-DA	C. Prop. (%)	Ages (Ma)	Err (2s)	CA-DA	C. Prop. (%)
548	8	18.0	1	603	10	123	1
552	7	22.0	1	608	21	138	1
553	8	23.0	2	608	8	138	2
562	10	32.0	3	609	8	139	3
564	9	34.0	4	610	16	140	4
568	10	38.0	4	611	11	141	4
568	5	38.0	5	612	12	142	5
574	17	44.0	6	618	7	148	6
574	8	44.0	6	619	12	149	7
575	11	45.0	7	623	9	153	7
579	8	49.0	8	629	12	159	8
582	10	52.0	9	630	17	160	9
586	8	56.0	9	636	12	166	9
588	4	58.0	10	643	11	173	10
592	8	62.0	11	646	7	176	11
592	8	62.0	11	647	6	177	12
593	7	63.0	12	651	10	181	12
594	10	64.0	13	653	11	183	13
594	8	64.0	13	654	10	184	14
596	8	66.0	14	661	11	191	14
597	9	67.0	15	663	11	193	15
599	8	69.0	16	664	11	194	16
599	10	69.0	16	667	9	197	17
600	5	70.0	17	667	8	197	17
601	11	71.0	18	671	9	201	18
601	11	71.0	18	673	17	203	19
602	10	72.0	19	677	13	207	20
604	7	74.0	20	681	8	211	20
605	18	75.0	21	683	20	213	21
606	8	76.0	21	684	10	214	22
607	9	77.0	22	685	8	215	22
607	10	77.0	23	690	12	220	23
608	6	78.0	23	695	15	225	24
611	10	81.0	24	698	13	228	25
612	12	82.0	25	702	18	232	25
612	13	82.0	26	741	12	271	26
612	7	82.0	26	754	10	284	27

613	14	83.0	27	776	24	306	28
614	9	84.0	28	786	26	316	28
614	14	84.0	28	789	12	319	29
614	10	84.0	29	805	12	335	30
616	10	86.0	30	811	17	341	30
617	11	87.0	30	823	9	353	31
619	10	89.0	31	825	14	355	32
620	7	90.0	32	843	8	373	33
625	10	95.0	33	843	13	373	33
625	10	95.0	33	843	11	373	34
626	7	96.0	34	850	16	380	35
628	9	98.0	35	858	11	388	36
629	10	99.0	35	865	10	395	36
629	11	99.0	36	881	9	411	37
629	9	99.0	37	907	18	437	38
631	11	101.0	38	930	15	460	38
633	13	103.0	38	932	8	462	39
634	8	104.0	39	938	9	468	40
634	13	104.0	40	959	39	489	41
636	9	106.0	40	962	22	492	41
639	8	109.0	41	968	15	498	42
642	8	112.0	42	969	19	499	43
642	7	112.0	43	977	10	507	43
644	15	114.0	43	984	9	514	44
645	6	115.0	44	985	32	515	45
646	6	116.0	45	987	15	517	46
648	11	118.0	45	989	15	519	46
648	8	118.0	46	990	10	520	47
648	10	118.0	47	993	20	523	48
649	9	119.0	48	998	16	528	49
650	10	120.0	48	1003	12	533	49
655	19	125.0	49	1004	14	534	50
659	14	129.0	50	1007	11	537	51
661	15	131.0	50	1011	21	541	51
661	10	131.0	51	1021	14	551	52
661	13	131.0	52	1024	13	554	53
661	11	131.0	52	1025	16	555	54
662	11	132.0	53	1026	10	556	54
664	12	134.0	54	1026	20	556	55
665	11	135.0	55	1029	20	559	56
669	7	139.0	55	1036	14	566	57

674	8	144.0	56	1042	21	572	57
675	7	145.0	57	1051	20	581	58
681	9	151.0	57	1056	10	586	59
686	8	156.0	58	1057	22	587	59
688	12	158.0	59	1061	16	591	60
691	25	161.0	60	1061	23	591	61
694	9	164.0	60	1064	23	594	62
698	25	168.0	61	1067	15	597	62
698	14	168.0	62	1072	17	602	63
706	7	176.0	62	1073	12	603	64
708	11	178.0	63	1075	13	605	64
710	19	180.0	64	1078	12	608	65
719	9	189.0	65	1083	26	613	66
721	9	191.0	65	1093	11	623	67
731	12	201.0	66	1098	14	628	67
732	14	202.0	67	1101	15	631	68
743	15	213.0	67	1108	17	638	69
760	9	230.0	68	1127	8	657	70
761	14	231.0	69	1128	22	658	70
762	13	232.0	70	1147	15	677	71
765	12	235.0	70	1160	23	690	72
768	11	238.0	71	1268	17	798	72
775	11	245.0	72	1781	27	1311	73
781	10	251.0	72	1812	26	1342	74
800	25	270.0	73	1833	29	1363	75
821	12	291.0	74	1843	65	1373	75
830	10	300.0	74	1849	25	1379	76
841	19	311.0	75	1852	33	1382	77
875	9	345.0	76	1870	21	1400	78
894	13	364.0	77	1916	23	1446	78
901	23	371.0	77	1925	19	1455	79
935	12	405.0	78	1935	23	1465	80
941	21	411.0	79	1941	22	1471	80
947	15	417.0	79	1971	16	1501	81
951	27	421.0	80	1993	42	1523	82
970	26	440.0	81	2038	41	1568	83
974	19	444.0	82	2044	37	1574	83
974	19	444.0	82	2062	45	1592	84
983	11	453.0	83	2092	31	1622	85
1005	14	475.0	84	2106	27	1636	86
1017	14	487.0	84	2195	25	1725	86
1057	20	527.0	85	2212	11	1742	87

1079	10	549.0	86	2418	27	1948	88
1117	18	587.0	87	2532	16	2062	88
1166	21	636.0	87	2545	15	2075	89
1299	18	769.0	88	2567	15	2097	90
1375	29	845.0	89	2570	25	2100	91
1619	21	1089.0	89	2583	11	2113	91
1748	24	1218.0	90	2599	20	2129	92
1914	23	1384.0	91	2603	33	2133	93
1975	25	1445.0	91	2611	36	2141	93
2018	19	1488.0	92	2615	22	2145	94
2023	30	1493.0	93	2617	20	2147	95
2135	29	1605.0	94	2621	22	2151	96
2194	32	1664.0	94	2642	16	2172	96
2239	17	1709.0	95	2652	19	2182	97
2246	29	1716.0	96	2657	47	2187	98
2397	27	1867.0	96	2664	11	2194	99
2458	14	1928.0	97	2676	16	2206	99
2459	19	1929.0	98	2896	9	2426	100
2601	23	2071.0	99				
2666	21	2136.0	99				
3165	14	2635.0	100				

ETZ30 (DA~530 Ma)				S5 (DA~530Ma)			
Ages (Ma)	Err (2s)	CA-DA	C. Prop. (%)	Ages (Ma)	Err (2s)	CA-DA	C. Prop. (%)
539	10	0.0	1	621	14	91	2
539	13	0.0	3	650	9.5	120	3
540	12	1.0	4	651	12	121	5
544	11	5.0	5	664	12	134	6
549	11	10.0	7	669	21	139	8
550	16	11.0	8	671	12	141	10
551	10	12.0	9	677	16	147	11
552	11	13.0	11	679	15	149	13
552	11	13.0	12	688	35	158	14
554	12	15.0	13	698	20	168	16
554	13	15.0	15	702	17	172	17
556	13	17.0	16	709	32	179	19
556	12	17.0	17	714	17	184	21
556	14	17.0	19	719	19	189	22
561	15	22.0	20	734	17	204	24
566	12	27.0	21	735	19	205	25
575	12	36.0	23	736	16	206	27
580	14	41.0	24	736	13	206	29
587	12	48.0	25	737	20	207	30
591	12	52.0	27	740	22	210	32
592	11	53.0	28	743	16	213	33
597	12	58.0	29	748	35	218	35
599	11	60.0	31	752	21	222	37
600	11	61.0	32	766	9.1	236	38
601	14	62.0	33	784	19	254	40
601	15	62.0	35	799	24	269	41
604	14	65.0	36	825	33	295	43
605	12	66.0	37	825	14	295	44
607	21	68.0	39	834	29	304	46
614	12	75.0	40	839	15	309	48
616	13	77.0	41	841	21	311	49
617	13	78.0	43	842	31	312	51
620	14	81.0	44	845	26	315	52
621	14	82.0	45	868	16	338	54
631	14	92.0	47	880	40	350	56
633	12	94.0	48	910	38	380	57
634	13	95.0	49	910	15	380	59

641	16	102.0	51	917	14	387	60
649	24	110.0	52	943	25	413	62
649	14	110.0	53	972	32	442	63
660	15	121.0	55	994	25	464	65
662	22	123.0	56	995	22	465	67
668	17	129.0	57	1025	40	495	68
673	18	134.0	59	1036	60	506	70
678	13	139.0	60	1039	31	509	71
680	13	141.0	61	1050	44	520	73
684	17	145.0	63	1050	44	520	75
685	28	146.0	64	1067	36	537	76
694	15	155.0	65	1129	46	599	78
696	15	157.0	67	1368	101	838	79
696	15	157.0	68	1624	29	1094	81
737	20	198.0	69	2006	54	1476	83
745	17	206.0	71	2165	41	1635	84
758	17	219.0	72	2264	29	1734	86
764	30	225.0	73	2373	46	1843	87
2045	37	1506.0	75	2453	25	1923	89
2062	25	1523.0	76	2457	30	1927	90
2077	35	1538.0	77	2536	45	2006	92
2090	36	1551.0	79	2556	19	2026	94
2090	30	1551.0	80	2562	20	2032	95
2101	64	1562.0	81	2584	25	2054	97
2119	17	1580.0	83	2660	12	2130	98
2125	70	1586.0	84	2802	24	2272	100
2388	16	1849.0	85				
2389	17	1850.0	87				
2390	14	1851.0	88				
2467	32	1928.0	89				
2561	28	2022.0	91				
2715	23	2176.0	92				
2722	22	2183.0	93				
2895	28	2356.0	95				
2910	17	2371.0	96				
2928	32	2389.0	97				
3086	17	2547.0	99				
3258	11	2719.0	100				

Appendix 3 : Operating conditions for the LA-ICP-MS equipment

Laboratory & Sample Preparation	
Laboratory name	Géosciences Rennes, UMR CNRS 6118, Rennes, France
Sample type/mineral	zircon
Sample preparation	Conventional mineral separation, 1 inch resin mount, 1µm polish to finish
Imaging	(CL) imaging using a Quanta 200 SEM with centaurus detector at the Laboratoire Magmas d'océanologie et de geosciences, Université de Lille 1 (Lille, France).
Laser ablation system	
Make, Model & type	ESI NWR193UC, Excimer
Ablation cell	ESI NWR TwoVol2
Laser wavelength	193 nm
Pulse width	< 5 ns
Fluence	7 J/cm-2
Repetition rate	5 Hz
Spot size	25 µm
Sampling mode / pattern	Single spot
Carrier gas	100% He, Ar make-up gas and N2 (3 ml/mn) combined using in-house smoothing device
Background collection	20 seconds
Ablation duration	60 seconds
Wash-out delay	15 seconds
Cell carrier gas flow (He)	0.75 l/min
ICP-MS Instrument	
Make, Model & type	Agilent 7700x, Q-ICP-MS
Sample introduction	Via conventional tubing
RF power	1350W
Sampler, skimmer cones	Ni
Extraction lenses	X type
Make-up gas flow (Ar)	0.85 l/min
Detection system	Single collector secondary electron multiplier
Data acquisition protocol	Time-resolved analysis
Scanning mode	Peak hopping, one point per peak
Detector mode	Pulse counting, dead time correction applied, and analog mode when signal intensity > ~ 10^6 cps
Masses measured	^{204}(Hg + Pb), ^{206}Pb, ^{207}Pb, ^{208}Pb, ^{232}Th, ^{238}U
Integration time per peak	10-30 ms
Sensitivity / Efficiency	20000 cps/ppm Pb (50µm, 10Hz)
Data Processing	
Gas blank	20 seconds on-peak
Calibration strategy	GJ1 zircon standard used as primary reference material, Plešovice used as secondary reference material (quality control)
Reference Material info	GJ1 (Jackson et al., 2004) Plešovice (Slama et al., 2008)
Data processing package used	GLITTER ® (van Achterbergh et al., 2001)
Quality control / Validation	Plešovice: concordia age = 336.7 ± 0.75Ma (N=36; MSWD=0.33)